ELASTIC-PLASTIC BENDING ANALYSIS OF PLATES AND SLABS BY THE FINITE ELEMENT METHOD

A THESIS SUBMITTED TO THE UNIVERSITY
OF LONDON FOR THE DEGREE OF
DOCTOR OF PHILOSOPHY

BY

GREGORY MALCOLM McNEICE, B.A.Sc., A.M.E.I.C.

DEPARTMENT OF CIVIL AND MUNICIPAL ENGINEERING
UNIVERSITY COLLEGE LONDON

November 1967

TO THE MEMORY OF

L.G. McNEICE

SYNOPSIS

The finite element method is applied to elastic-plastic plate bending analysis. Square plates are divided into square elements with corner nodes at which plastic rotations are introduced whenever the internal principal generalized stress states satisfy a square yield criterion. The analytical response of plates and slabs to monotonically increasing applied load is traced in a step-by-step manner by digital computer. A complete history of displacements and generalized stresses is developed through the elastic phase to collapse.

Results obtained from experiments on plates and slabs are compared with those produced analytically inorder to assess the validity of the finite element model.

ACKNOWLEDGEMENTS

I take this opportunity to express my sincere gratitude to Dr. K.O. Kemp for the guidance and personal support afforded me during this study.

I should like to thank Professor A.H. Chilver for providing the facilities required to conduct this research.

I should also like to thank Messrs D. Vale, T. Gurman, A. Jenkins, J. Jackson, D. Tillman, M. Gregory and D. Marner for their assistance and advice in preparing the experimental equipment. I should like to express my appreciation of Mrs. L. Moore and Misses G. Davidson, D. Lawrence and J. Shane at the University of London Computer Centre for their assistance in the preparation and operation of the computer program.

I gratefully acknowledge the financial support given me by the British Board of Trade through the Athlone Fellowship scheme and by the National Research Council of Canada.

Finally I should like to thank my wife for having the patience to type a difficult manuscript.

TABLE OF CONTENTS

NOMENCLATURE

General

x y z	- Cartesian reference system
ν	- Poisson ratio
E	- modulus of elasticity
G	- modulus of rigidity
J	- polar moment of inertia
I	- moment of inertia
L	- square plate span length
t	- plate thickness where appropriate
$D = Et^3/12(1-\nu^2)$	- plate flexural stiffnesses
$Dx = D$	
$D_1 = \tau \cdot D$	
$Dy = \sigma D$	
$Dxy = \mu D = (1-\nu)D/2$	
Mx My Mxy	- bending and twisting generalized stresses
M^1 M^2	- principal generalized stresses
Mx_b	- beam bending moment along x axis
M	- limiting yield value of generalized stresses
M_b	- limiting yield value of beam bending moment
$\gamma_e = \frac{EI}{DL} = \frac{D_b}{DL}$	- flexural stiffness ratio, beam/plate
$\gamma_p = \frac{M_b}{ML}$	- limiting strength ratio, beam/plate
$\gamma_t = \frac{GJ}{EI}$	- beam stiffness ratio, torsional/bending
V	- vertical edge reaction on plate

$\left.\begin{matrix}(\;) \\ [\;] \\ \{ \; \}\end{matrix}\right\}$	- brackets
$\left\| \; \right\|$	- denotes matrix when the elements are displayed
$(\cdot)^T$	- transpose of matrix(ces) in brackets
i j k l m n p q	- subscripts for use in summation convention
s t	- superscripts for use in summation convention
w_i	- vertical displacement at node i
θx_i	- slope about y axis at node i
θy_i	- slope about x axis at node i
P	- computer applied load
P_e	- computer elastic limit load
P_c	- limit analysis collapse load
F.E.M.	- finite element method
w,x	$- \partial w / \partial x$
w,y	$- \partial w / \partial y$
w,xy	$- \partial^2 w / \partial x \partial y$
$M^{1,2}$, xy	$- \partial^2 M^1 / \partial x \partial y$ or $\partial^2 M^2 / \partial x \partial y$
ϕ	- orientation angle of principal planes measured clockwise positive from x axis
$\Phi^1_q \quad \Phi^2_q$	- orientation of plastic flow lines measured clockwise positive from x axis, resulting from M^1 and M^2 satisfying yield criterion at node q
$\left\|\text{cosine } \Phi^t_q\right\|$	- modulus of cosine Φ^t_q

$\left|\text{sine } \Phi^{t}_{q}\right|$ - modulus of sine Φ^{t}_{q}

C^{t}_{q} - $-\left|\text{ cosine } \Phi^{t}_{q}\right|$

S^{t}_{q} - $+\left|\text{sine } \Phi^{t}_{q}\right|$

α_i - plastic rotation at node i

αx_i, αy_i - components of plastic rotation α_i along x and y axes

D_n - matrix of nodal displacements at node n

R^{s}_{p} - matrix of plastic rotations resulting from the principal generalized stresses M^s satisfying yield criterion at node p

F_m - matrix of nodal forces for node m

M^{t}_{q} - matrix of principal generalized stresses M^t at node q

K_{mn}, K^{s}_{mp}, K^{t}_{qn}, K^{ts}_{qp} - submatrices of elastic-plastic stiffness matrix

K^{II}_{mn} - 2nd column of K_{mn} matrix

K^{tIII}_{q1} - 3rd column of K^{t}_{q1} matrix

Chapter 1

q - uniformly distributed load

L - long span for slabs

l	- short span for slabs
$\psi = l/L$	- aspect ratio

Chapter 3

a, b	- dimensions of element in Figure 3.2 only
a	- matrix of coefficients from equation 3.7
b	- matrix of coefficients from equation 3.73
We	- external work
Wi	- internal work
μ	- coefficient of orthotropy for equation 3.27 only
C, k, B, I, D, K, G, H	- matrices
M	- matrix in equations 3.12, 3.13 and 3.15

Appendix I

A	- matrix in equations A1.3, A1.4 and A1.7, otherwise the non-dimensional length of an element
a	- matrix in equations A1.18, otherwise a constant
B	- matrix in equations A1.7 and A1.8, otherwise a constant
q	- uniformly distributed load

K - curvature matrix in equations A1.7

M - matrix in equation A1.8

w - matrix in equations A1.17, A1.18, and A1.19

L - matrix in equation A1.18

Appendix III

I - total moment of inertia of section

Ic - moment of inertia due to concrete

Is - moment of inertia due to reinforcing steel

b - width of slab section

SUMMATION CONVENTION

Example

Expansion of equations 3.60 for principal generalized stress M^1 at node q only.

- summation of repeated subscripts is independent of summation of repeated superscripts
- values of subscripts and superscripts for rectangular element are:

$$\left.\begin{matrix} m \\ n \end{matrix}\right\} 1\ 2\ 3\ 4 \quad \left.\begin{matrix} p \\ q \end{matrix}\right\} 1\ 2\ 3 \quad \left.\begin{matrix} s \\ t \end{matrix}\right\} 1\ 2$$

$$M_q^t = \begin{vmatrix} K_{qn}^t & K_{qp}^{ts} \end{vmatrix} \begin{vmatrix} D_n \\ R_p^s \end{vmatrix} = K_{qn}^t D_n + K_{qp}^{ts} R_p^s$$

$$M_q^1 = K_{qn}^1 D_n + K_{qp}^{1s} R_p^s$$

$$= K_{q1}^1 D_1 + K_{q2}^1 D_2 + K_{q3}^1 D_3 + K_{q4}^1 D_4 + K_{qp}^{11} R_p^1 + K_{qp}^{12} R_p^2$$

$$= (\quad \text{ditto} \quad) + K_{q1}^{11} R_1^1 + K_{q2}^{11} R_2^1 + K_{q3}^{11} R_3^1 + K_{q1}^{12} R_1^2 + K_{q2}^{12} R_2^2 + K_{q3}^{12} R_3^2$$

For further expansion of the K_{q1}^1 and K_{q1}^{11} etc. matrices see equations 3.59 and 3.63.

INTRODUCTION

Most of the existing analytical methods used in plate or slab bending problems are restricted in their application to either a purely elastic response or to a limiting (collapse) behaviour. The fundamental principles characteristic of elastic analysis have been well established for more than a century. The principles underlying the limit analyses of plates and slabs have been developed since the early 1940's resulting from the pioneering work of Johansen in Denmark and Prager in the U.S.A.

Probably the most informative contributions to the collapse analyses of reinforced concrete slabs have been made by British researchers, in particular the work of Wood at the Building Research Station.

Because of the nature of the two types of analyses existing at present there is a severe gap in our knowledge of the behaviour between the end of the elastic stage and the final or collapse stage. To bridge this gap a unified approach must be developed that will include both types of behaviour and still produce a realistic complete analysis throughout the elastic-to-collapse response. This type of analysis is becoming increasingly more important as more slab designs are made using limit methods. The importance of being able to estimate deflections, extent of cracking and the general behaviour of the slab before collapse is certainly realized by present code committees.

Wood suggested as far back as 1955 and again in 1961 that this type of elastic-plastic analysis should be attempted. Few attempts have been made until very recently since the complexity of the problem required solution by computers which until recently did not have sufficient

The purpose of the present study reported in this thesis is to present an elastic-plastic bending analysis for plates and slabs based on well established fundamentals of structural mechanics and on currently accepted principles of plastic theory for ductile metals.

In view of the complexity of plate bending problems it is hardly surprising that numerical methods are being applied to their solution. One such method that has gained appreciable popularity in recent years is the finite element method. This method is a more physically obvious one than previous methods such as finite difference and Fourier series solutions. The structure, in the present case a plate or slab, is divided into a number of small but finite elements. These elements are connected only at their nodal points where displacement continuity (in the purely elastic case) or discontinuity (by introducing plastic rotations for the present study), together with equilibrium of nodal forces is established. The solution of the problem follows using standard structural procedures (such as the displacement method in the present study).

The method originated from research carried out by aeronautical analysts in the U.S.A. in 1956. Although it has been applied to many types of problems (not only in the structural field) during the past decade, few plate bending problems had been attempted until 1964 when British academics began examining the method and applying it to slab problems.

Because of the philosophy of the method and the accuracy obtainable in elastic plate bending analyses, it was adopted as the analytical tool in producing the elastic-plastic analyses reported herein. To the writer's knowledge this method has not been applied previously to

elastic-plastic plate bending analysis.

The application of the finite element method to the present study does not introduce any new fundamental principles for the method but does involve the use of existing principles in a way that has not been previously reported.

The thesis consists of seven chapters and three appendices. Chapters 1 and 2 serve as an introductory background to the present study by describing existing types of inelastic analyses and summarizing the finite element method. Chapter 3 contains the theoretical procedures developed for the analysis. The experimental tests are described and reported in Chapters 4 and 5 respectively.

In Chapter 6 three analytical solutions are presented for reinforced concrete slabs carrying uniformly distributed loads. These are compared with available unique solutions presented in Chapter 1.

Chapter 7 summarizes the results (analytical and experimental) of the study from which certain conclusions are drawn and suggestions for further research presented.

Appendix I contains the matrices used in developing the rectangular element stiffness and generalized stress matrices. These are presented in explicit form for completeness of presentation.

Appendix II summarizes the computer program developed for the Atlas computer housed at the University of London Computer Center.

Appendix III contains miscellaneous experimental data for the tests reported.

References to existing literature are numbered such as Westergaard[1] in consecutive order as they appear in the text.

CHAPTER 1 - EXISTING INELASTIC PLATE BENDING ANALYSES

1.1 General Remarks

The behaviour of plates bending under transverse loading has received considerable attention since the first attempts at plate analysis in the early 1800's. For well over a century many analysts developed and improved upon the theories of plate bending for elastic analysis. Westergaard[1] has summarized the historical development of plate theory and described the early tests to investigate the collapse behaviour of reinforced concrete slabs by Bach and Graf[2] in 1911. A comprehensive works on the theory of plates and shells by Timoshenko and Woinowsky - Krieger[3] now forms the standard reference for most investigators.

Although the elastic behaviour of plate bending has retained the interest of many present day engineers and researchers, the collapse behaviour has also attracted many workers, notably Johansen in Denmark and Prager with his team in the U.S.A. In England, Wood[4] has given an excellent account of the plastic theories for the collapse analyses of reinforced concrete slabs and metal plates. This text has been well received and has stimulated much of the current research in this field.

From the existing literature it would appear that the missing link in the complete knowledge of plate bending behaviour is the absence of any unified theory that encompasses the existing elastic and limit theories and allows complete elastic-plastic analysis. There have been few attempts to do this but two recent approaches are outlined in section 1.5.

1.2 The Yield Line Method of Analysis for Reinforced Concrete Slabs

This method of analysis predicts a possible collapse load for reinforced concrete slabs and was pioneered by Johansen[5,6,7] in 1943. It has been accepted by many design code committees principally in Europe. The Comité Européen du Béton has organized extensive research in many laboratories and has published a number of bulletins[8,9,10] on the subject.

The theory is based on energy and kinematic principles and leads to an upper bound on the collapse load. That is, the true collapse load is either equal to or less than that calculated by yield line analysis and therefore essentially unsafe predictions are made. The collapse loads are determined by equating the external work done by applied loads to that dissipated internally along the yield lines of an assumed collapse mechanism. This leaves much choice to the analyst in selecting the collapse configuration. Although there are certain well defined procedures to aid in the proper selection, one is never sure that the lowest possible collapse load has been determined even after analysing many possible mechanism patterns.

The greatest drawback of the method is the impossibility of predicting what internal generalized stress states exist within the portions of the slab bounded by supports and/or yield lines.

A further limitation is the absence from the analyses of the effects of membrane action on the collapse load. This has lead to very conservative estimates of the collapse load for slabs in which in-plane forces are significant. Recently, an upper bound on the collapse load for a simply supported square slab carrying uniformly distributed load was developed by Kemp[11]. The increase in collapse

load was found to be as much as 20% greater than that determined by excluding membrane action.

Even with its limitations, the yield line method has and continues to stimulate interest in the limit behaviour of concrete slabs. Its greatest advantage is its simplicity of application and even though theoretically it leads to an upper bound on the collapse load, it seldom overestimates the experimental collapse load. This is primarily why it has been so well accepted.

For practical application of the yield line method excellent texts have been produced by Jones[12] and Wood and Jones[13].

1.3 Limit Analysis of Metal Plates

The application of limit analysis theory to perfectly plastic (ductile) metals in plate bending was mainly due to Prager and his team at Brown University[14], U.S.A. The theorems of limit analysis were introduced by Drucker, Greenberg and Prager[15]. From these theorems the unique collapse load can be defined. A uniqueness theorem was first established by Hill[16] for regular yield loci (no flats nor corners). Corollaries of this theorem were extended by Haythornthwaite and Shield[17] to include singular yield loci. For plates, unique collapse loads are produced whenever the static and kinematic theorems are satisfied and the collapse loads given by lower bound and upper bound procedures are identical.

From the existing limit solutions of metal plates it is clear that researchers have concentrated on producing unique solutions and have not considered upper bounds of much importance without accompanying lower bounds to help establish the validity of the collapse load. The only unique solutions that exist are for circular plates. Radial

symmetry of plate geometry, loading and boundary conditions permits the formulation of unique solutions with little difficulty[18].

Prager[19] and Hodge[20] have presented upper and lower bound solutions for simply supported square plates carrying uniformly distributed loads. More recently Shull and Hu[21] presented upper and lower bounds for rectangular metal plates based on the Tresca yield criterion. Again, no unique solutions were obtained since the difference in the upper and lower bounds for the collapse load varied from 10% to 33⅓% for various aspect ratios.

Although the correct collapse load will be given by unique solutions, the question will always remain as to how realistic the statical stress fields are as determined by limit analysis.

1.4 Existing Unique Solutions for Non-Circular Slabs

The object of this section is to present existing unique solutions for non-circular slabs to illustrate how few solutions exist and the similarity between them. Unfortunately only slab solutions exist based on a square yield criterion. No metal plate unique solutions using Tresca or von Mises yield criteria exist to date.

Wood[4] has presented a number of unique solutions for slabs. Those for non-circular slabs are summarized here without derivation. The general geometrical arrangement common to these solutions is given in Figure 1.1.

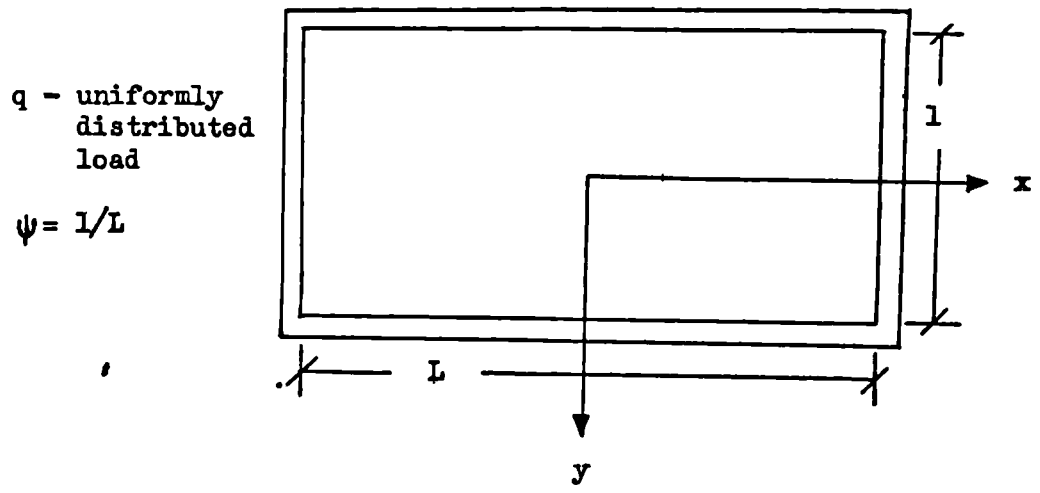

Non-Circular Slabs for Unique Solutions

Figure 1.1

(1) Simply supported square slab carrying uniformly distributed load. (Prager)

This solution was produced by Prager. The lower bound is derived from the radial generalized stress pattern for a fixed circular plate.

(i) Collapse load from a kinematically admissible velocity field (Upper bound).

$$q = 24M/L^2 \qquad 1.1$$

(ii) Statically admissible generalized stress field.

$$Mx = q(L-2x)(L+2x)/24 \qquad 1.2$$

$$My = q(L-2y)(L+2y)/24 \qquad 1.3$$

$$Mxy = qxy/6 \qquad 1.4$$

(iii) Vertical edge reaction acting upwards on slab.

$$V = qL/3 \qquad 1.5$$

(iv) Collapse load from a statically admissible generalized stress field (lower bound).

$$q = 24M/L^2 \qquad 1.6$$

(2) Simply supported square slab carrying uniformly distributed load. (Vallance)

(i) Upper bound on collapse load.

$$q = 24M/L^2 \qquad 1.7$$

(ii) Statically admissible generalized stress field.

$$Mx = My = \frac{q(L-2x)(L+2x)(L-2y)(L+2y)}{24\sqrt{(L-\sqrt{2}x)(L+\sqrt{2}x)(L-\sqrt{2}y)(L+\sqrt{2}y)}} \qquad 1.8$$

$$M_{xy} = q_{xy}\left\{\frac{1+1}{2}\frac{1}{24}\left[\frac{\left(\frac{4x^2}{L^2}-3\right)\sqrt{1-\frac{2y^2}{L^2}}}{\left(1-\frac{2x^2}{L^2}\right)^{3/2}}+\frac{\left(\frac{4y^2}{L^2}-3\right)\sqrt{1-\frac{2x^2}{L^2}}}{\left(1-\frac{2y^2}{L^2}\right)^{3/2}}\right]\right\} \quad 1.9$$

(iii) Vertical edge reaction acting upwards on the slab.

$$(\text{at } x' = L/2) \qquad V = \tfrac{1}{2}qL\left[1-\frac{1}{\left(2-\frac{4y^2}{L^2}\right)^{3/2}}\right] \quad 1.10$$

(iv) Lower bound on collapse load.

$$q = 24M/L^2 \quad 1.11$$

(3) Square slabs supported by edge beams with slab carrying uniformly distributed load. (Wood)

For this solution the key parameter that determines the collapse mode is

$$\gamma_p = \frac{M_b}{ML} \quad 1.12$$

Wood[4,22] has shown that the composite collapse mode of beams and slab occurs for $\gamma_p \leq 1$. For $\gamma_p > 1$ only the slab collapses by a diagonal mode. In the following the range of γ_p is restricted to

$$0 \leq \gamma_p \leq 1 \quad 1.13$$

(i) Upper bound on collapse load.

$$q = 8M(1+2\gamma_p)/L^2 \qquad 1.14$$

(ii) Statically admissible generalized stress field.

$$Mx = q(L-2x)(L+2x)/8(1+2\gamma_p) \qquad 1.15$$

$$My = q(L-2y)(L+2y)/8(1+2\gamma_p) \qquad 1.16$$

$$Mxy = qxy(2\gamma_p-1)/2(2\gamma_p+1) \qquad 1.17$$

(iii) Vertical edge reaction acting upwards on slab.

$$(\text{at } x = L/2) \quad V = qL\gamma_p/(1+2\gamma_p) \qquad 1.18$$

(iv) Lower bound on collapse load.

$$q = 8M(1+2\gamma_p)/L^2 \qquad 1.19$$

(4) Rectangular slabs simply supported carrying uniformly distributed load. (Wood)

This solution is not strictly unique except for aspect ratios ($\psi = l/L$) of unity and infinity. But the difference between the upper

and lower bounds on the collapse load is within $1\frac{1}{2}\%$.

(i) Upper bound on collapse load.

$$q = 24M/\psi^2L^2(\sqrt{3+\psi^2}-\psi)^2 \qquad 1.20$$

(ii) Statically admissible generalized stress field.

$$Mx = q\psi^2(L-2x)(L+2x)/8(1+\psi+\psi^2) \qquad 1.21$$

$$My = q\psi^2(L-2y)(L+2y)/8(1+\psi+\psi^2) \qquad 1.22$$

$$Mxy = q\psi xy/2(1+\psi+\psi^2) \qquad 1.23$$

(iii) Vertical edge reaction acting upwards on slab.

$$(\text{at } x = \frac{L}{2} \text{ or } \frac{1}{2}) \qquad V = \frac{q\psi L}{2}\left(1 - \frac{1}{1+\frac{1}{\psi}+\frac{1}{\psi^2}}\right) \qquad 1.24$$

(iv) Lower bound on collapse load.

$$q = 8M(1+\psi+\psi^2)/\psi^2L^2 \qquad 1.25$$

(5) Rectangular slabs supported by edge beams with slab carrying uniformly distributed load. (Wood)

The most general case for these slabs occurs when two different limiting values M and m exist for the slab in the directions parallel to the long and short beams respectively. If B refers to the long beams and b the short beams then

$$\gamma_b = \frac{M_b}{ML} \quad \text{and} \quad \gamma_B = \frac{M_B}{Ml} \qquad 1.26$$

(a) Case I - Long beams collapse with slab.

(i) Upper bound on collapse load.

$$q = 8M(1+2\gamma_B)/L^2 \qquad 1.27$$

(ii) Statically admissible generalized stress field.

$$Mx = q(L-2x)(L+2x)/8(1+2\gamma_B) \qquad 1.28$$

$$My = m(\psi - \frac{2y}{L})(\psi + \frac{2y}{L})/\psi^2 \qquad 1.29$$

$$Mxy = \frac{qxy}{2}(1 - \frac{1}{1+2\gamma_B}) - \frac{4mxy}{\psi^2 L^2} \qquad 1.30$$

(iii) Vertical edge reaction acting upwards on slab.

$$(\text{at } y = \frac{l}{2}) \qquad V = \frac{qL}{2}(1 - \frac{1}{1+2\gamma_B}) \qquad 1.31$$

(iv) Lower bound on collapse load.

$$q = 8M(1+2\gamma_B)/L^2 \qquad 1.32$$

(v) Additional requirements.

$$2\gamma_B \leq \frac{1+\frac{m}{M}}{\psi}\frac{1}{\psi 2} \qquad 1.33$$

(b) Case II - Collapse load to be equal to or less than the load for independent collapse of slab.

$$2\gamma_B \leq \frac{1+1}{\psi\ \psi^2} \qquad 1.34$$

(c) Case III - Slab only collapses.

$$2\gamma_B \geq \frac{1+1}{\psi\ \psi^2} \qquad 1.35$$

Very recently Massonnet[23] presented a number of unique solutions for reinforced concrete slabs. He builds these solutions using the fundamental equations governing complete solutions of rigid plastic slabs formulated by Hopkins. Massonnet states that for the five differential equations presented, no general method of integration is known and that this is why very few complete solutions exist.

Massonnet develops a theorem for producing a family of unique solutions by combining linearly two known complete solutions for the same problem. As an example, he selected the solutions for the square simply supported slabs of groups (1) and (2) above. He shows that there are a number of unique solutions within the family developed. The resulting generalized stress field for any one member of the family is governed by the amount selected from each of the two initial solutions. However interesting these results are, it remains to be shown that these families of solutions are other than of academic interest. Undoubtedly there is only one true solution to any one problem in reality and it is this solution we should strive to find.

The importance of lower bound and unique solutions for practical design cannot be assessed until the generalized stress fields are investigated experimentally. There does not appear to have been any attempts made to study lower bound solutions by experiment. For concrete slabs, previous experiments have been confined to the overall collapse behaviour and checking the validity of upper bounds on the collapse load.

A lower bound approach to slab design was introduced in 1960 by Hillerborg[24]. In this method the slab is divided into strips in two

orthogonal directions. Discontinuous moment fields obtained by uni-directional strip action are employed. It is a simple approach and results in economical placing of reinforcement. This method has been given a good deal of attention lately especially by Wood and his team at the Building Research Station.

1.5 Numerical Methods for Elastic-Plastic Slab Analysis

(a) The method proposed by Levi and applied by Callari.

This method was first proposed by Levi[25] in 1950. The general approach was outlined by Callari[26] and later applied by him[27].

The slab is divided into a number of squares by mesh lines. The method of finite differences is used to represent the Lagrange plate equation at each mesh point. To represent the effects of inelastic behaviour, plastic rotations are introduced at mesh points representing plastic curvatures occuring over one mesh length. The type of plastic distorsion imposed was first studied by Somigliana[28] in 1908. It is assumed that by imposing plastic rotations along the axes of the mesh, the effect of rotations at some other orientation can be represented. In the special case where the maximum generalized stresses occur at 45 degrees to the mesh directions, two equal rotations are imposed along the mesh lines. It follows, necessarily, that at some other point where the actual rotation is inclinded at other than 45 degrees, unequal component effects should be used.

The slab analysed was a simply supported square carrying four vertical point loads at the one quarter points along the diagonals. The maximum generalized stresses producing inelastic behaviour were directed along the mesh lines since Callari assumed that the twisting generalized stress vanished whenever cracking of concrete occured.

To determine the various levels of inelastic behaviour at a mesh point, a generalized stress-plastic rotation diagram was used. This had a trilinear variation for a cracking analysis and bilinear for studying the collapse behaviour. Perfect plasticity was not allowed in any of the cases. Two types of solutions were produced for the slab presented, one for cracking only and a second for the bilinear elastic-plastic collapse.

To determine the generalized stress field at any stage of external loading and internal plastic behaviour, the Lagrange equation written in terms of total curvature (elastic plus plastic) was solved at each mesh point. By suppressing the plastic rotation (plastic curvature multiplied by one mesh length) at all mesh points except one, the influence of a unit rotation on the vertical displacements was determined. This was then repeated for each plastic point in turn requiring a solution to the total set of Lagrangian finite difference equations. From the influence of unit rotations, the resulting increments of generalized stresses Mx, My and Mxy could be determined at all points. This procedure then produced generalized stress influence coefficients to be used in the elastic-plastic analysis. These multipliers were set aside and only used when the particular mesh points satisfied the inelastic requirements as presented by the generalized stress-rotation diagrams.

From the purely elastic response of the slab, the effect of applied loading on the generalized stresses was solved once, at the outset of the analysis. During the inelastic response the elastic effects were always available between any two load stages. The end result required for any application of load was the final generalized stresses Mx and

My at each mesh point. These were determined by knowledge of the initial values (at the end of the last load stage) causing inelasticity, the increments of the elastic generalized stresses and the influence of the increase in plastic rotations at affected points. The influence of the plastic rotations was determined from the generalized stress-rotation diagram and the previously computed influence coefficients. The total number of characteristic equations solved was equal to the number of mesh points that became inelastic. In this manner a history of cracking or a build up of a collapse behaviour was traced.

The general approach to this problem is quite good. Nevertheless, there are a number of points worth mentioning in connection with the method and the particular results that Callari obtained.

The assumption that the true plastic rotation can be represented by independent rotations in component directions without knowing the magnitude and direction of the true rotations requires some justification. For the particular solution presented, the true rotations were determined since Callari assumed that the twisting generalized stresses vanish once the concrete cracks. If this were not the case, the principal directions would have to be determined and in some manner two component rotations introduced along the mesh lines.

The so-called "characteristic equations" that are used to compute the final generalized stresses would have to be written in terms of principal values. If the orientations of the principal planes changed during loading the characteristic equations would have to be constantly corrected. This severely complicates the procedure and it is likely that principal generalized stresses could not be dealt with using the plastic distorsions presented.

From the computer analyses the first solution (cracking only) gave cracking loads in excess of experimental values in all cases. The cracking loads determined by any analytical means will probably never give an accurate picture since there are many factors which govern crack formation. The higher values might suggest that the actual maximum generalized stresses are greater than those produced analytically. The question of load application and internal stress concentrations mentioned by Callari are certainly local governing factors.

The largest error was found in the apparent collapse load in the second solution. Strictly speaking there was no collapse load since perfectly plastic behaviour was not allowed. The computed collapse load, defined when the displacements increase rapidly with a small increase in load, was 13% above the experimental value and 24% above the yield-line upper bound load. These results seem too high and throw doubt on the analytical procedures. The slab in question will experience tensile membrane action within the square bounded by the concentrated loads as the Johansen collapse load is exceeded. Experimentally the slab collapsed at 10% to 12% above the yield line value. Since membrane behaviour was not included in the analysis, it seems unreasonable to expect higher loads analytically than those given experimentally.

Callari is to be congratulated on attempting a solution to a most complex problem. However, the one slab example given does not establish its validity as a sound elastic-plastic approach.

(b) The method proposed by Massonnet and applied by Cornelis.

This method proposed by Massonnet[29] is very similar in principle to that just described. The fundamental difference is the way in which

plastic distorsions are introduced. In the Levi method plastic rotations were imposed in vectoral form. Massonnet introduces tensoral components of total curvature rates and adopts the incremental type of stress-strain law from the general theory of plasticity.

Although a concrete slab problem is presented by Cornelis[30], the generality of the method allows the solution of metal plate problems by adopting the appropriate yield criterion and associated flow rule. In fact, Massonnet describes the method with reference to the von Mises criterion for ductile metals.

The analysis begins by solving a set of Lagrangian equilibrium equations in finite difference form for a purely elastic response to applied load. From the resulting displacements, the generalized stresses Mx, My and Mxy are computed at each mesh point. The principal generalized stresses are computed at all mesh points and scaled until only one point becomes plastic. This constitutes the end of the elastic response. This procedure establishes the starting point for the elastic-plastic analysis. Next the Lagrangian equations are modified to include plastic curvatures in the x, y and xy directions. The resulting expressions that include plastic curvature appear as fictitious load terms. The modified Lagrangian or "characteristic equation" is written in finite difference form for each mesh point. With no applied load on the plate these equations are solved a number of times to determine the effects of unit plastic distorsions imposed one at a time at each point for each of the x, y and xy directions. From each solution of the "characteristic equations" the displacements allow a set of generalized stress influence coefficients to be determined for each

point affected by the unit distorsions. These coefficients are stored for later use.

The generalized stresses obtained at the end of the elastic stage are scaled up by a small load factor. The principal generalized stresses are computed and those points where the yield criterion is violated are noted. The next step is to establish what actual plastic distorsions must be introduced to maintain the yield requirements under this small increase in load. This is done by writing the yield function, at each point that is plastic, in terms of the generalized stresses produced by the scale up of preceding values, the influence of distorsions at other points and the influence of the unknown distorsion at the current point. This results in a number of yield equations equal to the number of existing plastic points. These equations are solved for the unknown distorsions, one at each plastic point. With these distorsions and the influence coefficients previously determined, the increases of generalized stresses are found. The principal generalized stresses are again computed to ensure that the yield criterion is not violated at any point. If more points appear plastic, the yield equations are solved again, now including additional equations to account for the new plastic points. This cycle is repeated within this one load increment until no point violates the yield criterion.

It should be mentioned here that throughout any one load increment, the directions of principal planes at each point are assumed constant. Since this is not strictly true the yield equations mentioned above are only approximations to the actual ones. Therefore, at the end of any one load stage these angles should be recomputed and the principal generalized stresses recalculated to test the degree of approximation. If the approximation is not within acceptable limits, the new angles

are substituted into the appropriate yield equations and the distorsions determined again. If acceptable, then an additional load increment is added and the calculation of distorsions etc. repeated. If after applying an additional load increment, no further points become plastic and the yield condition approximations are acceptable, then an additional load increment is applied and the procedure repeated. Collapse of the plate is defined when the displacements resulting from plastic distorsions increase rapidly.

This method has two definite advantages over a finite element approach. The number of Lagrangian or equilibrium equations is equal to the number of mesh points and consequently the accuracy obtained should be good even for a large number of points. Furthermore, the size of computer program required will most likely be sufficiently small to enable compilation on medium sized computers. These two features must be considered for elastic-plastic plate analyses.

The analysis example presented by Cornelis is for a rectangular slab simply supported on four boundaries. The square yield criterion for isotropically reinforced concrete with elastic perfectly plastic characteristics was assumed. Very good accuracy was obtained for the collapse load resulting in a 2% increase over the yield line upper bound value. Collapse was defined by a rapid increase in vertical displacements.

The overestimate of collapse load is to be expected since the yield function was only approximately satisfied at plastic mesh points off lines of symmetry. The actual principal generalized stresses are greater than those assumed. Consequently an underestimate of internal

energy dissipation resulted in more external work required for collapse. The equation selected to represent the yield function (see section 3.4e) is a poor choice for elastic-plastic plate analysis. Using this equation and assuming that the orientation of principal planes remains constant during one load increment results in an approximation to the true limiting yield value. This approximation is a function of the actual change in orientation and the magnitude of the angle assumed to be constant. This is further discussed in detail in section 3.4e where it is shown that a much better approximation can be made. The yield function used by Cornelis was satisfactory in his example since the plastic zones were close to a line of symmetry where little change in orientation is to be expected.

There does not appear to have been a definite collapse mechanism from the results presented. The plastic points are located close to and along the central axis of symmetry but do not extend the plastic zone to the supports in any direction.

There are two particular aspects of Levi's and Massonnet's methods which could limit their usefulness. The first is the problem of using finite difference techniques to establish the plastic distorsion influence coefficients. The accuracy of the difference technique for small distorsions poses the question as to whether the effect of imposing unit distorsions will produce changes of vertical displacements of the proper order. The mesh size employed and the choice of difference approximations[31] becomes much more important for determining the influence coefficients. These facts alone might lead to substantial error since vertical displacements may not in general be very sensitive to localized plastic behaviour.

The second is the question of introducing other types of structural members, such as edge beams on plates. Just what the composite yield behaviour would be and how it could be incorporated is not clear. Unless such support conditions can be dealt with, these methods have limited application. Perhaps these questions should be investigated more thoroughly before attempts are made to include other behaviour such as membrane action as was mentioned by Massonnet.

On the whole, Massonnet's approach is based on sound principles of structural mechanics and plastic theory.

(c) The method proposed by Parkhill.

In this method an elastic bending analysis using finite differences is performed on the "rigid" portions of the slab that form a collapse mechanism and leads to a lower bound generalized stress field for the assumed mechanism. Since the generalized stress field is statically admissible and nowhere exceeds the yield criterion, and is established in accordance with a kinematically admissible velocity field, the solution contains the required uniqueness properties of a complete limit analysis solution.

Parkhill[32] first establishes a possible collapse mechanism by applying yield line analysis. Then the "rigid" segments of the slab are analysed separately by purely elastic considerations using finite differences. The boundary conditions imposed on each segment are assumed to represent those existing in the original slab. Plastic generalized stresses are applied along yield lines and displacements are allowed in accordance with those that exist in the slab. The elastic analysis gives the internal stress fields for the segments.

If after the segments are analysed it is found that the yield criterion is violated within the boundary of the element then an incorrect collapse mechanism has been selected and a different mechanism must be used.

Although Parkhill presents a solution to a square simply supported slab carrying a uniformly distributed load, he implies that other shapes can also be analysed.

At first sight this method looks inviting since for many practical slabs the mechanism pattern is fairly well known or could be determined experimentally. However, Kemp[33] has explained why this method will not work in all but the simplest symmetrical cases of which the one presented is an example. The difficulties arise whenever the segments of slab adjacent to a yield line are non-symmetrical. Of the three quantities (normal and twisting generalized stresses and vertical shear force) on the yield line, only two may be specified and made continuous across the yield line. This problem occurs in classical plate flexure where not more than two boundary conditions may be specified. Therefore, the solutions will not necessarily satisfy both the equilibrium and yield conditions.

In the discussion of Parkhill's paper McNeice[34] presented a statically admissible generalized stress field for the square plate obtained from an elastic-plastic approach using finite elements. There was no similarity to Parkhill's results. It was implied by McNeice that the field presented by Parkhill seemed far from a realistic one.

Upon further consideration it does appear that Parkhill selected fictitious boundary points along the central axis and imposes two boundary conditions ($M_{xy} = 0$ and normal slope = 0). Unless the use of these fictitious points also maintains the absence of vertical

shear forces along this boundary, Parkhill's solution is incorrect. This may explain the equality of principal generalized stresses along the central axis. This would mean that the results are not even a valid lower bound field for the square slab but simply an elastic solution to a triangular slab with certain boundary and loading conditions. It has not been established that incorrect boundary procedures have been followed. However, Kemp's discussion clearly indicates the limitation of the Parkhill method.

CHAPTER 2 - THE FINITE ELEMENT METHOD

2.1 Origin

The finite element method was developed in the U.S.A. in 1956[35]. Since its beginning in the aircraft industry, the method has become very popular in many other fields. Principal researchers into the development and application of finite elements have been Clough[36] et al in U.S.A. and Zienkiewicz[37,38] et al in the United Kingdom. Many other authors have contributed to the popularity of the method. Almost all available literature on the procedures and use of finite elements is reported in two texts[36,38]. The latest text[38] also refers to many of the relevant papers presented at the Conference[39] on Matrix Methods in Structural Mechanics held in the U.S.A.

2.2 The Philosophy of the Finite Element Method

The finite element method is essentially a generalization to three dimensions of the classical structural analyses of skeletal structures. The basic concept of the method is not new. The structure when analysed consists of a finite number of elements connected to one another at nodal points. The structure is a mathematical assembly of physical elements. There is no approximation required in the mathematical procedures, only in the choice and physical assembly of the elements. This is the basic difference between the finite element and finite difference methods. The finite difference method gives an approximate mathematical solution to the exact continuum whereas the finite element method gives an exact mathematical solution to an approximate continuum.

By dividing the continuum into elements of various sizes and shapes, all material properties of the original system can be retained within the individual elements. This capacity of the method to cope with

arbitrary material properties is a principal attribute of the method. Of equal importance, is the facility to deal with cutouts, irregularly shaped boundaries and any type of applied loading.

The three basic steps in any finite element analysis are the structural idealization or subdivision into elements, the derivation of individual element properties and the assembly of elements into a physical structure. Sound judgement is required in subdividing the structure. If boundary stresses are required finer divisions should be used along such boundaries. The number of different shaped elements should be kept to a minimum. This will reduce the amount of initial computation of element stiffness characteristics.

The element stiffness properties describe the nodal force - displacement response of the element.. These properties are the governing factors in assessing the validity of the discretization. It is this second basic step that has been investigated the most in recent years. The primary concern is to establish a response function that will describe the element behaviour under various types of traction.

The final step is the assembly of the elements into a substitute structure. This is done using the well known matrix structural methods, satisfying equilibrium of nodal forces and compatibility of corresponding displacements.

Either of the two approaches to matrix analysis (force or displacement approach) can be used in the finite element formulation. The development of the force method has been traced by Argyris[40]. A summary of both and a comparison have been made by Gallagher[41]. The displacement approach has been selected for the present study.

2.3 Finite Elements for Plate Bending

Although the finite element method is by no means restricted to structural problems, the remaining discussion will be confined to plate bending analysis since this aspect of the method is of primary interest in this thesis. An up-to-date account of the method as applied to plate bending problems has been given by Zienkiewicz[38].

The most difficult item in a bending analysis is the selection of a function that will ensure displacement continuity between elements. Functions which fail to maintain normal slope continuity have been labelled "non-conforming" by Zienkiewicz. The complexity of the function will depend on the number of degrees of displacement freedom allowed at the nodes of the element. For example, for the present study a cubic polynomial with twelve coefficients was chosen to represent the displacement response of a rectangular element with three degrees of freedom at each of four corner nodes. This function was adopted by Zienkiewicz and Cheung[42] and is a non-conforming type since it does not ensure that the normal slopes to element boundaries are continuous across the boundaries. Vertical displacement and slopes tengential to boundaries are maintained continuous. All three displacements are continuous at nodes and it is only at these points that internal stress fields and other quantities are computed.

The cubic polynomial mentioned here is one of the simplest that have been developed for plate bending problems. It has resulted in extremely good accuracy where rectangular elements were used. Attempts[36,37] to reduce this function to nine coefficients for triangular elements have not met with much success. Unfortunately, rectangular elements have

limited use since they are not suitable for irregular boundaries.

Zienkiewicz[38] has developed shape functions for triangular elements by employing a method of area coordinates. He obtains better results than previous attempts at using triangular elements but still not as good as the non-conforming rectangular elements. In an attempt to produce better shape functions Bazeley[43] et al developed conforming functions for triangular elements by applying corrective functions to non-conforming shaped functions and thereby maintaining continuous normal slope. Similar techniques were also used by Clough and Tocher[44]. From the results presented the non-conforming triangular element solutions gave better accuracy especially for coarse subdivision. Corrective functions do not seem to be the immediate answer for triangular elements in bending.

A novel approach to triangular elements has been developed recently by Herrmann[45]. He introduces a functional that permits both vertical displacement and generalized stress (w, Mx, My and Mxy) variation at element nodes. These quantities become the basic unknowns at the nodes. By allowing only first order derivatives in the functional, continuity of vertical displacement and generalized stresses is maintained along and across the element boundaries. The results presented show excellent agreement with exact solutions.

The question of normal slope continuity for rectangular elements based on a displacement function has been successfully solved by Hansteen[46]. He introduces four degrees of displacement freedom (w, θx, θy, θxy) at each of the four nodes. Here the normal slope is continuous across element boundaries and the results presented are

excellent even for a coarse subdivision. These latter two analyses are good examples of the diversified approaches currently being investigated.

The application of finite elements to bending problems has just begun. With the current interest in this application it will soon be possible to solve many complex and very interesting plate problems that to date have defied analysis. Even though many questions remain to be answered in applying the method to purely elastic problems, there is evidence of application being made to non-linear elastic and elastic-plastic problems.

2.4 Existing Elastic-Plastic Analyses Using Finite Elements

Available literature on elastic-plastic analyses using finite elements is confined to plane stress problems. Argyris[47] has presented the fundamentals involved for elastic-plastic analyses of three dimensional media. He gives solutions to plane stress plate problems by employing a step-by-step formulation of non-linear plastic behaviour in a series of linear steps. He describes the procedures in a collapse analysis by adopting either a force or displacement approach. He compares these approaches and concludes that the force method is easier to program by computer and is more suitable for problems were the degree of redundancy is much smaller than the number of structural elements. The redundancies must be chosen with care if the solution is not to be sensitive to round off error. He further states that the displacement method is more suitable for structures with many redundancies and that once the program is written, the problem can be solved by comparatively unskilled operators.

In the delta wing problem presented, the force method was used to determine the lower bound on the collapse load. The displacement method was used to give an upper bound on the load by establishing a kinematically admissible velocity field (mechanism) by considering a combination of possible mechanisms. No correct collapse load by the upper bound approach was determined. This method of applying finite elements to a three dimensional problem only gives a limit solution with no information about the behaviour before collapse. Argyris also applied the element method in plane stress to flat plates with a central hole. Here a complete history of inelastic behaviour was recorded.

Another example of plane stress elastic-plastic analysis has been given by Pope[48]. A rectangular panel with uniform edge members is divided into triangular elements and stressed in two orthogonal directions. The von Mises yield criterion is used with both elastic-perfectly plastic and elastic linear strain hardening properties. Earlier attempts at elastic-plastic plane stress analysis have been reported by Clough[36].

One of the latest applications of the method to plane stress problems has been made by Ngo and Scordelis[49]. Here the application is to reinforced concrete beams. The authors have developed a "linkage element" comprising linear springs in two orthogonal directions to simulate the bond link between concrete and the reinforcing steel. They investigate single reinforced concrete beams under two point loading by imposing various crack formations of both a vertical and diagonal nature. Steel and concrete stresses are computed along with bond forces for each crack pattern selected.

This quite novel approach to solving a very complex problem is

a further example of the importance of the finite element method.

Although only a few problems have been briefly mentioned above to account for some of the areas in which the finite element method has been applied to elastic-plastic problems, it is by no means a complete resumé of those that have been tackled.

However, there does not appear to have been any attempts made to analyse elastic-plastic plate bending problems. For this reason the present study was begun in 1965 with the hope that successful use of the method could be made to analyse simple plate problems.

CHAPTER 3 - THEORETICAL DEVELOPMENT

3.1 General Discussion of the Method

The procedures developed for the present study are presented in detail in this chapter. The following discussion is confined to the general aspects of these procedures and their method of application.

The theory of small deflections in plate bending is adopted with all its assumptions assumed to hold throughout the elastic-plastic bending behaviour. The effects of membrane straining are excluded inorder not to complicate the investigation. Plates and slabs that deform into developable surfaces under transverse loading are exempt from in-plane strains of sufficient magnitude to affect basic bending behaviour. This is particularly true for plates of so-called medium thickness. Most concrete slabs and certain metal plate applications are contained within this category.

Only square plates are analysed by the following procedures. Symmetrical loading and boundary conditions are selected to reduce the size of the computer program required.

To represent the plate in mathematical terms, the concept of finite elements is applied. The plate is divided into square elements each joined at their corners to adjacent elements. For each element a third order polynomial displacement function is used. This function ensures continuity of vertical displacement everywhere on the boundaries of adjacent elements. Continuity of slope at junctions or nodes is also maintained but normal slopes across element boundaries between any two nodes of an element are not necessarily continuous. However, at the nodes, equilibrium of forces and compatibility of displacement are maintained in the elastic portion of the analysis. Since the elements

are considered to be joined only at their corners, the bending and twisting internal generalized stresses are only approximations to the actual values.

With this displacement method of finite elements, the basic unknowns are the nodal displacements. Through proper force-displacement relationships the stiffness matrices for each element are derived. In addition, the elastic bending theory provides the necessary internal generalized stress relationships and when combined with the assumed displacement function the internal generalized stress matrices are established. By applying the usual procedures of structural stiffness matrix methods, the plate continuum can be assembled once the element stiffness matrices are known.

The effect of edge beams is included in this study. The procedures outlined above apply for beam elements as well. In the inelastic behaviour of plates with edge beams the question of yield behaviour at nodes where plate and beam elements join is dealt with separately in this chapter. For the present discussion the edge beam effects will be omitted, although certain aspects of the following also apply to the beam elements.

Once the plate structure is assembled the resulting nodal force-displacement relationships form a set of simultaneous linear equations. Since the nodal forces must be in equilibrium with any applied loading, the matrix of nodal forces can be replaced by a matrix of applied loads. Solution of these equations produces the nodal displacements for the entire structure. From the displacements, the internal generalized stress state is determined at each node.

Applied loading can consist of point loads, distributed loads,

bending moments or any combination of these. In all cases, the loads are monotonically increasing with no reversal possible for an elastic-plastic analysis. The load matrices required for the present study are developed in Appendix I.

Wherever the principal generalized stresses satisfy the yield criterion, plastic behaviour results. The resulting generalized strain rates are curvature rates. The concept of plastic rotations is introduced by allowing discontinuities in slope at the nodes and are effectively curvature rates over an infinitesmal length of the plate.

For each principal generalized stress that satisfies the yield criterion, one additional nodal displacement (plastic rotation) is introduced. Upon further increase of load these principal generalized stresses must be maintained at the limiting generalized stress value. This is accomplished by introducing the equation for the principal generalized stress into the force-displacement relationships for the elements at the plastic nodes. When the elements are joined to represent the plate structure this equation enters the total set of simultaneous linear equations. These additional equations allow for the solution of the plastic rotations. In this way the total stiffness of the structure is reduced as more nodes become plastic. The final collapse of the plate occurs when no solution to the equations is possible. Mathematically this is implied when the stiffness matrix of the plate becomes singular.

Inorder to trace the spread of plasticity from node to node the behaviour is assumed to be a linear function of the displacements. This is certainly true in the elastic response but not in the plastic. However, by adopting an incremental linear approach for the applied

load-internal generalized stress behaviour it is possible to obtain approximate elastic-plastic behaviour with sufficient accuracy to warrant a linear analysis.

This linear method can be applied in different ways depending on the accuracy desired. One approach is to apply small increments of load in the order of .1% of the estimated collapse load. Once the increment is applied the generalized stress state is computed at all nodes. If none of the nodes becomes plastic, further small increments of the same order are applied consecutively until at least one additional node is plastic. If the yield criterion is violated at one or more nodes, the generalized stresses (Mx, My and Mxy) are scaled linearly within this last increment until only one additional node is plastic.

A second approach which results in slightly less accuracy is to apply load sufficiently large to ensure that all nodes become plastic. That is, a load well above the estimated collapse load. The generalized stresses are scaled down until only one node becomes plastic within this increment. The same load is again applied and the scaling procedure repeated until a further node becomes plastic and so on.

For additional accuracy in either of the two methods, an iterative procedure can be adopted within each load increment. However, this would result in much more computational time since each iteration would require the solution of the force-displacement equations.

For the present study the first method was selected initially but because it required more computer time than was available for any one solution, it had to be abandoned. The second method was therefore used.

The principal generalized stresses at plastic nodes off lines of

symmetry vary non-linearly with load and therefore the directions of the plastic generalized strain rates do not remain constant throughout subsequent applications of load. Since the components of the plastic rotations are required in the directions of the coordinate axes, the orientation of principal planes must be known throughout the analysis. By assuming a linear variation of principal generalized stresses in any one plastic load increment (that contained between two nodes becoming plastic) it is implied that the directions of the plastic generalized strain rates remain constant within this increment. These directions are computed at the beginning and end of each plastic load increment and if the changes in directions are within certain limits, the same directions can be assumed for the next applied load increment. If this change is not acceptable for one or more of these nodes and the yield criterion is severely violated, then these directions are recalculated for use for the next application of load. In this way, the yield function is linearized during each applied load increment and is adjusted if necessary after each plastic load increment to bring it closer to the actual non-linear variation.

Although this updating procedure can be used, it is not possible to determine the exact degree of approximation involved without applying an iterative procedure within applied load increments in addition to the above corrections.

On lines of symmetry the yield function varies linearly with displacements and the directions of the plastic generalized strain rates are constant throughout the elastic-plastic behaviour. Therefore the "true" inelastic behaviour is only determined in cases where all plastic nodes are located on lines of symmetry.

The word "true" applies here only in the sense of the mathematical means of representing the plate continuum. In the finite element method "true" takes on different meanings depending on the initial approximations made in the structural idealization.

For best results the continuum should be divided into a large number of elements. This is important in the elastic analysis but even more so in the elastic-plastic analysis. When there are many nodal points the resulting load increments between subsequent stages of plastic behaviour will be small and the linear approximation discussed above will be less restrictive on the yield behaviour.

It is conceivable that arguments could develop in favour of using elements with shapes different from those adopted in the present study. For example when the plate is divided physically into finite elements, it is difficult to visualize lines of plastic action (yield lines in concrete slab terminology) forming in directions other than along element boundaries. The use of square elements would mean that collapse mechanisms would be confined to rectangular patterns and therefore diagonal modes would not be permissible for a realistic solution. Such a simple physical thought is not as restrictive as one might think. It is true that element shape has an influence on the accuracy of the collapse load since kinematically only the nodes of the element contain the displacement discontinuities with the element still remaining continuous in displacement within its boundaries. However, it would appear from the results of the analyses presented that the effective reduction in the bending stiffness of an element with one or more plastic nodes is sufficient to allow the element to function as though it had a

plastic zone across or along some portion of its section. This fact is evident from the solution for a simply supported square plate carrying a uniformly distributed load in which a diagonal collapse mechanism forms. The collapse load was approximately two percent above that determined by limit analysis.

Therefore it seems unnecessary to use elements where boundaries are on the lines of plastic action. This is an important feature of the present proposal since the aim is to allow the plate to develop the collapse mechanism without imposing any initial conditions on the kinematics of the collapse mechanism or having to change the element shapes before a complete solution is obtained.

3.2 Small Deflection Theory of Plate Bending

(a) Assumptions

The classical theory of small deflections in plate bending is based on certain assumptions as to the deformation and straining characteristics of the middle surface of the plate. This theory is adopted for the present study and is assumed to be valid throughout the elastic-plastic analysis.

The assumptions normally used in this theory are as follows:

(1) The plate is considered to be medium-thick. That is, it is neither so thick in proportion to the span that vertical stresses must be considered, nor so thin that stretching and/or shrinking of the middle plane occurs when the plate is bent into a doubly-curved surface.

(2) The plate has uniform thickness and is composed of material of a homogeneous character. Consequently, the modulus of elasticity for horizontal stresses and the Poisson ratio for lateral contraction to

longitudinal elongation are the only two material constants necessary to specify the elastic properties of the plate.

(3) Vertical plane sections drawn through the plate before bending remain plane after bending. This implies that horizontal stresses vary linearly with depth at all cross-sections of the plate.

(4) Transverse bending deflections are considered small compared with the plate thickness.

(b) Plate Bending Formulae

The problem of determining the stresses and deflections of the plate is essentially a three dimensional problem in elasticity. By making the assumptions stated above the problem is reduced to two dimensions. Norris and Wilbur[50] have shown that these approximations can be justified by considering the order of magnitude of the six independent stress components that are involved. The equations for plate bending can be found in standard texts. The best account of their derivation is given by Timoshenko[3]. These equations are used here with the sign convention for internal bending given in Figure 3.1.

The term" generalized stresses" is used throughout this thesis to denote bending and twisting moments per unit length of the plate. This terminology was selected to be consistent with that used in discussing the yield criterion.

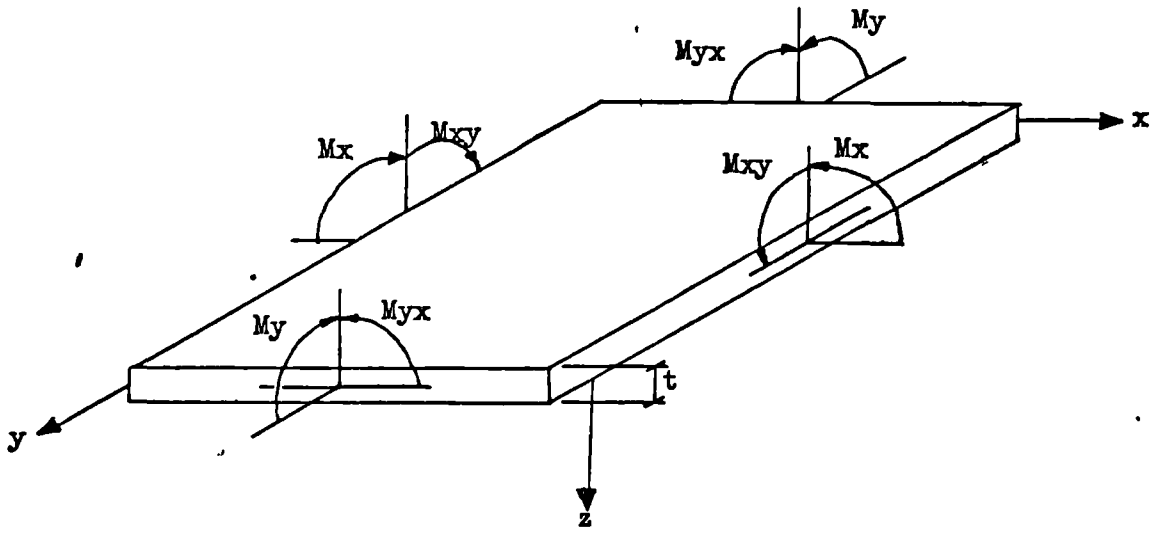

Generalized Stresses - Positive as Shown

Figure 3.1

The generalized stresses illustrated in Figure 3.1 for elastic anisotropic plate bending are determined from the following equations:

$$\begin{aligned} Mx &= -(Dx\ w,xx+D_1\ w,yy) \\ My &= -(Dy\ w,yy+D_1\ w,xx) \\ Mxy &= 2Dxy\ w,xy \end{aligned} \qquad 3.1$$

In equations 3.1, Dx, Dy, D_1, Dxy represent the bending stiffnesses of the plate. If ν is the Poisson ratio of lateral to longitudinal

strain, then for an isotropic and homogeneous plate $D_x = D_y = D$, $D_1 = \nu D$ and $D_{xy} = (1 - \nu)D/2$ where

$$D = \frac{Et^3}{12(1-\nu^2)} \qquad 3.2$$

E denotes the modulus of elasticity.

Although the conditions of isotropy and homogenity are assumed for the analyses presented, the generalized stress and stiffness matrices are derived here for anisotropic rectangular plate elements of constant thickness. These matrices are presented in explicit form in Appendix I.

3.3 The Finite Element Method in Elastic Plate Bending Analysis

(a) The Elastic Element Stiffness Matrix

The philosophy of the finite element method has been summarized in Chapter 2. In the present study the displacement approach is used in deriving the element force-displacement characteristics. Clough[36] has outlined the basic steps in determining the element stiffness properties Similar steps were adopted here in deriving the stiffness matrix for a rectangular element. These procedures are explained for a two dimensional element in bending.

(1) Select a displacement function that satisfies compatibility of displacement within the boundaries of the element and also maintains the best possible displacement compatibility along the boundary between adjacent elements.

This function takes a form dictated by the number of degrees of displacement freedom selected at the nodes of the element. If the node

displacements are given by the matrix

$$u_i = \begin{vmatrix} w_i \\ \theta x_i \\ \theta y_i \end{vmatrix} \qquad 3.3$$

for node i, then the matrix of element displacements for an element with nodes i,j,k and l is given by

$$u = \begin{vmatrix} u_i \\ u_j \\ u_k \\ u_l \end{vmatrix} \qquad 3.4$$

A typical rectangular plate element is shown in Figure 3.2. The sign convention for nodal displacements and external nodal forces is a "right-handed screw rule" convention.

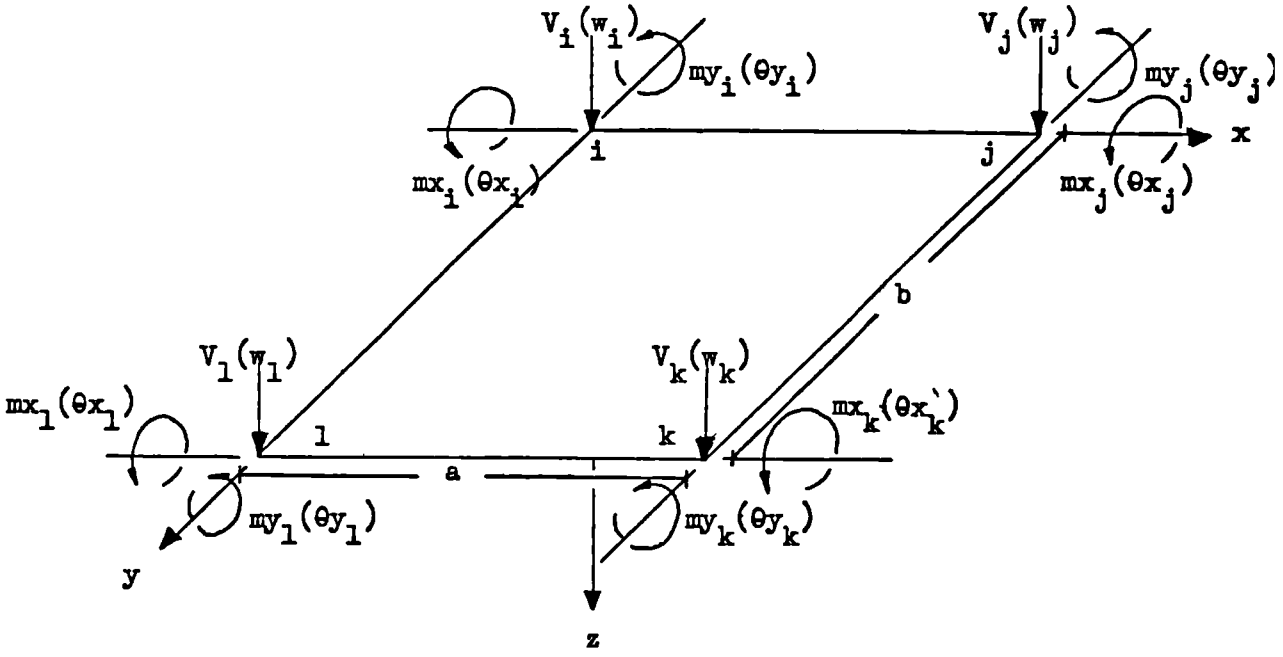

Typical Rectangular Plate Element
with Positive Nodal Forces and Corresponding Displacements

Figure 3.2

(2) Corresponding to the nodal displacements of equations 3.3 and 3.4, there exist nodal forces (one vertical force and two moments). These forces are a fictitious concept[38] and in some way represent the shear forces, bending and twisting moments per unit length distributed along the element boundaries. For node i these forces are

$$F_i = \begin{vmatrix} V_i \\ mx_i \\ my_i \end{vmatrix} \qquad 3.5$$

For the element there are twelve forces given by

$$F = \begin{vmatrix} F_i \\ F_j \\ F_k \\ F_l \end{vmatrix} \qquad 3.6$$

(3) The displacement function selected for the rectangular element is a cubic polynomial in x and y. This function is given by

$$w = a_1+a_2x+a_3y+a_4x^2+a_5xy+a_6y^2+a_7x^3+a_8x^2y+a_9xy^2+a_{10}y^3+a_{11}x^3y+a_{12}xy^3 \qquad 3.7$$

In accordance with the sign convention for nodal displacements illustrated in Figure 3.2, the displacement at node i (and all other nodes) becomes

$$u_i = \begin{vmatrix} w_i \\ \theta x_i \\ \theta y_i \end{vmatrix} = \begin{vmatrix} w \\ w,y \\ -w,x \end{vmatrix}_i = \left| u(x,y) \right|_i \left| a \right| \qquad 3.8$$

Similarly if all the element nodal displacements are written in terms of w and its first derivatives, these can be written in matrix form as

$$u = Ca \qquad 3.9$$

In equations 3.9 the matrix a contains the coefficients of equation 3.7. The matrix C contains all the u(x,y) functions as in equations 3.8. The variables x and y are given values to describe the node position relative to the element coordinate axes.

(4) Next, the internal generalized stress relationships are derived. These relationships depend upon the element nodal displacements such that all internal generalized stresses can be determined at each node in the plate, once the displacements are known.

The bending and twisting curvatures are formulated once the displacement function of equation 3.7 is chosen since these curvatures are simply

$$k = \begin{vmatrix} -w,xx \\ -w,yy \\ w,xy \end{vmatrix} = Ba \qquad 3.10$$

The generalized stresses for anisotropic plate bending are given by

$$\begin{vmatrix} Mx \\ My \\ Mxy \end{vmatrix} = \begin{vmatrix} Dx & D_1 & 0 \\ D_1 & Dy & 0 \\ 0 & 0 & 2Dxy \end{vmatrix} \begin{vmatrix} -w,xx \\ -w,yy \\ w,xy \end{vmatrix} \qquad 3.11$$

In general matrix terms equations 3.11 can be stated as

$$M = Dk \qquad 3.12$$

Since $k = Ba$ from equations 3.10 and $a = C^{-1}u$ from equations 3.9, equations 3.12 can be established in terms of the element nodal displacements. That is, the generalized stresses become

$$M = DBC^{-1}u \qquad 3.13$$

(5) The next step is to determine the nodal force-displacement response of the element when subjected to external loading. These relationships contain the stiffness matrix of the element. One approach leading to the formation of this stiffness matrix is the use of the principle of virtual work. If the nodal forces are moved through a set of virtual displacements, the resulting external work done must be equal to the internal work given by the product of the generalized stresses and their corresponding curvatures. If virtual displacements of unit magnitudes are imposed at the element nodes in the directions of the external nodal forces, the external work will have the same value as the nodal forces. If the unit virtual displacements are given by $\delta u = I$ (the identity matrix) and are imposed in turn at each of the element nodes, then the external work done is

$$We = \delta uF = IF = F \qquad 3.14$$

If the resulting internal curvatures are δk, then the internal work becomes

$$Wi = \iint (\delta k)^T M dx dy \qquad 3.15$$

Since $\delta k = BC^{-1}\ \delta u = BC^{-1}I = BC^{-1}$ and substituting equations 3.13 into 3.15, the internal work becomes

$$Wi = \iint (BC^{-1})^T D BC^{-1} u\,dx\,dy \qquad 3.16$$

Equating the internal and external work the nodal forces become

$$F = \left[(C^{-1})^T \iint B^T D B\,dx\,dy C^{-1}\right] u \qquad 3.17$$

The elastic element stiffness matrix is therefore

$$K = (C^{-1})^T \iint B^T D B\,dx\,dy C^{-1} \qquad 3.18$$

(6) After each element in the structure is considered and its stiffness matrix derived relative to the element coordinate axes, the assembly of these elements into the final structure is a simple procedure. If the coordinate axes of the element are not directed along those of the global system, the element force-displacement relationships must be transformed into the directions of the global system coordinates. Once all transformations are performed, equilibrium of nodal forces and compatibility of nodal displacements can be achieved. For the particular steps necessary in this general formulation, the reader is referred to Livesley[51]. No transformations were necessary in the present study since the global axes system coincided with those of all the elements in the plate.

The matrices involved in the above steps are presented in explicit form in Appendix I for a single rectangular element of anisotropic composition.

(b) The Square Plate Idealization

For the present study only square plates are analysed. These are divided into square finite elements as illustrated in Figure 3.3. The 12 x 12 mesh shown was selected on the basis of the accuracy obtained from elastic solutions based on this subdivision.

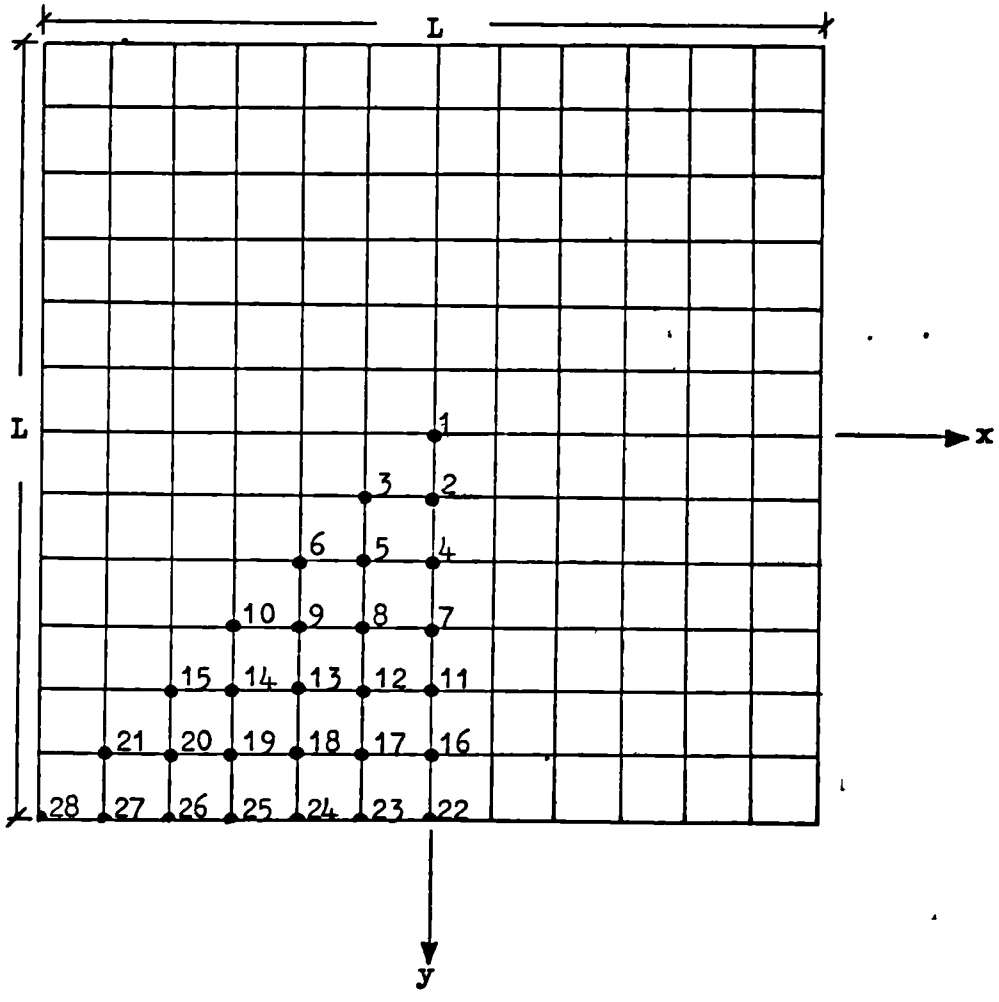

Subdivision of Square Plate into Finite Elements

Figure 3.3

All loading and boundary conditions are symmetrical about the x and y axes and the diagonals of the plate. Therefore only one eighth of the plate had to be analysed.

The numbering of the nodes is also shown in Figure 3.3. It is worth noting that although the numbering of nodes is completely arbitrary, there is a definite advantage in numbering them such that the difference between any two adjacent node numbers is kept to a minimum. This will ensure that the band width of stiffness coefficients in the total structural stiffness matrix is kept ot a minimum. A narrow band width increases the accuracy of solution and also reduces the amount of computer storage required for the coefficients in an elastic analysis.

(c) Discontinuities in Generalized Stresses

At a node common to two or more elements the generalized stresses should be identical for each element. That is, in reality there is only one stress condition at any one point in the plate provided no discontinuity in plate flexural stiffness occurs at that point. However, for rectangular elements of the type described above for which the stiffness matrices are derived by the displacement function of equation 3.7, slight discontinuities in the generalized stresses occur across element boundaries. This discrepancy exists because the displacement function selected does not maintain continuity of curvatures at nodes. For evidence of these discontinuities or steps in the generalized stresses, the reader is referred to Zienkiewicz[38].

For the present analyses the generalized stresses Mx, My and Mxy were each averaged at common nodes such that for elements of the same bending properties, there was only one set of principal generalized stresses..

(d) The Variation of Principal Generalized Stresses within one Element

The variation of internal generalized stresses within the boundaries of an element can be determined from the second derivatives of the displace ment function. From equations 3.11 these generalized stresses can be written as

$$\begin{aligned}
\frac{Mx}{D} &= -\left|0\ 0\ 0\ 2\ 0\ 2\nu\ 6x\ 2y\ 2\nu x\ 6\nu y\ 6xy\ 6\nu xy\right|\left|a\right| \\
\frac{My}{D} &= -\left|0\ 0\ 0\ 2\nu\ 0\ 2\ 6\nu x\ 2\nu y\ 2x\ 6y\ 6\nu xy\ 6xy\right|\left|a\right| \\
\frac{Mxy}{D} &= \left|0\ 0\ 0\ 0\ (1-\nu)\ 0\ 0\ 2(1-\nu)x\ 2(1-\nu)y\ 0\ 3(1-\nu)x^2\ 3(1-\nu)y^2\right|\left|a\right|
\end{aligned} \qquad 3.19$$

In equations 3.19 the generalized stresses Mx and My vary linearly and Mxy parabolically within or along the element boundaries. With these distributions it is possible for the principal generalized stresses which are given by

$$M^{1,2} = 1/2\left[Mx+My \pm \sqrt{(Mx-My)^2+4Mxy^2}\right] \qquad 3.20$$

to have a maximum value within the element boundaries. This is an important consideration for an elastic-plastic analysis since the yield criterion could be violated at points away from the nodes.

The necessary condition for a stationary value of principal generalized stresses at a point (x,y) is that

$$M^t,\ x = o \qquad 3.21$$

and

$$M^t,\ y = o \qquad 3.22$$

simultaneously. For this stationary value to be a maximum

$$(M^t,_{xx})\ (M^t,_{yy}) > (M^t,_{xy})^2 \qquad 3.23$$

with

$$\left.\begin{matrix} M^t,_{xx} \\ M^t,_{yy} \end{matrix}\right\} < o \qquad 3.24$$

The position (x,y) for a possible maximum depends on the coefficients a in equations 3.19 which in turn depend on nodal values of displacements. Once these coefficients are known, the distributions of generalized stresses within the element (equations 3.19) are specified. The next step is to satisfy equations 3.21 and 3.22 and determine (using conditions 3.23 and 3.24) if a maximum exists.

However, because of the form of equations 3.20 it is not possible to establish algebraically the coordinates (x,y). Consequently, a numerical approach is required.

For the present study a number of spot checks were made within elements to assess the violation of the yield criterion. These are presented and discussed in Addendum I. In general, it can be said that for the analyses presented herein, the selection of nodal principal generalized stresses as maxima is justified.

3.4 Yield Criteria for Metals and Reinforced Concrete

(a) General

A fundamental requirement for an elastic-plastic bending analysis is the selection of a yield criterion for the plate material. In the

present study both metal plates and reinforced concrete slabs are considered. Consequently, separate yield criteria for these materials should be used. However, by limiting the analyses to plates and slabs with similar limiting stress states, it was possible to adopt one yield criterion that satisfies closely, the yield properties of both materials.

The terminology appearing in this section is consistent for the most part with that used in the theories of plasticity and limit analysis. The terms generalized stress (bending, twisting and principal) and generalized strain rates (curvature rates) are used to indicate that the variables specifying the states of stress and strain need not have the dimensions of stress or strain. The concept of plastic rotations is adopted to represent slope discontinuity after yielding of the plate material occurs. These rotations are curvatures over an infinitesmal length of the plate.

The term "plastic flow line" is here introduced to describe an imaginary line of infinitesmal length across which the plastic generalized strain rate occurs. For reinforced concrete slabs these lines when joined correspond to yield lines.

(b) Yield Criterion for Metals

The two well known yield criteria for ductile metals are illustrated in Figure 3.4

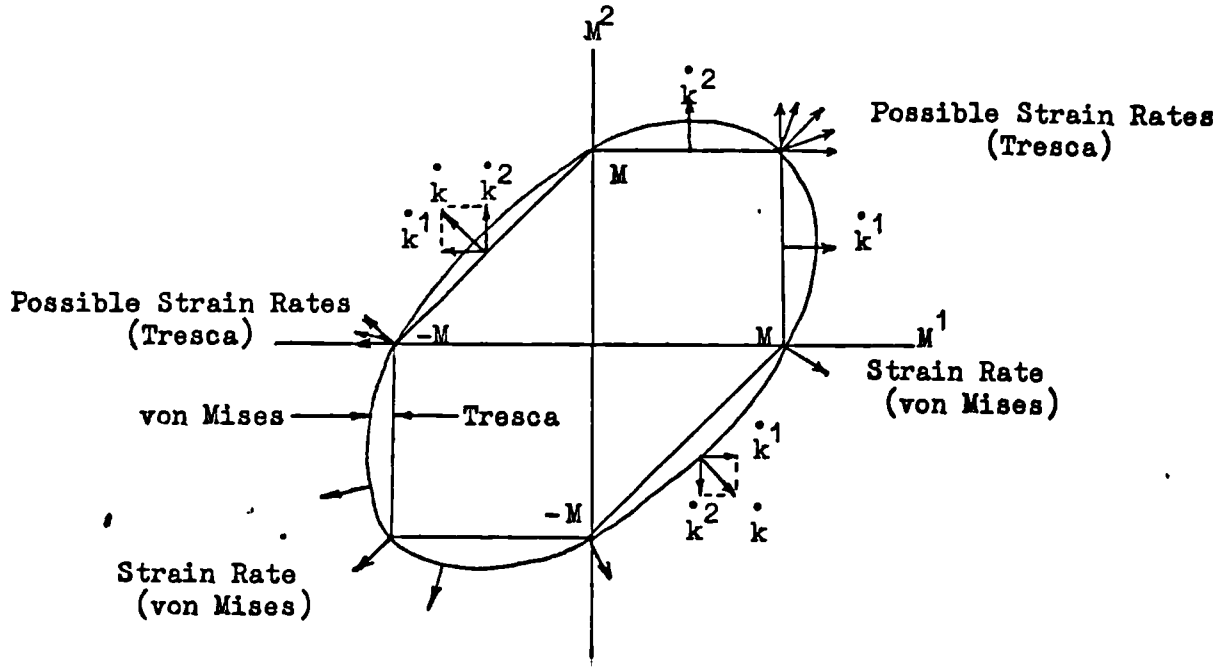

Yield Criteria for Ductile Metals
in $M^{1,2}$ Generalized Stress Space

Figure 3.4

The directions of the generalized strain rates are indicated. These directions are established by the theory of the plastic potential due to von Mises in 1928. In 1953 Koiter[52] generalized this theorem and removed the restriction of the yield locus having to be a continuous, piecewise differentiable function. This generalization enabled the plastic potential to be applied to the Tresca criterion and therefore established the flow rule. This flow rule states that except at the corners of the yield locus, the generalized strain rates are directed along the outward normal to the yield locus. At corners generalized strain rates are permissible in any direction between those that are perpendicular to the yield locus.

The limiting generalized stress condition for the Tresca criterion can be specified by several yield functions in the sense of Koiter. That is

$$(M^1-M)(M^2-M)(M^2-M^1-M)(-M^1-M)(-M^2-M)(M^1-M^2-M) = 0 \qquad 3.25$$

In equation 3.25, the state of generalized stress is below the yield limit if all these yield functions have negative values. For a state of stress at the yield limit, at least one of these functions must vanish while none has a positive value.

The von Mises yield criterion in two dimensional plane space forms an ellipse. For any one combination of the principal generalized stresses that satisfy this criterion, there is only one state of generalized strain rates that can be determined by the theory of the plastic-potential. The yield function for the von Mises criterion in bending is

$$(M^1)^2+(M^2)^2-M^1M^2-(M)^2 = 0 \qquad 3.26$$

For a complete discussion of the theory of the plastic potential and the yield criteria for metals, the reader is referred to Hill[53]. Hill also describes anisotropic criteria for metals.

(c) The Yield Criteria for Reinforced Concrete

Since any yield criterion is simply a hypothesis concerning the limit of elastic behaviour of a material subjected to certain combinations of stresses, its validity must be established by experimentation. For metals the criteria mentioned above have been investigated experimentally with most evidence supporting their basic concepts. For plain and reinforced concrete no yield criteria have been so firmly established

as for the case of metals. Recent research into the yield criteria for isotropic and orthotropic reinforced concrete slabs has developed as a result of the increased acceptance in design practice of the yield line theory of analysis for reinforced concrete slabs pioneered by Johansen[7]. British researchers have produced the most note worthy works on many aspects of the limit analysis and design of reinforced concrete slabs. The principal stimulus has been the work of Wood[4] at the Building Research Station.

Most exponents of yield line theory have assumed that the yield of a Johansen slab is governed by a square form of yield criterion. This, of course, is a false assumption when one considers the criterion stated by Johansen.

For an orthotropically reinforced concrete slab in which the ultimate bending resistances are M and μM in the x and y directions respectively, the Johansen criterion is

$$\begin{aligned} Mn &= M(\text{cosine}^2\phi + \mu\ \text{sine}^2\phi) \\ Mt &= M(\text{sine}^2\phi + \mu\ \text{cosine}^2\phi) \\ Mnt &= M(1-\mu)\text{sine}\phi\text{cosine}\phi \end{aligned} \qquad 3.27$$

The generalized stresses are shown in Figure 3.5.

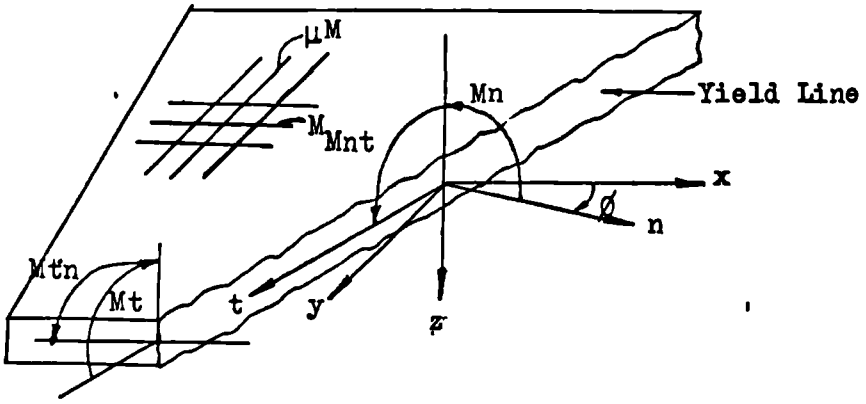

Normal, Tangential and Twisting
Generalized Stresses on Yield Lines

Figure 3.5

This yield criterion implies that the x and y directions are principal and the twisting generalized stress Mxy is zero. For the isotropic case with $\mu = 1$ equations 3.27 reduce to

$$\begin{aligned} Mn &= M \\ Mt &= M \\ Mnt &= 0 \end{aligned} \qquad 3.28$$

If a top layer of reinforcing steel exists with an ultimate

bending resistance m then the yield criterion for negative bending is

$$Mn = -m$$
$$Mt = -m \qquad 3.29$$
$$Mnt = 0$$

Equations 3.28 and 3.29 represent two points on the yield locus for the criterion of equations 3.27 when $\mu = 1$. Furthermore, these are the only points that exist for the isotropic case since $M_n = M_t$ for positive or negative bending and therefore it is impossible to have a positive-negative bending combination. Consequently the Johansen criterion is far from a square criterion. Only the +,+ or -,- corners of the souare criterion for the isotropic case are coincident with the Johansen criterion. The square criterion is illustrated in principal generalized stress plane space in Figure 3.6 of the next section.

When the static theorem of limit analysis was applied to a Johansen slab it was found that inorder to satisfy the equilibrium equation

$$Mn,nn+Mt,tt-2Mnt,nt = -q/D \qquad 3.30$$

at all points along a yield line, the tangential generalized stress M_t must be made to vary. This variation removes the restriction of not being able to represent a positive-negative generalized stress state and consequently a square criterion can be assumed. This is tantamount to rejecting the M_t condition of Johansen's original yield criterion (equations 3.27). Therefore the square yield criterion was never really implied by Johansen although it has been assumed by many

as a result of applying the lower bound techniques of limit analysis to Johansen slabs.

A different yield criterion from that of equations 3.27 for orthotropically reinforced slabs has been established in the principal generalized stress space by Kemp[54]. He establishes the flow rule associated with this criterion and shows that it is consistent with the predictions of the plastic potential theory. More recently Save[55] has presented the same criterion in generalized stress space. Kemp's criterion reduces to the square yield criterion for isotropic slabs.

Experimental evidence on the yield criterion for isotropically reinforced slabs has recently been published by Morley[56] in England and by Lenschow and Sozen[57] in the United States. Morley used rhomboid slabs loaded at the corners to investigate principal generalized stresses of opposite sign. The results support the idea of a square yield criterion for isotropic reinforcement. Lenschow and Sozen performed tests on two different types of slab configuration loaded by flexible cables to reduce the effects of possible membrane action. They applied separately, uniaxial and twisting external bending moments to rectangular slab elements and equal biaxial bending moments to regular hexagonal shaped slabs. This latter slab shape allows bending moments to be applied in three different directions at sixty degrees to each other. These experimental results for isotropically reinforced slabs also support the square yield criterion form in principal generalized stress plane space.

The square yield criterion is accepted by many at present as a good approximation for isotropically reinforced slabs.

(d) The Yield Criterion Adopted for the Present Analyses

The criterion adopted for the present study is the "square criterion" in principal generalized stress plane space of M^1, M^2. This criterion is illustrated in Figure 3.6 and is identical to that presently employed for reinforced concrete. It is also identical to the Tresca criterion when the principal generalized stresses have the same sign. It was assumed that by selecting certain metal plate bending problems, internal generalized stress states producing principal generalized stresses of opposite sign would occur at only a few locations in the plate (near corners for the plates analysed herein) and that yielding at these points would not occur until much of the plate away from these locations had become plastic.

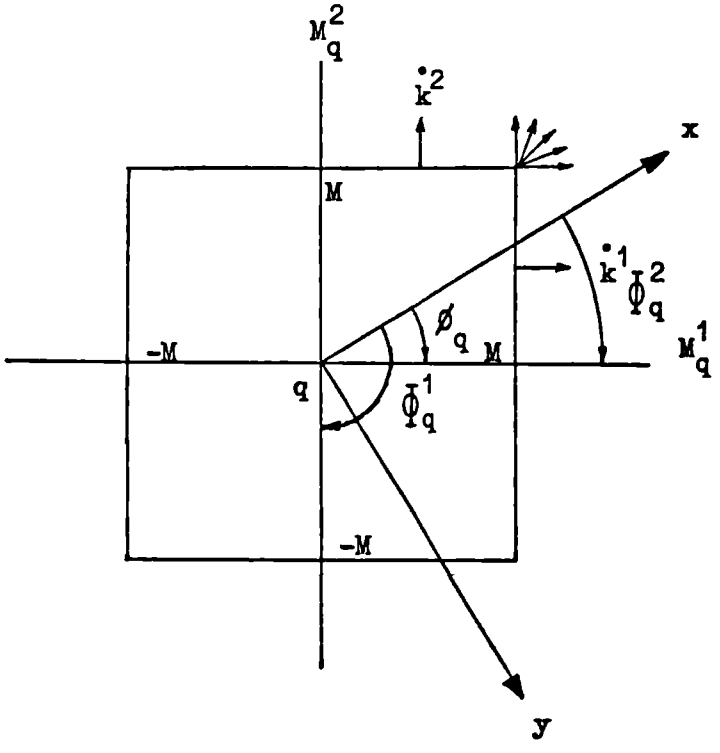

The Square Yield Criterion in $M_q^{1,2}$ Generalized Stress Space

Figure 3.6

In discussing this criterion and its associated flow rule, it is supposed that the generalized stress state is determined at some point in the plate. In the context of the finite element method, let this point coincide with some node q at the corner of an element. The x and y axes shown represent the orientation of the global coordinate axes of the plate in a Cartesian reference system. If the generalized stresses in bending are Mx, My and Mxy given by equations 3.1, then the principal generalized stresses determined from a Mohr generalized stress circle, are simply

$$M_q^{1,2} = \frac{1}{2}\left[Mx+My \pm \sqrt{(Mx-My)^2+4Mxy^2}\right] \qquad 3.31$$

In addition, the directions of these principal values can be specified by the angle ϕ_q of which the

$$\text{Tangent}(2\phi_q) = 2Mxy/(My-Mx) \qquad 3.32$$

The yield requirement for this criterion is that whenever a principal generalized stress attains the limiting value of M, plastic straining takes place. The flow rule associated with this generalized stress state is such that the plastic strains occur in the direction of the responsible principal generalized stress. The resulting generalized strain rates for bending are curvature rates and are idealized in the present study by employing the concept of plastic rotations. Since these rotations have both magnitude and direction, they can be represented as vectors, the directions of which are

perpendicular to the actual plastic strains (adopting a right-handed screw rule). . These rotations concentrated at nodes of an element are considered to produce "plastic flow lines" directed at right angles to that of the responsible principal generalized stresses. The directions of these flow lines are given by the angles Φ_q^1 and Φ_q^2 measured clockwise positive from the x axis in Figure 3.6. These angles and the kinematics of displacement behaviour at plastic nodes are discussed in the following section of this chapter.

The flow rule described above satisfies the requirements of the plastic potential theory since if the yield function is given by

$$f(Mx,My,Mxy) = Mx+My \pm \sqrt{(Mx-My)^2+4Mxy^2} - 2M = 0 \qquad 3.33$$

and the generalized strain rates by

$$\dot{k}x = \rho f,x \quad \dot{k}y = \rho f,y \quad \dot{k}xy = \rho f,xy \qquad 3.34$$

then the directions of the principal generalized strain rates measured clockwise positive from the x axis should be

$$\text{Tangent}(2\phi_q) = 2\dot{k}xy/(\dot{k}y-\dot{k}x) \qquad 3.35$$

Partial differentiation of the yield function required by equations 3.34 (ρ is an arbitrary positive constant) produces

$$\text{Tangent}(2\phi_q) = 2Mxy/(My-Mx) \qquad 3.36$$

which is identical to the flow condition initially assumed by equation 3.32.

However, this flow rule cannot be strictly enforced using the finite element method presented here. The problem of imposing plastic rotations in plate elements is discussed in section 3.5b where it is shown that only an approximation to this flow rule can be made.

(e) Linear Approximations to the Yield Function

The non-linear form of equations 3.31 presents certain difficulties for use in an elastic-plastic bending analysis using matrix algebra. These difficulties develop at plastic nodes off lines of symmetry where the generalized stresses Mx and My are not equal and Mxy is non-zero. At these nodes the yield function cannot be written in matrix terms unless it is restated in an approximate linear form.

Therefore at a plastic node where the non-linear form of equations 3.31 governs, it is necessary to maintain the limiting value M by using and approximate yield function throughout the remainder of the analysis. This can be done by assuming that the angle ϕ_q in Figure 3.6 remains constant during each plastic load increment. The plastic load increment is the increment of applied load between any one node becoming plastic and the next. Thus the angle assumed for any one plastic load increment has the value obtained at the end of the previous plastic load increment. This approximation will have little effect on the accuracy of the solution if the change in this angle is small when determined at the beginning and end of the increment.

Massonnet[29] and Cornelis[30] adopted an approximation to equations

3.31 in the form

$$M_q^{1,2} = \tfrac{1}{2}\left[Mx+My \pm (Mx-My)\,\text{secant}(2\phi_q)\right] \qquad 3.37$$

The same approximate equation was independently chosen initially for the present finite element approach previous to the publication of these papers. However, it was abandoned in favour of a more accurate equation in the form

$$M_q^{1,2} = \tfrac{1}{2}\left\{Mx+My \pm \left[(Mx-My)\,\text{cosine}(2\phi_q) - 2Mxy\ \text{sine}(2\phi_q)\right]\right\} \qquad 3.38$$

The Mohrs circles of Figures 3.7 and 3.8 illustrate geometrically the differences between the approximate equations 3.37 and 3.38 and the actual equation 3.31.

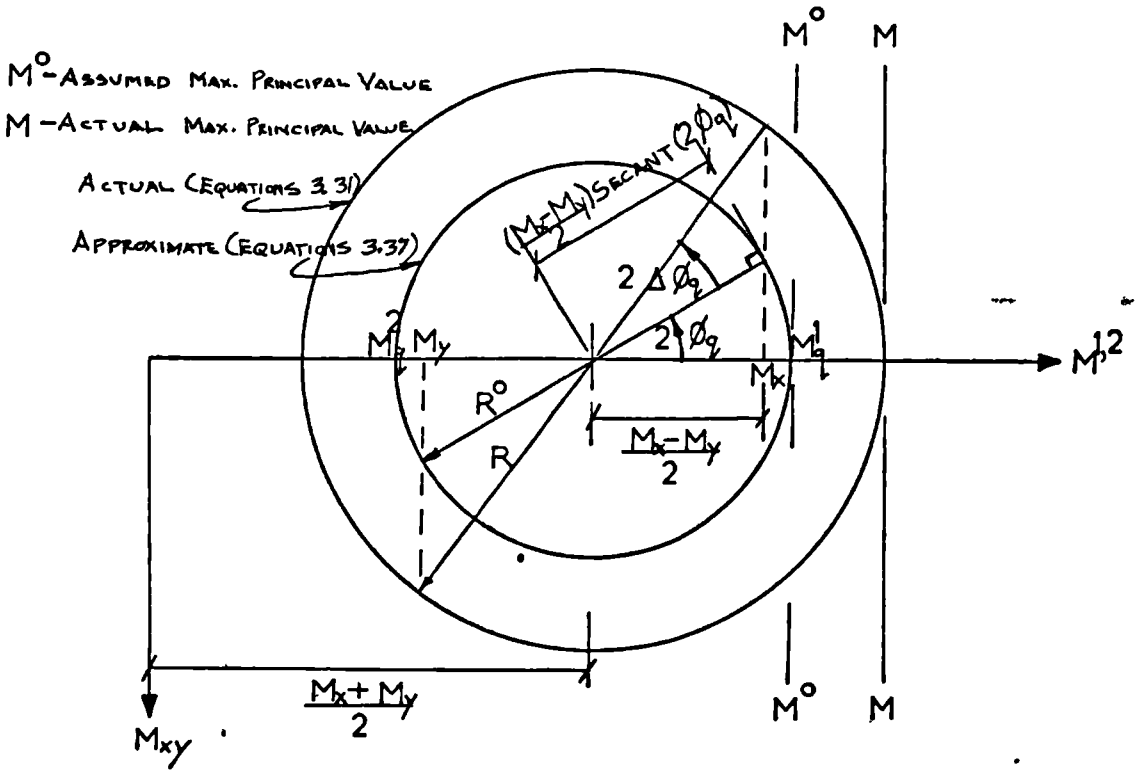

Figure 3.7

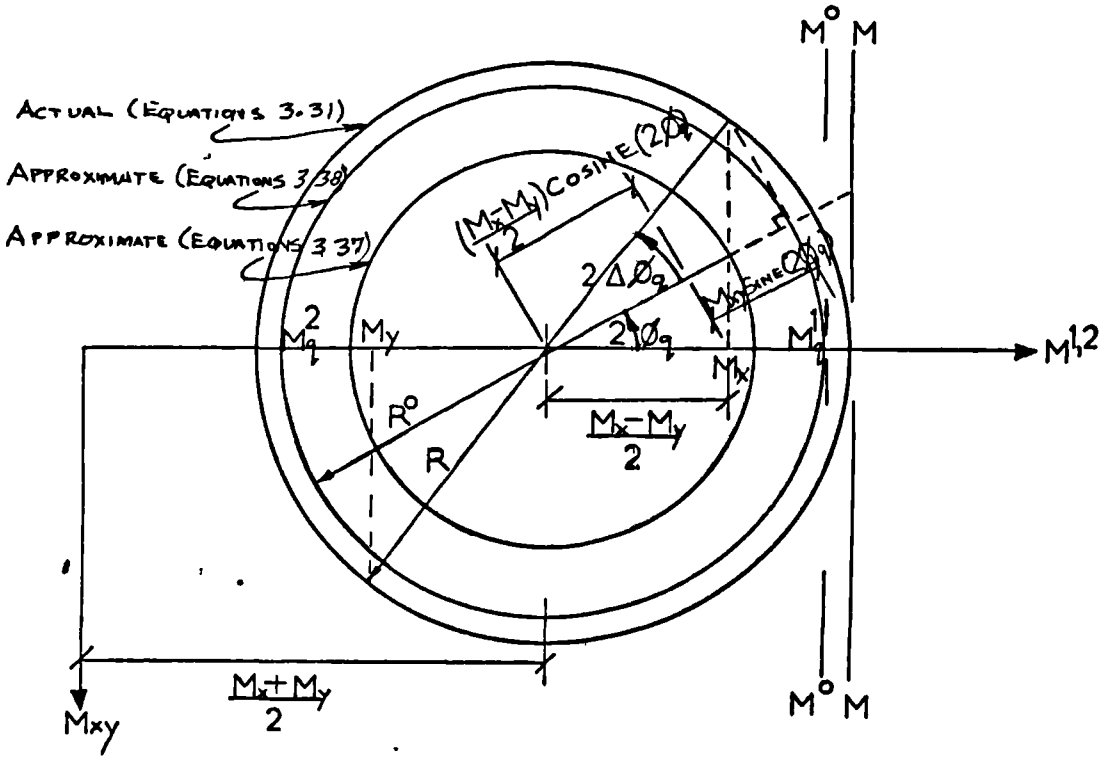

Figure 3.8

The angle ϕ_q and the assumed generalized stresses in Figure 3.8 have the same values as those in Figure 3.7. The change in ϕ_q is shown as $\Delta\phi_q$ and represents the change in orientation of the principal planes as the load is increased from the beginning of a plastic load increment to the end of this increment.

It is clear geometrically that the approximation made using equation 3.38 by assuming ϕ_q is constant during the plastic increment is far superior to that of equations 3.37.

To illustrate the differences between these equations when various angles ϕ_q are assumed constant, the ratio of actual to approximate radii (R^o/R) is plotted against changes $\Delta\phi_q$ of up to 10 degrees

in Figure 3.9. From Figure 3.7 the radii ratio is

$$\frac{R^o}{R} = \frac{\text{cosine}(2\phi_q + 2\Delta\phi_q)}{\text{cosine}(2\phi_q)} \qquad 3.39$$

and from Figure 3.8 this ratio is simply

$$\frac{R^o}{R} = \text{cosine}(2\Delta\phi_q) \qquad 3.40$$

Of the two ratios in equations 3.39 and 3.40 the first is a function of both ϕ_q and its change $\Delta\phi_q$ whereas the latter is only a function of $\Delta\phi_q$. In Figure 3.9 for the case of $\phi_q = 0$ degrees, the radii ratios are identical for either of the approximate equations. However, for any other angle ϕ_q and an accompanying change $\Delta\phi_q$, the superiority of equations 3.38 becomes quite evident. In equations 3.38 the approximation to the radius of the circle is the same for any <u>one</u> $\Delta\phi_q$ regardless of the orientation (ϕ_q) of the principal directions. On the other hand equations 3.37 can give as much as 100% error as ϕ_q approaches 45^o with the change $\Delta\phi_q$ only a fraction of a degree.

The error introduced by using R^o rather than R is not, however, the error in the principal generalized stresses. The error in the principal generalized stresses (and therefore violation of the yield criterion) can only be assessed if the center of the circle, and R^o and R are known. If Mx = -My then the error implied by the radii ratio is also the error in the principal generalized stresses.

The importance of employing equations 3.38 as an approximation to equations 3.31 for elastic-plastic analysis is that the angle ϕ_q need not be changed for a plastic node after each plastic load increment.

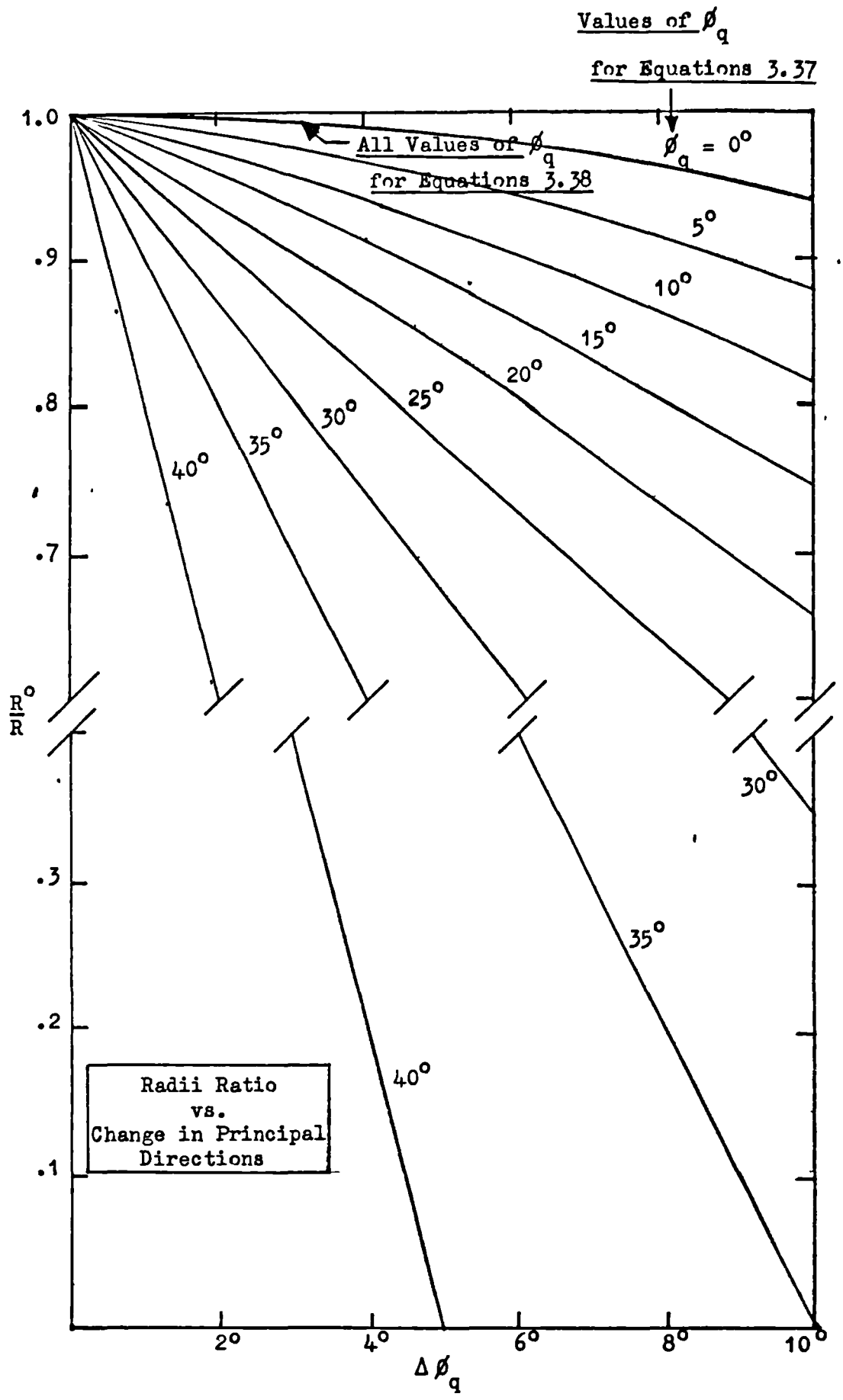
Values of ϕ_q
for Equations 3.37
All Values of ϕ_q
for Equations 3.38
$\phi_q = 0^\circ$
5°
10°
15°
20°
25°
30°
35°
40°
1.0
.9
.8
.7
.3
.2
.1
$\frac{R^\circ}{R}$
Radii Ratio
vs.
Change in Principal
Directions
2°
4°
6°
8°
10°
$\Delta\phi_q$

Figure 3.9

Indeed from Figure 3.9 it is evident that even a change of $\Delta \phi_q = 10$ degrees gives at the most 6% error in principal generalized stresses (in the extreme case of Mx = -My).

Equations 3.38 have been used in producing the solutions presented in this thesis. From the results it appears to be an excellent approximation to the actual principal generalized stresses.

3.5 The Elastic-Plastic Bending Behaviour of Rectangular Elements

(a) General

The elastic stiffness matrix for the rectangular element (the basic steps apply to any element) was derived in section 3.3a. For an elastic-plastic analysis the resulting stiffness matrix becomes an extension of the elastic matrix with additional coefficients describing the internal generalized stress state at the plastic nodes of the element. Its final form is dictated by the way in which the node displacements are allowed to become discontinuous (that is, how the flow rule is applied). In the present proposal, slope discontinuities at nodes occur whenever plastic rotations are introduced. The components of the plastic rotation are determined once the rotation and its orientation to the coordinate axes are known.

(b) The Approximate Nature of Plastic Flow in Finite Elements

In general the finite element idealization of the plate results in a substitute structure that deforms in accordance with the kinematics allowed by the nodal displacements. At a plastic node common to four rectangular elements the idealized plastic behaviour between elements is only an approximation to the actual plastic flow. It is impossible to introduce a <u>single</u> plastic rotation that enforces the elements to deform

physically in the correct manner. This follows from the fact that when yield occurs in the real plate discontinuous slopes form in the direction of the plastic strains but in the substitute plate, the only nodal slope discontinuities (plastic rotations) that can be dealt with are those normal to the element boundaries.

With the displacement function adopted in this study, the plastic rotation must be divided vectorally into two orthogonal components, each of which is introduced between adjacent elements and directed along their boundaries. In Figure 3.10 this idealized plastic flow is shown.

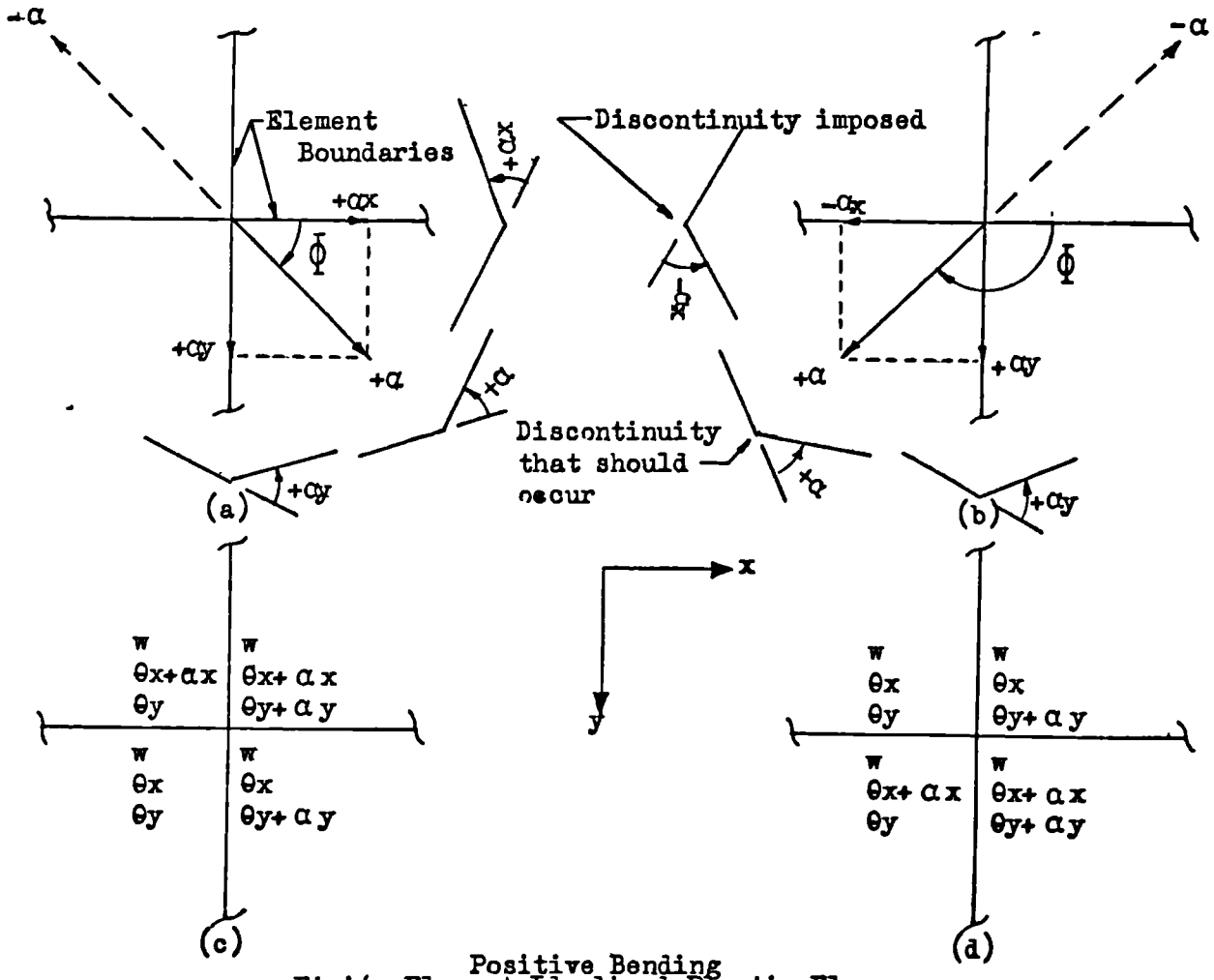

Positive Bending
Finite Element Idealized Plastic Flow

Figure 3.10

Plastic behaviour at a typical node is illustrated in Figure 3.10a and b. Positive plastic rotations result from positive bending. For negative bending the direction of the plastic rotation is simply reversed. Figures 3.10c and d are displacement patterns for elements with plastic rotations of Figures 3.10a and b respectively.

The discontinuity that should occur cannot since the slopes perpendicular to α are not determined at the node. To approximate the true behaviour, the components of the plastic rotation are determined in the directions of the element boundaries and these result in a double fold between elements. If the angle Φ is measured clockwise positive from the x axis then

$$\alpha x = \alpha \text{cosine } \Phi$$
$$\text{and} \qquad \alpha y = \alpha \text{sine } \Phi \qquad 3.41$$

for positive or negative bending in Figures 3.10a and b.

From Figures 3.10c and d it is evident that two situations develop for specifying how the displacements are donated to each element. The elastic-plastic stiffness matrix for any one element in Figure 3.10c will have a different form from that for the same element in Figure 3.10d. However, the components of plastic rotations for either displacement pattern are determined from equations 3.41.

It is preferable to have only one displacement pattern for any plastic rotation that might occur. This will reduce the complexity of the computer program required. The configuration of Figure 3.10d is selected for the present study. To make Figure 3.10c consistent with this choice,

equations 3.41 are restated as

$$\alpha x = -\alpha|\text{cosine}\,\Phi| \qquad 3.42$$

and

$$\alpha y = \alpha|\text{sine}\,\Phi|$$

Equations 3.42 simply maintain a negative αx and a positive αy for positive bending and vice versa for negative bending.

Because the components of plastic rotations are imposed between elements in two orthogonal directions, the flow rule associated with the square yield criterion is not in general satisfied at a plastic node. If the direction of the plastic rotation vector is along an element boundary then the flow rule is properly satisfied since the correct discontinuity is allowed.

(c) Node Displacements Including Finite Rotations

Figure 3.11 illustrates the node displacements at a plastic node j. Only the boundaries of two elements along the x axis are shown. The y axis is directed out of the plane of the page. Vector directions for displacements are positive if along the positive axes directions. All the slopes shown are negative. The vertical displacements and the component αy_j of the plastic rotation are positive. The superscript o denotes displacements at the node before the principal generalized stress state of node j satisfies the yield conditions.

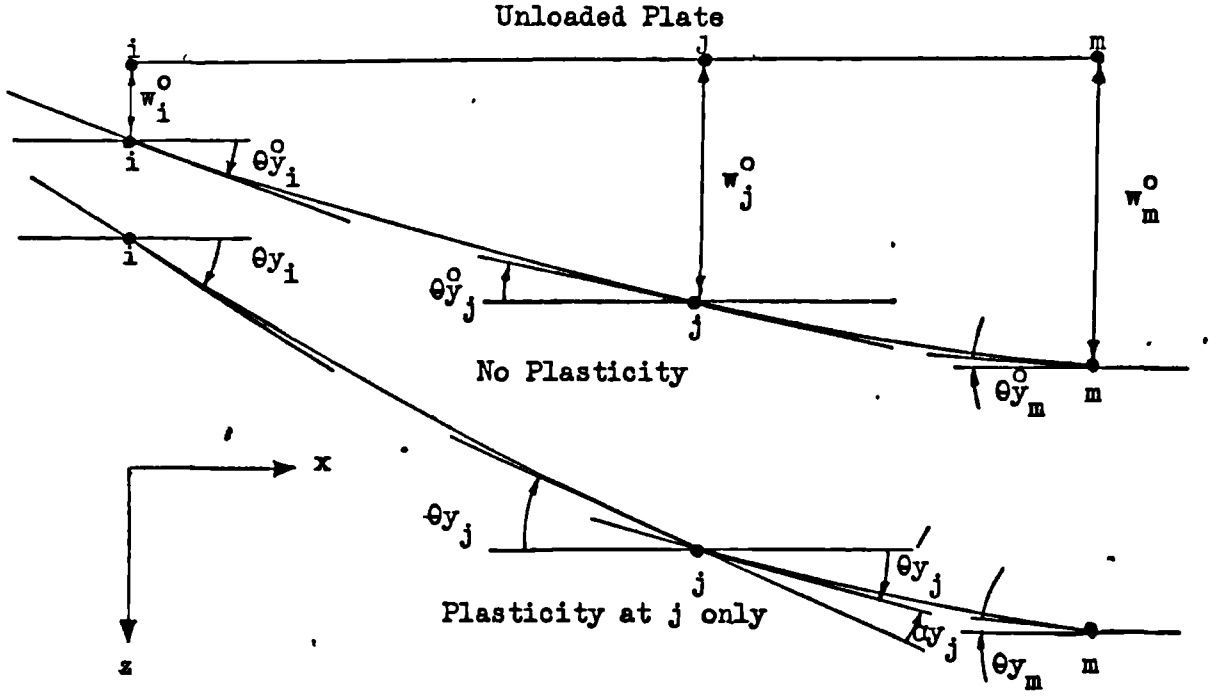

Node Displacements - Slopes and Rotation Components About y Axis

Figure 3.11

From Figure 3.11 the slope

$$\theta y_j' = \theta y_j + \alpha y_j \qquad 3.43$$

A similar situation occurs along the x axis if the vector direction of the plastic rotation α_j is other than along the y axis. That is, there would be components of the plastic rotation directed along both the x and y axes. If the generalized stress condition at node j is such that both principal generalized stresses M_j^1 and M_j^2 satisfy the yield criterion at different load stages, there would be components in the x and y axes due to both plastic rotations.

Equation 3.43 implies that the component αy_j is donated to element jm. Consequently, the stiffness matrix of this element will contain coefficients that relate the external nodal forces (V_j, mx_j and my_j) and the internal responsible principal generalized stress at j to this component. Similar relationships will exist for the same quantities with respect to the component αx_j when the elements are viewed along the y axis bearing in mind that equations 3.42 determine the plastic rotation components.

If, this method of introducing the components of the plastic rotations is applied at all four corners of a rectangular element, it would result in each node having the displacements shown in Figure 3.12.

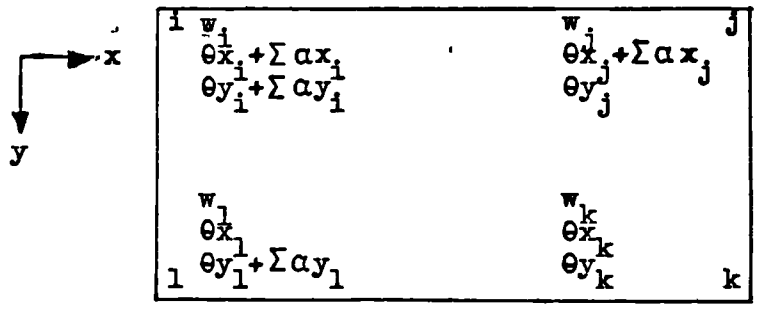

Node Displacements for Rectangular Element — . —
All Nodes Plastic

Figure 3.12

Only nodes i, j and l have components of the plastic rotations within these nodal displacements. $\Sigma \alpha x_i$ etc. represent the summation of components due to all principal generalized stresses M_i^1 and M_i^2 etc. satisfying the yield criterion. This represents the most general case of node plasticity for a rectangular element.

(d) Plastic Behaviour at a Common Node for Four Rectangular Elements

The method of introducing plastic rotations and resolving them into coordinate components as described above will now be applied to a typical node i. It is assumed that both principal generalized stresses M_i^1 and M_i^2 have independently satisfied the yield criterion at two different plastic load stages. A section taken from the plan view of these elements is shown in Figure 3.13.

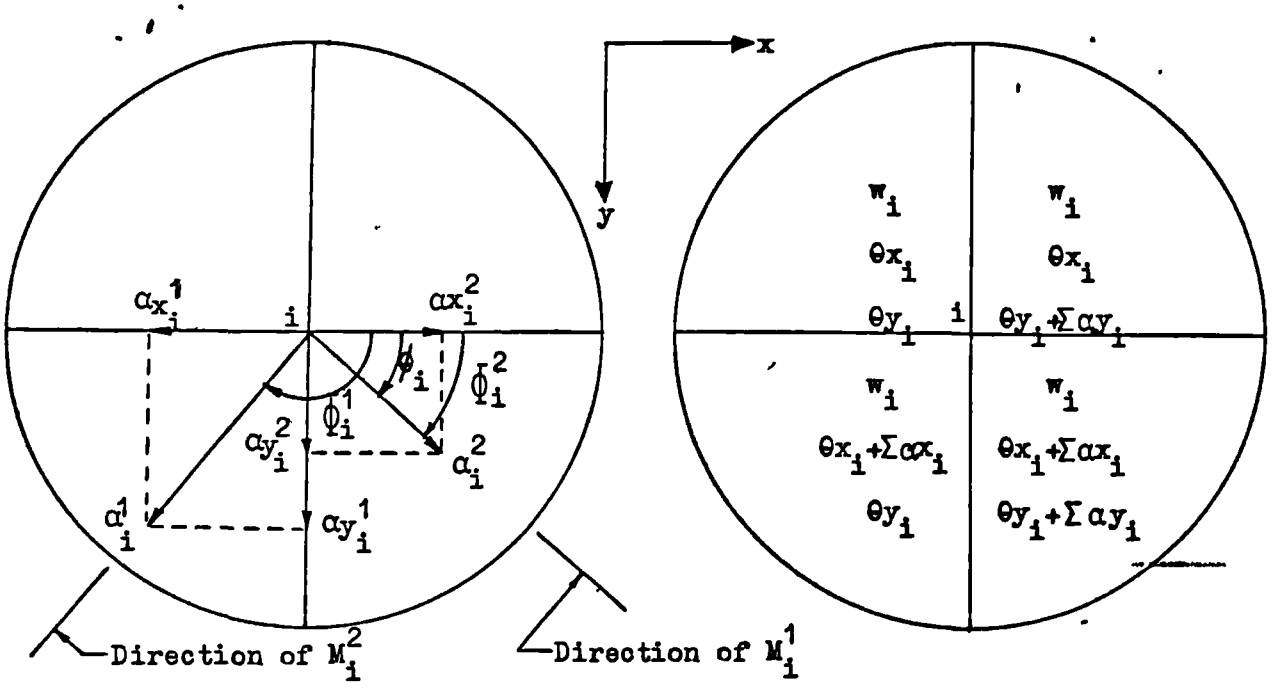

Vector Directions of Plastic Rotations and Directions of Principal Generalized Stresses

(a)

Resulting Node Displacements

(b)

Typical Plastic Node Behaviour

Figure 3.13

Once the plastic rotations form, the four elements become discontinuous in slope in both the x and y directions since components of these rotations act about both axes. Each plastic rotation that forms constitutes one additional independent displacement. For the case of node i the unknown displacements are five in number. That is, one vertical deflection, two slopes and two independent rotations. A column matrix of these displacements for node i is

$$\begin{vmatrix} w_i \\ \theta x_i \\ \theta y_i \\ \alpha_i^1 \\ \alpha_i^2 \end{vmatrix} \qquad 3.44$$

The superscripts on the rotations denote which of the principal generalized stresses was responsible for its formation.

In Figure 3.13 the angle ϕ_i has been described previously (see equation 3.32). The angles Φ_i^1 and Φ_i^2 have also been described previously (see Figure 3.6) and are given by

$$\Phi_i^t = \tfrac{1}{2}(t-2)\pi + \phi_i \qquad 3.45$$

in which t = 1 or 2 for M_i^1 or M_i^2 respectively. Therefore the components of the plastic rotations (recalling equations 3.42) in Figure 3.13 are simply

$$\begin{aligned} \Sigma \alpha x_i &= -\alpha_i^1 \left|\text{cosine } \Phi_i^1\right| - \alpha_i^2 \left|\text{cosine } \Phi_i^2\right| \\ \Sigma \alpha y_i &= \alpha_i^1 \left|\text{sine } \Phi_i^1\right| + \alpha_i^2 \left|\text{sine } \Phi_i^2\right| \end{aligned} \qquad 3.46$$

t

Now that the displacements have been described, the elastic-plastic stiffness matrix for the rectangular element of Figure 3.12 can be established.

(e) The Elastic-Plastic Stiffness Matrix

Whatever the form of the stiffness matrix is, its coefficients must relate the nodal forces to the corresponding nodal displacements. If any of the element nodes are plastic, additional nodal displacements (plastic rotations) must be determined. Therefore additional equations must be available to solve for these. These equations are simply principal generalized stress equations that satisfy the yield conditions. In the general case for a node p where the principal generalized stresses M_p^1 and M_p^2 attain the limiting yield value, the rotations α^1 and α^2 can be expressed in a column matrix

$$\begin{vmatrix} R_p^1 \\ R_p^2 \end{vmatrix} = \begin{vmatrix} \alpha_p^1 \\ \alpha_p^2 \end{vmatrix} \qquad 3.47$$

or in a general form as

$$R_p^s = \left|\alpha_p^s\right| \qquad 3.48$$

The other three independent displacements are simply

$$D_p = \begin{vmatrix} w_p \\ \theta x_p \\ \theta y_p \end{vmatrix} \qquad 3.49$$

If the same procedure is applied to four nodes numbered 1,2,3 and 4 of a rectangular element then the displacements for the element can be assembled into one single column matrix

$$\left|\begin{matrix} D_n \\ R_p^s \end{matrix}\right| = \left|\begin{matrix} D_1 \\ D_2 \\ D_3 \\ D_4 \\ R_1^1 \\ R_1^2 \\ R_2^1 \\ R_2^2 \\ R_4^1 \\ R_4^2 \end{matrix}\right| \qquad 3.50$$

The omission of independent rotations at node 3 follows from Figure 3.12 if i = 1, j = 2, k = 3 and l = 4 for the present example. The introduction of the subscript n implies that n and p can have different node number values.

The external nodal forces corresponding to the displacements D_n for the element node n are simply

$$F_n = \left|\begin{matrix} V_n \\ mx_n \\ my_n \end{matrix}\right| \qquad 3.51$$

If the subscript m is introduced such that it has the same range of values as n in equations 3.50, the nodal forces for the element are

$$F_m = \left|\begin{matrix} F_1 \\ F_2 \\ F_3 \\ F_4 \end{matrix}\right| \qquad 3.52$$

All of the internal principal generalized stresses at the nodes have attained the limiting value M. They can therefore be established in matrix form to read

$$M_q^t = \begin{vmatrix} M_1^1 \\ M_1^2 \\ M_2^1 \\ M_2^2 \\ M_4^1 \\ M_4^2 \end{vmatrix} = \begin{vmatrix} M \\ M \\ M \\ M \\ M \\ M \end{vmatrix} \qquad 3.53$$

The complete force vector (external nodal forces and internal principal generalized stresses) can be written by combining equations 3.52 and 3.53 in the form

$$\begin{vmatrix} F_m \\ M_q^t \end{vmatrix} = \begin{vmatrix} F_1 \\ F_2 \\ F_3 \\ F_4 \\ M_1^1 \\ M_1^2 \\ M_2^1 \\ M_2^2 \\ M_4^1 \\ M_4^2 \end{vmatrix} \qquad 3.54$$

The submatrices F_m and M_q^t in equations 3.54 are related to the D_n and R_p^s matrices of equations 3.50 by elastic-plastic stiffness coefficients.

To determine these coefficients the following are required for the element:

(1) The elastic stiffness coefficients determined from equations 3.18.

(2) The principal generalized stress equations 3.31 established in matrix form through knowledge of equations 3.13.

(3) The angles Φ_q^t determined from equations 3.45.

To simplify the discussion of the formation of the stiffness coefficients only the forces at node 1 will be considered. The forces

at node i (i = 1) in Figure 3.12 are given by the equations

$$F_1 = \left|K_{11},K_{12},K_{13},K_{14}\right| \begin{vmatrix} w_1 \\ \theta x_1 + \Sigma \alpha x_1 \\ \theta y_1 + \Sigma \alpha y_1 \\ w_2 \\ \theta x_2 + \Sigma \alpha x_2 \\ \theta y_2 \\ w_3 \\ \theta x_3 \\ \theta y_3 \\ w_4 \\ \theta x_4 \\ \theta y_4 + \Sigma \alpha y_4 \end{vmatrix} \qquad 3.55$$

The submatrices K_{mn} are 3 x 3 in size for the rectangular element since there are three degrees of displacement freedom corresponding to F_1. If the components of rotation αx_1 etc. are replaced by the relationships of equation 3.46 and separated from the slopes, equations 3.55 can be written as

$$F_1 = \left|K_{11},K_{12},K_{13},K_{14},K_{11}^{II},K_{11}^{III},K_{12}^{II},K_{14}^{III}\right| \begin{vmatrix} w_1 \\ \theta x_1 \\ \theta y_1 \\ w_2 \\ \theta x_2 \\ \theta y_2 \\ w_3 \\ \theta x_3 \\ \theta y_3 \\ w_4 \\ \theta x_4 \\ \theta y_4 \\ \alpha_1^1 c_1^1 + \alpha_1^2 c_1^2 \\ \alpha_1^1 s_1^1 + \alpha_1^2 s_1^2 \\ \alpha_2^1 c_2^1 + \alpha_2^2 c_2^2 \\ \alpha_4^1 s_4^1 + \alpha_4^2 s_4^2 \end{vmatrix} \qquad 3.56$$

The matrices K_{11}^{II} etc. are 3 x 1 in size and are simply columns of coefficients repeated from the matrices K_{11} etc. For example K_{11}^{II} is the second column of the matrix K_{11}. This column of coefficients multiplies the displacements θx_1 and $\alpha_1^1 C_1^1 + \alpha_1^2 C_1^2$. The Roman numeral denotes which of the columns (2nd or 3rd) is repeated. C_1^1 and S_1^1 etc. represent $(-\left|\text{cosine}\,\phi_1^{I\,1}\right|)$ and $(\left|\text{sine}\,\phi_1^{I\,1}\right|)$ respectively where the subscripts denote node numbers and the superscripts, the principal generalized stresses.

Once again equations 3.56 can be rearranged by multiplying the sines and cosines of the angles $\phi_i^{I\,t}$ by the stiffness coefficients. Restating equations 3.56 in this manner the forces become

$$F_1 = \left|K_{11}, K_{12}, K_{13}, K_{14}, K_{11}^{II}C_1^1 + K_{11}^{III}S_1^1, K_{11}^{II}C_1^2 + K_{11}^{III}S_1^2, K_{12}^{II}C_2^1, K_{12}^{II}C_2^2, K_{14}^{III}S_4^1, K_{14}^{III}S_4^2\right| \left|\begin{matrix} D_1 \\ D_2 \\ D_3 \\ D_4 \\ \alpha_1^1 \\ \alpha_1^2 \\ \alpha_2^1 \\ \alpha_2^2 \\ \alpha_4^1 \\ \alpha_4^2 \end{matrix}\right| \qquad 3.57$$

To simplify these equations a summation convention can be used to advantage and allows the following generalization of the external nodal force-displacement equations.

$$F_m = \left|K_{mn} \quad K_{mp}^{s}\right| \left|\begin{matrix} D_n \\ R_p^s \end{matrix}\right| \qquad 3.58$$

The summation convention applied here is the same as that explained by Hill[53] except here it applies independently to both subscripts and superscripts. For the rectangular element the subscripts and superscripts

have the following values:

$$\left.\begin{matrix} m \\ n \end{matrix}\right\} 1,2,3,4 \quad \left.\begin{matrix} p \\ q \end{matrix}\right\} 1,2,3 \quad \left.\begin{matrix} s \\ t \end{matrix}\right\} 1,2$$

The use of superscript t is shown in equations 3.54.

The next requirement is to establish, in matrix form, the internal principal generalized stress conditions that satisfy the yield criterion. By substituting the generalized stress equations 3.13 into equations 3.31 the principal generalized stresses can be written in matrix form as

$$\begin{vmatrix} M_1^1 \\ M_1^2 \end{vmatrix} = \begin{vmatrix} K_{11}^1, K_{12}^1, K_{13}^1, K_{14}^1, K_{11}^{1II}C_1^1 + K_{11}^{1III}S_1^1, K_{11}^{1II}C_1^2 + K_{11}^{1III}S_1^2, \\ K_{12}^{1II}C_2^1, K_{12}^{1II}C_2^2, K_{14}^{1III}S_4^1, K_{14}^{1III}S_4^2 \\ K_{11}^2, K_{12}^2, K_{13}^2, K_{14}^2, K_{11}^{2II}C_1^1 + K_{11}^{2III}S_1^1, K_{11}^{2II}C_1^2 + K_{11}^{2III}S_1^2, \\ K_{12}^{2II}C_2^1, K_{12}^{2II}C_2^2, K_{14}^{2III}S_4^1, K_{14}^{2III}S_4^2 \end{vmatrix} \begin{vmatrix} D_1 \\ D_2 \\ D_3 \\ D_4 \\ \alpha_1^1 \\ \alpha_1^2 \\ \alpha_2^1 \\ \alpha_2^2 \\ \alpha_4^1 \\ \alpha_4^2 \end{vmatrix} \qquad 3.59$$

These equations can also be stated generally by using the summation convention. That is

$$M_q^t = \left| K_{qn}^t \quad K_{qp}^{ts} \right| \left| \begin{matrix} D_n \\ s \\ R_p \end{matrix} \right| \qquad 3.60$$

Equations 3.58 and 3.60 can now be combined to form the required elastic-plastic nodal force-displacement relationships.

$$\left| \begin{matrix} F_m \\ M_q^t \end{matrix} \right| = \left| \begin{matrix} K_{mn} & K_{mp}^s \\ K_{qn}^t & K_{qp}^{ts} \end{matrix} \right| \left| \begin{matrix} D_n \\ R_p^s \end{matrix} \right| \qquad 3.61$$

The coefficients K_{mp}^s and K_{qp}^{ts} are determined systematically from the following equations. The Kronecker Delta δ_{ip} has its usual meaning:

$$\delta_{ip} = 0 \text{ if } i \neq p \text{ and } \delta_{ip} = 1 \text{ if } i = p$$

The coefficients are

$$K_{mp}^{s} = \delta_{1p}(K_{m1}^{II}C_1^s + K_{m1}^{III}S_1^s) + \delta_{2p}(K_{m2}^{II}C_2^s) + \delta_{4p}(K_{m4}^{III}S_4^s) \qquad 3.62$$

and

$$K_{qp}^{ts} = \delta_{1p}(K_{q1}^{tII}C_1^s + K_{q1}^{tIII}S_1^s) + \delta_{2p}(K_{q2}^{tII}C_2^s) + \delta_{4p}(K_{q4}^{tIII}S_4^s) \qquad 3.63$$

The summation convention which allows the generalization of the force-displacement equations (equations 3.61, 3.62 and 3.63) can be employed in deriving the stiffness relationships by computer.

3.6 The Total Structural Stiffness Matrix

Livesley[51] has outlined the procedures to follow in formulating the total structural stiffness matrix once the individual element stiffnesses have been established. To satisfy both equilibrium and compatibility for an elastic solution, the structural stiffness matrix can be assembled at the outset and need not be altered during the analysis. However, for an elastic-plastic solution this is no longer true. As the structure develops more plasticity, its total stiffness matrix must be altered in such a way that the stiffness of the structure is progressively reduced.

For elastic-plastic analyses of skeletal structures the reduction of stiffness can be achieved by two different methods. One method results in a decrease in the total number of stiffness equations by eliminating the displacement corresponding to the force which satisfies the yield condition. For members such as beams and columns the external nodal forces such as mx or my are the same quantities as the internal nodal bending moments. Therefore when the internal bending moment

attains the limiting yield value the external nodal force (say mx) also has this value. Consequently the corresponding displacement (slope θx) at that node can be eliminated from all the stiffness equations since mx is known. This reduces the total number of equations by one. Each of the remaining equations will include the limiting yield value which thereafter results in the internal bending moment at that node maintaining the yield condition.

A second method requires additional equations, one for each additional unknown plastic rotation. For uniaxial members (beams or columns) these rotations will occur at right angles to the longitudinal bending axis. The additional equations specify that the internal bending moments equal the limiting value. Both methods are identical with respect to the equilibrium of external nodal moments and internal bending moments. The first is an implicit formulation whereas the second is an explicit one.

For elastic-plastic bending of plate elements using the displacement approach of the present study, only an explicit formulation is possible. This follows from the fact that the external nodal forces such as mx and my are not the same quantities as the internal generalized stresses Mx and My. (Even if their dependence on one another were exactly known, the principal generalized stresses would have to be established in terms of these external nodal forces. The resulting non-linear relationship would make the elimination of the corresponding displacements θx or θy impossible). Consequently the total plate stiffness must be reduced by the addition of yield function equations. These equations prevent any increase in principal generalized stresses at plastic nodes when

the applied load is increased and the bending resistance of the plate is therefore reduced.

The stiffness equations for the plate resemble those of equations 3.61. If the displacement vector for the plate is

$$\left|\begin{matrix} Q \\ P \end{matrix}\right| = \left|\begin{matrix} D_1 \\ \vdots \\ R_1^1 \\ \vdots \end{matrix}\right| \qquad 3.64$$

and the force vector

$$\left|\begin{matrix} L \\ S \end{matrix}\right| = \left|\begin{matrix} \Sigma F_1 \\ \vdots \\ \Sigma M_1^1 \\ \vdots \end{matrix}\right| \qquad 3.65$$

then the total structural stiffness equations are

$$\left|\begin{matrix} L \\ S \end{matrix}\right| = \left|\begin{matrix} K(E.E) & K(E.P) \\ K(P.E) & K(P.P) \end{matrix}\right| \left|\begin{matrix} Q \\ P \end{matrix}\right| \qquad 3.66$$

The four groups of submatrices in the total stiffness matrix have coefficients that connect the following parameters;

K(E.E) - The external nodal forces L to the nodal slopes and vertical displacements Q.

K(E.P) - The external nodal forces L to the nodal plastic rotations P.

K(P.E) - The internal principal generalized stresses S to the nodal slopes and vertical displacements Q.

K(P.P) - The internal principal generalized stresses S to the nodal plastic rotations P.

The summation of the external nodal forces (see equations 3.65) must provide equilibrium with the applied loading at the nodes. Therefore the column matrix of equations 3.65 can be replaced by a column matrix

of applied loads. The solution of these equations determines the nodal displacements and these in turn allow the internal generalized stresses to be computed at each node of the plate.

In equations 3.66 the coefficients in the K(E.E) matrix are additions of those taken from the K_{mn} matrices in equations 3.61 for each element. These coefficients remain the same throughout the elastic-plastic analysis. The K(E.P), K(P.E) and K(P.P) matrices form from additions of the K_{mp}^{s}, K_{qm}^{t} and $K_{.qp}^{ts}$ matrices respectively. It is the formulation of these latter matrices for an elastic-plastic analysis that requires a much more sophisticated computer program than does an elastic analysis. However, the procedures required are systematic and lend themselves to a computerized formulation. Because of the non-linear form of equations 3.31 for certain plastic nodes, some of the coefficients in the K(E.P), K(P.E) and K(P.P) matrices may have to be changed after each plastic load increment since the directions of the principal planes and the plastic flow lines change (see sections 3.4e and 3.5d).

For a general plate structure with n nodes there would be 3n external nodal forces and 2n possible independent principal generalized stresses. Correspondingly, there would be 3n nodal displacements and a possible 2n independent plastic rotations. Therefore the total number of equations possible in equations 3.66 would be 5n. The size of sub-matrices in equations 3.66 would be

$$\begin{vmatrix} 3nx1 \\ 2nx1 \end{vmatrix} = \begin{vmatrix} 3nx3n & 3nx2n \\ 2nx3n & 2nx2n \end{vmatrix} \begin{vmatrix} 3nx1 \\ 2nx1 \end{vmatrix} \qquad 3.67$$

For a symmetrical plate structure the total number of equations can be reduced. For example, for the plates analysed in this study symmetry of plate geometry, loading and boundary conditions reduced 845 possible equations to 140 independent equations.

3.7 Load Application and Scaling Technique

(a) A Simplified Example

To illustrate the general procedures for determining plastic nodes and the final collapse of a plate, a simplified example is given in which only three plastic nodes cause the plate to collapse. The plastic nodes are i, j and k at which only the principal generalized stresses M_i^1, $M_j^{1;2}$ and M_k^1 satisfy the yield conditions. The larger principal generalized stress M_1^2 at node 1 is presented with those above to illustrate typical behaviour at a non-plastic node.

(b) Principal Generalized Stress-Applied Load Characteristics

If the principal generalized stress and applied load characteristics of each of the four nodes are plotted for each load stage causing plasticity, the complete elastic-plastic solution would result in five diagrams as in Figure 3.14.

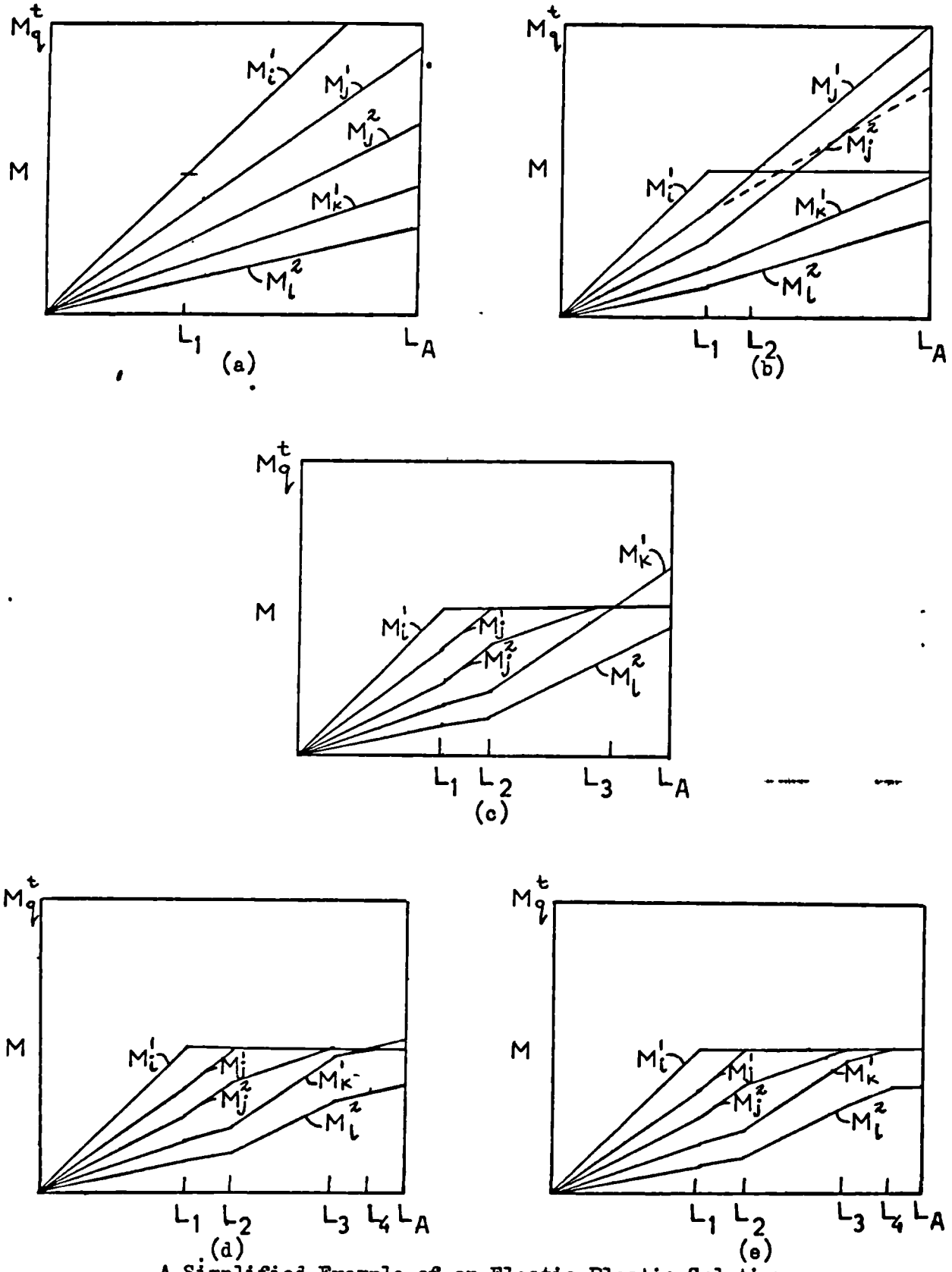

A Simplified Example of an Elastic-Plastic Solution

Figure 3.14

The load is applied in large increments and scaled until only one node becomes plastic within each increment. In the present study only scaling down procedures were adopted. Consequently the applied load had to be sufficiently large to form a collapse mechanism.

In Figure 3.14 the load L_A is applied and from the nodal displacements the generalized stresses (Mx, My and Mxy) are computed at all nodes. The principal generalized stresses are then determined. Those for the four nodes are shown in Figure 3.14a. The largest principal value at L_A is M_i^1. A scale factor is next computed such that $M_i^1 = M$, resulting in load stage L_1. The generalized stresses at L_A are scaled to L_1 and recorded for the next application of load (L_A). At node i the yield conditions ($M_i^1 = M$) is now maintained for the remainder of the analysis by introducing this condition into the stiffness equations for all elements joining at node i (see equation 3.60).

The load L_A is again applied and the principal generalized stresses computed. The variation in principal values between L_1 and L_A is different from before since the plate bending stiffness has been reduced (Figure 3.14b).

The largest principal value at L_A is now M_j^1. Again a scale factor is determined that results in node j becoming plastic at load L_2. The generalized stress field is scaled down to L_2 and recorded for the next increment of load. These steps are repeated until the third node becomes plastic with $M_k^1 = M$ at L_4. If the load L_A is again applied, no solution to the equations exists and this defines collapse of the plate.

The plastic load increments are o to L_1, L_1 to L_2, L_2 to L_3 and L_3 to L_4. The scale factors that determine the plastic behaviour are

computed from the generalized stresses (Mx, My and Mxy) at the beginning of a plastic load increment, the slopes of their variations and the principal generalized stress equations (either equations 3.31 if the node was previously non-plastic or 3.38 if previously plastic).

There are two types of scale factors, one for non-plastic nodes based on a non-linear variation of principal generalized stress and a second for nodes that were previously plastic due to one principal value and subsequently become plastic due to the second principal generalized stress. In Figure 3.14, the first type was used for nodes i, j and k in Figures 3.14a, b and d respectively. The second type was used in Figure 3.14c for node j.

To illustrate the calculation of these scale factors consider node j. Before plasticity occurs at j, the principal values M_j^1 and M_j^2 are computed by equations 3.31. If at node j, M_x^o, M_y^o , and M_{xy}^o are the generalized stresses at load L_1 with the orientation of principal planes given by ϕ_j^o , then the generalized stresses at some load stage between L_1 and L_A are simply

$$\begin{aligned} Mx &= M_x^o + \lambda_j \Delta Mx \\ My &= M_x^o + \lambda_j \Delta My \\ Mxy &= M_{xy}^o + \lambda_j \Delta Mxy \end{aligned} \qquad 3.68$$

since the generalized stresses vary linearly with displacements. In equations 3.68, λ_j is the required scale factor and ΔMx etc. are the rises of the generalized stress slopes between L_1 and L_A. Substituting equations 3.68 into equations 3.31 and rearranging to form a quadratic equation in λ_j gives

$$\lambda_j^{1,2} = (-B \pm \sqrt{B^2-4AC})/2A \qquad 3.69$$

in which

$$A = \Delta Mx\,\Delta My-(\Delta Mxy)^2$$
$$B = \Delta Mx M_y^o+\Delta My M_x^o-2\Delta Mxy M_{xy}^o-M(\Delta Mx+\Delta My) \qquad 3.70$$
$$C = M_x^o M_y^o-(M_{xy}^o)^2+(M)^2-M(M_x^o+M_y^o)$$

For negative bending, M is replaced by -M. The smallest positive λj from equations 3.69 is the relevant scale factor. Since $M_j^1 = M$ at L_2, let the scale factor be λ_j^1. In Figure 3.14b this scale factor leads to load L_2. With further increase in load, the principal generalized stresses M_j^1 and M_j^2 are assumed to vary linearly with displacements by maintaining ϕ_j^o (now computed at L_2) constant for load stage L_2 to L_A. This step requires that the principal generalized stresses be given by equations 3.38. If M_x^o, M_y^o and M_{xy}^o are recorded at L_2 (scaled from L_A by λ_j^1) a set of equations like that of 3.68 is substituted into equations 3.38 giving

$$\lambda_j^{1,2} = \frac{2M-(M_x^o+M_y^o)\mp(M_x^o-M_y^o)\cos(2\phi_j^o)\pm 2M_{xy}^o \sin(2\phi_j^o)}{\Delta Mx+\Delta My\pm(\Delta Mx-\Delta My)\cos(2\phi_j^o)\mp 2\Delta Mxy \sin(2\phi_j^o)} \qquad 3.71$$

The scale factor λ_j^2 results in $M_j^2 = M$ at L_3.

In Figures 3.14a to d the largest principal generalized stress at load L_A indicated which node was the next to become plastic. This is not always the case since the variation of principal values may result in some other node becoming plastic before the one indicated at L_A. For example in Figure 3.14b, if the variation of M_j^1 followed the broken line, M_j^2 would have exceeded M_j^1 at L_A. This would have led to a load causing $M_j^2 = M$ with $M_j^1 > M$. Therefore, once the scale factor is determined on the basis of the largest principal value at L_A and the generalized stress field scaled down, it is necessary to recompute

all principal generalized stresses at this scaled load stage to test for a violation of the yield criterion. If such a condition exists, then a new scale factor must be established to produce a lower load. This is repeated if necessary until only one additional node becomes plastic for each application of L_A.

3.8 Edge Beam Elements for Plates

(a) General

Beam elements can be readily included in the finite element method when applied to elastic plate bending analysis. Once the beam element stiffness matrices are determined, these elements can be joined to plate elements by the usual matrix methods.

The effects of edge beam elements on the elastic-plastic behaviour of plates is included in this study. The concept of plastic beam rotation is retained with the general formulation of the edge beam behaviour based on well established principles of structural mechanics. The simple principles involved in the composite yield behaviour between plate and beam elements illustrate how easily beam elements can be included in the present proposal.

(b) The Elastic Stiffness Matrix for Beam Elements in Bending

A typical beam element is shown in Figure 3.15. The convention for external nodal forces and corresponding displacements is the same as that for the plate elements. For beam elements the vertical shear forces are the same as the external nodal vertical forces V. Also the external nodal forces my and mx are the same quantities as the internal bending and twisting moments respectively. This was not the case for

plate elements.

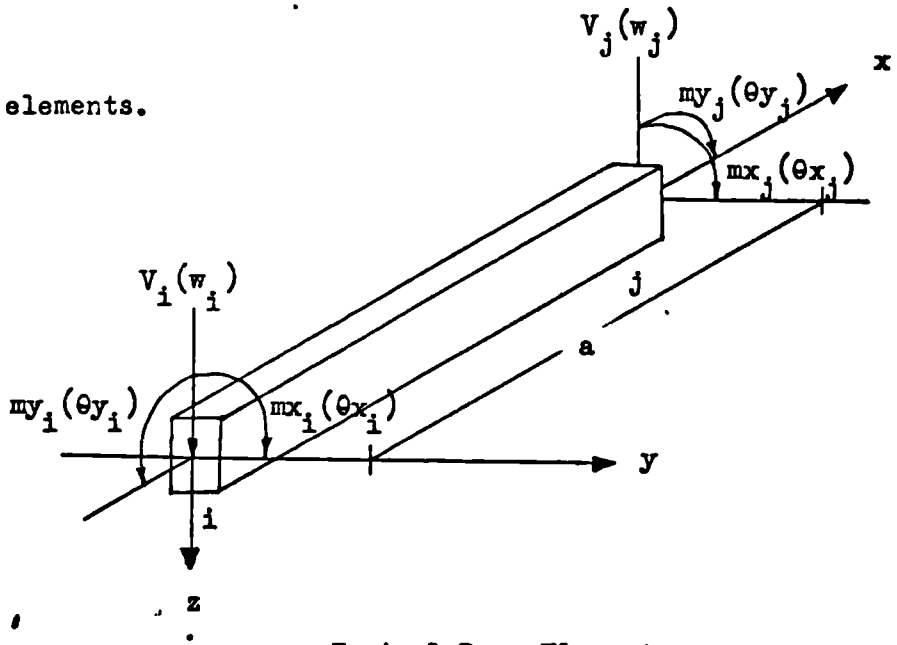

Typical Beam Element
with Positive Nodal Forces
and Corresponding Displacements

Figure 3.15

The internal shears and moments are based on the normal convention in which positive curvature is produced when beam fibres below the neutral axis are in tension. Shear forces are positive when their summation in the positive x direction acts downwards. This convention is consistent with that adopted for the plate elements (Figure 3.1) and is illustrated for a beam element in Figure 3.16.

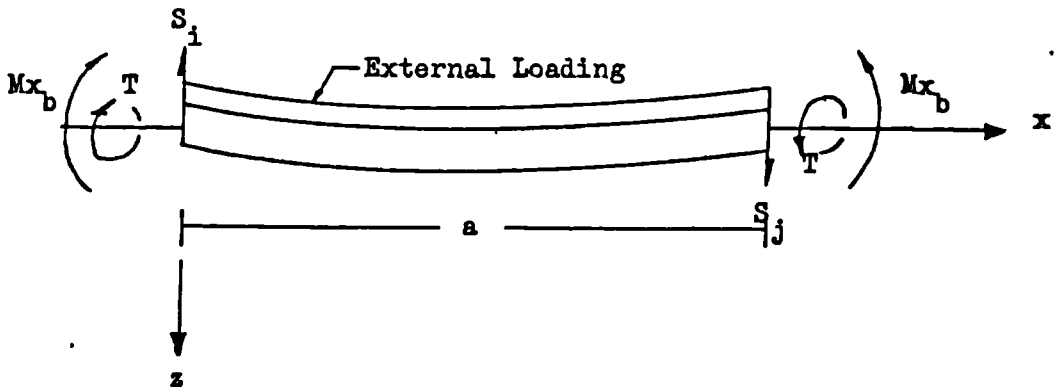

Beam Element
Internal Shear and Moment Convention

Figure 3.16

If EI is the flexural stiffness of the beam element, the bending moment in Figure 3.16 is simply

$$Mx_b = -EI\ w,xx \qquad 3.72$$

Following the same procedures of section 3.3 the stiffness matrix of the beam is next derived. The assumed displacement function of the beam is

$$w = b_1+b_2x+b_3x^2+b_4x^3 \qquad 3.73$$

The nodal displacements are functions of x and can be written as

$$u_i = \begin{vmatrix} w_i \\ \theta x_i \\ \theta y_i \end{vmatrix} = |u(x)|_i\,|\,b\,| \qquad 3.74$$

In general the displacements for both nodes of any beam element become

$$u = Gb \qquad 3.75$$

The corresponding external nodal forces at node i are

$$F_i = \begin{vmatrix} V_i \\ mx_i \\ my_i \end{vmatrix} \qquad 3.76$$

For the two nodes the force vector becomes

$$F = \begin{vmatrix} F \\ F^i_j \end{vmatrix} \qquad 3.77$$

By equation 3.72, if D_b = EI, the internal bending moments are

$$M = D_b\ k = D_b\ H\ b \qquad 3.78$$

In deriving the bending stiffness matrix the torsional behaviour can be excluded initially. The external work done by the nodal forces

in bending (F^*) acting through unit virtual displacements $\delta u^* = I$ is given by

$$We = \delta u^* F^* = IF^* = F^* \qquad 3.79$$

The internal work done by the bending moments through resulting curvatures δk is

$$Wi = \int (\delta k)^T M dx \qquad 3.80$$

From equations 3.75, $b = G^{-1}u$ and when substituted into equations 3.78 the moments become

$$M = D_b H G^{-1} u \qquad 3.81$$

For virtual displacements the resulting curvatures are simply

$$\delta k = H b = H G^{-1} \delta u^* . \qquad 3.82$$

Equating internal and external work in bending the nodal forces become

$$\begin{aligned} F^* &= \int (H G^{-1} \delta u^*)^T D_b H G^{-1} u dx \\ &= \left\{ (G^{-1})^T \left[\int H^T D_b H dx \right] G^{-1} \right\} u \end{aligned} \qquad 3.83$$

The quantity in the curled brackets is therefore the bending stiffness matrix for the beam element. This matrix is presented explicitly in Appendix I.

The torsional components of the element stiffness matrix can now be included. The torsional stiffness is the product of the polar moment of inertia of the cross-section and the modulus of elasticity in shear.

If the angle of twist per unit length of the beam element in Figure 3.15 is

$$(\theta x_i - \theta x_j)/a \qquad 3.84$$

then the external torsional moments mx_i and mx_j are

$$\begin{vmatrix} mx_i \\ mx_j \end{vmatrix} = GJ \begin{vmatrix} 0 & \frac{1}{a} & 0 & 0 & -\frac{1}{a} & 0 \\ 0 & -\frac{1}{a} & 0 & 0 & \frac{1}{a} & 0 \end{vmatrix} \begin{vmatrix} w_i \\ \theta x_i \\ \theta y_i \\ w_j \\ \theta x_j \\ \theta y_j \end{vmatrix} \qquad 3.85$$

By combining equations 3.83 and 3.85 the complete stiffness relationship between nodal forces and corresponding displacements can be determined for the beam in the matrix form

$$F = Ku \qquad 3.86$$

At nodes where beam and plate elements join there will be three displacements common to both elements. The assembly of the elements follows in the conventional manner by summing stiffness coefficients for each element. Therefore in the elastic response both equilibrium and compatibility are satisfied in the usual way.

3.9 Composite Yield Behaviour of Plates and Edge Beam Elements

(a) General

Wood[22] has developed the mathematical relationships for the elastic behaviour of plate-beam systems based on the small deflection theories of plate and beam bending. He included the effects of in-plane or membrane forces which occur when the centroids of the plate and beam do not coincide. The numerical solutions presented were based on the method of finite differences and the particular problems solved excluded the

effects of membrane forces, twisting moments in the beams and beam width.

In the present study similar simplifications are employed. The effects of membrane forces are excluded by maintaining plate and beam centroids at the same position. The beam elements have zero width so that the beam and plate have the same vertical displacement along their boundaries in the elastic case but not necessarily in the plastic case. However, at their junctions or nodes, they have the same vertical displacement throughout the elastic-plastic analysis.

The effects of torsional stiffness of beams are included in the structural interaction of plate and beam elements. The twisting moments are excluded from the yield criterion for the beams.

The neglect of membrane action was made not because its effect was considered negligible but rather to allow the development of the present elastic-plastic approach to proceed as a first approximation to what is in reality a complex structural problem.

(b) The Yield Behaviour of Beam Elements only.

It is assumed in the following presentation that a beam becomes plastic whenever the internal bending moment at a node attains a limiting value M_b. The effects of strain hardening are excluded but it need not be if a linear rule is selected. Once the limiting value is reached, displacement discontinuities (plastic rotations) are allowed at the node. The vector direction of these rotations is always perpendicular to the longitudinal bending axis of the beam.

A typical situation which illustrates the yield behaviour of two beam elements joined at node i is seen in Figure 3.17.

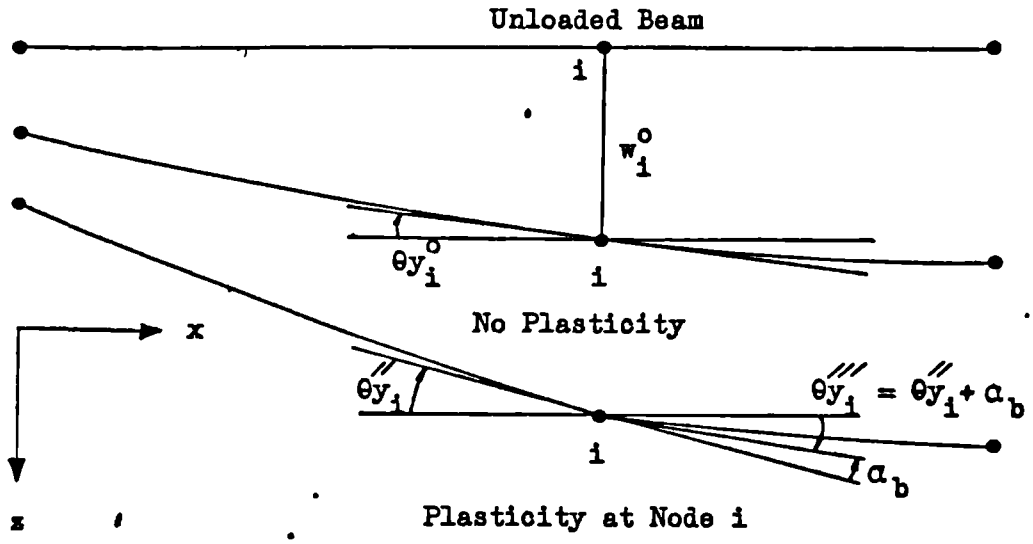

Plastic Behaviour of Beam Elements

Figure 3.17

Here the right-hand screw rule is applied to the displacements. The plastic rotation α_b is positive as shown since its vector direction is perpendicular to the plane of the page along the positive y axis. The introduction of beam elements and plastic rotations follows directly from the procedures adopted for plate elements.

The elastic-plastic stiffness matrix for beam elements that have plastic nodes can be derived by the methods of sections 3.5. The result would take the form of equations 3.61. For each new unknown (beam plastic rotation) there will be one additional equation to be satisfied ($Mx_b = M_b$).

(c). Composite Yield Behaviour at Nodes Common to Plate and Beam Elements.

Now that the yield behaviours of beam and plate elements have been developed separately the next step is to establish the composite yield behaviour for these elements when joined at common nodes. It is important to realize that a complex stress state exists at such interfaces and that only an idealized interaction of elements can be used to produce a tractable solution. From a stress analysis point of view the yield characteristics of the combined system cannot be separated into one system for beams and another for the plate. The following proposal is not based on the knowledge of the actual stress situation at such an interface but rather on well established theories of structural analysis and idealized material behaviour.

In this approach there are separate stress states in each of the two types of members. That is, the principal generalized stresses in the plate can occur in any direction relative to the bending axis of the beam but the beam bending stresses will always produce bending moments along the longitudinal bending axis. Therefore, if the yield behaviour of plate-beam elements is based on independent stress states, the resulting plastic flows in these elements are also independent of each other.

With the method of finite elements the separation of nodal force equilibrium and displacement compatibility between beam and plate elements allows the composite yield behaviour to develop in a manner consistent with the force-displacement approach to matrix structural analysis and the simple plastic theories of idealized member behaviour.

The fundamental idea adopted in the composite yield mechanism is that of a structural pin connection between plate and beam elements. This

pin allows the beam to bend and/or rotate freely about an axis normal to the plate elements at the common node. This results in different slopes occuring between plate and beam elements along the direction of the beam axis. These slopes are made independent of one another by separating the total equilibrium of nodal forces into one equilibrium condition for beam elements and another for plate elements. This pin concept then allows plastic rotations to develop separately in the plate and/or beam elements.

The differences between the composite yield behaviour of plate and beam elements and that for four plate elements are the introduction of different slopes about the y axis (see Figure 3.18) and the fact that the beam plastic rotation vector is always perpendicular to the beam bending axis and is independent of the yield behaviour of the plate elements.

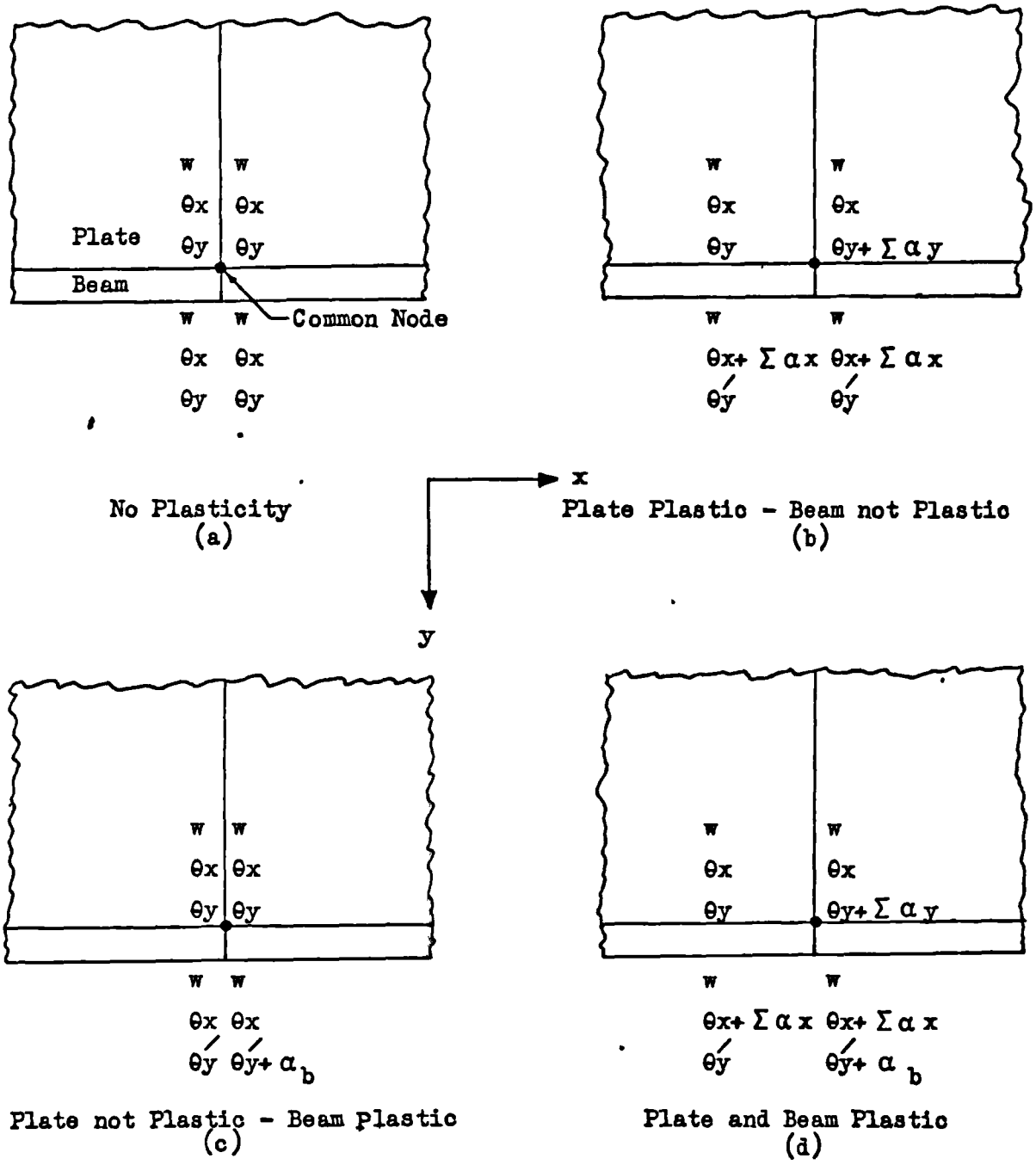

Composite Yield Behaviour at Plate-Beam Common Nodes

Figure 3.18

Figure 3.18 illustrates four possible displacement patterns for beam-plate nodes. Comparing Figure 3.18d with Figure 3.13b, the essential differences are $\theta y'$ (the beam slope) instead of θy for the beam elements and α_b rather than $\Sigma \alpha y$. The displacements $\theta y'$ and α_b are independent from those of the plate elements (θy and $\Sigma \alpha y$) and therefore additional independent equations must be available for their solution. For α_b the yield condition is simply that the beam bending moment

$$M_{Beam} = M_b \qquad 3.87$$

For $\theta y'$ the equilibrium of nodal forces on the beam elements requires that

$$\Sigma my_b = 0 \qquad 3.88$$

The subscript b denotes beam. In the plate element equilibrium of forces corresponding to θy requires that

$$\Sigma my_p = 0 \qquad 3.89$$

in which p denotes plate elements. When no plasticity occurs (Figure 3.18a) the slope $\theta y' = \theta y$ and the normal equilibrium of nodal forces requires that

$$\Sigma my_b + \Sigma my_p = 0 \qquad 3.90$$

The equilibrium of vertical and twisting (mx) nodal forces remains the same whether the node is plastic or not. That is

$$\Sigma V_b + \Sigma V_p = 0 \qquad 3.91$$

and $$\Sigma mx_b + \Sigma mx_p = 0 \qquad 3.92$$

Table 3.1 is a summary of the composite yield behaviour of plate and beam elements. For each yield condition the independent unknown displacements are given accompanied by the equations required to solve for these unknowns. Of the eight yield conditions presented there are only four different combinations of unknown displacements that must be allowed for in the elastic-plastic analysis.

Yield Conditions at Common Node	Independent Displacement Unknowns						Available Independent Equations						
	w	θ_x	θ_y	$\alpha^{1,2}$	θ_y'	α_b	$\Sigma V_p + \Sigma V_b = 0$	$\Sigma mx_p + \Sigma mx_b = 0$	$\Sigma my_p + \Sigma my_b = 0$	$M^{1,2} = M$	$\Sigma my_p = 0$	$\Sigma my_b = 0$	$M_{Beam} = M_b$
1. No Plasticity	x	x	x				x	x	x				
2. Plate only Plastic, One Flow Line only Parallel to Beam	x	x	x	x			x	x	x	x			
3. Plate only Plastic, One Flow Line only not Parallel to Beam	x	x	x	x	x		x	x		x	x	x	
4. Plate only Plastic, Two Flow Lines in any Direction	x	x	x	x	x		x	x		x	x	x	
5. Beam only Plastic	x	x	x		x	x	x	x			x	x	x
6. Beam and Plate Plastic at Different Times	x	x	x	x	x	x	x	x		x	x	x	x
7. Beam and Plate Plastic at Same Time	x	x	x	x	x	x	x	x		x	x	x	x
8. Beam Plastic with Plate Previously Plastic	x	x	x	x	x	x	x	x		x	x	x	x
9. Plate Plastic with Beam Previously Plastic	x	x	x	x	x	x	x	x		x	x	x	x

Plate-Beam Composite Yield Behaviour

Table 3.1

CHAPTER 4 - EXPERIMENTAL TESTS ON PLATES AND SLABS

4.1 General Remarks

To establish the validity of the analytical model a series of experiments was performed on four reinforced concrete slabs and four mild steel plates. The investigation includes the effects of two different point load arrangements on the metal plates and the effect of edge beams on the elastic-plastic response of both plates and slabs.

The plates, slabs and test procedures are described in this chapter; the results of the tests and their comparison with analytical results are presented in Chapter 5.

Reinforced Concrete Slab Tests

4.2 Purpose of Slab Tests and Quantities Measured

The basic purpose of the slab tests was to obtain certain data for comparison with the analytical results. Wherever possible the following items were recorded:

(i) Deflection contours.

(ii) General cracking behaviour and final collapse mechanism.

(iii) Internal generalized stresses in the slab.

(iv) Bending moments in the edge beams.

(v) The collapse load.

A summary of the slabs tested is presented in Table 4.1.

Description of Slabs Tested

Slab No.	Span L	Thickness t	$\frac{L}{t}$	Type of R/s	% R/s	Type of Concrete	Strength of Conc. Cube p.s.i.	Av. Depth to Steel d_1	Loading	Boundary Conditions	Items Recorded
1	36" x 36"	$1\frac{3}{4}$"	25.7	3/16" Ø M.S. @ 3" o.c.	.855	1:2:3 Mix $\frac{3}{8}$" Max. Agg.	6800 6970 7400	$1\frac{1}{4}$"	Central Point Load	Free Edges	Load, Deflections, Crack Pattern Formation
2	36" x 36"	$1\frac{3}{4}$"	25.7	$\frac{1}{8}$" x $\frac{3}{8}$" Flat M.S. @ 4" o.c.	.892	1:2:3 Mix $\frac{3}{8}$" Max. Agg.	6500 6650 7220	$1\frac{3}{8}$"		$\frac{3}{8}$" x $1\frac{1}{2}$" M.S. Edge Beam	Load, Deflections, Crack Pattern Formation, Strains for Beam Moments and Generalized Stresses
3	16" x 16"	$\frac{3}{4}$"	21.3	.040" x .25" M.S. @ 1" o.c. Perforated Sheet	1.20	1:2:3 Mix 3/16" Max. Agg.	6100 6455 6675	$\frac{5}{8}$"		Free Edges	Load, Deflections, Collapse Crack Pattern
4	16" x 16"	$\frac{3}{4}$"	21.3	.040" x .25" M.S. @ 1" o.c. Perforated Sheet	1.20	1:2:3 Mix 3/16" Max. Agg.	6250 6375 6500	$\frac{5}{8}$"		$\frac{5}{16}$" x $\frac{5}{16}$" M.S. Edge Beam	Load, Deflections, Strains for Beam Moments, Collapse Crack Pattern

Table 4.1

4.3 Generalized Stresses in Reinforced Concrete Slabs

It was realized at the outset of this investigation that the measurement and interpretation of bending strains in reinforced concrete is a difficult task. The approach adopted for the slab tests consisted of measuring strains on the top surface of the slabs and on the reinforcing steel. This provides an estimate of bending curvature.

The generalized stress-curvature characteristics of the slab were determined from a statically determinate bending test on a control beam specimen. From this test the applied bending moment per unit width of specimen (generalized stress) was known and the strain measurements (concrete compressive strain and reinforcing steel tensile strain) provided an estimate of bending curvature. Once this relationship was established and the curvatures measured in the slabs, the generalized stresses were determined.

4.4 Metal Edge Beams

Mild steel edge beams were used on slabs No. 2 and No. 4. Metal beams simplified casting of the slab structure and provided a more accurate means of measuring bending strains than would reinforced concrete beams. Furthermore, the neutral axis of the steel beam would be maintained close to the center of the beam, a condition that was assumed in the analytical study.

The bending moment-curvature characteristics of the edge beams were determined from a control specimen following the usual procedures discussed above.

The beams were connected to the slabs by threaded shear connectors that were wired firmly to the slab reinforcing steel. For the $\frac{3}{8}$" x $1\frac{1}{2}$" beams of slab No. 2, $\frac{1}{4}$" diameter bright mild steel connectors were used.

For slab No. 4, 3/32" diameter high strength steel screws were used. At the corners of the slabs, the beams were welded together. The beams were made of mild steel, British Standard 115.

4.5 Slab Reinforcement

The steel reinforcement for slabs No. 1 and No. 2 consisted of commercial black mild steel. For slab No. 1 round bars were used at approximately 3" spacing both ways. The two layers of steel had different total steel areas in an attempt to produce equal ultimate bending strength in the two orthogonal direction. However, this was not entirely successful since under test, slab No. 1 showed a definite weakness in one direction. Therefore, for slab No. 2 a flat bar rectangular cross-section was selected. The bars in one direction were staggered above and below those of the orthogonal direction. With this facility and the flat cross-sectional shape the effective steel layer depth was almost constant in all directions. This arrangement of reinforcement produced a more symmetrical pattern of cracks and deflections than did that for slab No. 1.

For the small slabs No.3 and No.4 the problem of unequal effective steel depths and unequal ultimate bending resistances was a more serious item to be considered than for the larger slabs. To overcome these difficulties a perforated sheet type of reinforcement was used. This was produced by punching 1" square holes in .040" thick mild steel sheet (British Standard En.3 series). The center of the holes were spaced 1¼" apart in two orthogonal directions. This gave a reinforcement mesh with steel strips .25" wide by .040" thick. This type of reinforcement reduced the effective bond between steel and concrete but the general performance of the slabs under test was good.

4.6 Strain Measurement

Electrical resistance foil type strain gauges were used. These gauges were purchased from Westland Aircraft Limited, Saunders-Roe Division, Osborne, East Cowes, Isle of Wight. Gauges of 1" gauge length were used on the surface of the concrete for slab No. 2 along with $\frac{1}{2}$" gauge lengths on the reinforcing steel and metal edge beams. For the edge beams of slab No. 4, $\frac{1}{4}$" gauge lengths were used. For the gauges on the reinforcement protection against water damage was provided by a covering of Araldite and a rubberized coating. All exterior surface mounted gauges were covered with a temperature protecting grease and polythene sheeting. Some gauges were connected to dummy gauges to compensate for strain errors resulting from temperature changes during the tests. Other pairs of gauges were wired to read only bending strain.

All strain recordings were made by a 10 channel portable data logger manufactured by Westland Aircraft Limited. This logger was extended to 20 channels, each channel requiring $1\frac{1}{2}$ seconds to register a reading.

4.7 Slabs No. 1 and No. 2

These slabs were cast in the mould shown in Photo 4.1. The mould was covered with contact paper to prevent water entering the shuttering and to produce smooth surfaces on the slabs. In this photo are pictured the reinforcement, strain gauge positions, edge beams with shear connectors for slab No. 2. For each slab a control beam specimen was also cast. This specimen represented $\frac{1}{3}$ the width of the slabs. The mould used is pictured in Photo 4.2. Also shown are the gauges for determining the steel tensile strain leading to curvature measurements. Three positions were used in determining the bending-curvature characteristics as a check against faulty readings. Two point loading was applied approximately at one

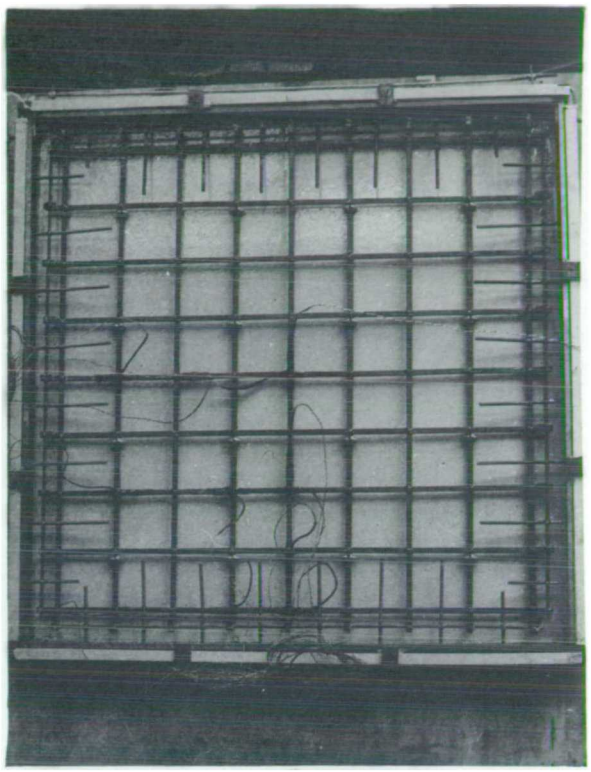

Photo 4.1

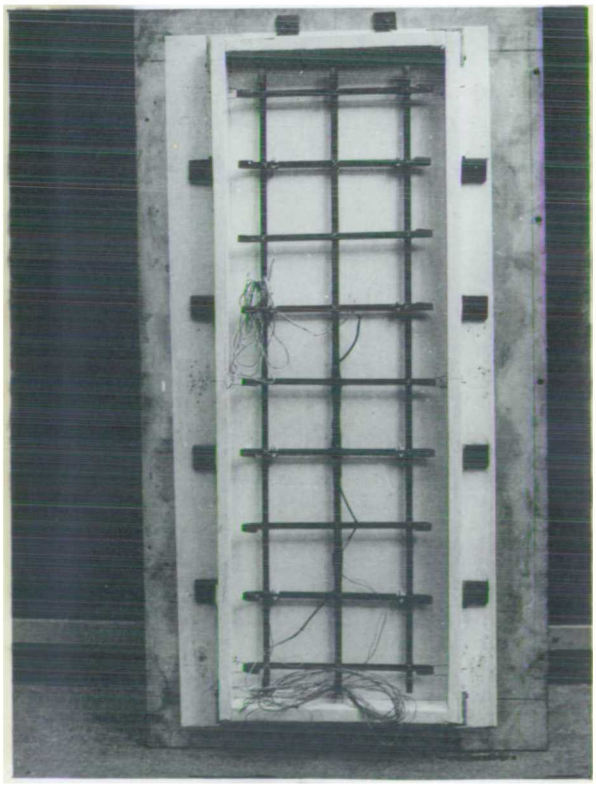

Photo 4.2

third span intervals resulting in constant moment over the middle third of the span.

The general arrangement for tests No. 1 and No. 2 is shown in Photo 4.3. The slabs were tested vertically to permit the taking of photographs of crack patterns as they developed during the test. The underside of each slab was covered with a fine coating of white Snowcem to help detect cracking. A 3" square grid was marked out to correspond to the 12 x 12 mesh of finite elements adopted for the analytical model.

Each corner of the slab was supported against transverse displacement by 1" diameter steel balls. In-plane movement was allowed. A central point load was applied by hydraulic jack, the load being distributed over a 3" diameter hard rubber pad $\frac{1}{4}$" thick. The load was measured using a high strength steel proving ring as well as a load cell as a double check.

Deflections were recorded by the dial gauges shown in Photo 4.3. These gauges were connected by fine high tensile steel wire to the top surface of the slab. Readings were recorded by a 35mm. camera. Photo 4.4 is a typical set of deflection readings. Also shown are the surface mounted adapters for connecting the wire to the slab surface. Deflections were measured over $\frac{1}{8}$th of the slab area at 3" intervals as shown. Deflections at a number of other points were also measured to check symmetry of transverse movement.

The data logger and load cell measuring equipment are also pictured in Photo 4.3.

4.8 Slabs No. 3 and No. 4

These slabs were tested using the apparatus designed for the metal plate tests. They were corner supported and centrally loaded. Slab No.4

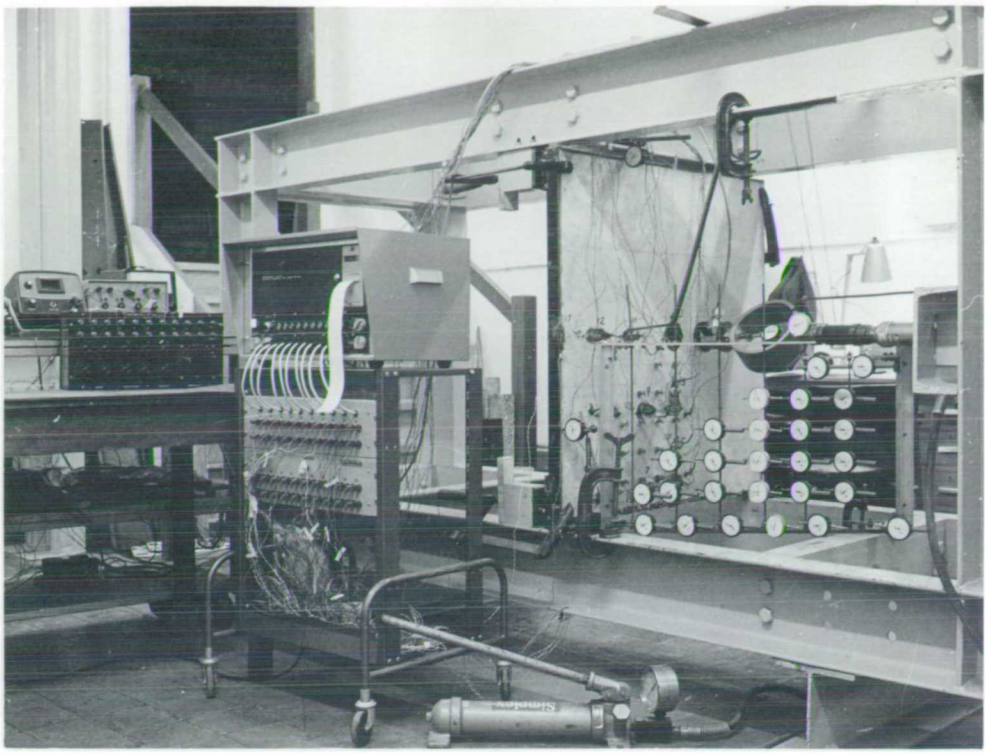

Photo 4.3

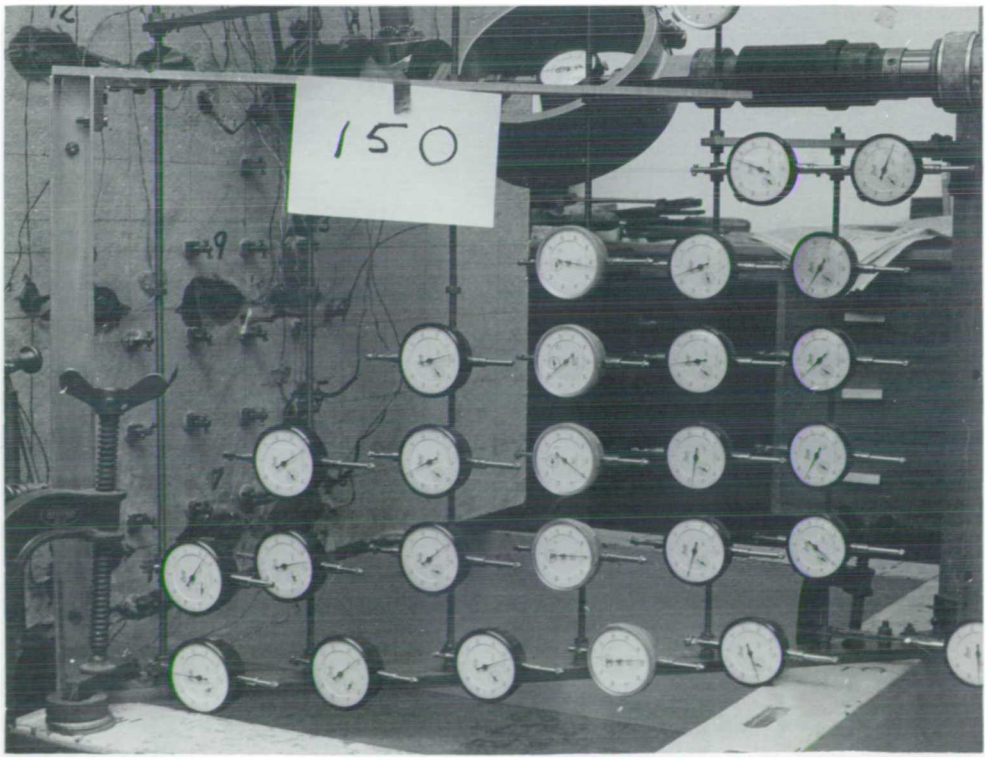

Photo 4.4

had square cross-sectional metal edge beams. Strain measurements were made on these edge beams but no attempt was made to place gauges in the slabs on the reinforcement. Photographs were taken of the crack patterns at collapse. Deflections were recorded at two positions; at the center and at mid-span along the edge.

These tests were performed to check the analytical results with small scale or model slabs.

Mild Steel Plate Tests

4.9 Purpose of Plate Tests and Quantities Measured

The following items were measured in the metal plate tests for comparison with analytical results:

(i) Deflections at center of plate and/or at mid-span on the edges.

(ii) Internal generalized stresses.

(iii) Bending moments in the edge beams.

(iv) The collapse load.

A summary of the plates tested is presented in Table 4.2.

Description of Plates Tested

Plate No.	Span L	Thickness t	$\frac{L}{t}$	Type of Steel	Treatment	Loading	Boundary Conditions	Items Recorded
1	16" x 16"	$\frac{1}{2}$"	32	Mild Steel B.S.115	Tested as Purchased	Central Point Load	Free Edges and Corner Supports	Load, Deflections, Strain for Generalized Stresses
2	16" x 16"	$\frac{1}{2}$"	32	Mild Steel B.S.115	Normalized	Central Point Load	$\frac{3}{4}$" x $1\frac{1}{2}$" Channel Mild Steel Edge Beams and Corner Supports	Load, Deflections, Strain for Edge Beam Moments and Generalized Stresses
3	16" x 16"	$\frac{1}{2}$"	32	Mild Steel B.S.115	Normalized	Four Point Loads	Free Edges and Corner Supports	Load, Deflections, Strain for Generalized Stresses
4	16" x 16"	$\frac{1}{2}$"	32	Mild Steel B.S.115	Normalized	Four Point Loads	$\frac{3}{4}$" x $1\frac{1}{2}$" Channel Mild Steel Edge Beams and Corner Supports	Load Deflections, Strain for Edge Beam Moments and Generalized Stresses

Table 4.2

4.10 Generalized Stresses in Metal Plates

The measurement of generalized stresses in metal plates did not present any particular difficulties. Foil type electrical resistance strain gauges with $\frac{1}{2}$" gauge lengths were used on all plates and edge beams. Principal generalized stresses were determined at certain locations by using a rectangular type of strain rosette.

The generalized stresses were determined using generalized stress-curvature characteristics computed from bending tests on control beam specimens. Bending moment-curvature relationships for the metal edge beams were also determined from control specimen tests.

Strain gauges were placed on the top and bottom surfaces of the plates and edge beams for curvature measurement. Both bending and in-plane strains were measured. Dummy gauges were used in conjunction with certain active gauges. All gauges were protected against the effects of temperature differentials and air currents on strain measurement.

4.11 Metal Edge Beams

Metal edge beams were welded on plates No. 2 and No. 4. These beams were made from commercial black mild steel and had a $\frac{3}{4}$" x $1\frac{1}{2}$" channel cross-section. The ends of the beams were mitred and welded together at the corners of the plates. The beams were welded to the plates (continuous fillet welds on top and bottom of plate) such that the centroid of the beam coincided with the middle plane of the plate.

4.12 Metal Plates No. 1 and No. 2

All the plate tests were performed using a Denison tension-compression machine. Plates No. 1 and No. 2 were loaded at their centers by a point load distributed over a $\frac{3}{4}$" diameter circle. Plate No. 1 had free edges

with vertical corner supports. This plate is shown in Photo 4.5 prior to testing. Plate No. 2 had the same loading and general test arrangement except for metal edge beams around its periphery. The steel support plates at the corners housing the 1" diameter steel balls were attached to the plate specimens by three high tensile $\frac{1}{4}$" diameter screws. The 1" diameter balls were held in position under the corner of the plates by countersunk holes in the corner support plates.

4.13 Corner Support Columns

The loading and boundary conditions selected for all the tests (plates and slabs) were selected to allow the plates and slabs to deform into developable surfaces and thereby reduce the chance of membrane forces developing. For the metal plates, special corner support columns were constructed to allow freedom of horizontal movement and also rotation in the vertical plane.

Photo 4.6 shows the pipe column support with the lower distribution plate welded to the top of the column and carrying an array of $\frac{3}{8}$" diameter steel balls set in a perspex mould. The purpose of these balls is to allow horizontal movement. An upper distribution plate was placed on top of these balls (Photo 4.5) and it in turn supported the 1" diameter ball and plate structure. The exposed faces of the upper and lower distribution plates were covered with spring steel sheet material to prevent indentation of steel balls under load.

These supports proved very valuable in eliminating in-plane forces and allowed the plates to develop definite collapse mechanisms. The supports were also lubricated with oil to further reduce frictional effects.

Photo 4.5

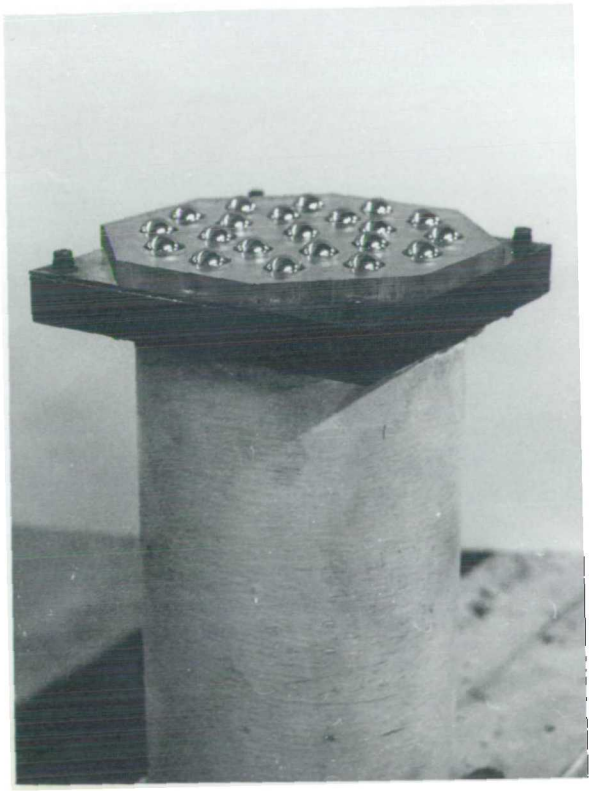

Photo 4.6

4.14 Metal Plates No. 3 and No. 4

These plates were made identical to plates No. 1 and No. 2 respectively. However, plates No. 3 and No. 4 were loaded by four point loads positioned as shown on plate No. 4 in Photo 4.7. The steel core cables shown were purchased from British Ropes Limited.

To apply the load from under the plates, a loading yoke was constructed for use on the compression head of the Denson machine. This yoke is shown in Photo 4.8 along with a statically determinate system of load distribution beams. The four uppermost cables in Photo 4.8 are the same cables pictured in Photo 4.7. The top center of the yoke was fastened to the compression head. The yoke and distribution beams were assembled around the plate structure. A typical arrangement of applying the four point loads (in this case plate No. 3) is seen in Photo 4.9.

The general test arrangement is shown in Photo 4.10. All strain measurements were recorded by the data logger previously mentioned. As an added precaution against effects of temperature change and drafts on the strain measurements, the entire loading area of the Denson machine was enclosed in polythene.

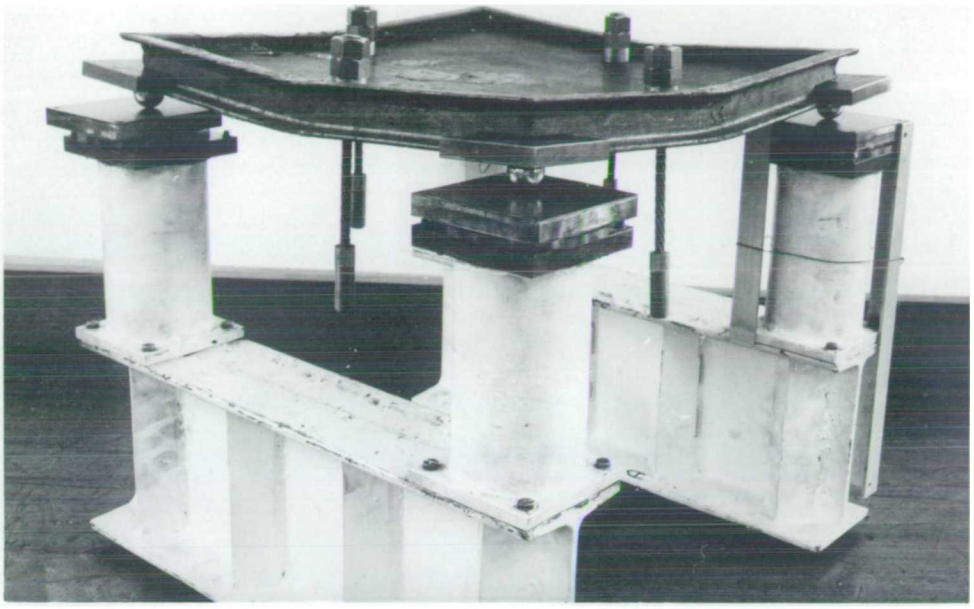

Photo 4.7

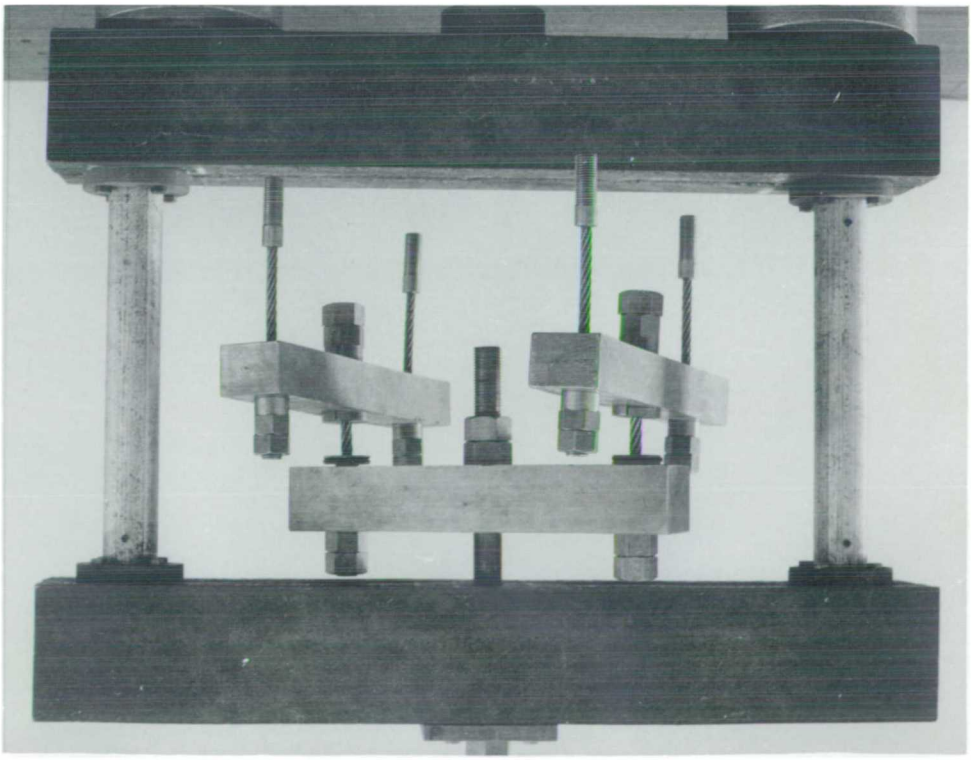

Photo 4.8

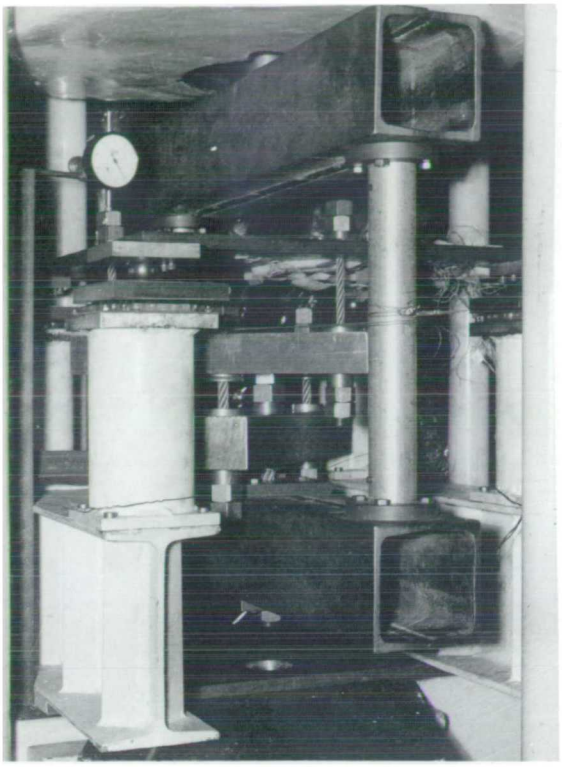

Photo 4.9

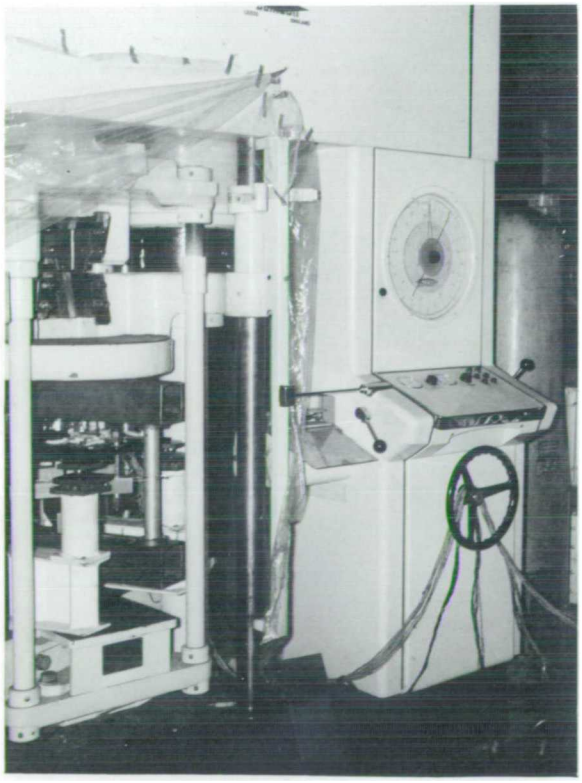

Photo 4.10

CHAPTER 5 - COMPARISON OF EXPERIMENTAL AND ANALYTICAL RESULTS

5.1 General Remarks

In this chapter the experimental results from the tests of plates and slabs described in Chapter 4 are presented and compared with those produced by analytical analyses based on the theory of Chapter 3.

The test results for slabs are presented in four separate groups, one for each slab test. Deflections for all slabs measured at mid-span on the slab boundaries and under the point load are presented at the end of the slab tests. For slabs No. 1 and 2 crack formations and deflection contours were recorded over most of the applied load range. For brevity only the crack patterns and contours for the elastic limit stage (according to the analyses) and one other load stage within the elastic-plastic behaviour are presented. For slab No. 1 the last recorded contours were measured at 85.5% of the analytical collapse load.

The metal plate results follow those for the slabs and are presented in the same fashion. In addition to the grouping of deflections at the end of the plate tests, results from the measurements of principal plane directions are presented. Also evidence of inhomogeneous plastic deformation is reported with photographs from two plate tests showing the formation of Lüders lines. An explanation of the stress states is given with analytical predictions of their formation.

The results of both plate and slab tests are presented in separate sections independent of each other. No comparisons of plate or slab tests with each other are made although the tests were organized so that such comparisons would be possible. They are not reported since the primary purpose of the tests was to assess the validity of the

analytical model.

The graphs are numbered with reference to test type and number. For example P4.6 refers to the sixth graph of results from plate test No. 4. The ordinates on graphs of generalized stresses and edge beam bending moments are labeled M/M_c where M refers to the item measured (indicated at the top center of the graph) and M_c has the meanings: Mu for the ultimate bending resistance of reinforced concrete, M_p for metal plate sections and M_b for metal edge beams. In Chapter 3, M_c was called M to prevent possible confusion with the use of suffix notation. The generalized stresses M_{LP} and M_{SP} denote largest and smallest principal values respectively. M_{bm} refers to beam bending moment.

For the graphs of deflections, the abscissa (W/t) is the ratio of transverse displacement to the total thickness of plate or slab. The label P/P_c in all graphs is the ratio of applied load to the collapse load determined from limit analysis.

The estimation of collapse load for the slab tests reported was a simple matter. However, for the metal plates although the same could not be said, there was a definite indication of limit behaviour in all the plate tests. The maximum load reached was governed to a large extent by the rate at which load was applied. For example in plate test No. 1 the maximu[illegible]ad reached was about 20% above the limit analysis value. This p[illegible] from increasing the load too rapidly without allowing th[illegible] deform sufficiently between load stages. For the three [illegible]s, the load was allowed to remain constant until all t[illegible] ceased. The limiting loads for these tests were quite [illegible]d collapse load. The freedom of movement

given by the support columns described in Chapter 4 were primarily responsible for allowing the plates to deform into collapse mechanisms.

Most of the experimental results were processed by computer. Separate computer programs were written for each of the metal plate tests and for slabs No. 2 and No. 4. Many readings were recorded especially of strain by the data logger to eliminate gross errors due to faulty recordings. The accuracy (with respect to strain measurement) in determining generalized stresses is in the order of $\pm$ 10%. Only a sample of the experimental results was selected for the graphs presented. Approximately three times as many recordings were made as are shown on the graphs. The analytical results, however, are shown at each stage of plasticity (where possible) causing plastic nodes.

The analytical results were determined from computer solutions for each plate and slab tested. These solutions were based on the theoretical procedures of Chapter 3 and give complete generalized stress and displacement fields for each load causing a plastic node. For a general account of the elastic-plastic behaviour, plastic flow patterns are presented at the beginning of each test description. Each pattern consists of a 12 x 12 mesh of square finite elements showing the plastic flow lines inclinded to the element boundaries at the appropriate angles. These flow lines are really only tangents to the actual flow line trajectories. The configuration shown in each pattern represents the collapse stage pattern of flow lines. However, patterns developed at other load stages before collapse can also be determined since on the left of the pattern is listed the ratio of applied (computer) load P to the limit analysis collapse load P_c for each stage of plasticity.

The final collapse pattern is simply a superposition of patterns for each plastic node. The order in which plasticity occurs is also given with the load ratios. These integers are shown beside the plastic nodes corresponding to the load ratios.

Below the pattern, the collapse load by computer (P) is stated to three decimal places. Also shown is the limit analysis collapse pattern giving an upper bound P_c to the collapse load. To the right of the limit analysis collapse mechanism, the ratios of computer elastic limit and collapse loads to the limit analysis value are indicated.

To the left of the limit analysis solution is listed the strength and stiffness parameters used in the computer solution. Each solution is based on a non-dimensional limiting generalized stress value of unity so that the generalized stress fields were output in the ratio of M/M_c. To determine other quantities that are not ratios of M_c, the computer results were multiplied by the experimental limiting values (M_cL/D) of Tables 5.1 and 5.2. The Poisson ratio used for concrete was .15 and for steel .30.

When reference is made to the finite element method, the abbreviation F.E.M. will be used.

Reinforced Concrete Slab Tests

5.2 Stiffness and Strength Parameters

These parameters pertaining to the slab tests are presented in Table 5.1. Most of the items shown have been measured experimentally. The measurements and calculations for these quantities are presented in

Item	Slab No.1	Slab No.2	Slab No.3	Slab No.4
D Lb in.	354,000	353,000	58,800	58,800
$\frac{M_u L}{D}$	.1280	.1060	.0464	.0464
EI $Lb\ in.^2$	0	3,640,000	0	16,200
$\frac{M_b}{D}$	0	.0226	0	.00493
$\gamma_e = \frac{EI}{DL}$	0	.2860	0	.0172
$\gamma_p = \frac{M_b}{M_u L}$	0	.2140	0	.1065
$\gamma_t = \frac{GJ}{EI}$	0	.00705	0	0.480

Stiffness and Strength Parameters for Slab Tests

Table 5.1

Appendix III. The polar moments of inertia in the γ_t ratio for the edge beams on plates and slabs were determined from the results of St. Venant's analysis on torsion of non-circular cross-sections reported by Seely and Smith[58]. The analytical solutions are also based on the parameters of Table 5.1 and are therefore directly comparable with the experimental results.

The slab stiffness D for slab No. 2 was determined from the moment-curvature relationship for the concrete control specimen (see Appendix III). The stiffnesses for the other slabs were determinded on the basis of a "cracked to the neutral axis" cross-section. That is, the entire slab was considered cracked with a constant flexural stiffness maintained throughout the analysis.

5.3 Slab No. 1

(a) Plastic Flow Pattern

Pattern No. 1 shows the directions of the plastic flow lines that form at the nodes where the limiting principal generalized stress is attained.

In this computer solution the end of the elastic limit occurred when the center of the slab became plastic at 55.7% of the collapse load. A total of eight plastic points reduces the plate to a mechanism with a collapse load identical to that given by limit analysis. The only difference between the plastic flow pattern shown and the mechanism of limit analysis is the indication of plasticity on the diagonals close to the point load. This local plastic behaviour is to be expected and spreads radially from the center of the plate.

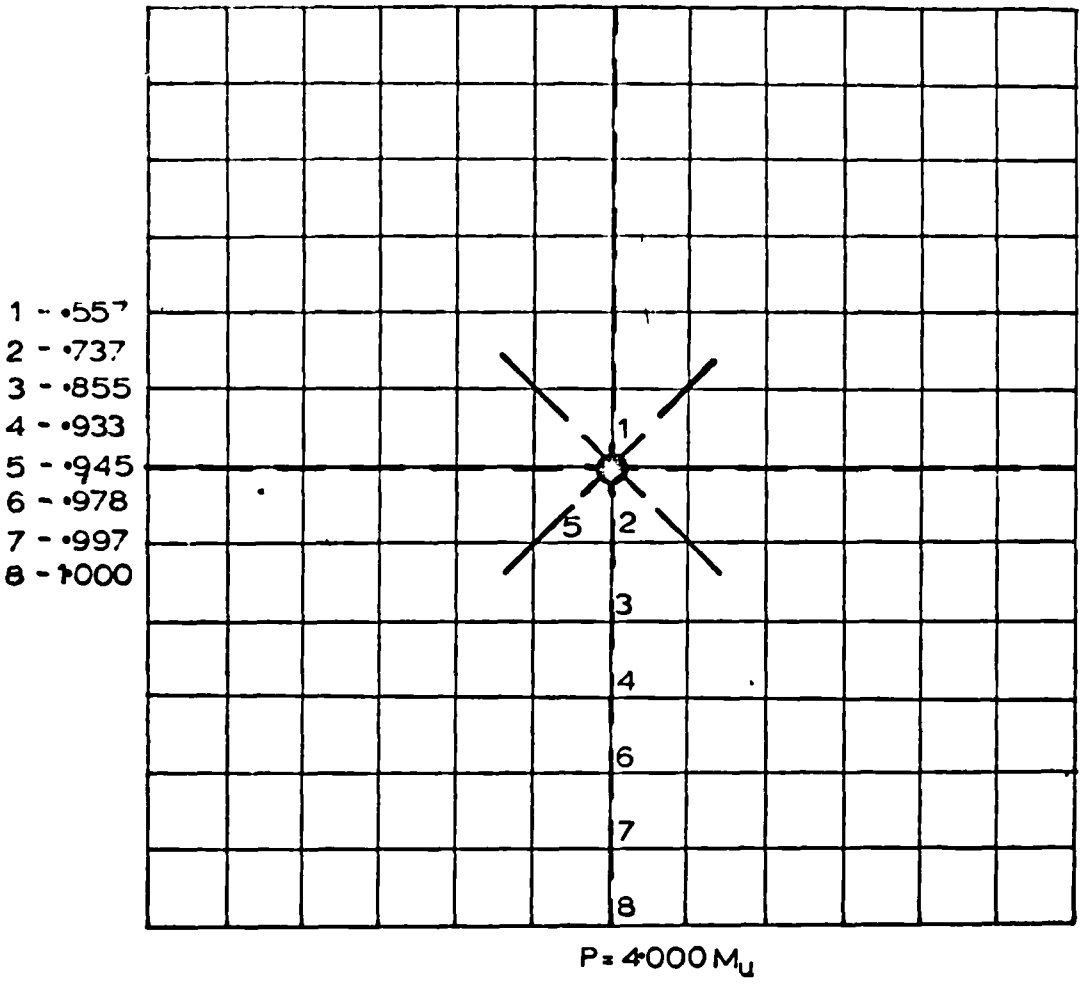

ν = ·15

M_u = 1·0 D/L

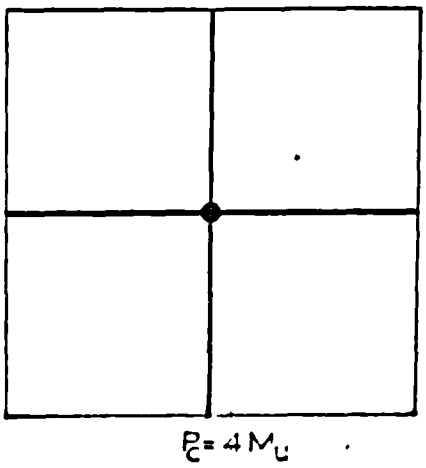

$\frac{P_e}{P_c}$ = ·557

$\frac{P}{P_c}$ = 1·000

Pattern No. 1

(b) Crack Pattern at End of Elastic Behaviour

The crack pattern which developed at the end of the elastic behaviour (P/P_c = .557 as predicted by computer) is shown in Figure 5.1. These cracks were visible to the naked eye. Most cracks formed at about 35% of the collapse load. The corresponding analytical plastic flow is superimposed on this crack pattern in Figure 5.1.

(c) Deflection Contours at End of Elastic Behaviour

The contours of Figure 5.2 show symmetry of transverse displacement. During the test, deflections were recorded at mid-span on all the edges to establish the degree of symmetrical behaviour. The deflections in one direction exceeded those of the orthogonal direction by as much as 30%. Therefore deflections recorded by the bank of gauges had to be adjusted by an averaging process governed by the corresponding deflections in other parts of the slab. The maximum deflection at the center under the point load represents approximately 1/80 of the span.

From Figure 5.2 it is clear that the finite element model underestimates the stiffness of the slab resulting in displacements far greater than actually occur. This is to be expected since the stiffness used in the analyses was based on the cracked concrete section. In Figure 5.1 although a substantial area of the slab is cracked, these had not penetrated far enough into the slab section to reduce the stiffness to the degree assumed.

(d) Crack Pattern at 85.5% of Collapse Load

Figure 5.3 indicates the formation of additional cracks to those of Figure 5.1 and also the opening of those where the ultimate bending

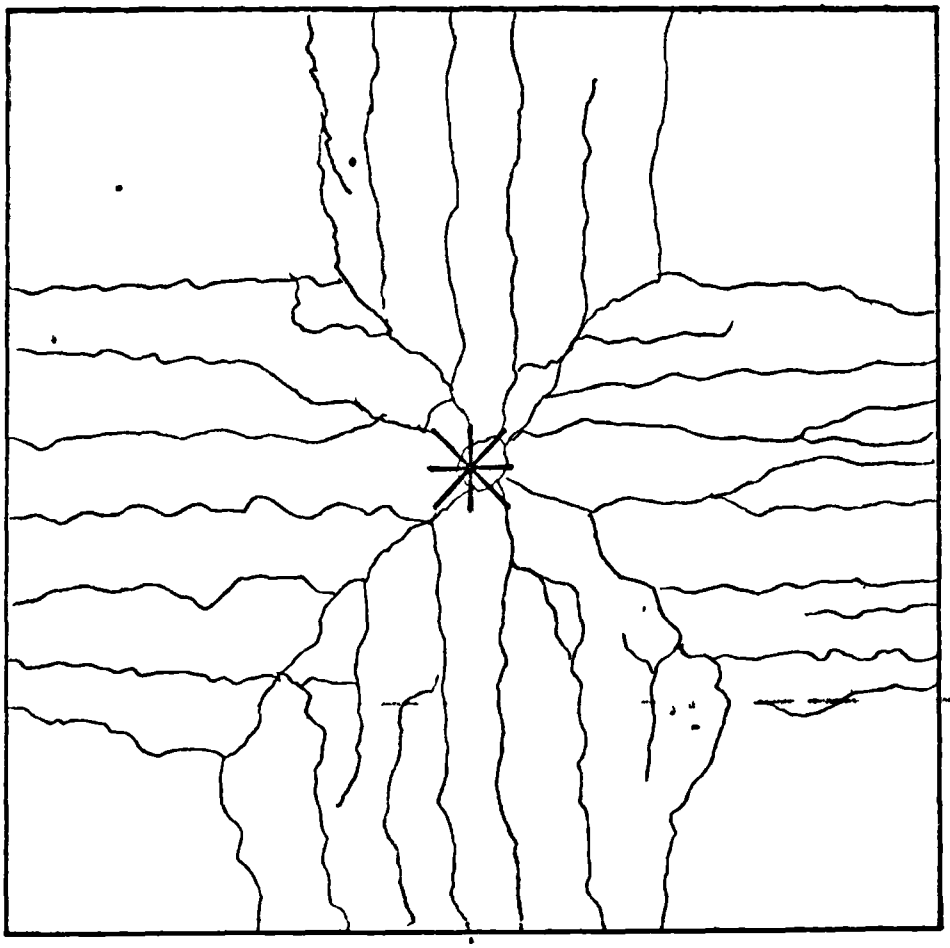

Slab No.1 - Crack Pattern at $P/P_c = .557$

Figure 5.1

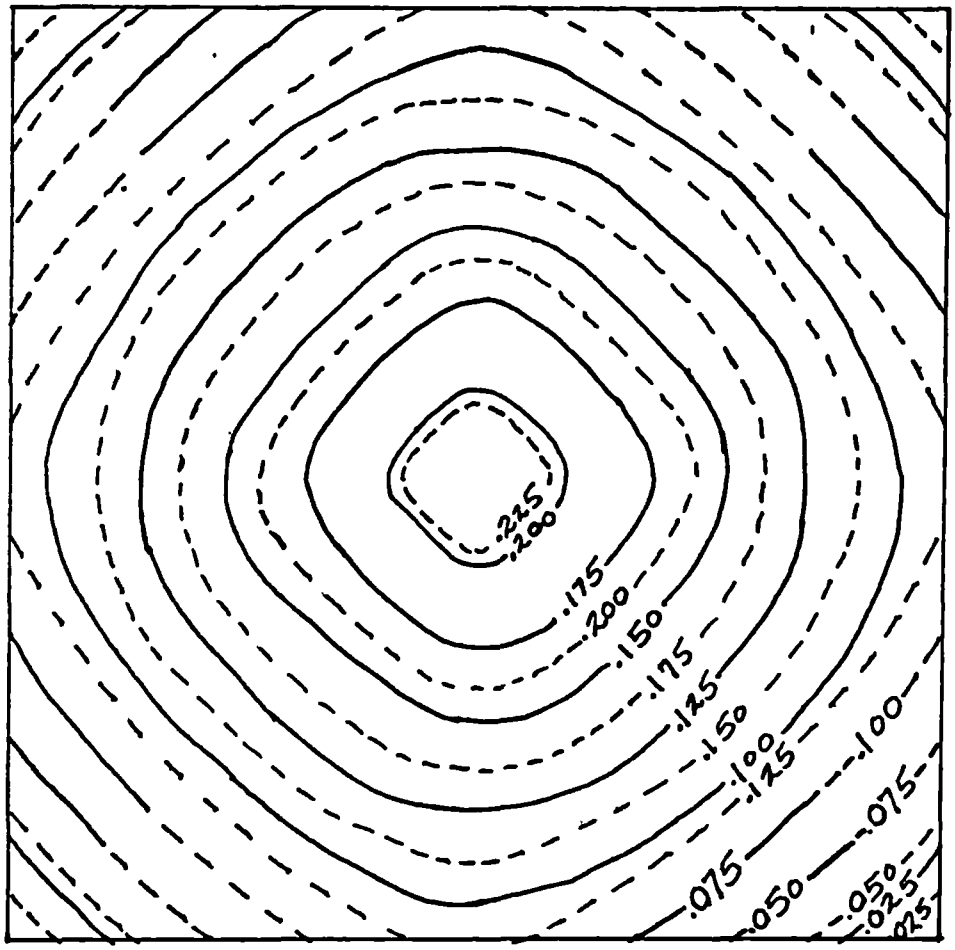

Computer - - - -
Experimental ———

Slab No.1 - Deflection Contours at P/P_c = .557

Figure 5.2

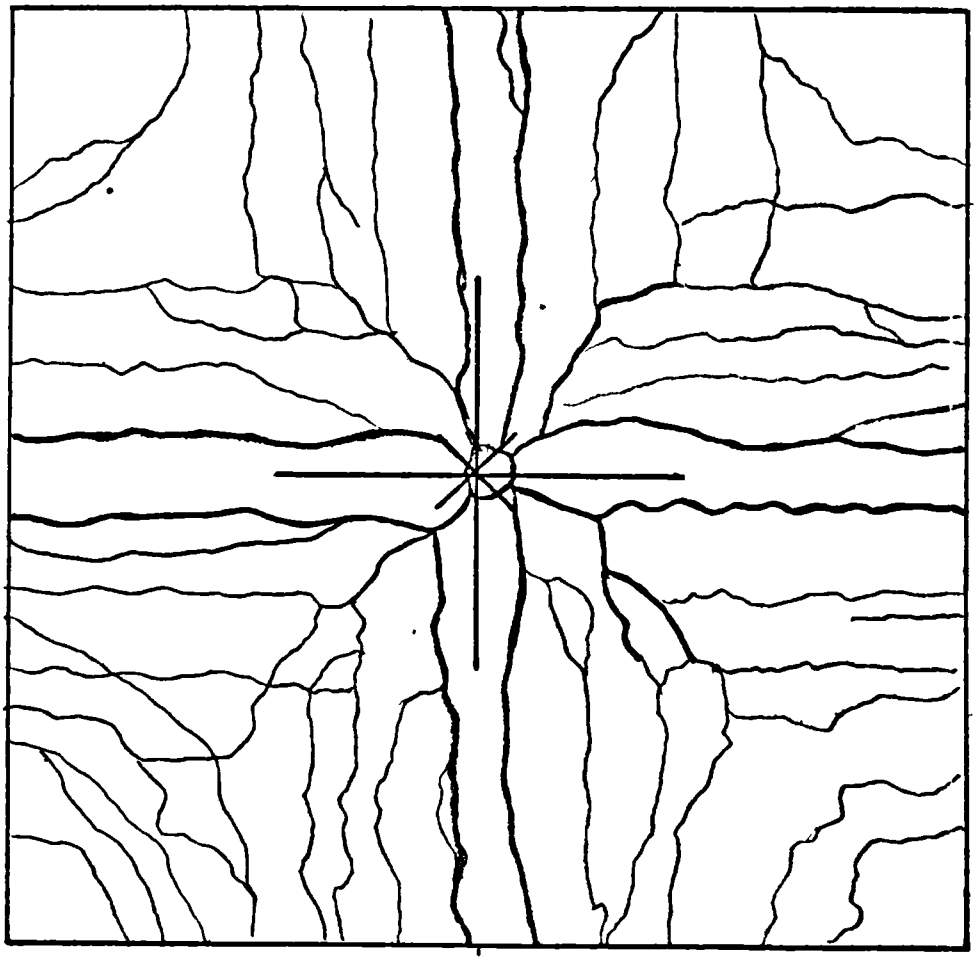

Slab No.1 - Crack Pattern at $P/P_c = .855$

Figure 5.3

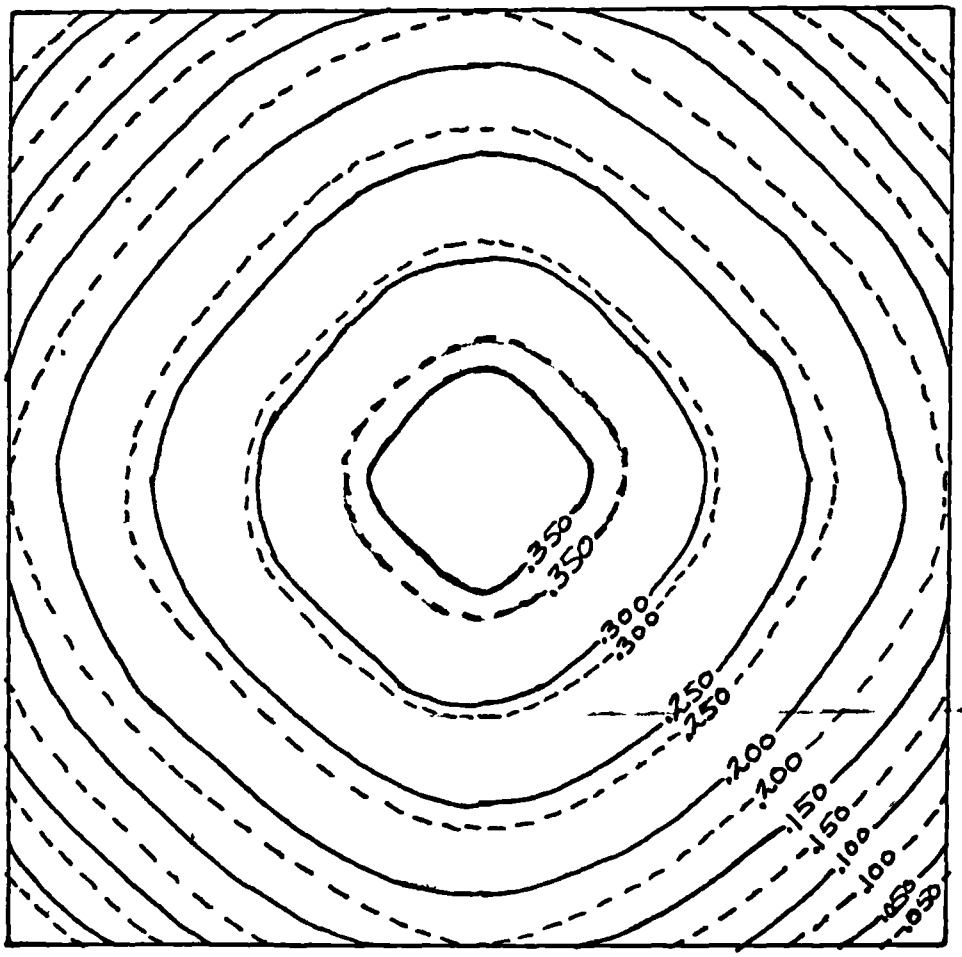

Computer - - - - -
Experimental ———

Slab No.1 - Deflection Contours at P/P_o = .855

Figure 5.4

resistance is reached. Although the applied load was only 85.5% of the limit analysis collapse load, the final crack pattern had already formed. Upon further increase of load these cracks simply opened allowing the final mechanism to develop.

The F.E.M. flow pattern as developed at this load stage is also shown in Figure 5.3. This pattern indicates that yielding of the reinforcing bars across the central axes had occurred along half of the span length. The flow lines shown represent those existing after the third plastic node formed in Pattern No.1. The opening of cracks along the diagonals extending from the central point load appear to substaniate the formation of the fifth plastic node in Pattern No. 1.

The experimental collapse load for this slab was equal to the limit analysis prediction to within .5%.

(e) Deflection Contours at 85.5% of Collapse Load

Figure 5.4 is a sketch of the contours which indicate that the F.E.M. predictions are still in excess of measured values but are much closer to the real values than at the end of the elastic range. This is so because the extensive cracking has reduced the flexural stiffness to a value close to that assumed in the analysis.

5.4 Slab No. 2

(a) Plastic Flow Pattern

This slab was supported by rectangular metal edge beams and collapsed analytically into the flow pattern of Pattern No. 2. Here eleven stages of plastic behaviour were recorded with ten plastic nodes occurring in the slab. The first plastic node appeared under the point load at 43.3%

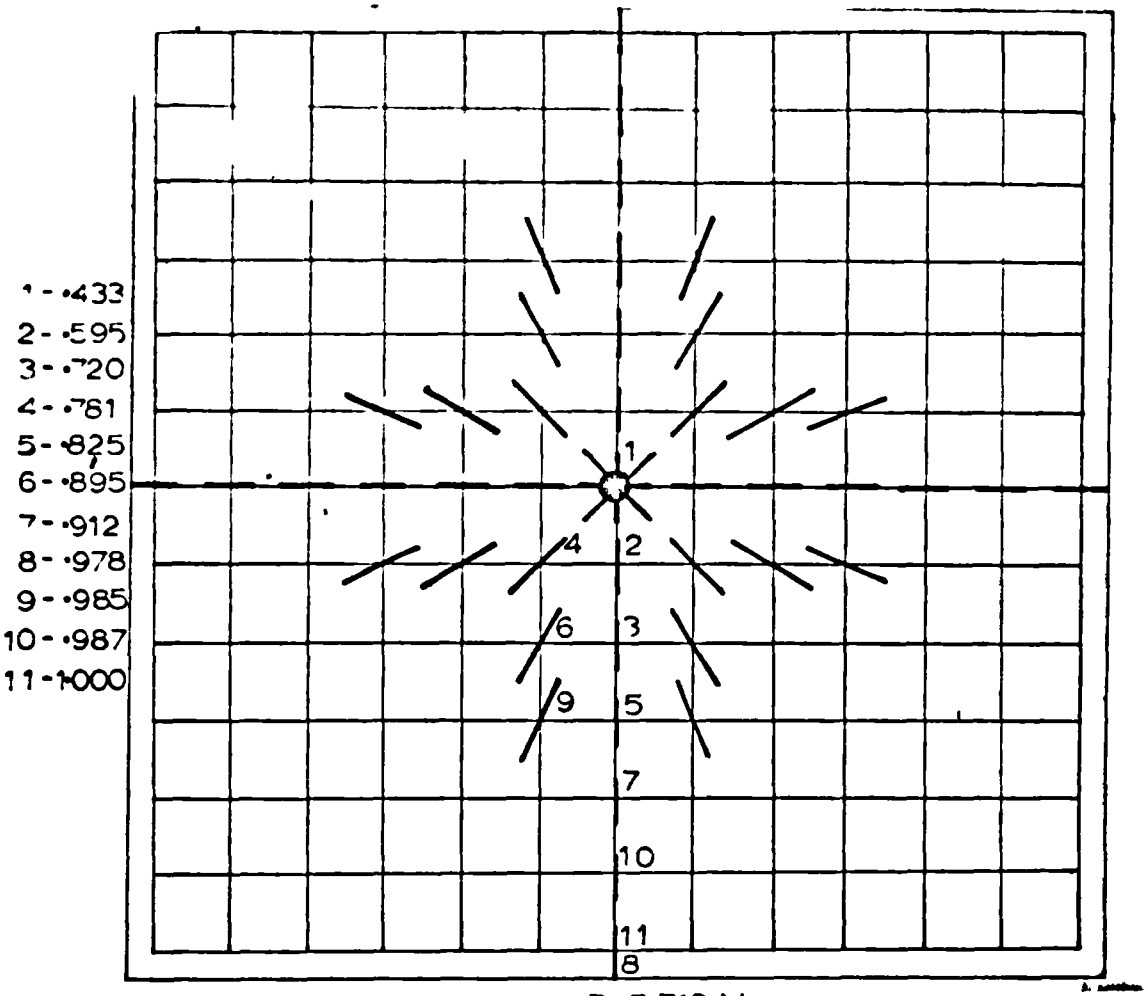

$P = 5 \cdot 712\ M_u$

$\nu = \cdot 15$

$M_u = 1 \cdot 0\ D/L$

$\gamma_e = \cdot 2860$

$\gamma_p = \cdot 2140$

$\gamma_t = \cdot 0071$

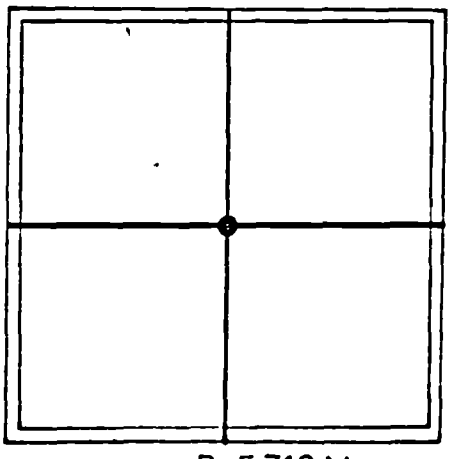

$\frac{P_e}{P_c} = \cdot 433$

$\frac{P_i}{P_c} = 1 \cdot 000$

$P_c = 5 \cdot 712\ M_u$

Pattern No.2

of the collapse load with the last indication of plastic behaviour occurring in the slab at the slab-beam interface at mid-span.

The pattern indicates a spread of plasticity in a radial direction from the center forming a wide band of yielding along most of the central axes. Only one plastic node appeared for the beam elements. This node became plastic at 97.8% of P_c and occurred independently of and before the adjacent slab element.

(b) Crack Pattern at End of Elastic Behaviour

Figure 5.5 shows the extent of cracking at $P/P_c = .433$ and also the superimposed flow lines from Pattern No. 2. The cracks shown were barely visible to the naked eye. As for the case of slab No. 1, most of these cracks had formed at 30% of the collapse load. However, with slab No. 2 the cracks had not opened to the same extent. In fact, strain measurement on the reinforcing steel under the point load indicated that first yield occurred at approximately 55% of the limit analysis collapse load. Therefore the $P/P_c = .433$ ratio predicted by the F.E.M. proved premature. Again the same reason applies as before since the actual slab stiffness is much greater than assumed in the analysis.

(c) Deflection Contours at End of Elastic Behaviour

Figure 5.6 shows the contours corresponding to the crack pattern of Figure 5.5. It is quite evident that the flexural stiffness of the slab has been greatly underestimated in the analytical model.

(d) Crack Pattern at Theoretical Collapse

This slab collapses at a load about 10% above the calculated computer and limit analysis values. The final crack pattern and evidence

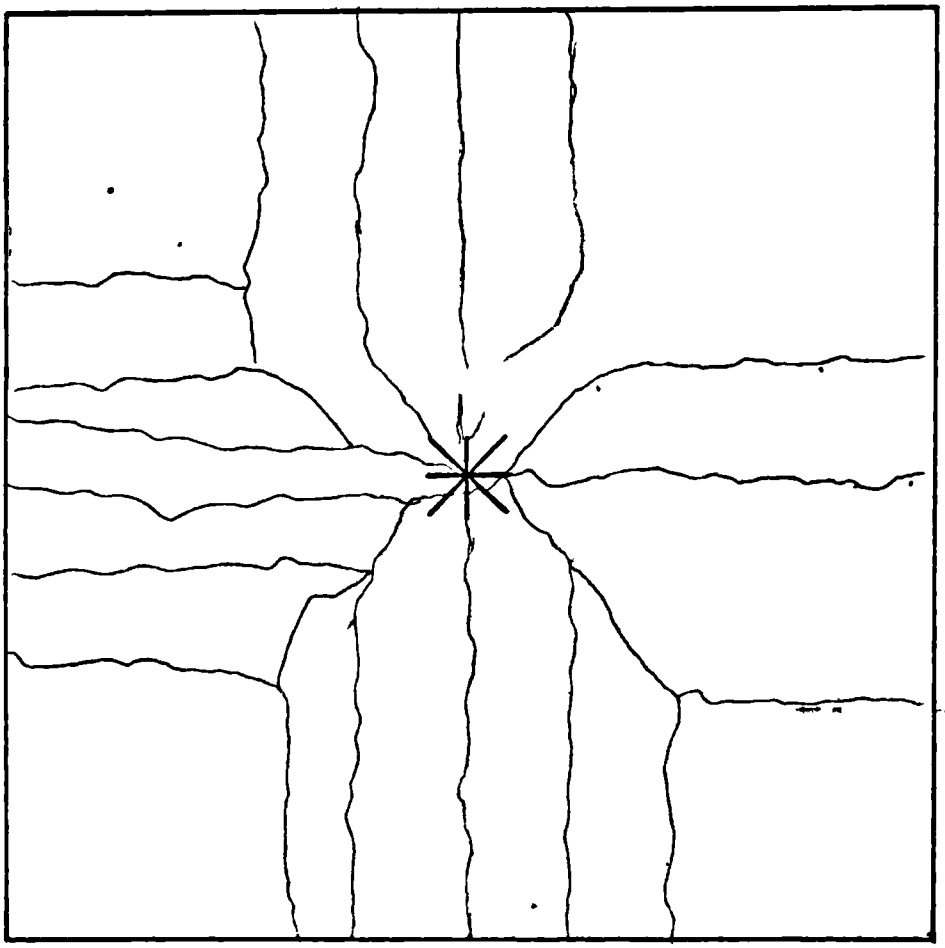

Slab No.2 - Crack Pattern at P/P_c = .443

Figure 5.5

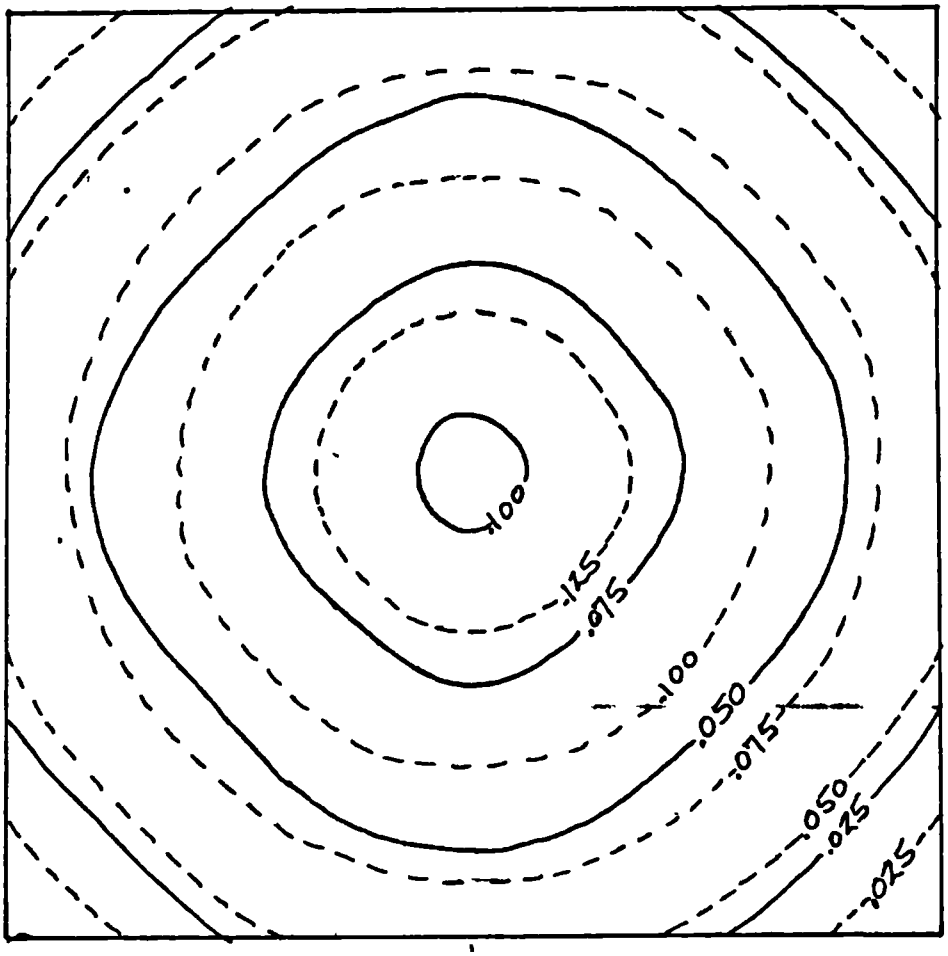

Computer - - - -
Experimental ———

Slab No.2 - Deflection Contours at P/P_o = .443

Figure 5.6

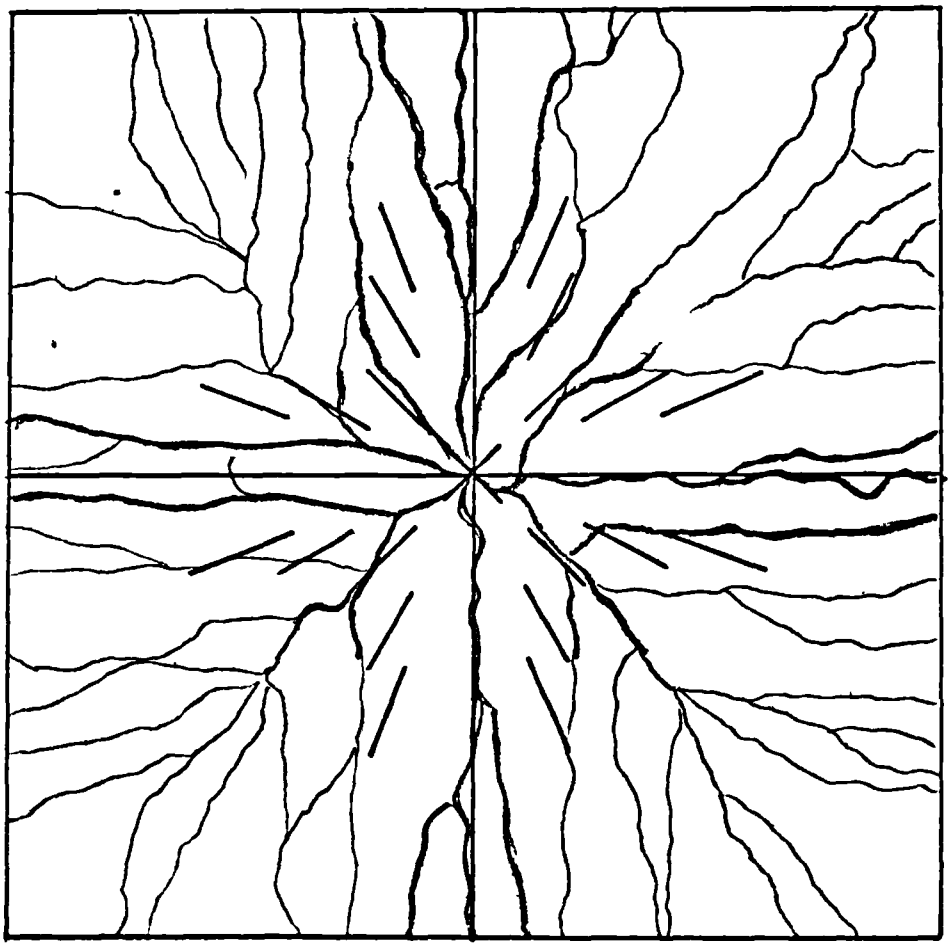

Slab No.2 - Crack Pattern at $P/P_c = 1.000$

Figure 5.7

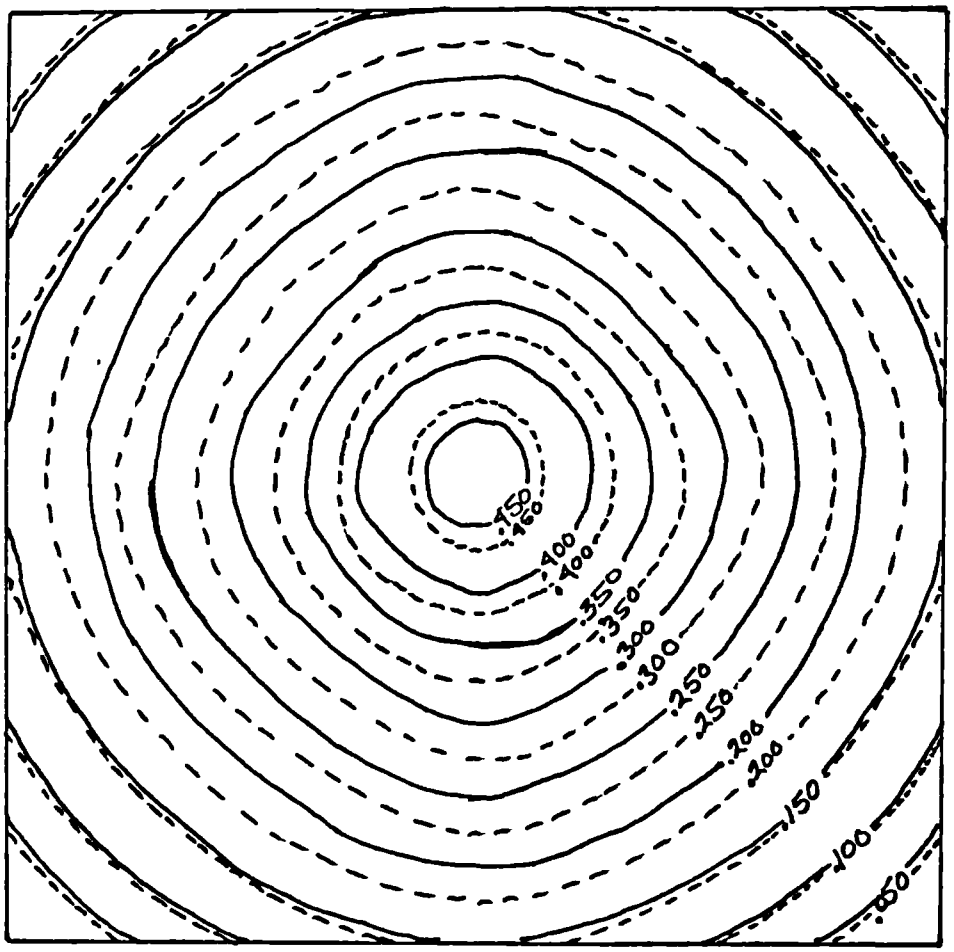

Computer – – – –
Experimental ———

Slab No.2 - Deflection Contours at $P/P_c = 1.000$

Figure 5.8

of the crack openings appear in Figure 5.7. The plastic flow of Pattern No. 2 is superimposed to compare the directions of the yield lines with those predicted by the F.E.M. model. For the most part the crack formations support the analytical results.

(e) Deflection Contours at Theoretical Collapse

The contours of Figure 5.8 were sketched from the results of deflection photographs previously described (see Chapter 4). In this test, symmetry of transverse deflection was well maintained and no averaging process was necessary to produce the contours.

The analytical results of Figure 5.8 show a close similarity to measured values, the analytical being slightly in excess of the experimental.

(f) Generalized Stresses and Beam Bending Moments

The generalized stresses in the slab were measured at six locations. These are presented on Graphs S2.1 to S2.6. These positions are indicated on the figure accompanying the graphs, representing $\frac{1}{4}$ of the slab area. Also shown on this figure are the four positions on the edge beams at which bending moments were determined.

In the case of slab generalized stresses, wherever the analytical elastic response deviates from experiment, the elastic-plastic portion of the analytical results have been superimposed on the experimental curve. These results are indicated by a broken line and are presented to compare the form of variation beyond the elastic limit of the analytical and experimental curves.

In all the graphs of generalized stresses except S2.2, the F.E.M. gives lower generalized stresses then determined experimentally because

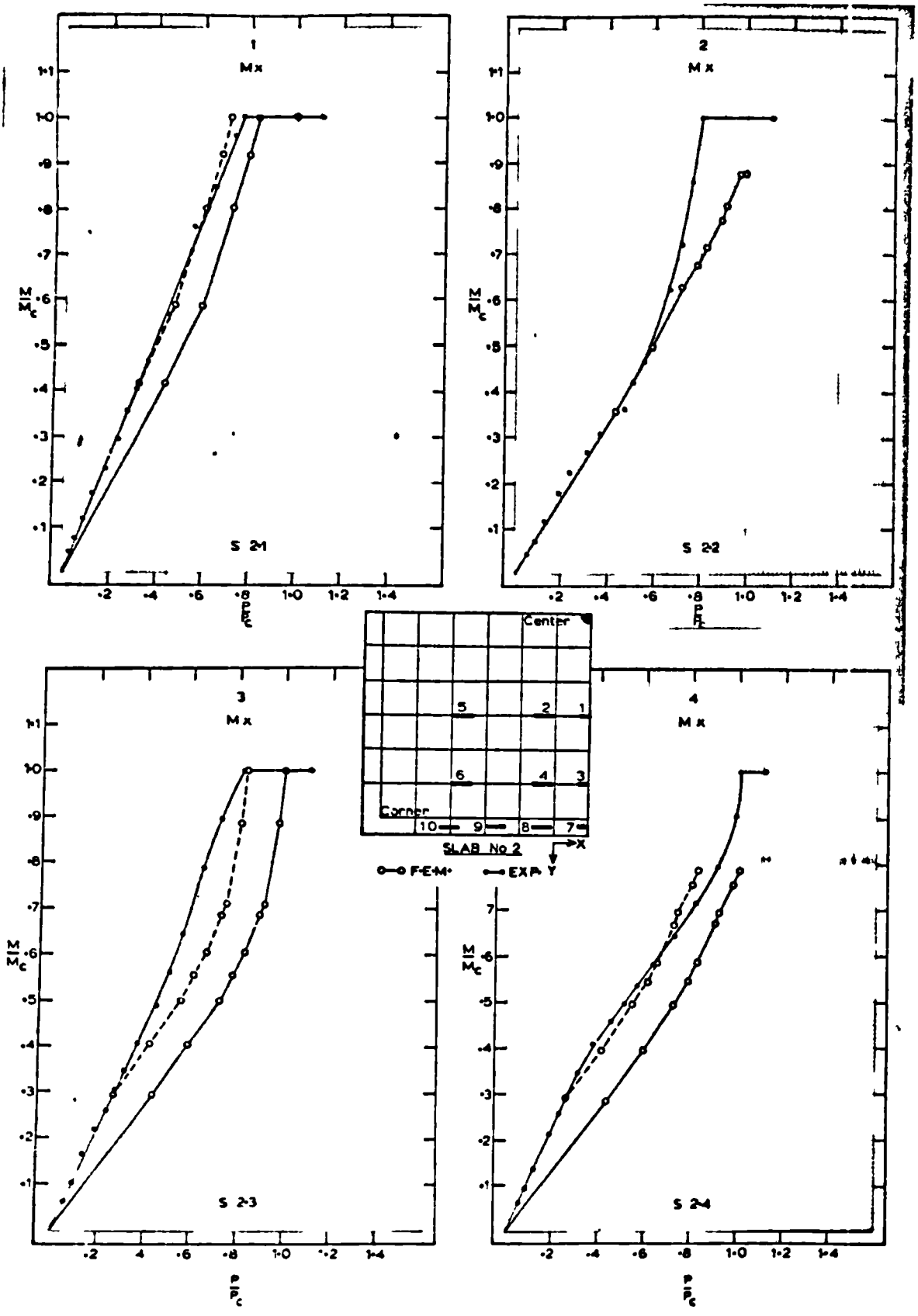
1
Mx
S 21
2
Mx
S 22
3
Mx
S 23
4
Mx
S 24
Center
Corner
SLAB No 2
FEM
EXP
X
Y

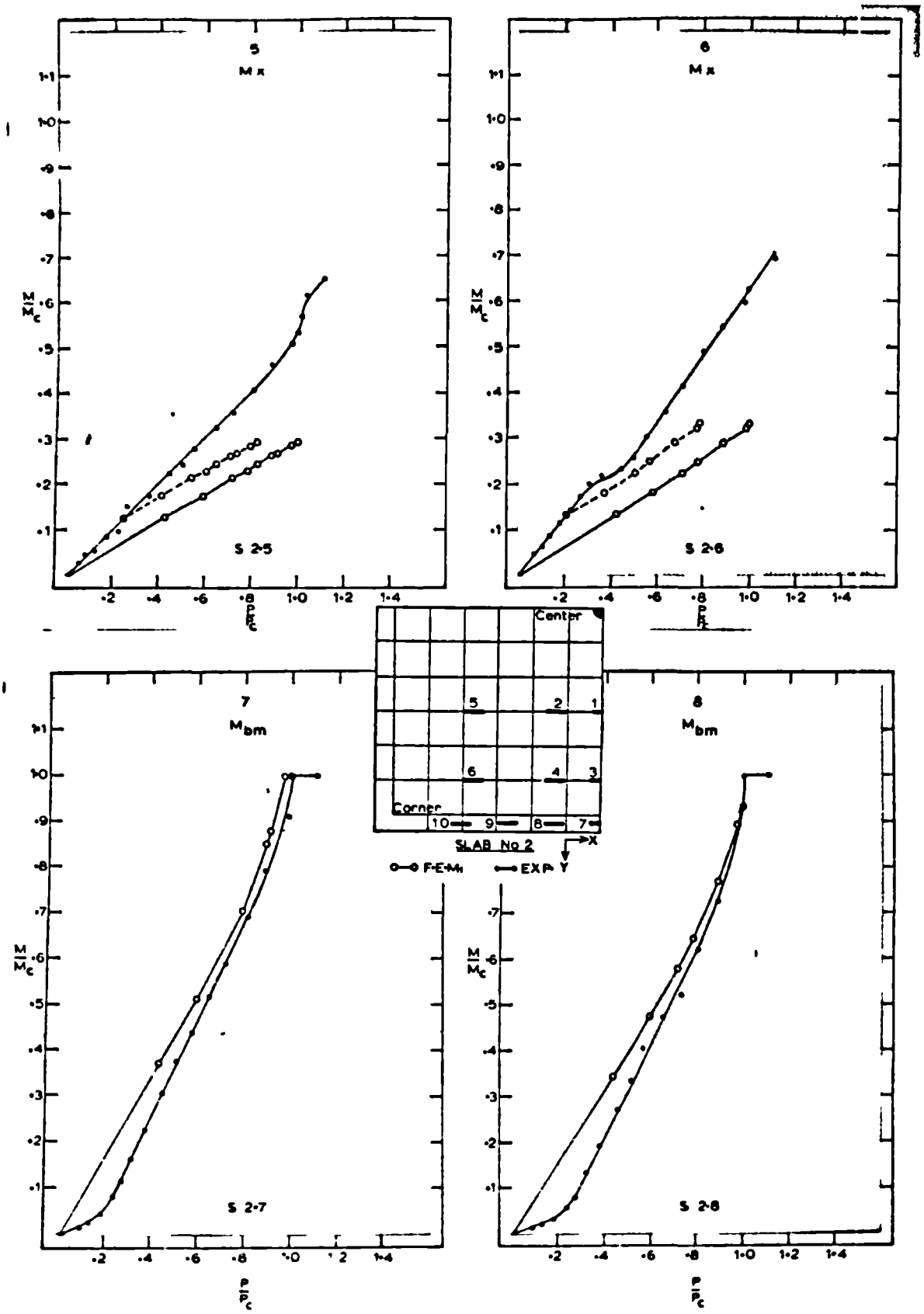
5
Mx
S 2-5
6
Mx
S 2-6
Center
Corner
5
2
1
6
4
3
10
9
8
7
SLAB No 2
X
Y
F-E-M
EXP
7
Mbm
S 2-7
8
Mbm
S 2-8

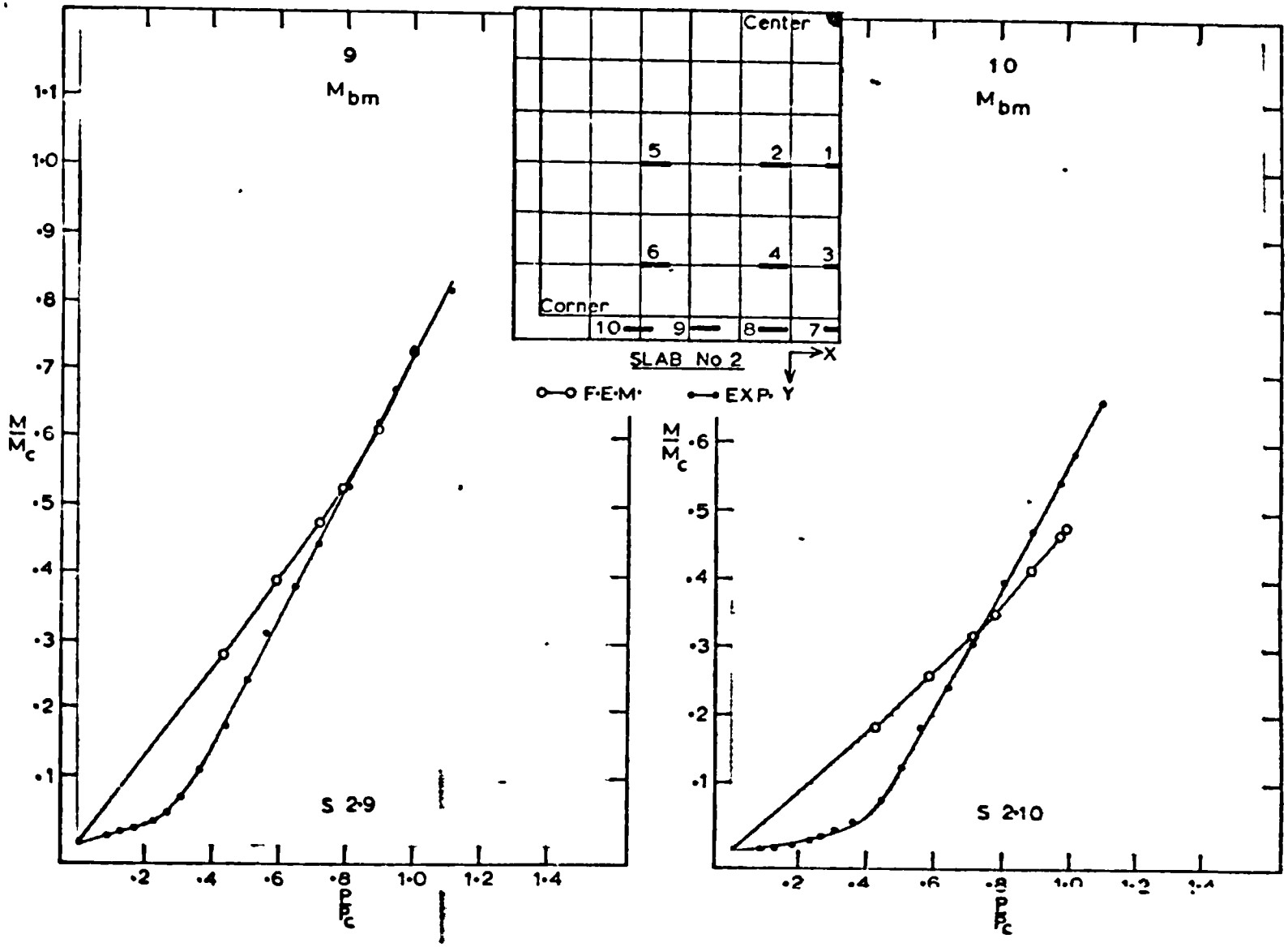
9
M_{bm}
10
M_{bm}
Center
Corner
5
2
1
6
4
3
10
9
8
7
SLAB No 2
X
Y
F·E·M·
EXP·
$\frac{M}{M_c}$
$\frac{P}{P_c}$
S 2·9
S 2·10
·1
·2
·3
·4
·5
·6
·7
·8
·9
1·0
1·1
·2
·4
·6
·8
1·0
1·2
1·4

of the underestimate of flexural stiffness. In general the analytical values are between 25% and 50% different from the measured values. It is difficult to assess the validity of the F.E.M. model for generalized stresses since the uncertainties in measuring bending strains do not allow a proper comparison to be made. However, it is clear from Graphs S2.1 to S2.4 that yielding of the reinforcing steel occurs experimentally over a wide band about the central axes. Only a portion of this band was predicted by computer.

Graphs S2.7 to S2.10 show the edge beam bending moments to be fairly closely predicted especially in the elastic-plastic range of behaviour. Once again the effects of slab stiffness during the uncracked load range ($0 < P/P_c < .3$) results in initial deviation between curves. This effect is less pronounced at position 7 since most of the slab in this area begins to crack at an early load stage ($P/P_c = 0.1$). The effects of uncracked stiffness are most pronounced in Graph S2.10 where the drop in slab flexural stiffness does not occur until about $P/P_c = .4$. This corresponds to the end of the analytical elastic response assuming a cracked section throughout the slab. On the whole, the beam bending moments are closely predicted by computer in the elastic-plastic range of behaviour.

5.5 Slab No. 3

(a) Plastic Flow Pattern

Pattern No. 3 is identical to that for slab No. 1 and the comments made in section 5.3a also apply here.

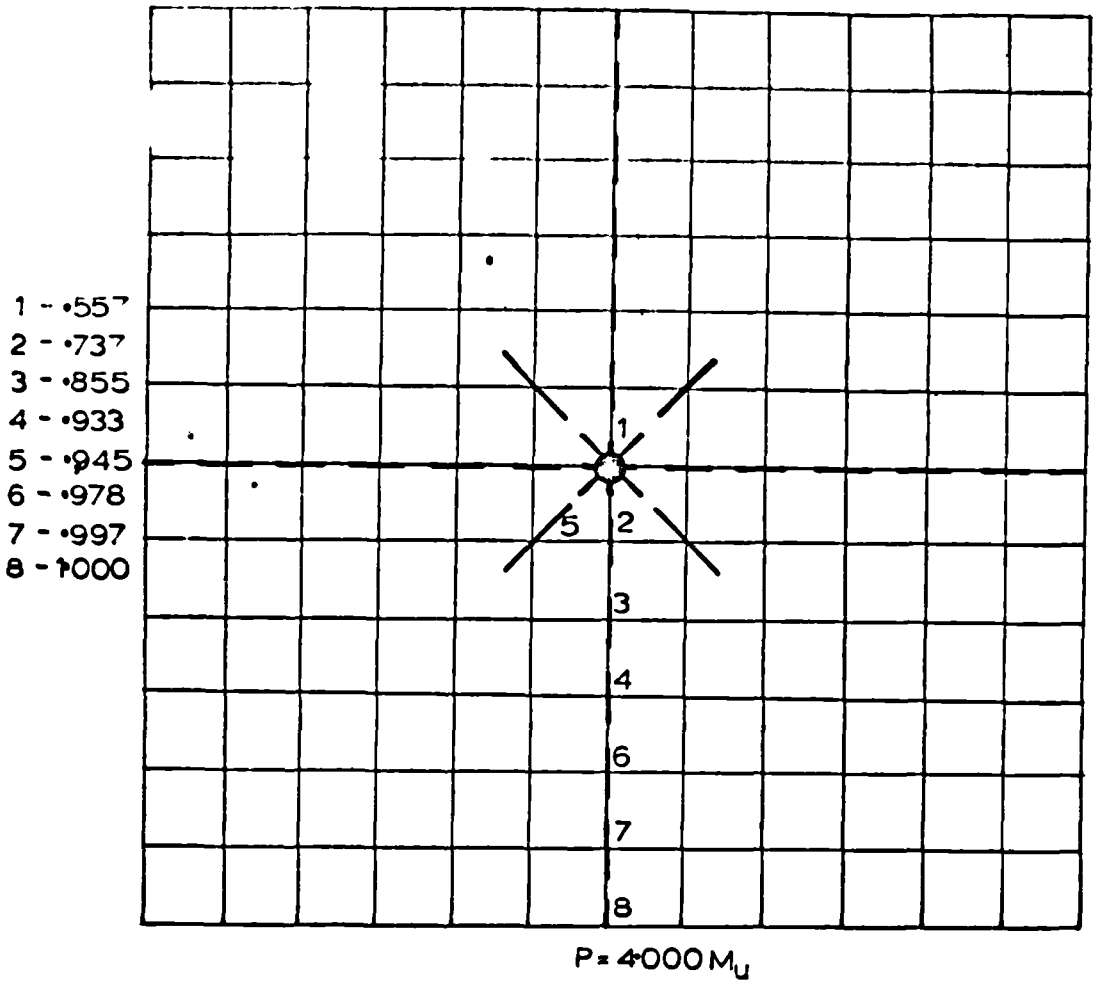

$\nu = \cdot 15$.

$M_u = 1 \cdot 0\ D/L$

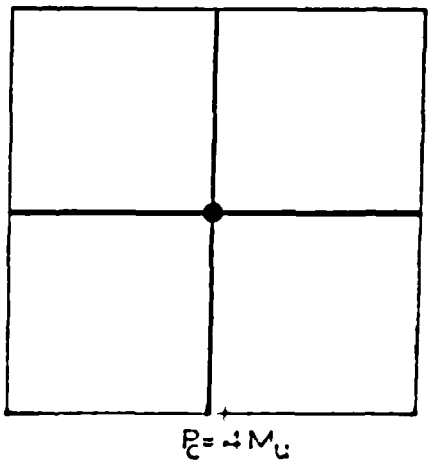

$\frac{P_e}{P_c} = \cdot 557$

$\frac{P_{1e}}{P_c} = 1 \cdot 000$

Pattern No. 3

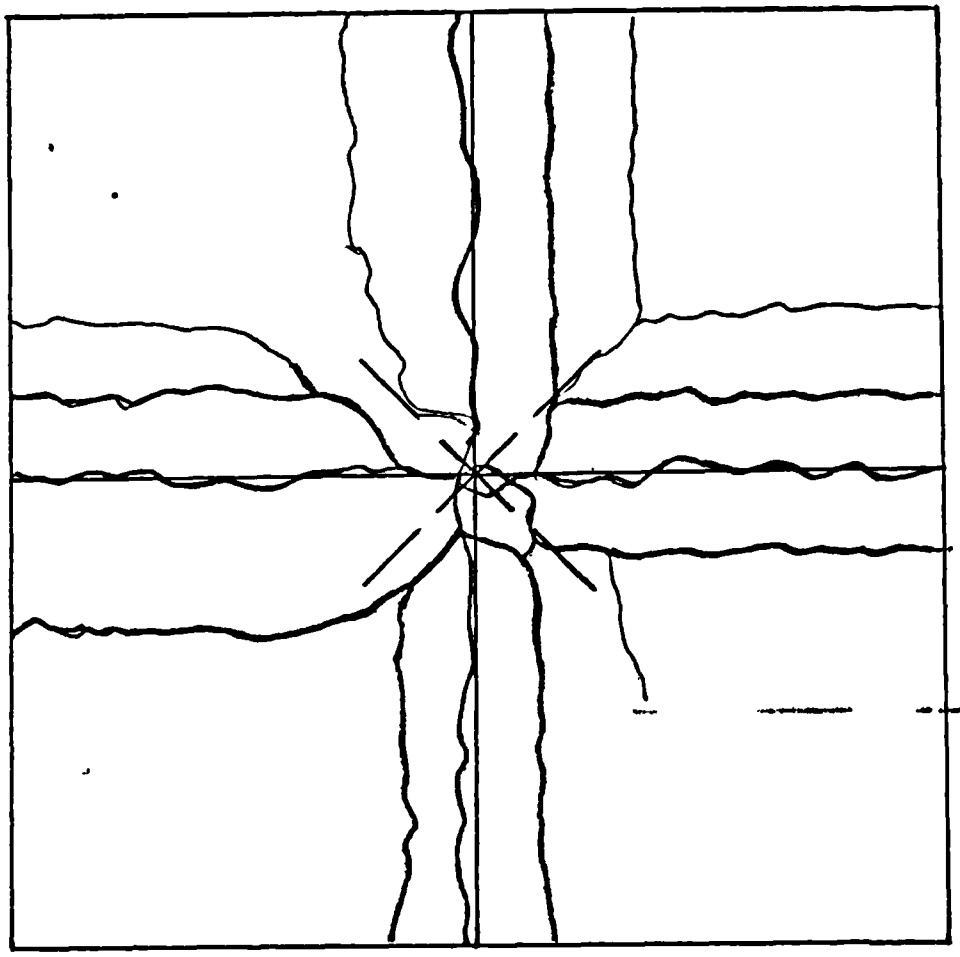

Slab No.3 - Crack Pattern at $P/P_c = 1.000$

Figure 5.9

(b) Crack Pattern at Collapse

The collapse load for this slab was identical to that predicted by limit analysis. The crack pattern at collapse is shown in Figure 5.9 on which is superimposed the plastic flow pattern for collapse given by the F.E.M. analysis.

The cracking began almost immediately upon load application. Due to the insufficient bonding properties between the concrete and the perforated sheet reinforcing steel, general cracking occured from the outset of the test. This results in a closer approximation to the analytical behaviour since the flexural stiffnesses are then similar.

The only other items recorded in this test were the deflections at two positions. These are presented later.

5.6 Slab No. 4

(a) Plastic Flow Pattern

The plastic flow lines are shown in Pattern No. 4 in which 18 stages of plastic behaviour occur before collapse of the slab. Again the analytical collapse load is identical to the limit analysis upper bound. According to the computer solution a wide band of plasticity occurs about the central axis. This occurs since the bending stiffness of the beam was small compared to that of the slab. Analytically at 75% of P_c the slab developed a continuous yield line across its span but an additional 15% of load was required until the beam developed a plastic hinge allowing the structure to collapse. During this latter load range, 9 additional positions became plastic forming the band indicated.

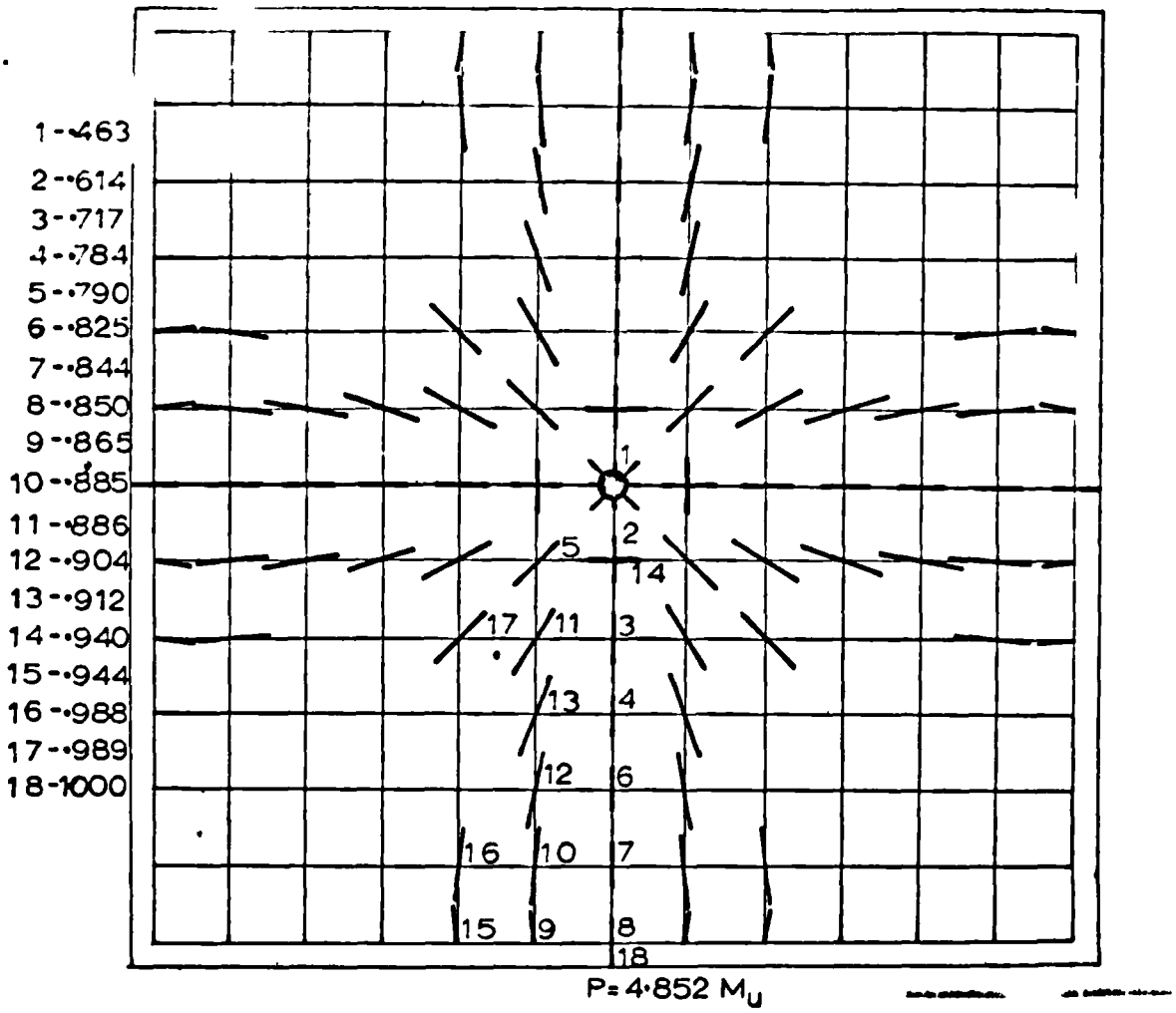

ν = ·15

M_u = 1·0 D/L

γ_e = ·0172

γ_p = ·1065

γ_t = ·4800

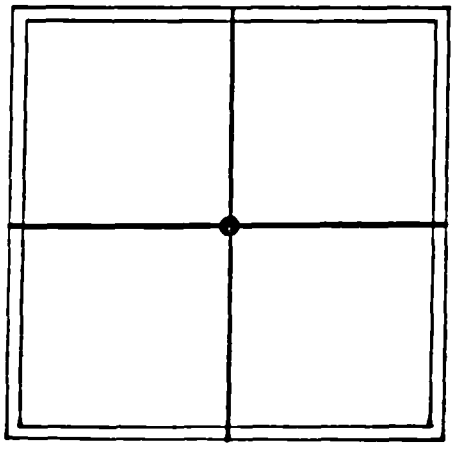

$\frac{P_e}{P_c}$ = ·463

$\frac{P}{P_c}$ = 1·000

Pattern No.4

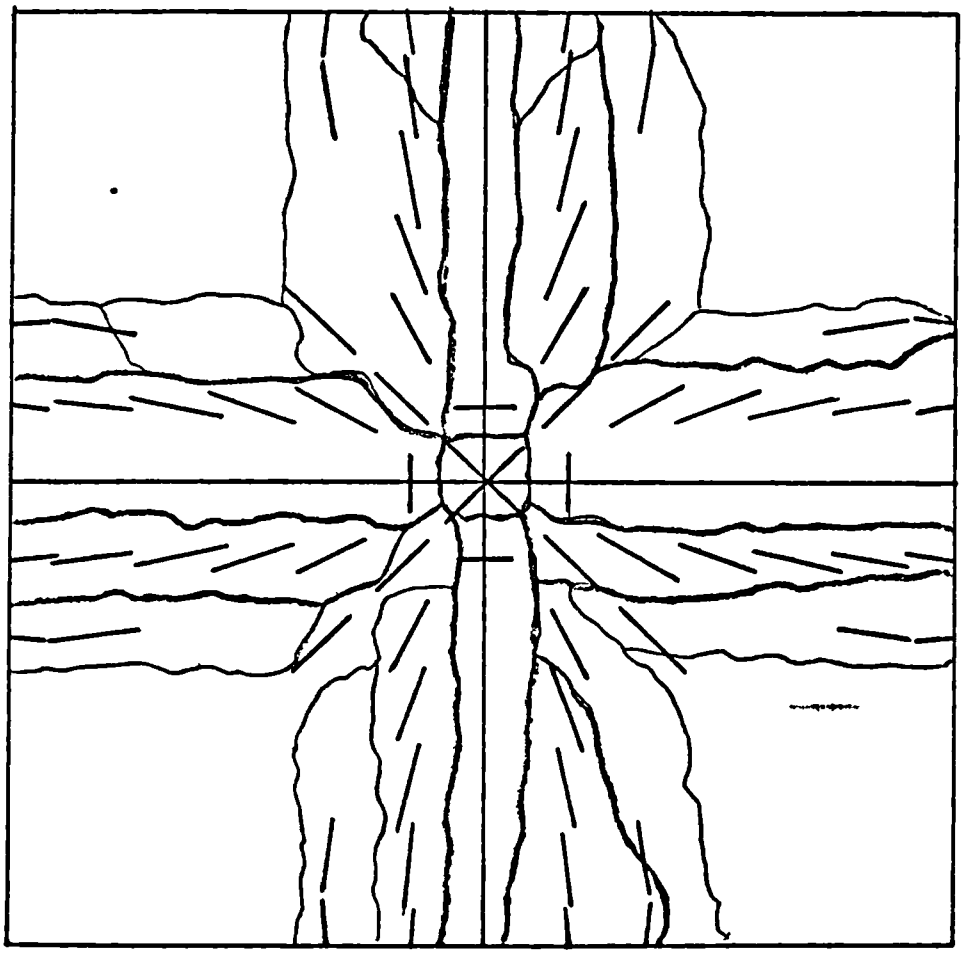

Slab No.4 - Crack Pattern at $P/P_c = 1.000$

Figure 5.10

(b) Crack Pattern at Theoretical Collapse

The collapse crack pattern is shown in Figure 5.10 with the flow pattern superimposed. Again the extent of cracking closely resembles the plastic flow pattern.

The experimental collapse load was about 10% above that predicted by limit analysis.

(c) Edge Beam Bending Moments

The edge beam bending moments at four positions are presented in Graphs S4.1 to S4.4. The effects on beam moments of gradual reductions in slab stiffness is seen as before. However, for this slab the cracking was continuous with no abrupt change in stiffness noticeable. Good accuracy is obtained until about 90% of P_c where although the analytical results overestimate the moments, the general performance is well reproduced.

5.7 Deflections - Slabs No. 1 to No. 4

The deflections of the slabs measured under the point load and at mid-span on the edge are presented in Graphs S1.0 to S4.0. The comments made previously about slab flexural stiffness also apply here. The analytical results show good agreement with experiment in most cases during the elastic-plastic behaviour.

5.8 Concluding Remarks - Slab Tests

From the results presented thus far it is difficult to establish the validity of the analytical model primarily because a variation of slab bending stiffness has not been allowed. Furthermore, the measurement of strain and subsequent calculation of generalized stresses in reinforced concrete is a difficult task. The resulting measurements are usually crude approximations to the actual strain distribution,

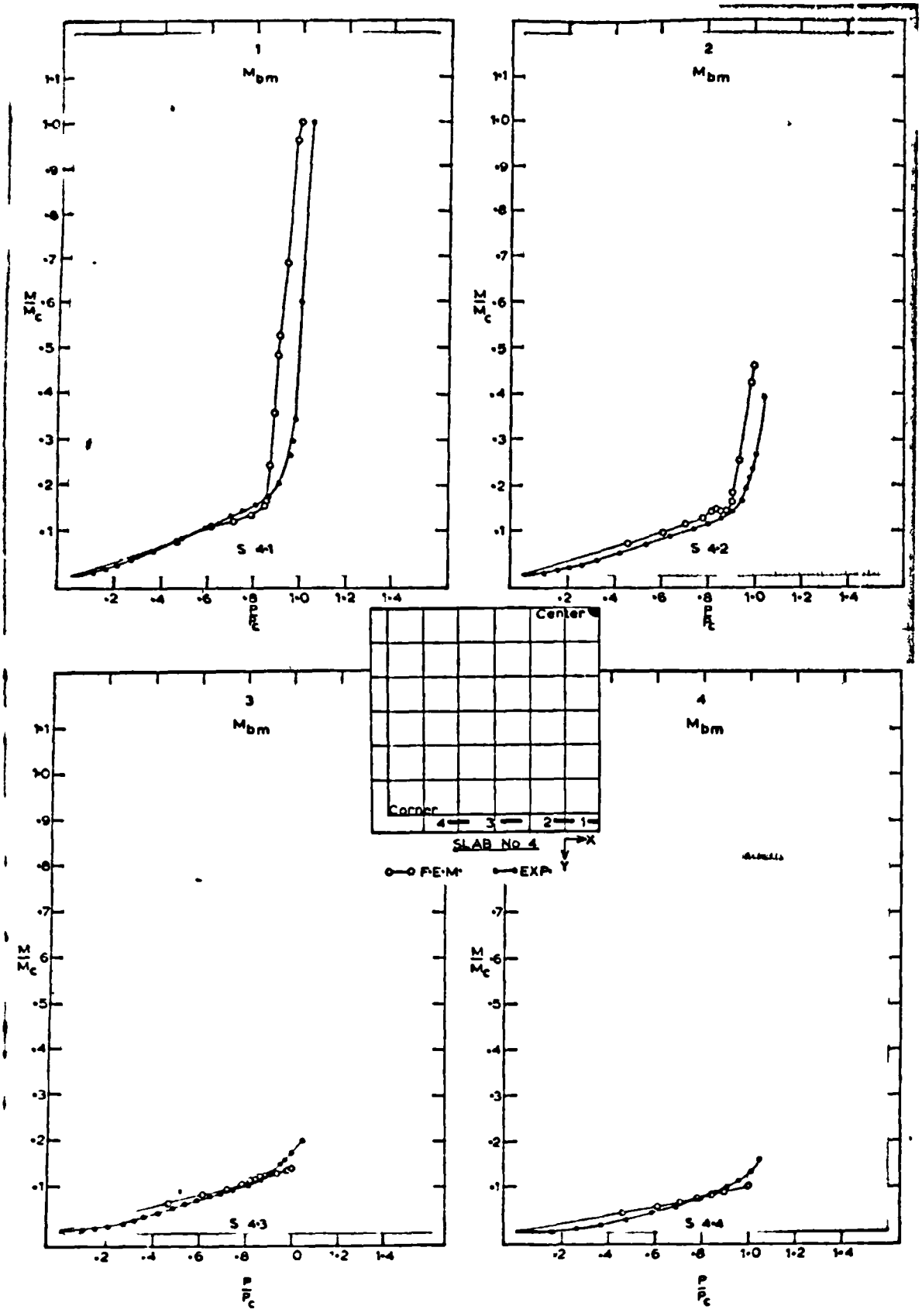
1
Mbm
S 4-1
2
Mbm
S 4-2
Center
Corner
4 3 2 1
SLAB No 4
X
Y
F·E·M·
EXP.
3
Mbm
S 4-3
4
Mbm
S 4-4
M/Mc
P/Pc

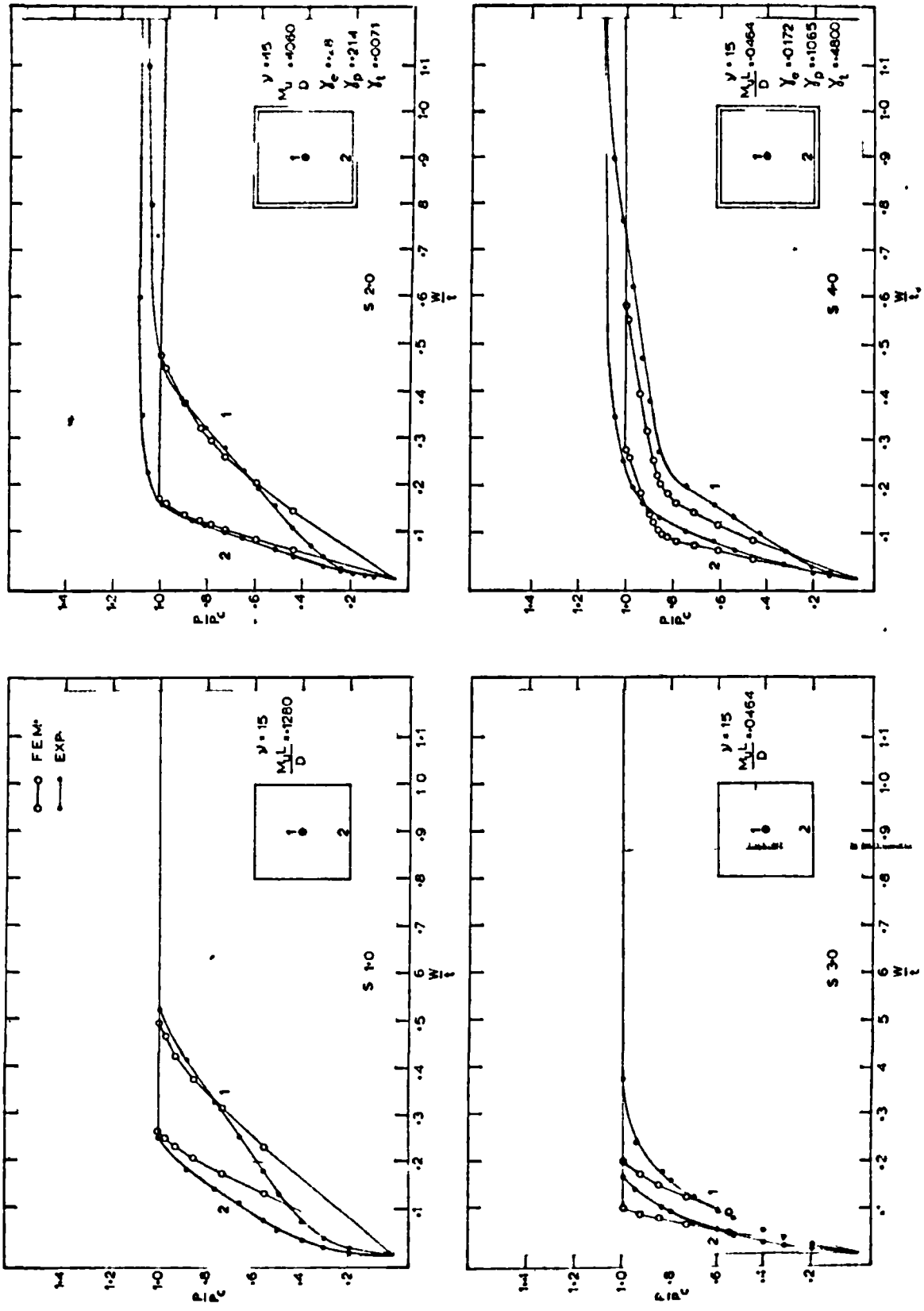
FEM
EXP
S 1·0
S 2·0
S 3·0
S 4·0
P/P_c
w/t

and the deduced stress distributions will be even less reliable.

However, the analytical predications of the overall yield behaviour and especially the collapse load are in good agreement with experiment. The yield patterns, deflection contours and beam moments are in good agreement in the elastic-plastic range of behaviour. In general, conservative predications are made by the F.E.M. model when compared with experiment.

Mild Steel Plate Tests

5.9 Stiffness and Strength Parameters

A summary of these parameters is given in Table 5.2. All quantities shown except γ_t (see section 5.2) were determined experimentally. Various data used in these calculations are presented in Appendix III.

All plates have the same flexural stiffness and fully plastic value of the limiting generalized stress. The properties of edge beams for plates No. 2 and No. 4 are identical. These plate tests could be compared with each other to investigate the effects of point load arrangement and edge supporting beams on the elastic-plastic behaviour. However, such comparisons have been left for future presentation since the purpose of these tests is to assess the validity of analytical results when applied to different plate problems.

The difficulty of determining the flexural stiffness does not arise for the metal plates as it did for the slabs since fracture of the plate material does not occur. Therefore, the experimental generalized stresses etc. presented in the next sections can be considered reliable for comparison with the analytical results.

Item	Plate No.1	Plate No.2	Plate No.3	Plate No.4
D Lb in.	325,000	325,000	325,000	325,000
$\frac{M_p L}{D}$	.1120	.1120	.1120	.1120
EI Lb in.^{2}	0	4,700,000	0	4,700,000
$\frac{M_b}{D}$	0	.0244	0	.0244
$\gamma_e = \frac{EI}{DL}$	0	.9050	0	.9050
$\gamma_p = \frac{M_b}{M_p L}$	0	.2180	0	.2180
$\gamma_t = \frac{GJ}{EI}$	0	.00484	0	.00484

Stiffness and Strength Parameters for Plate Tests

Table 5.2

5.10 Plate No. 1

(a) Plastic Flow Pattern

Pattern No. 5 for this plate is similar to those for slabs No. 1 and No. 3 except for the P/P_c ratios. The higher Poisson ratio results in less redistribution of generalized stress between the elastic limit and collapse.

(b) Generalized Stresses

Generalized stresses reported were measured at seven locations on Plate No. 1. These positions are indicated on $\frac{1}{4}$ of the plate in the figure shown with Graphs Pl.1 to Pl.10. The strain gauge positions are marked showing rectangular rosettes along the diagonal. Strain measurements were recorded at locations symmetrically opposite (across diagonal) the positions of 1,2 and 3 inorder to check symmetry of curvature. Also certain gauges measured membrane strains. These additional measurements are discussed in Appendix III. Similar discussions are also presented there for the other plate tests.

The analytical generalized stress of Graph Pl.1 is much greater than the experimental value because position 1 is located directly under the point load. Analytically the load is concentrated at one node and this results in very large displacement gradients in the vicinity of the load. Consequently, a direct comparison with experiment cannot be made. All of the remaining graphs for this plate show excellent agreement between the experimental and F.E.M. predictions with the exception of Graph Pl.6 in which the magnitudes are in error but the correct form of variation is produced by computer.

From the graphs it is clear that the plate was loaded to approximately

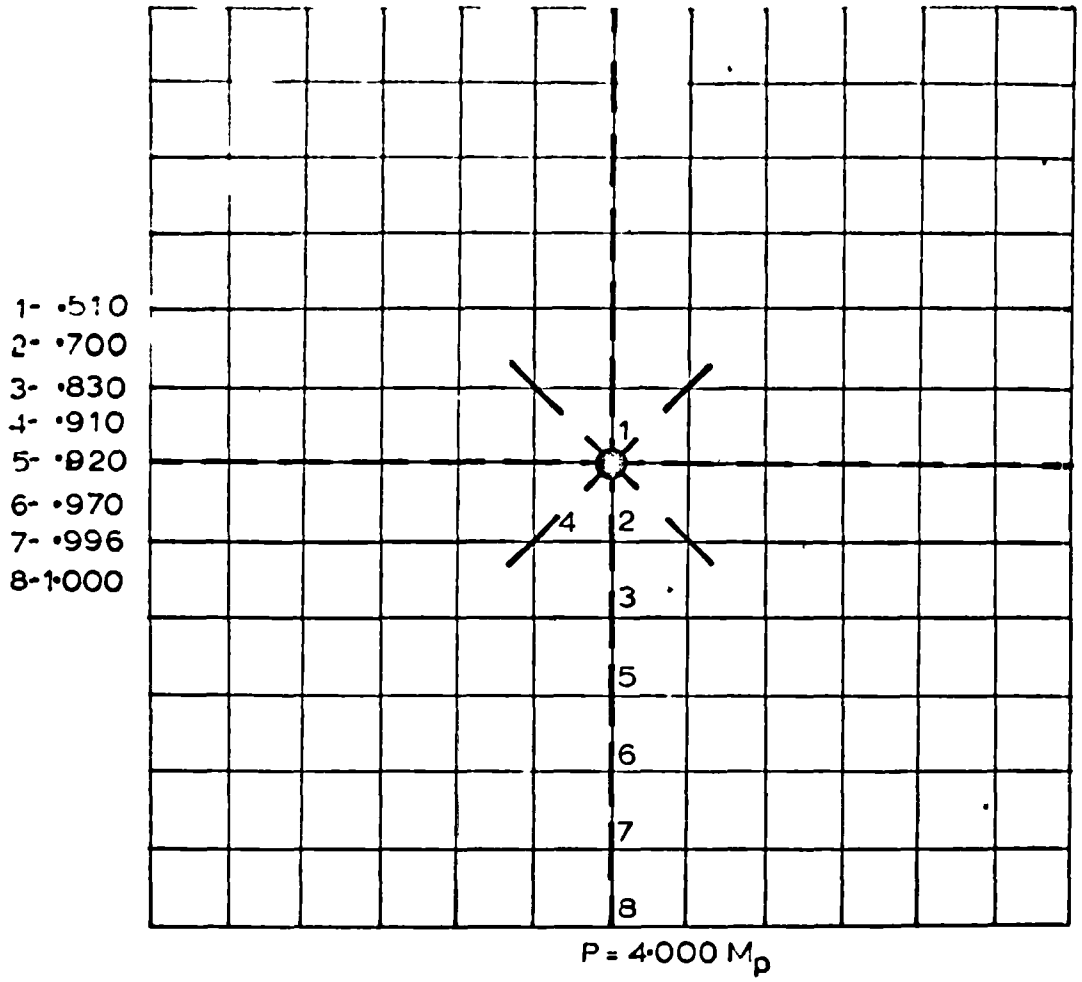

$\nu = .30$

$M_p = 1.0$ D/L

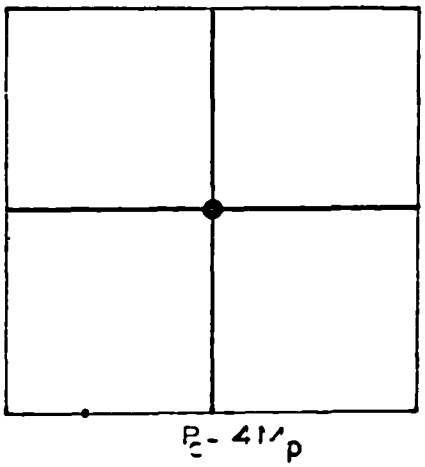

$\frac{P_e}{P_c} = .510$

$\frac{P}{P_c} = 1.000$

Pattern No.5

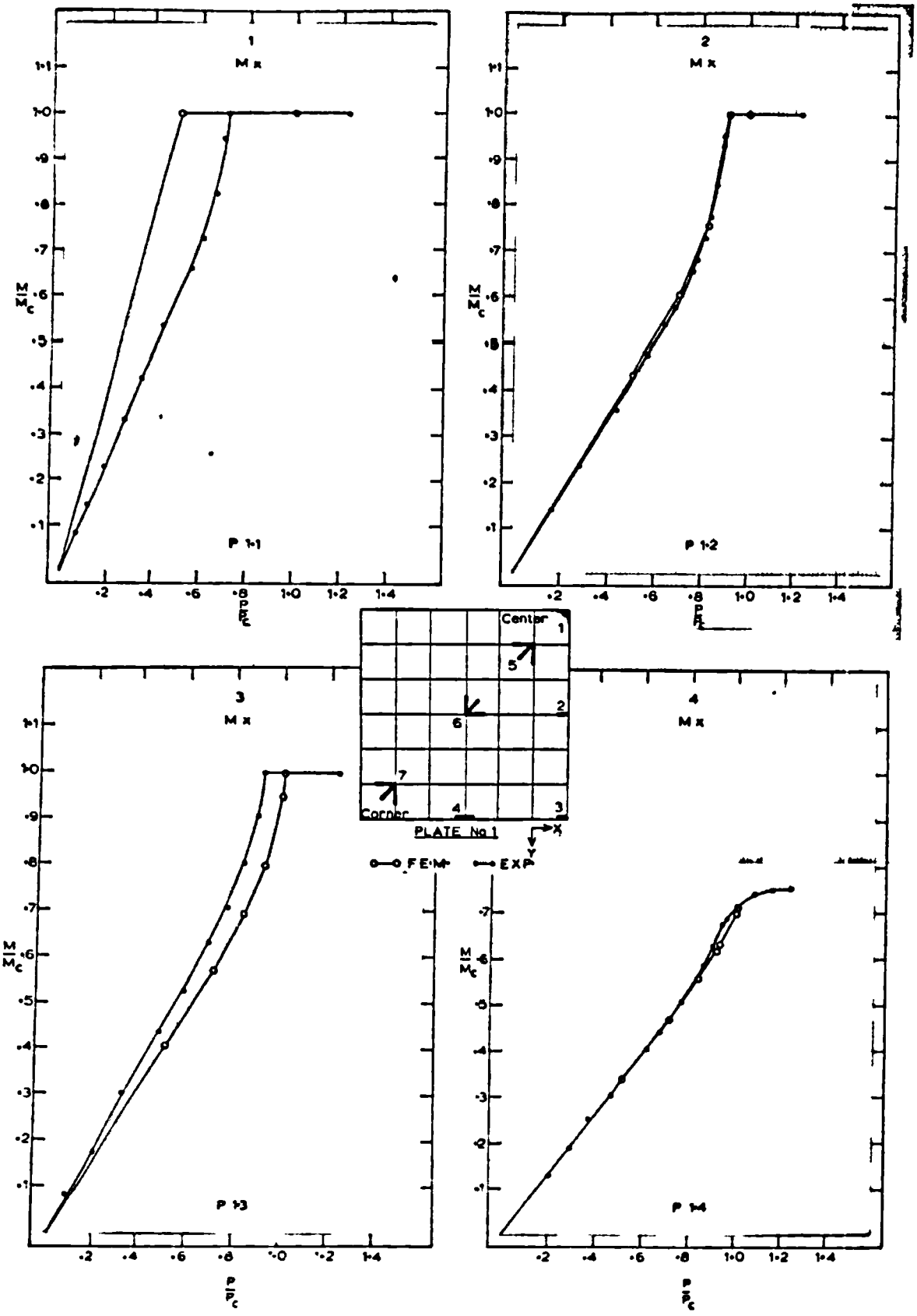
1
M x
P 1-1
2
M x
P 1-2
Center
Corner
PLATE No 1
FEM
EXP
3
M x
P 1-3
4
M x
P 1-4

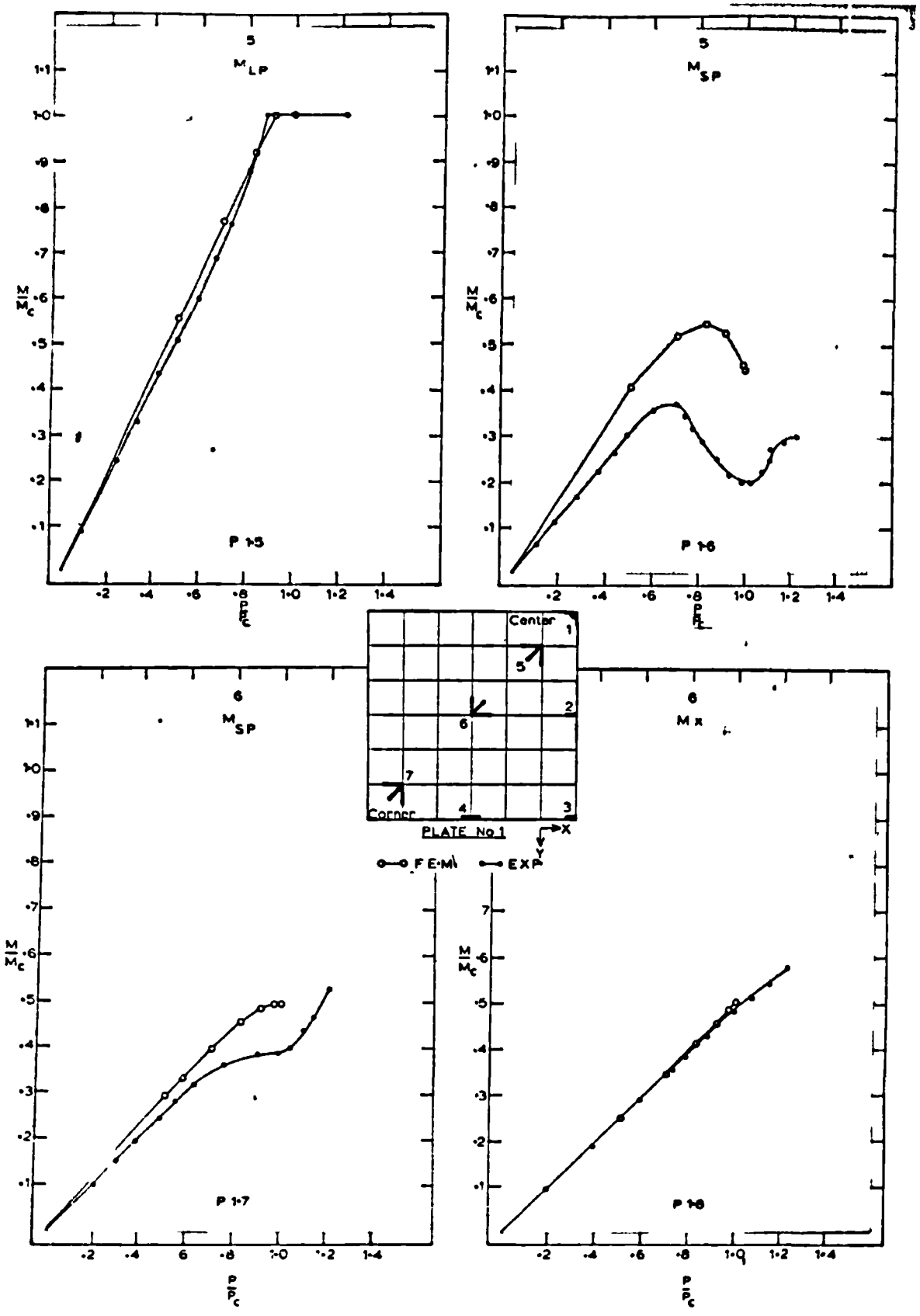
5
M LP
P 1-5
5
M SP
P 1-6
Center
1
5
2
6
7
Corner
4
3
PLATE No 1
X
Y
F E-M
EXP
6
M SP
P 1-7
6
M x
P 1-8
M/Mc
P/Pc

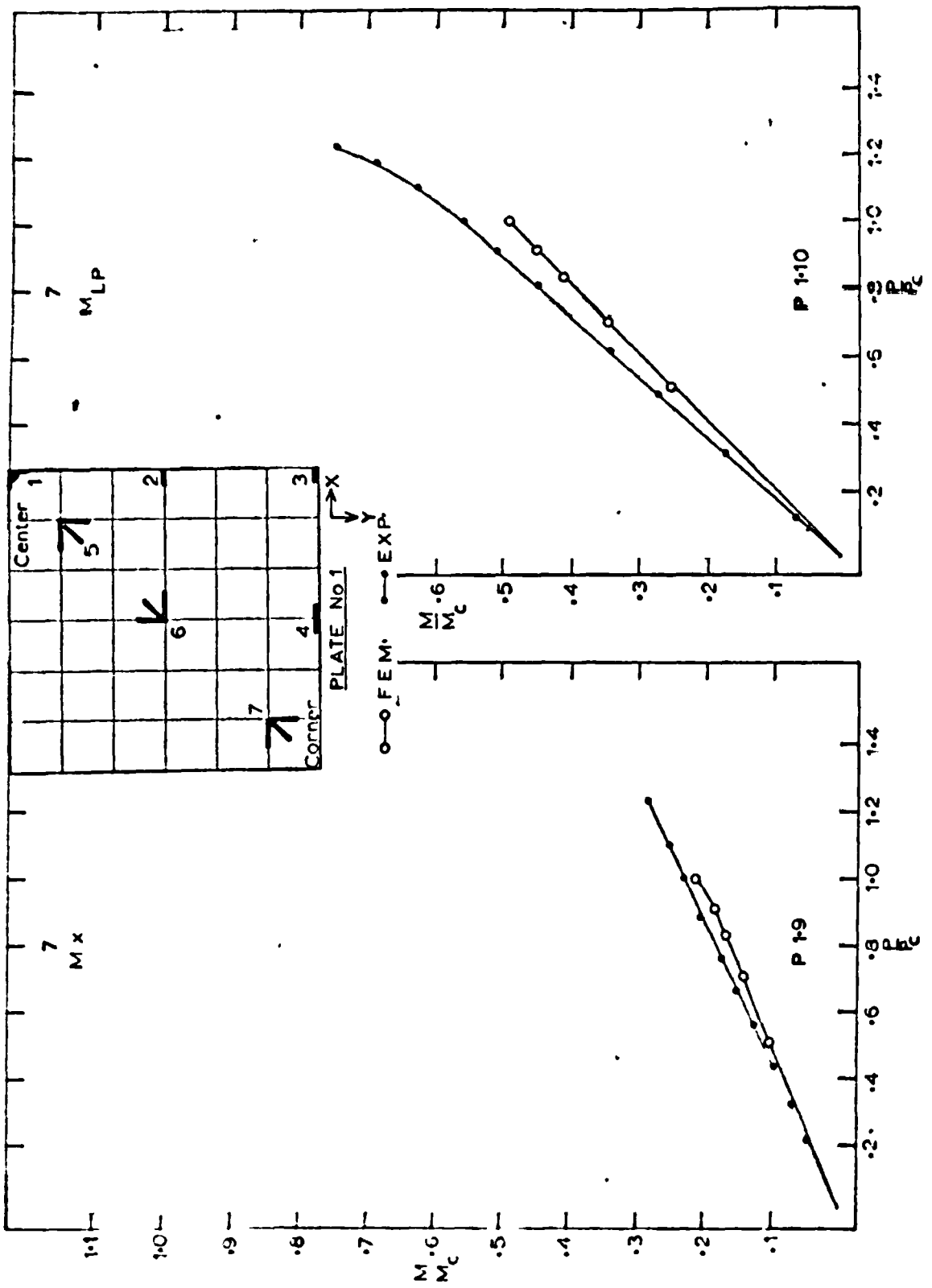
7
M_{LP}
P 1-10
$\frac{M}{M_c}$
$\frac{P}{P_c}$
EXP
FEM
Center
Corner
PLATE No 1
X
Y
7
M_x
P 1-9
$\frac{M}{M_c}$
$\frac{P}{P_c}$

2% above the limit analysis upper bound value. However, at load slightly above the theoretical collapse the deflections increased rapidly. This value of 2% would have been reduced had the load not been increased as rapidly as it was during the last stages of the test.

5.11 Plate No.2

(a) Plastic Flow Pattern

Pattern No. 6 indicates twelve stages of plastic behaviour. The independent plastic behaviour of edge beam elements is illustrated by this solution. Collapse does not occur until the plate becomes plastic at the beam interface at mid-span. The analytical collapse load is again identical to the limit analysis value. The experimental collapse load was approximately 10% above this value.

(b) Generalized Stresses and Beam Bending Moments

The generalized stresses for this plate are presented in Graphs P2.1 to P2.8. Again excellent correlation of results is seen with the exception of Graph P2.1 corresponding to the point load position. The beam bending moments at positions 7 and 8 have been closely reproduced by the finite element method.

5.12 Plate No. 3

(a) Plastic Flow Pattern

In this solution (see Pattern No. 7) almost one half of the plate material is plastic at collapse with a total of 15 stages of plasticity indicated. The computer collapse load is identical to that of limit analysis based on either of the collapse mechanisms shown. Experimentally

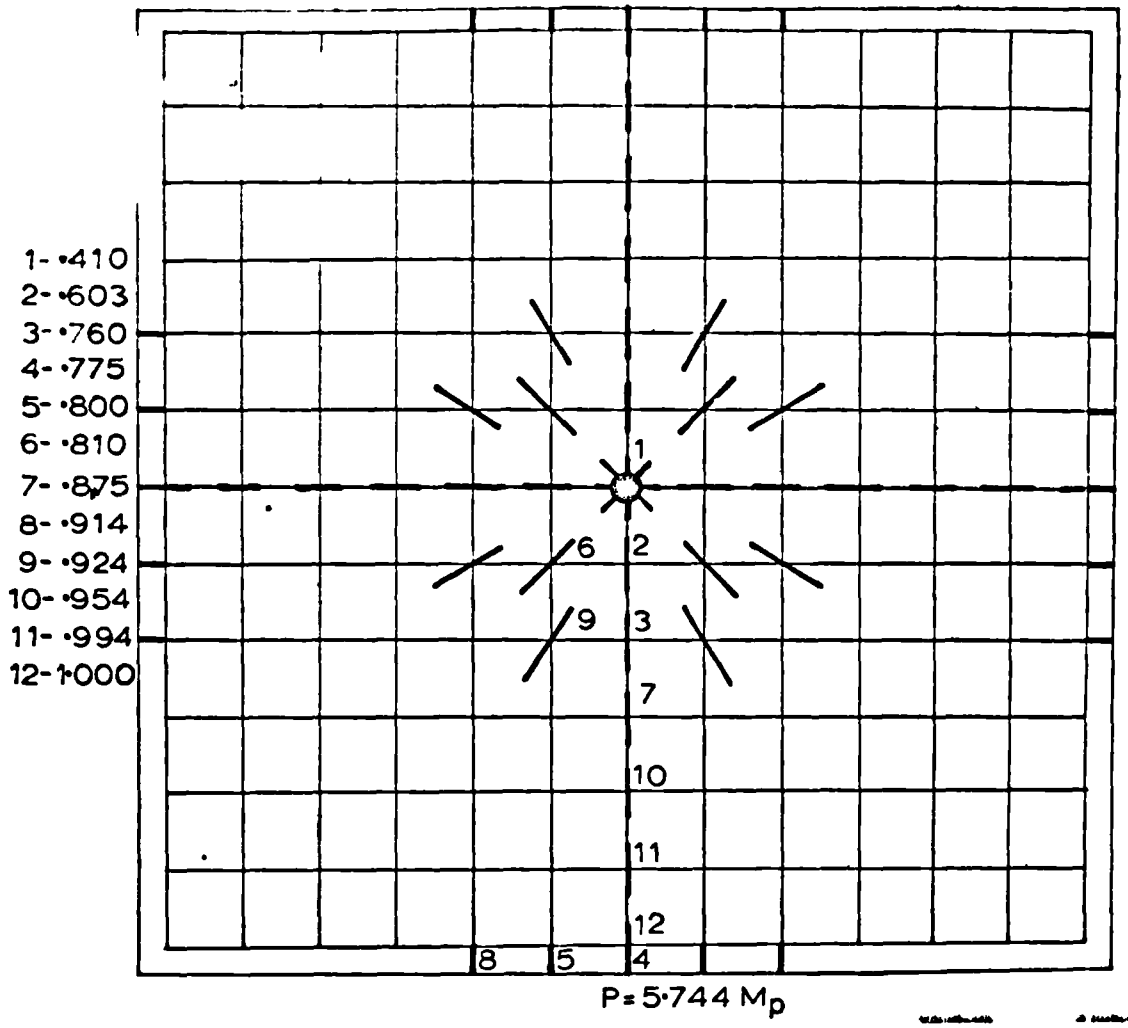

ν =·30

M_p= 1·0 D/L

γ_e =·9050

γ_p=·2180

γ_t =·0048

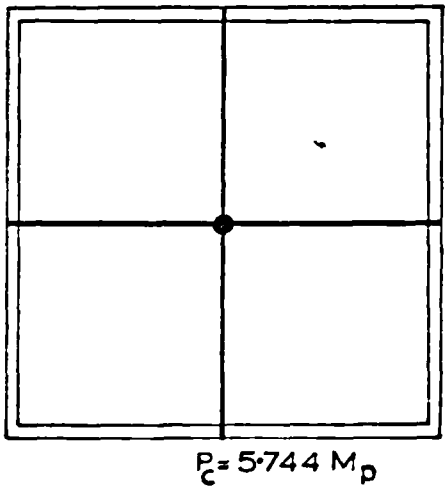

$\frac{P_e}{P_c}$ =·410

$\frac{P}{P_c}$ = 1·000

Pattern No.6

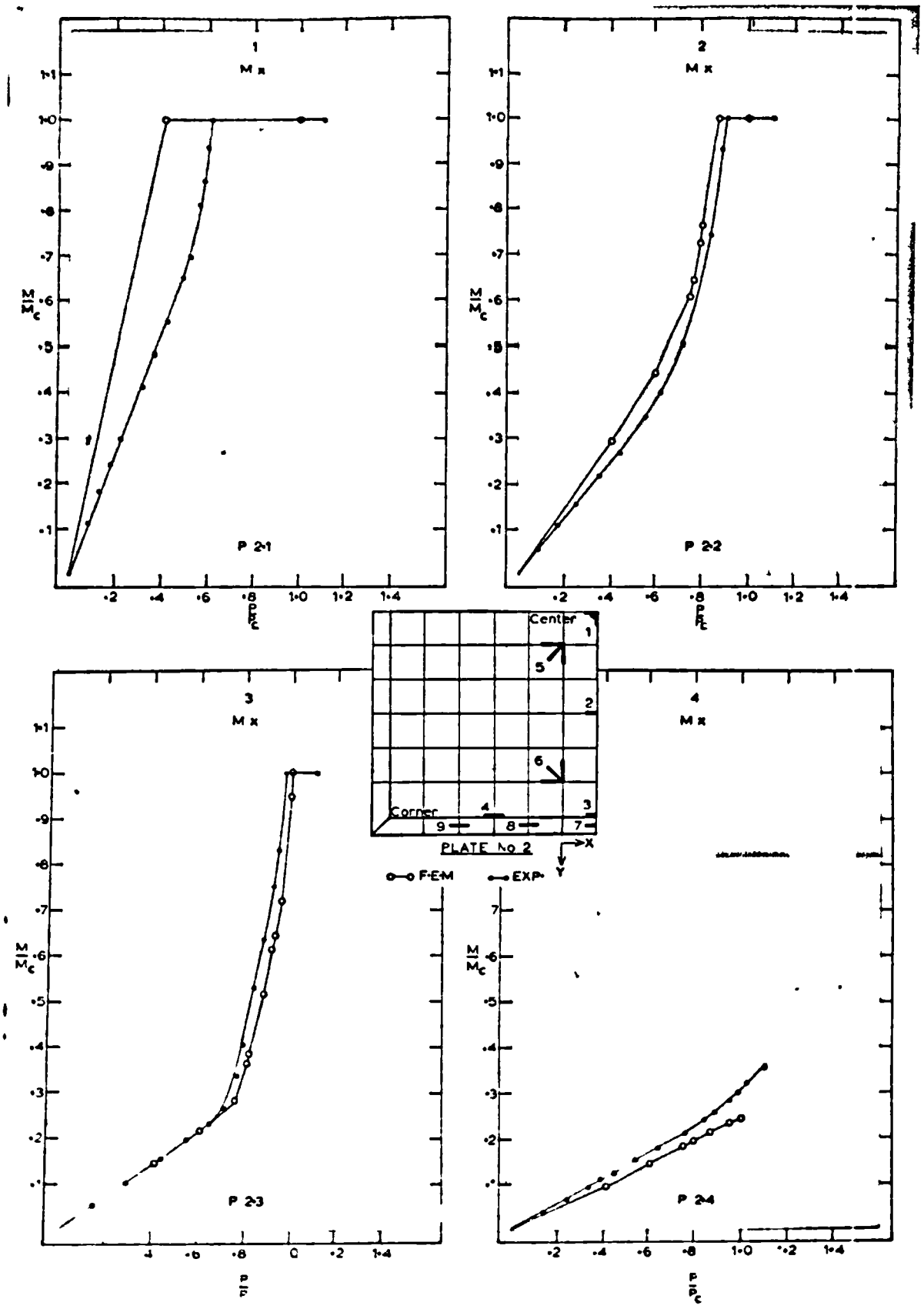
1
M x
P 2-1
2
M x
P 2-2
3
M x
P 2-3
4
M x
P 2-4
Center
Corner
PLATE No 2
F-E-M
EXP
M/Mc
P/Pc

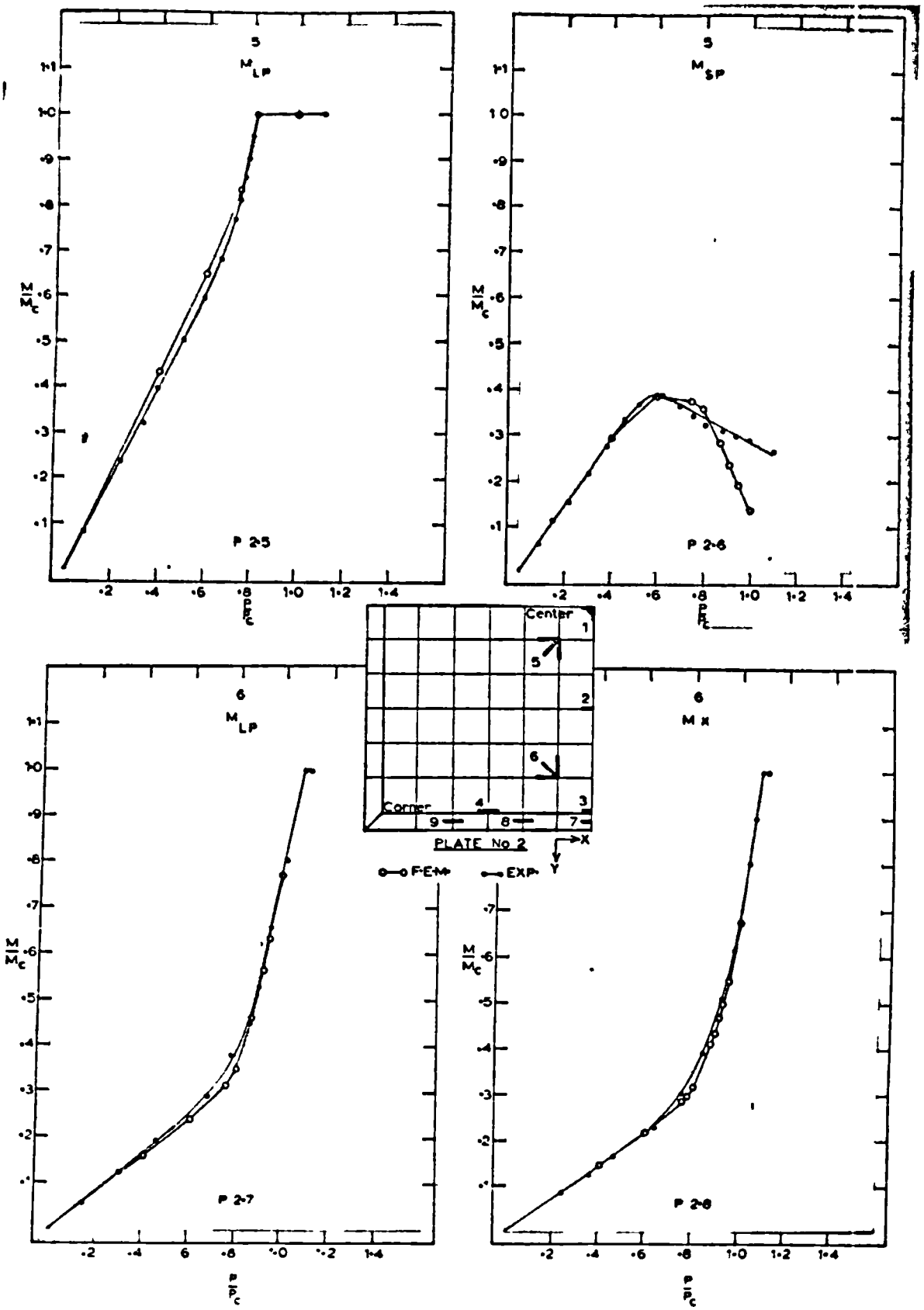
5
M_{LP}
P 2-5
5
M_{SP}
P 2-6
Center
Corner
PLATE No 2
6
M_{LP}
P 2-7
6
M x
P 2-8
F-E-M
EXP
$\frac{M}{M_c}$
$\frac{P}{P_c}$

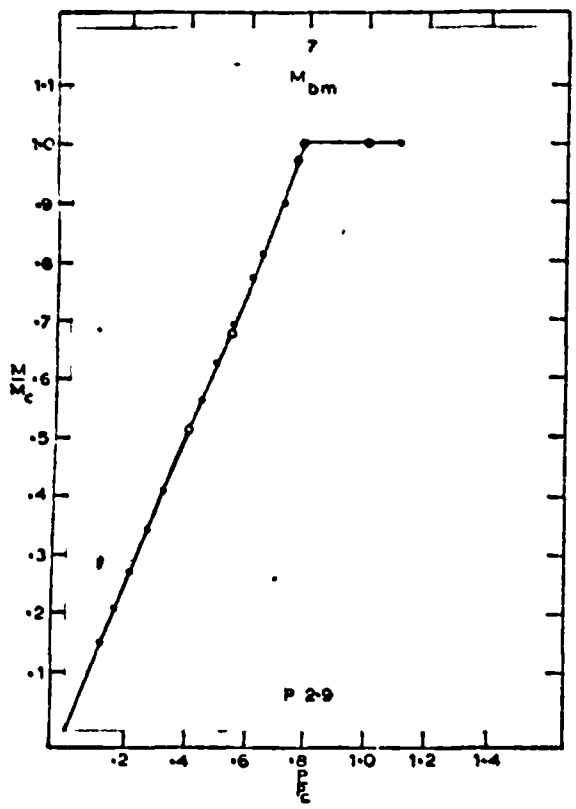
7
M_{bm}
P 2-9
$\frac{M}{M_c}$
$\frac{P}{P_c}$

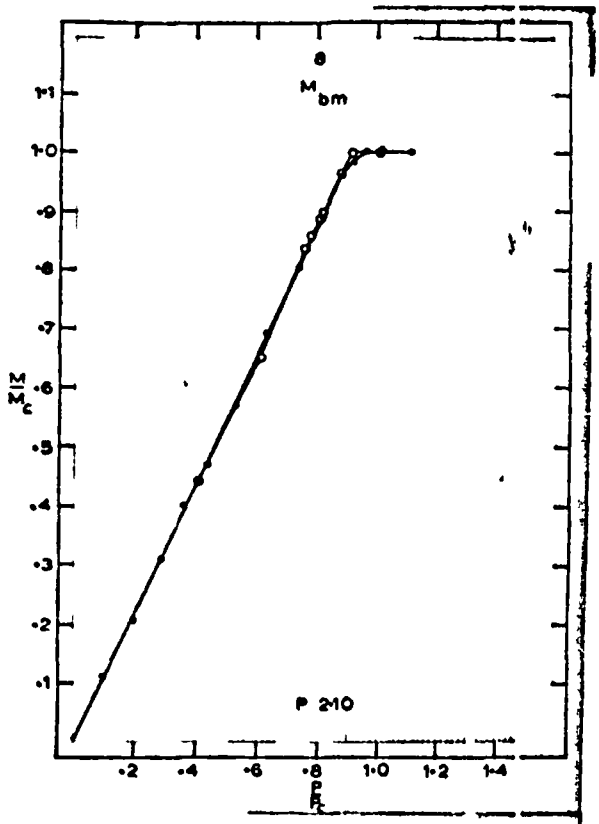
8
M_{bm}
P 2-10
$\frac{M}{M_c}$
$\frac{P}{P_c}$

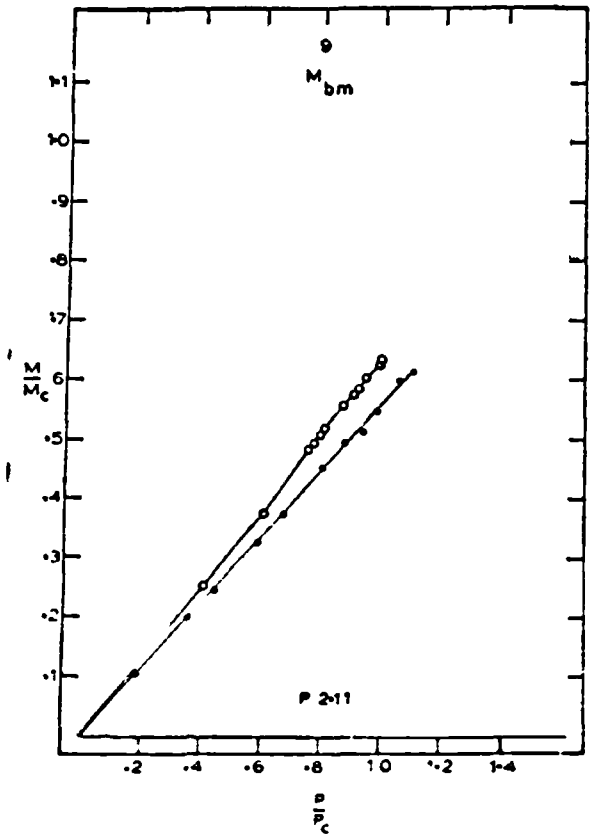
9
M_{bm}
P 2-11
$\frac{M}{M_c}$
$\frac{P}{P_c}$

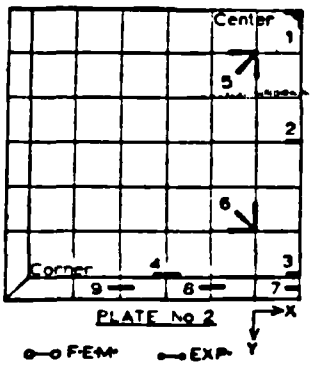
Center
Corner
PLATE No 2
F-E-M
EXP
X
Y

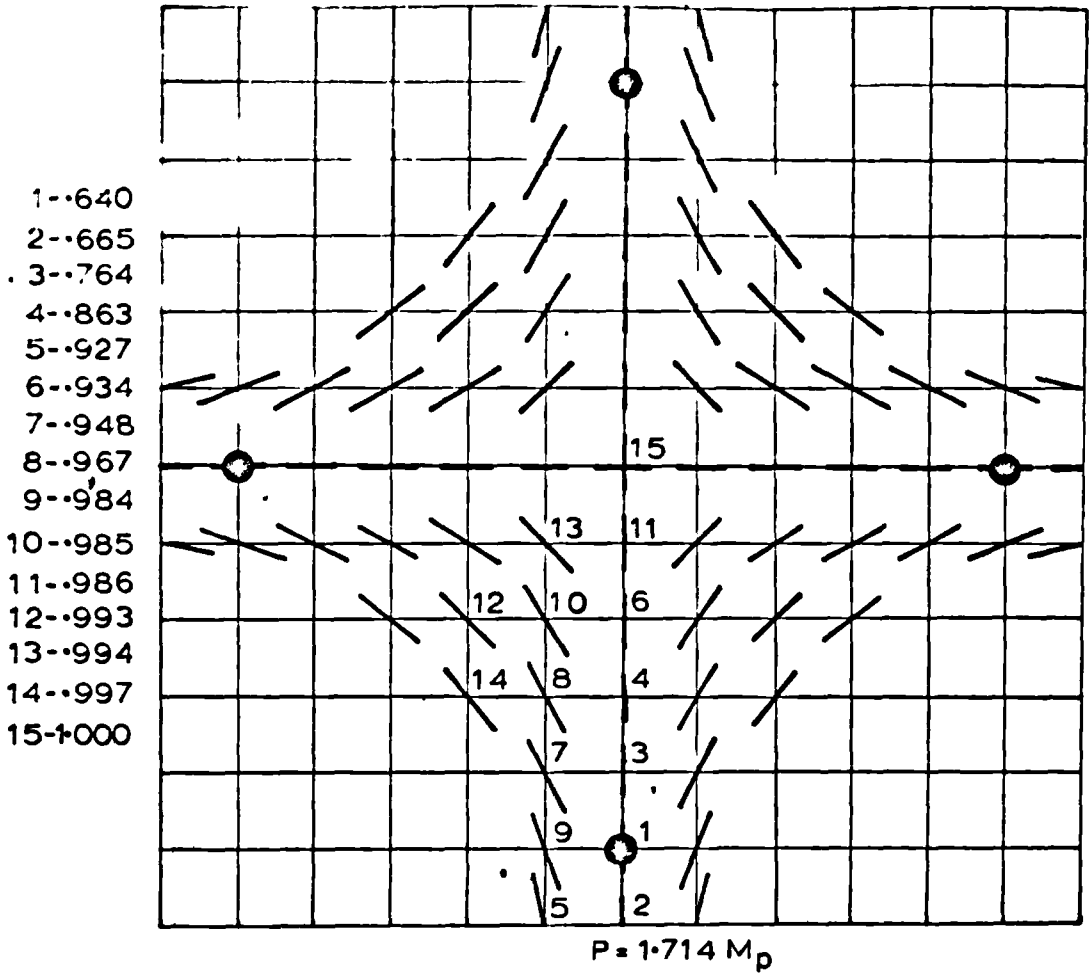

ν = ·30

M_p = 1·0 D/L

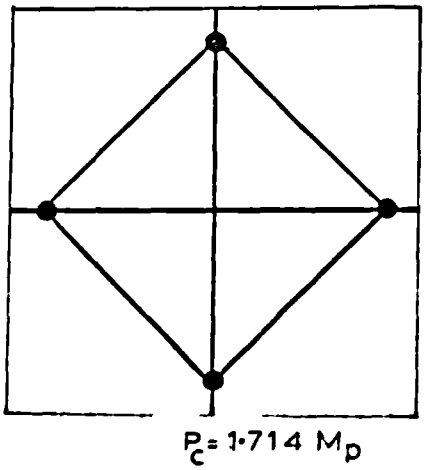

$\frac{P_e}{P_c}$ = ·640

$\frac{P}{P_c}$ = 1·000

Pattern No.7

the collapse load was about 3% below this value although the graphs do not show this.

(b) Generalized Stresses

With the exceptions of Mx at positions 1,5 and 6, the graphs of generalized stresses (P3.1 to P3.11) show good agreement. The spread of plasticity predicted by computer is quite evident experimentally. The largest discrepancy in generalized stress occurs around the center of the plate since the computer indicates that the center is the final plastic region before collapse but experimentally the plate reaches only 60% of the limiting generalized stress value. It was quite evident during the test that the central region was not developing plasticity and of the two possible collapse mechanisms of limit analysis, only the across-diagonal mode developed. The reason for this mode occuring rather than the rectangular one is found in the comparison of collapse loads for the mechanisms of Figure 5.11a and b.

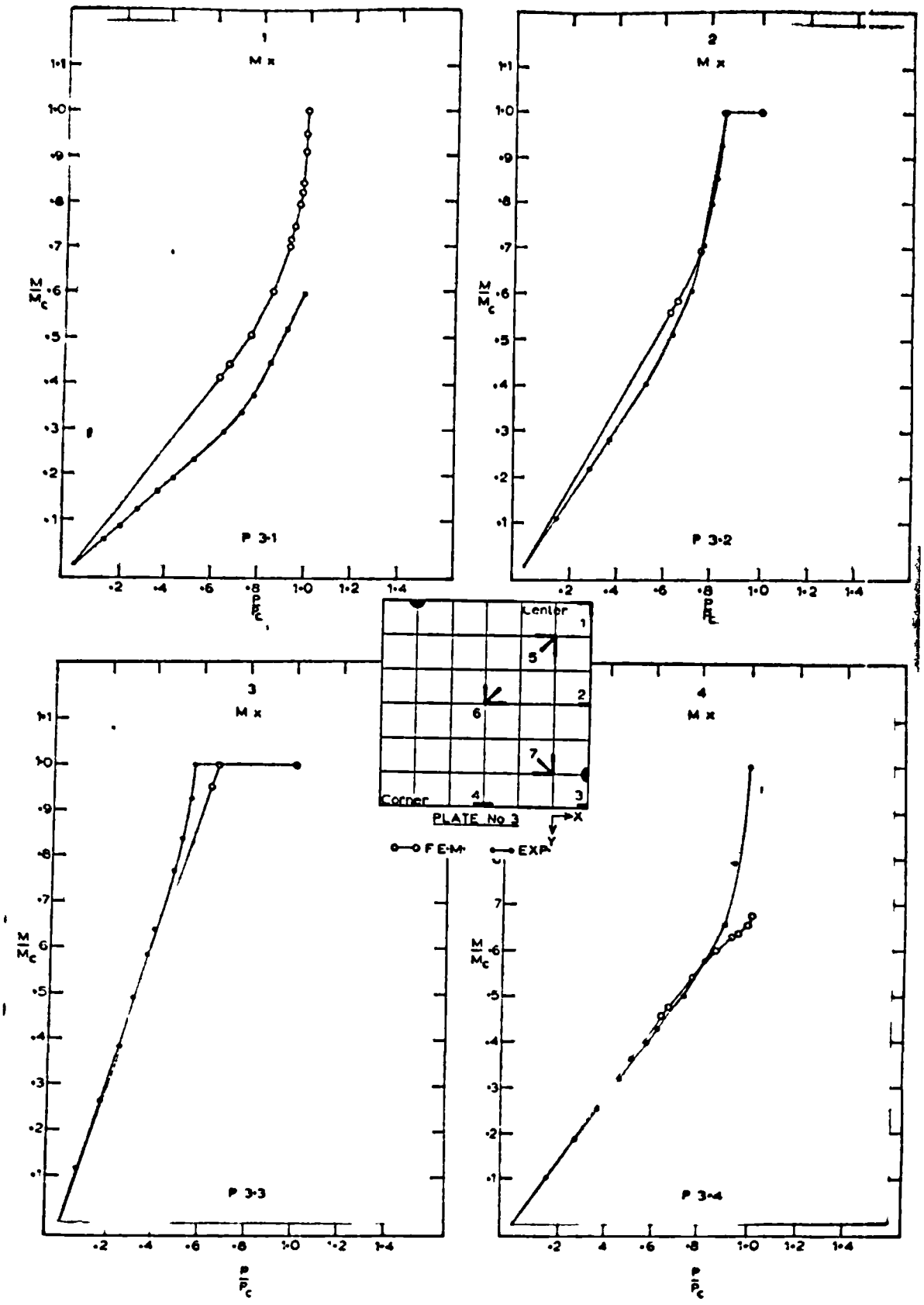
1
M x
P 3·1
2
M x
P 3·2
3
M x
P 3·3
4
M x
P 3·4
Center
Corner
PLATE No 3
FEM
EXP

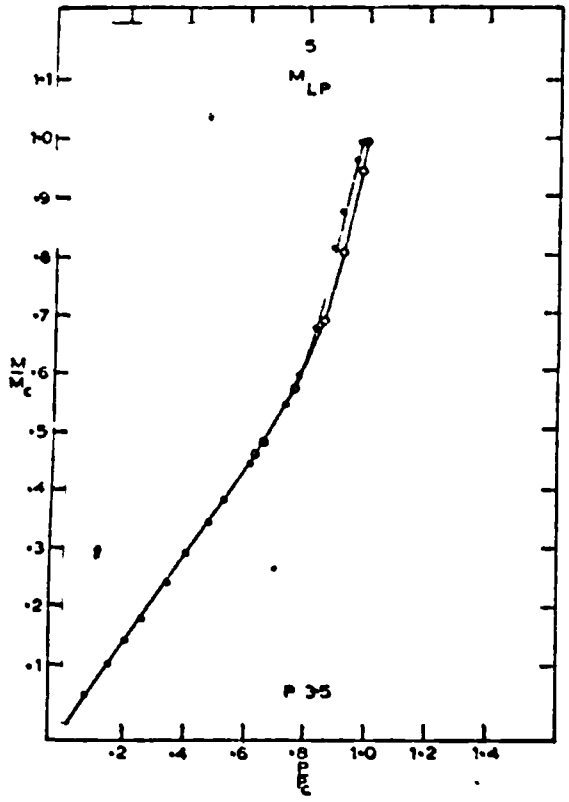
S
M LP
P 35
M/Mc
P/Pc

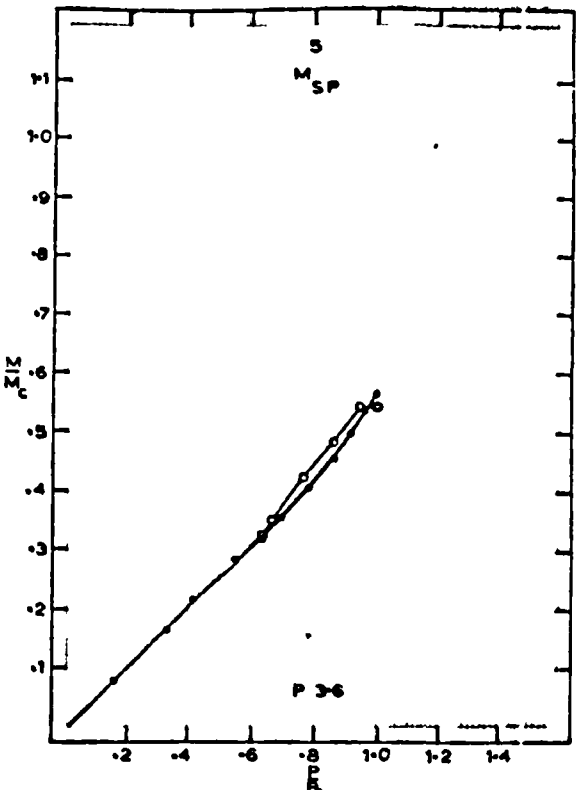
S
M SP
P 36
M/Mc
P/Pc

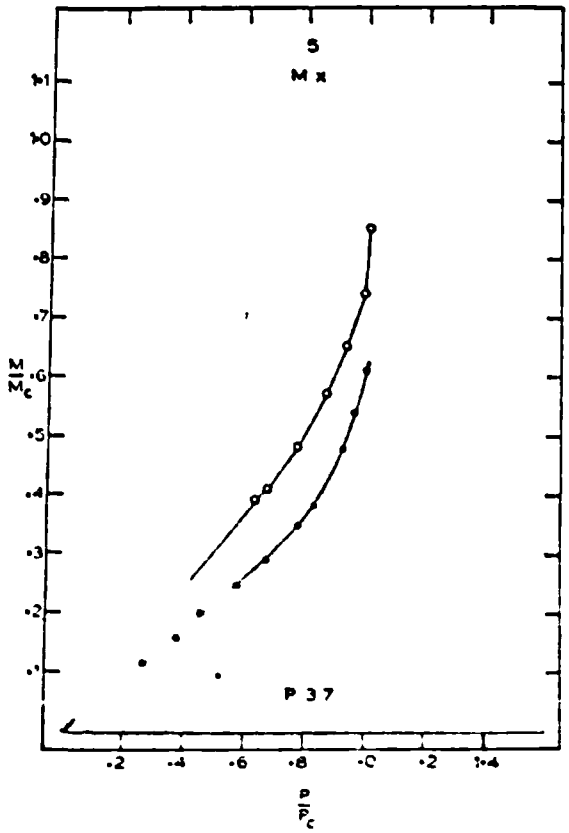
S
M x
P 37
M/Mc
P/Pc

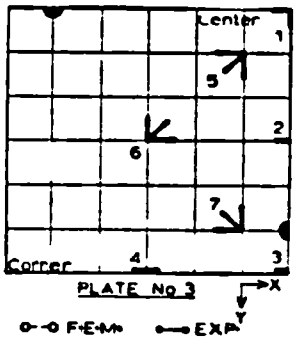
Center
Corner
PLATE No 3
X
Y
F-E-M
EXP

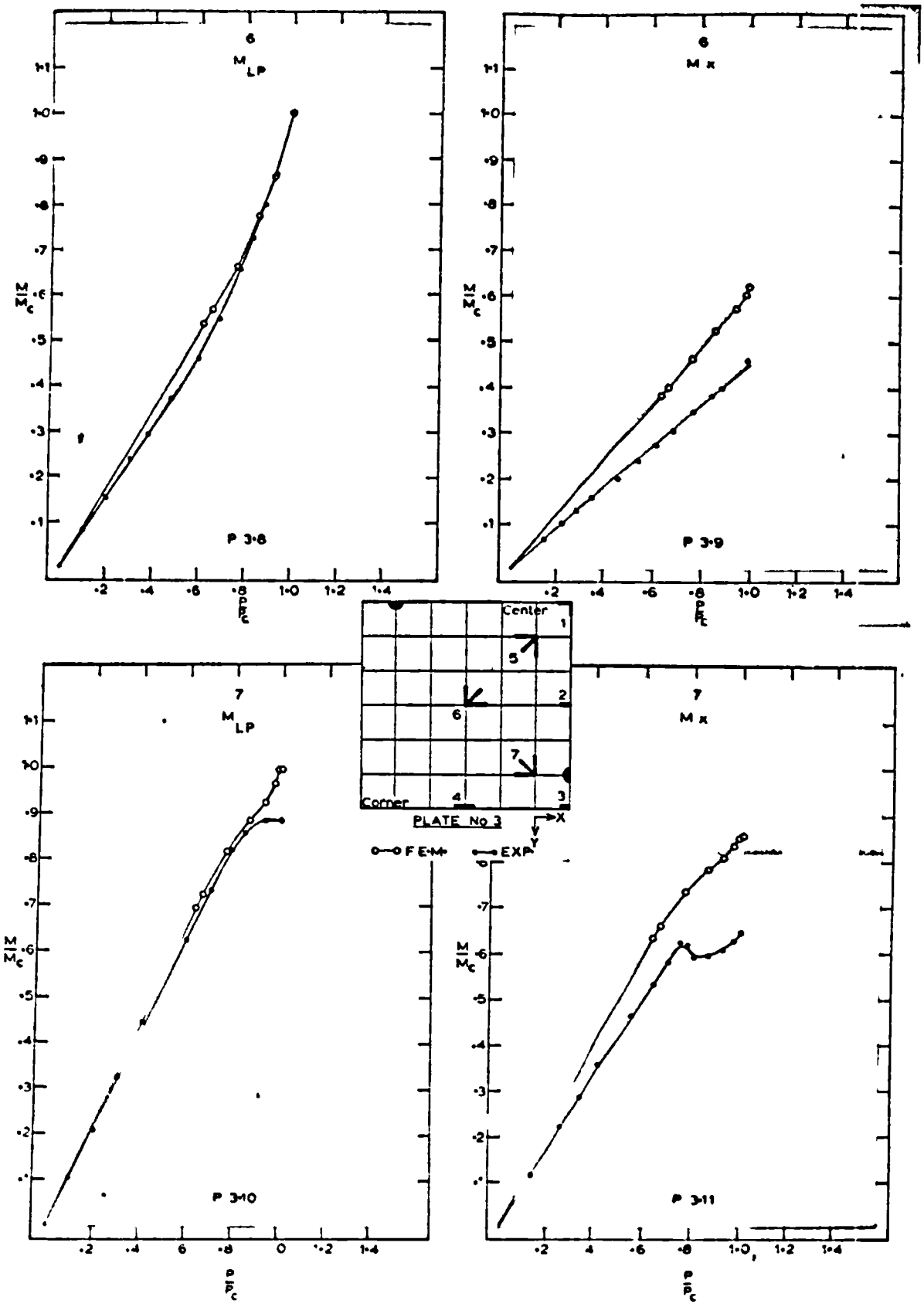
6
M_{LP}
P 3·8
6
M x
P 3·9
Center
Corner
1
2
3
4
5
6
7
PLATE No 3
X
Y
FEM
EXP
7
M_{LP}
P 3·10
7
M x
P 3·11
$\frac{M}{M_c}$
$\frac{P}{P_c}$

Effect of Circular Holes on Collapse Mode

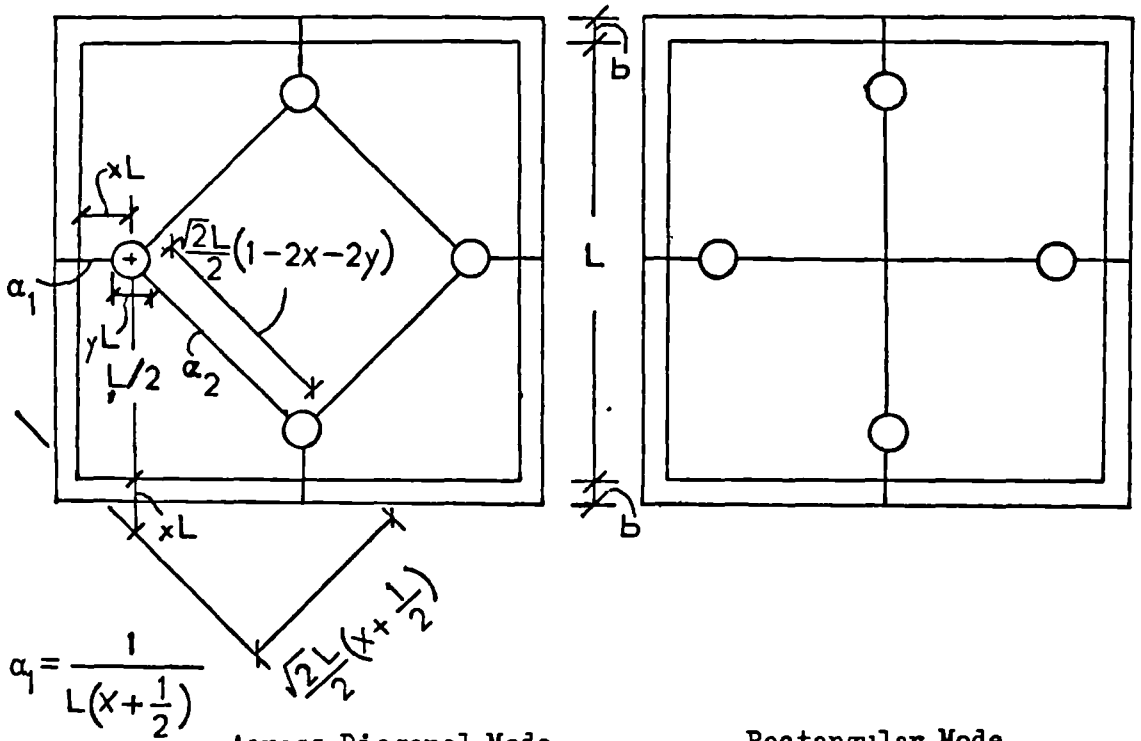

$$\alpha_1 = \frac{1}{L(x+\frac{1}{2})}$$

$$\alpha_2 = \frac{1}{\frac{\sqrt{2}L}{2}(x+\frac{1}{2})}$$

Across-Diagonal Mode (a)

Rectangular Mode (b)

Figure 5.11

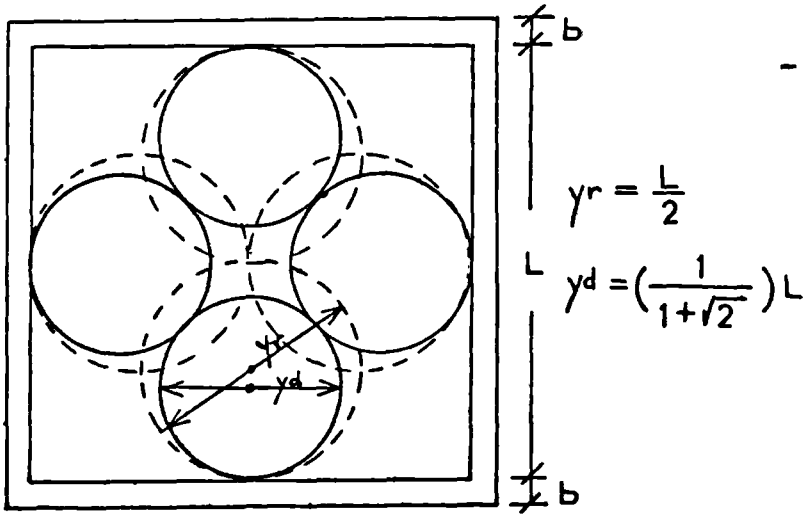

Limiting Size of Holes

Figure 5.12

Here the limit analysis loads are determined from the real geometry of the test plate. That is, including the effects of the holes made for the loading cables (see Photo 4.7). In Figure 5.11 edge beams are included since the next test (Plate No. 4) also failed by the across-diagonal mode. The collapse load for Figure 5.11a is

$$Pd = 2M_c \left[1-(1+\sqrt{2})y+2\gamma_p\right] /(1+2x) \qquad 5.1$$

The collapse load for Figure 5.11b is

$$Pr = 2M_c \ (1-2y+2\gamma_p) \ /(1+2x) \qquad 5.2$$

with their ratio as

$$\frac{Pd}{Pr} = \frac{1-(1+\sqrt{2})y+2\gamma_p}{1-2y+2\gamma_p} \qquad 5.3$$

For the present test, $\gamma_p = 0$ in equations 5.1, 5.2 and 5.3. The subscripts d and r denote diagonal and rectangular respectively when referring to the collapse loads. From equations 5.1 and 5.2 the limit analysis load P_c on Pattern No. 7 can be computed by setting $\gamma_p = 0$ and $y = 0$. Then both modes give identical collapse loads. However, when holes exist on the central axes, the rectangular mode does not occur. This becomes more obvious as the holes increase in size and approach, tangentially the diagonals of the plate. Figure 5.12 illustrates the limiting size of holes causing the collapse load to vanish. If the rectangular mode was assumed, the limiting value of y would be given by equation 5.2 by setting $Pr = 0$. This makes the hole diameter equal to one half the plate span (shown by dotted lines in Figure 5.12). It is obvious that the plate would collapse before $y = .5$. The limiting y value is given

in Figure 5.12 to be $y \doteq .414$.

Consequently, the presence of holes in plate No. 3 resulted in the across-diagonal mode. The experimental collapse load, although slightly lower than the computer and limit analysis ($y = 0$) value, was about 5% above that given for Pd in equations 5.1. That is, the experimental collapse load was between the calculated values based on plates with and without holes respectively.

The failure of the rectangular mode to develop experimentally explains the large differences between computer and experimental generalized stresses around the center of the plate (see Graph P3.1).

5.13 Plate No. 4

(a) Plastic Flow Pattern

Pattern No. 8 indicates composite collapse behaviour involving plate and beam elements resulting in a rectangular collapse mode. Of the 14 stages of plasticity, the first 2 occured in the beams with the final stage appearing at the center of the plate as was the case with plate No. 3. This pattern shows the band of plasticity closer to the central axes when compared with Pattern No. 7. Again the computer collapse load is identical to the limit analysis value (no holes in plate) based on either mechanism shown at the bottom of Pattern No.8. The maximum experimental collapse load attained was approximately 10% above this limit analysis value.

(b) Generalized Stresses

Graphs P4.1 to P4.9 again indicate the accuracy obtained using the element method. The discrepancy of Graph P4.1 has the same explanation

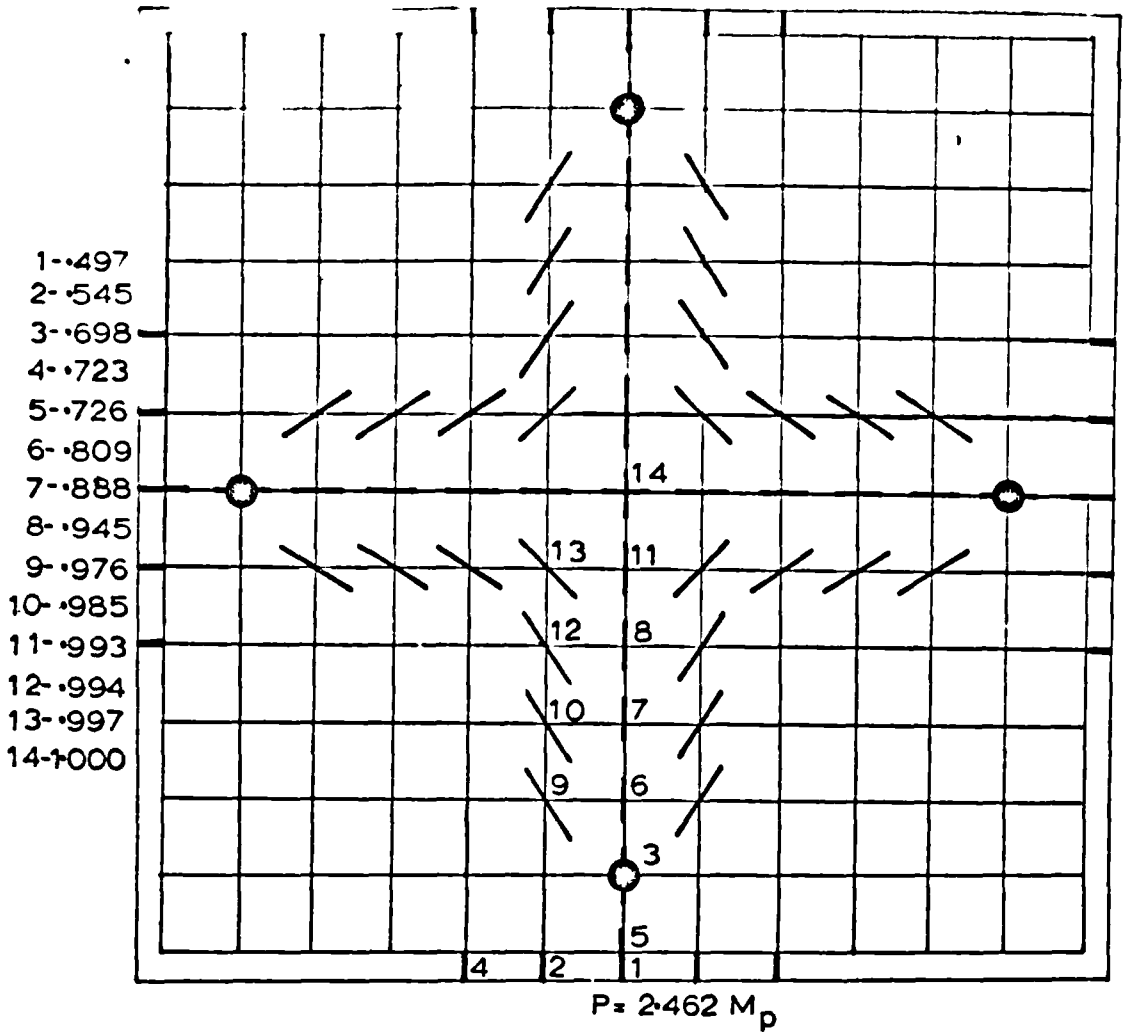

ν =·30

M_p = 1·0 D/L

γ_e =·9050

γ_p =·2180

γ_t =·0048

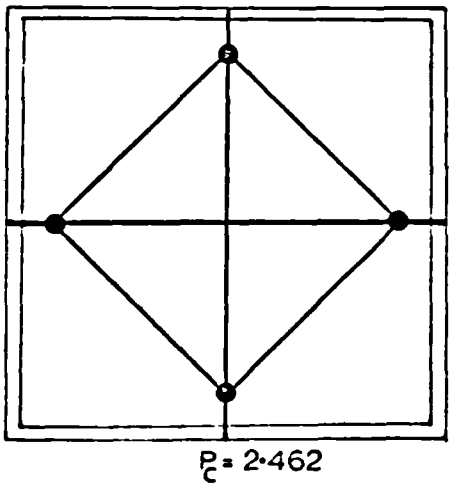

$\frac{P_e}{P_c}$ =·497

$\frac{P}{P_c}$ = 1·000

Pattern No.8

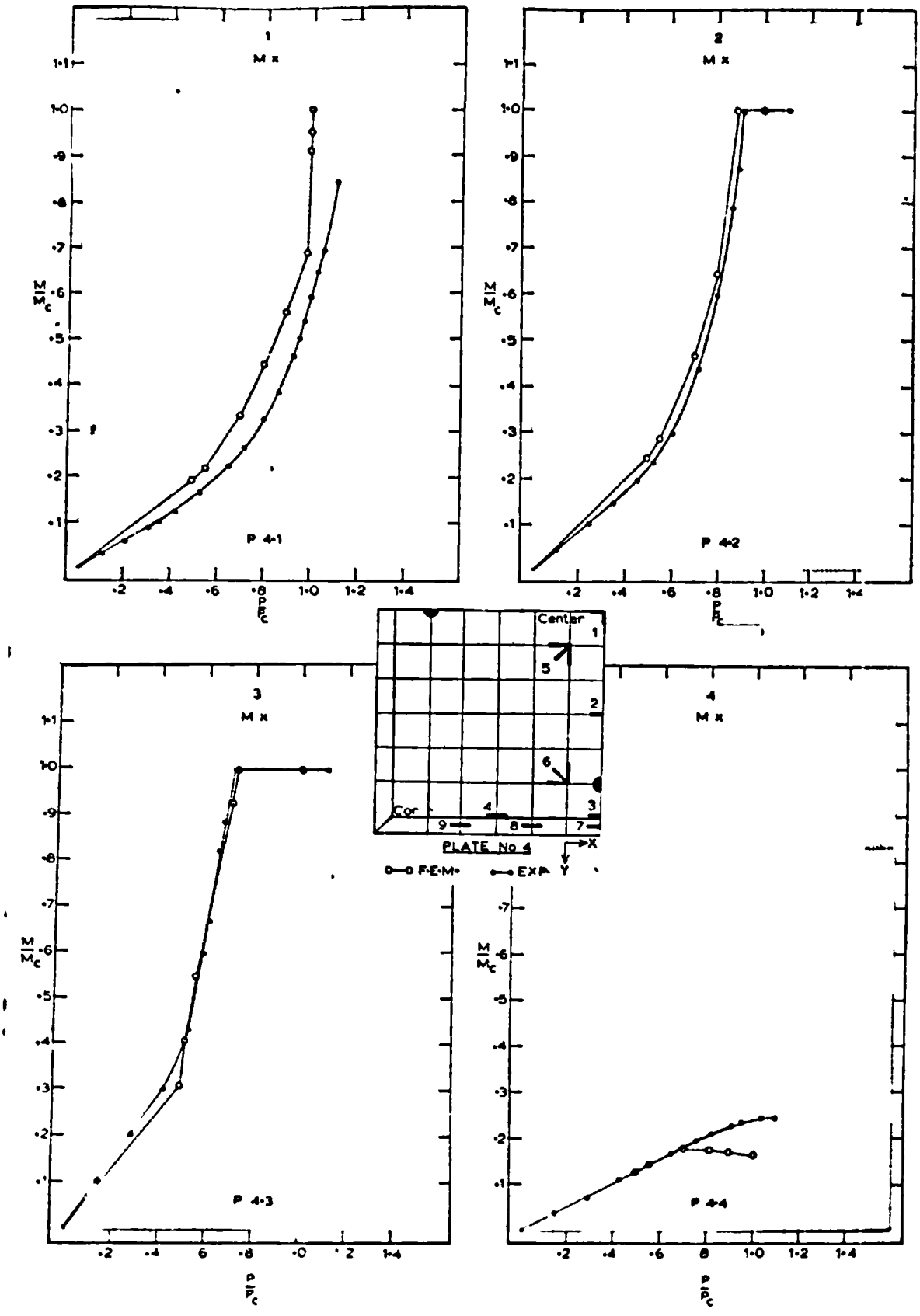
1
M x
P 4·1
2
M x
P 4·2
3
M x
P 4·3
4
M x
P 4·4
M/Mc
P/Pc
Center
Cor
PLATE No 4
F·E·M·
EXP
X
Y

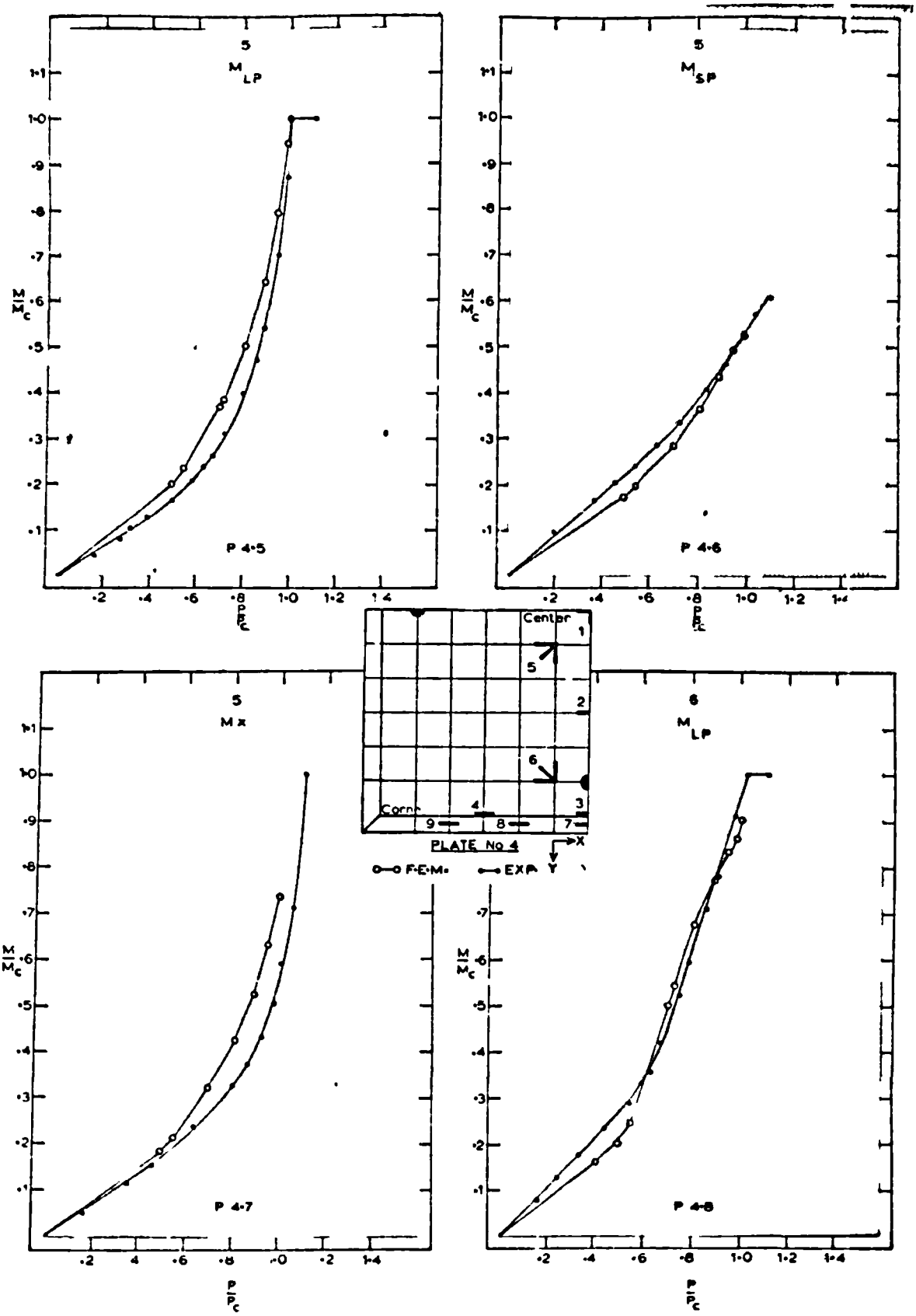
5
M LP
P 4-5
5
M SP
P 4-6
Center
PLATE No 4
F·E·M·
EXP
5
M x
P 4-7
6
M LP
P 4-8
M/Mc
P/Pc

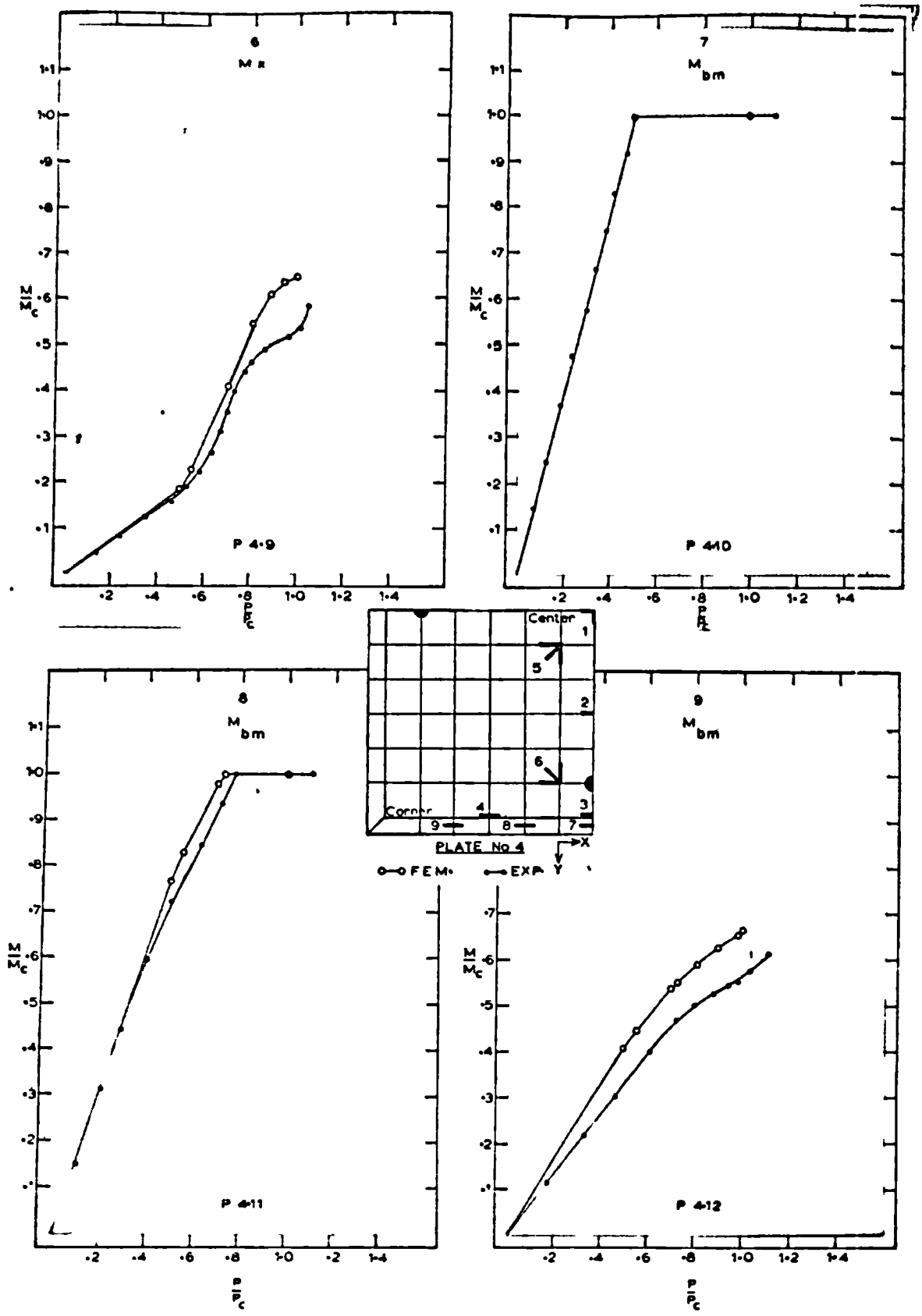
6
M x
P 4·9
7
M bm
P 4·10
8
M bm
P 4·11
9
M bm
P 4·12
M/Mc
P/Pc
Center
Corner
PLATE No 4
FEM
EXP
X
Y

as that for P3.1 except for plate No. 4 the comparison shows a slightly better correlation. The explanation for this can also be explained from the collapse loads for the modes of Figure 5.11. When edge beams are involved, the collapse load does not vanish when $y \doteq .414$ but now is governed solely by the γ_p value. For plates No. 3 and No. 4, $y = .04$. For plate No. 4, $\gamma_p = .218$. Therefore, for plate No. 3 equation 5.3 gives Pd/Pr = .980 and .988 for plate No. 4. Although this difference is small and the across-diagonal mode still governs for plate No. 4, it also indicates that the possibility of this mode occuring is less pronounced than for plate No. 3. This may result in higher generalized stresses in the central region for plate No. 4 than for plate No. 3 since the rectangular mode has a better chance of forming even though it cannot.

The experimental collapse load was approximately 10% above the limit analysis value when holes are excluded in the calculation. When compared with the limit analysis value based on holes with values $y = .04$ and $\gamma_p = .218$ in equation 5.1, the experimental value is about 16% above the true upper bound collapse value.

Good accuracy is again obtained for the beam bending moments with the greatest deviation occuring at points closer to the ends of the beams. This is not surprising since under test the corners of the plates with edge beams appeared to be quite rigid, preventing the beam curvature from attaining as high values as predicted by the F.E.M. model.

5.14 Deflections - Plates No. 1 to No. 4

Graphs P1.0 to P4.0 compare the analytical and experimental deflection at the center and mid-span on the edge of plates No. 1 and 2 and under the point load for plates No. 3 and 4. Reasonably good accuracy is obtained except for position 2 on Graph P2.0 and the deflections of

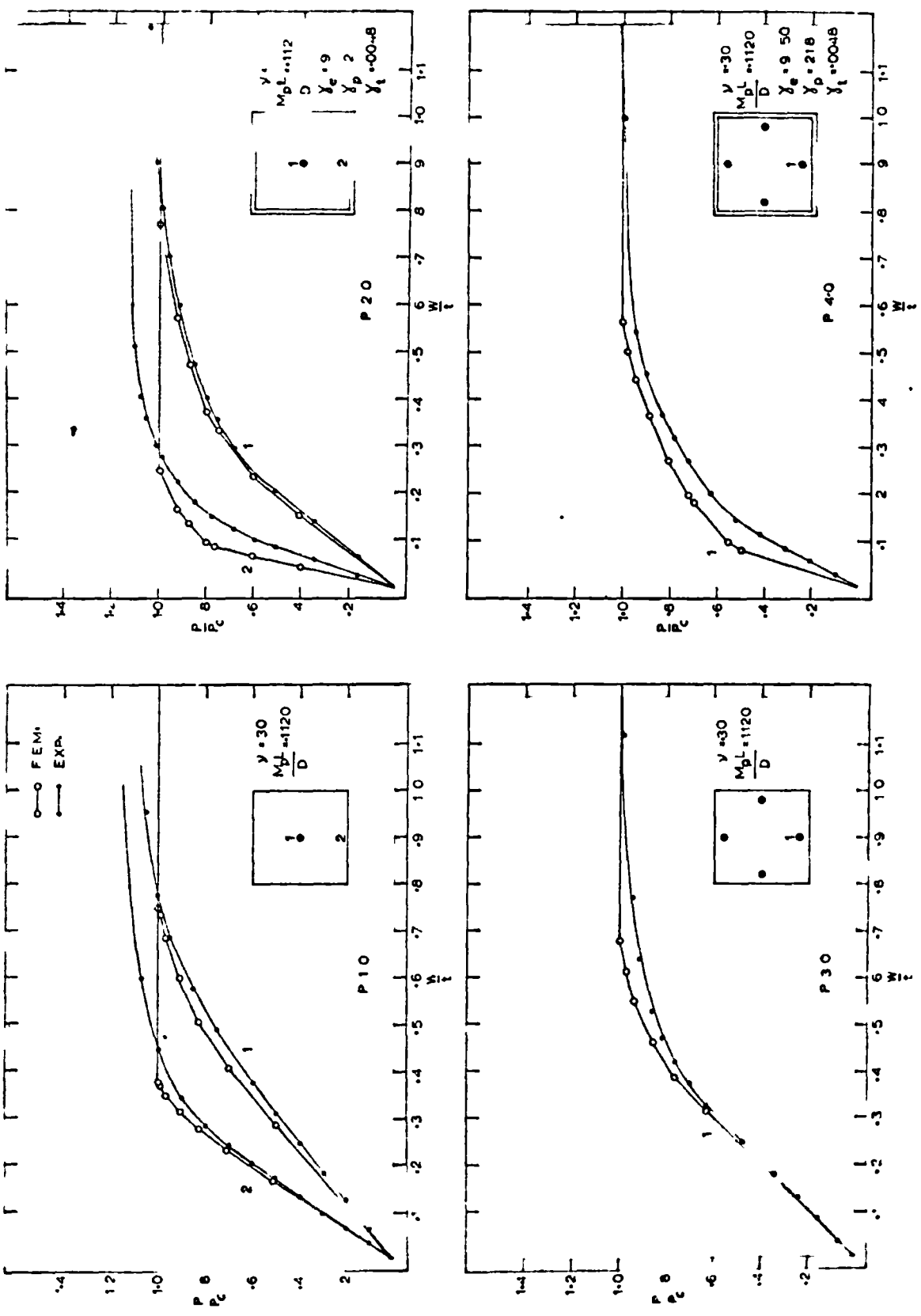
P 20
P 40
P 10
P 30
FEM
EXP
ν =30
ν =.112
ν =.218
γe =9
γe =9 50
γp =2
γp =218
γt =·0048
P/Pc
W/t

Graph P4.0.

Other deflection measurements were taken to check symmetry of transverse displacement. Excellent symmetry was produced in plates No.3 and No. 4 with approximately 10% difference for plate No. 1 and less than 5% for plate No. 2. Measurements could not be made at the centers of plates No. 3 and 4 for lack of space around the loading yoke.

5.15 Change in Directions of Principal Planes

The orientation of principal planes was measured on plates No. 2, No. 3 and No. 4 at one and the same location for each test. The results of these measurements are shown on Graphs P2.12, P3.12 and P4.13. The accompanying figure indicates the position where the angle ϕ was measured. This position corresponds to positions 6,7 and 6 on plate tests No. 2, No.3 and No. 4 respectively.

The object of determining these angles was twofold. Firstly, it was to compare the experimental variation in this angle with the predictions of the F.E.M. approach at some point that would remain non-plastic over a wide range of elastic-plastic behaviour. Consequently, the position shown was selected on plate No. 2. Secondly, it was to assess the reliability of the assumption of constant angle ϕ for plastic nodes during plastic load increments (see section 3.4e). Therefore, the same position was selected on plates No. 3 and No. 4. It was thought that these latter plates would show plasticity in this area during the early stages of elastic-plastic response.

The first objective was accomplished for plate No. 2. The second failed to materialize since experimentally neither plate No. 3 nor No. 4 reached plasticity during the load range indicated by computer.

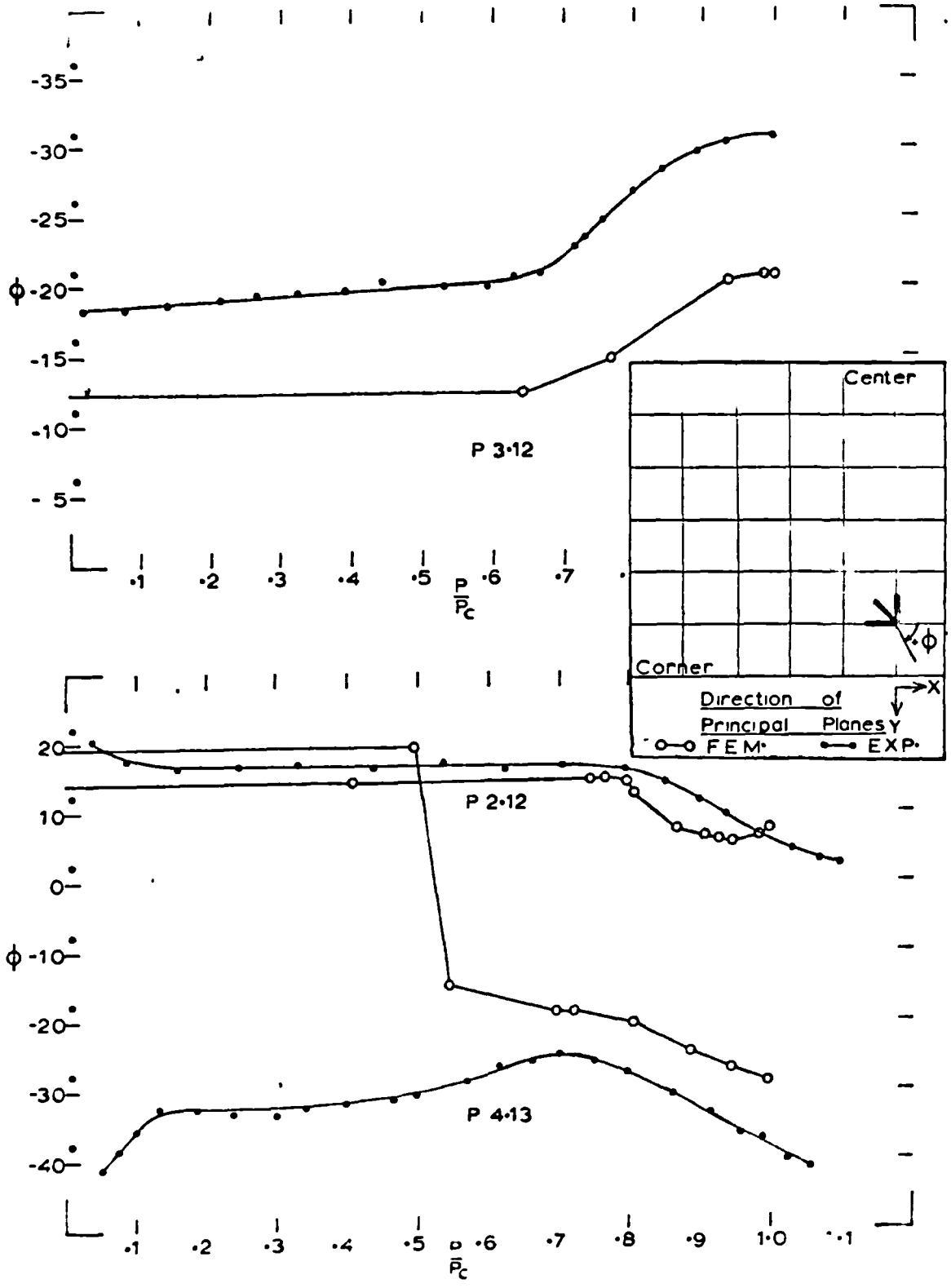
-35
-30
-25
φ -20
-15
-10
- 5
P 3·12
·1 ·2 ·3 ·4 ·5 ·6 ·7
P/Pc
Center
Corner
·φ
Direction of Principal Planes
X
Y
FEM·
EXP·
20
10
0
φ -10
-20
-30
-40
P 2·12
P 4·13
·1 ·2 ·3 ·4 ·5 ·6 ·7 ·8 ·9 1·0 ·1
P/Pc

Furthermore, from the computer results only plate No. 3 indicated plastic flow at the point chosen but this did not occur until 98.5% of the computer collapse load had been reached. This would have made a comparison with experimental plasticity impossible anyhow. It should be mentioned here that none of the computer solutions were available before the slab and plate tests were completed and therefore a proper choice of position for measuring strain could not be predetermined. As a result the graphs presented only satisfy the first objective.

However unsuccessful these attempts were, the results of Graphs P2.12, P3.12 and P4.13 are encouraging. With the exception of the results of Graph P4.13 during the first half of the load range, the form of variation in experimental results is closely reproduced by the F.E.M. model for all three tests. The differences between experimental and analytical are practically constant throughout the load range. That is, 3°, 5° and 8° for plates No.2, No. 3 and No. 4 respectively.

5.16 Evidence of Inhomogeneous Deformation

Photos 5.1 and 5.2 show evidence of inhomogeneous plastic deformation in the form of Lüder's lines appearing in the mill scale. These lines appear as a result of the maximum shearing generalized stress attaining one half the limiting fully plastic bending value (M_p). The plate material between the lines remains wholly elastic while the plastic straining occurs in the line.

In Photo 5.1 this phenomenon occurs as a result of the plate material shearing plate-to-atmosphere at an angle of 45° to the plate surface. This pattern appeared on plate No. 1 on the compression face only, at least to the naked eye. This plate had a mill scale that was not

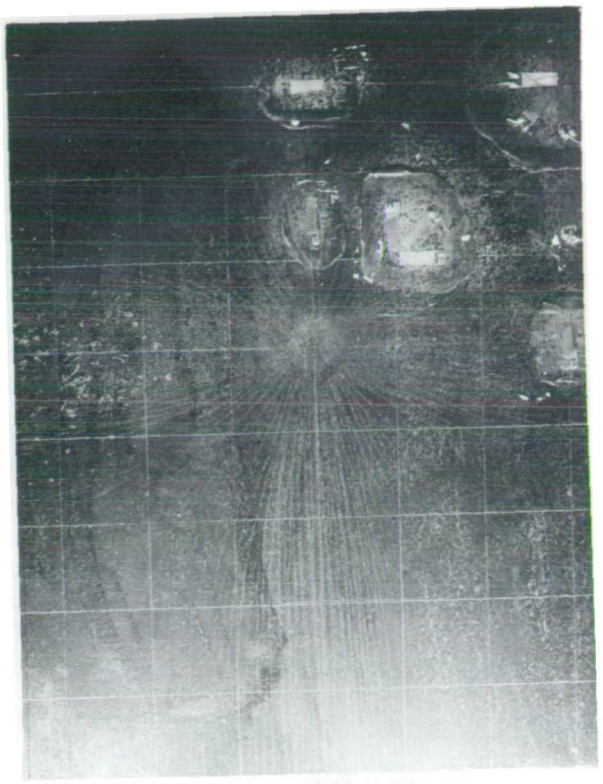

Photo 5.1

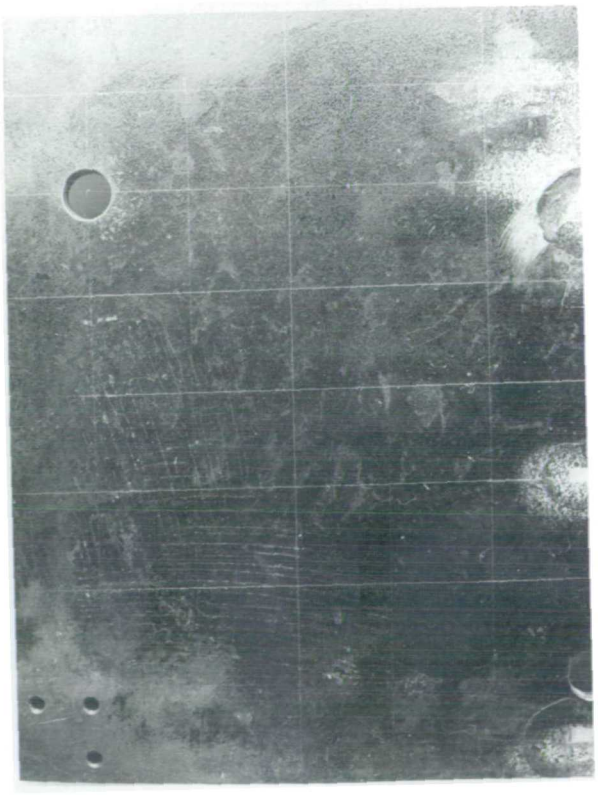

Photo 5.2

removed before testing since the plate was tested as purchased. The other three plates were normalized and the mill scale removed before testing. Consequently, similar patterns (shearing plate-to-atmosphere) did not appear, at least to the naked eye. On plate No. 3 Lüder's lines formed near the corners of the plate on the underside. As seen in Photo 5.2 these lines form a criss-cross pattern at approximately 45° to the principal plane directions. This represents plastic behaviour resulting from the maximum shearing generalized stress satisfying the Tresca +, - yield condition in the plane of the plate.

The only strain measurements made near the corners of the plates were made in plate No. 1. Unfortunately due to one faulty gauge in the strain rosette, only the largest of the principal generalized stresses could be determined by using the gauges on the diagonal. This principal value did not reach M_p at collapse and it was not possible to determine if the $|M^1 - M^2| = M_p$ state existed there or not. But since this plate had sufficient mill scale to show in-plane shear plastic straining and none was evidenced, it is reasonable to assume that the +, - Tresca condition was not satisfied.

To illustrate <u>possible</u> generalized stress states that could produce the effects indicated by Photo 5.1 and 5.2, Mohr circles are presented in Figure 5.13 accompanied by two-dimensional projections of the Tresca criterion and the possible stress state.

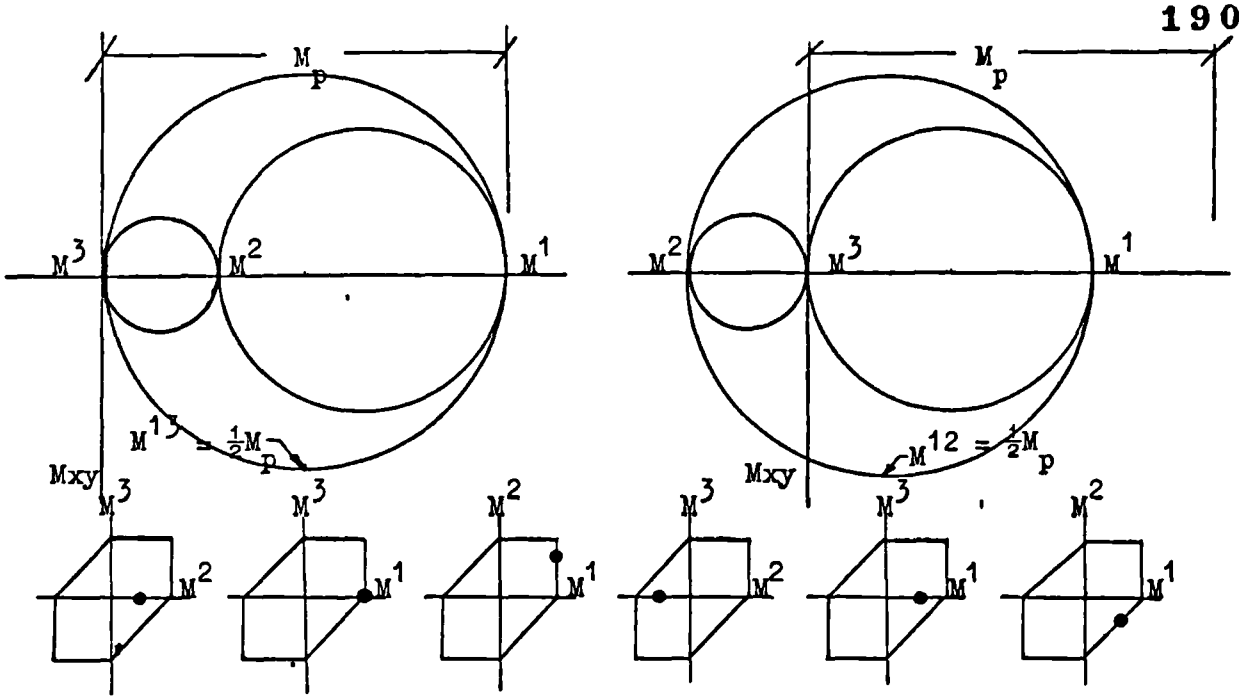

For Photo 5.1
(a)

For Photo 5.2
(b)

Possible Generalized Stress States for Photos 5.1 and 5.2

Figure 5.13

In each of Figures 5.13a and b the maximum shearing generalized stress has a value of $\frac{1}{2}$ Mp and therefore satisfies the Tresca criterion. From the projections of the stress state of Figure 5.13a onto the M^1,M^3 and M^1,M^2 planes, it is clear that both conditions indicate plastic straining in the plane of the plate. M^1 = Mp in the M^1, M^2 plane and in the M^1, M^3 plane plastic shear straining occurs at 45^o to this plane since M^3 = 0 and the stress state occurs at the obtuse angled corner of the yield locus.

The other stress situation that could have resulted in the lines on Photo 5.2 appears on the yield locus at only one point in Figure 5.11b (i.e. $|M^1 - M^2|$ = Mp). Therefore, in this case, the plastic straining is due to shearing failure in the plane of the plate and because of equal

shear stresses on orthogonal planes, a criss-cross pattern develops.

From the computer solutions for the metal plate tests, the formation of Lüder's lines on plate No. 3 is well substantiated since only plate No. 3 had a generalized stress state near its corners that would satisfy the Tresca criterion in the +,- quandrant. One corner of the plate analysed is shown in Figure 5.14 on which is superimposed the stress conditions $|M^1 - M^2| = Mp$ produced by computer at the collapse stage of the analysis. Also shown are the load ratios P/P_c at which the node had attained a value of $(M^1 - M^2)$ sufficient to satisfy the Tresca condition. The region over which the Lüder's lines have formed in Photo 5.2 is also shown.

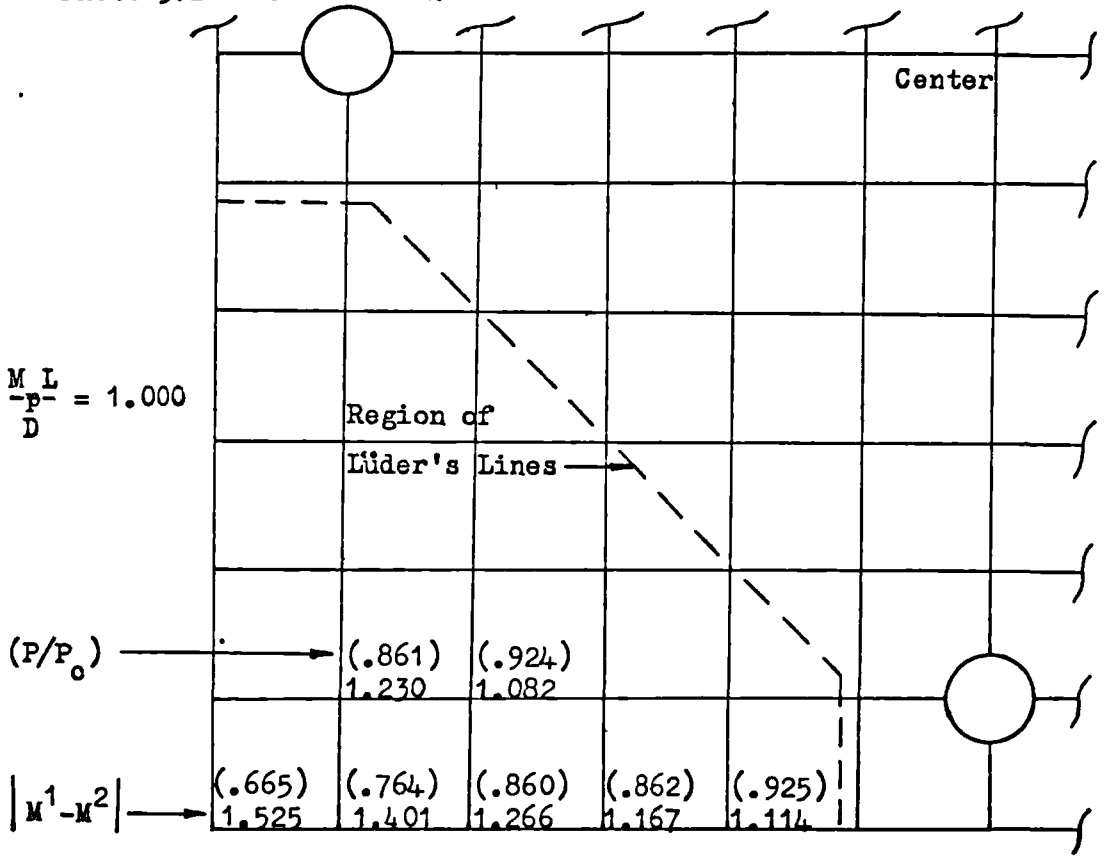

Plate No.3 - Analytical Evidence of +,- Tresca Yield

Figure 5.14

From the results shown it appears that analytically, the generalized stress conditions required to satisfy the $|M^1 - M^2| = Mp$ condition would occur near the corners at load ratios above .86. This is the only analytical solution in which the Tresca criterion is violated by assuming a square yield locus.

Since experimental evidence suggests that only one plate test involved a shearing type failure, it is reasonable to conclude that plastic straining in the other plate tests was caused by generalized stress states that can be positioned on a square yield locus. If so, then the use of a square criterion in the computer analyses for the plates tested is justified. The experimental-analytical comparisons of results previously presented seems to indicate that this is so.

CHAPTER 6 - ADDITIONAL COMPUTER SOLUTIONS

6.1 General Remarks

In this chapter three elastic-plastic slab analyses are presented and their collapse stage generalized stress fields are compared with certain lower bound solutions. Only the plastic flow patterns for the analyses are given, although the complete histories of generalized stress and displacement fields were also established.

The choice of solutions made here was influenced by the "junction modes" described by Wood[22] in which square slabs with edge beams of $\gamma_p = 1.0$ develop collapse mechanisms of a rectangular type, a diagonal type or any combination of either of these types. Consequently, the three analyses chosen were for the following square slabs each carrying a uniformly distributed load.

(1) Simply supported

(2) Free edges with corners supported vertically

(3) Edge beams with $\gamma_p = 1.0$ with corners supported vertically

The x direction for all the graphs of the chapter is directed along the line marked 1 from left to right on the figure accompanying the graphs. The y axis coincides with the center line shown and is directed from top to bottom of the figure.

Simply Supported Square Slab

6.2 Plastic Flow Pattern

The plastic flow pattern for this slab is shown by Pattern No. 9 in which a diagonal collapse mode appears. This solution results in

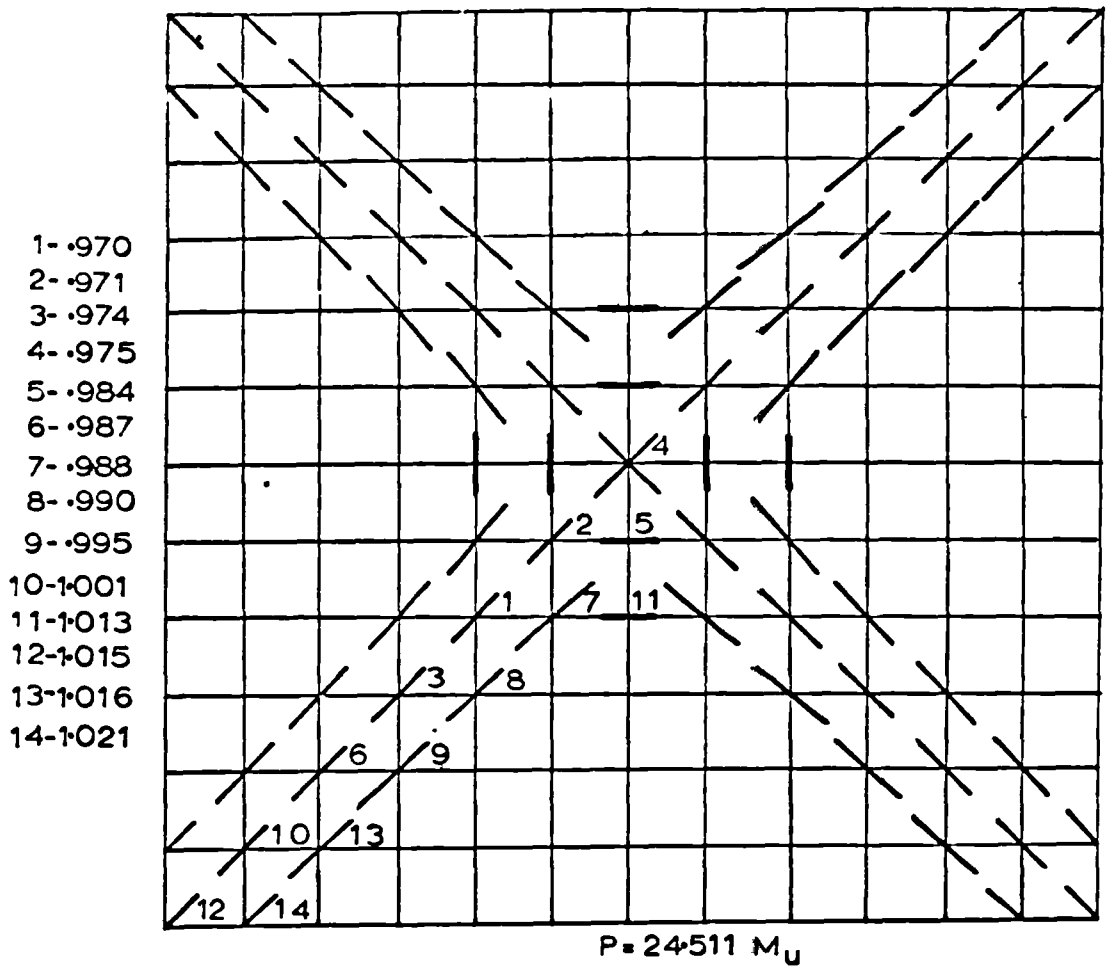

$y = \cdot 15$

$M_u = 1 \cdot 0\ D/L$

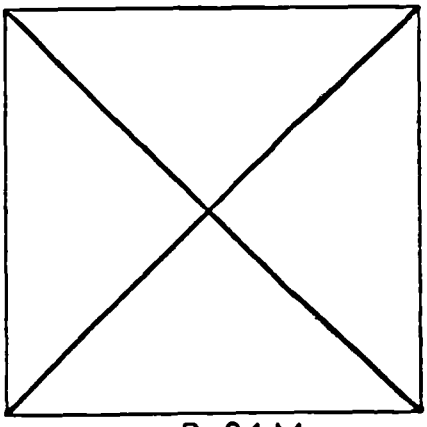

$\frac{P_e}{P_c} = \cdot 970$

$\frac{P}{P_c} = 1 \cdot 021$

Pattern No.9

very little redistribution of generalized stress between the elastic limit and collapse stages of load. As a result the final generalized stress field is much the same as the elastic one except, of course, close to and along the diagonals.

A definite band of plasticity develops about the diagonals with 14 stages of plastic behaviour resulting in a collapse load 2% above the limit analysis value. One explanation for this discrepancy is the fact that the directions of plastic flow lines are diagonally across the elements and since the elements remain wholly elastic within their boundaries the mechanism cannot form entirely in accordance with the kinematics required for a diagonal mode.

Before collapse could occur the outer boundaries of the band had to reach the support (plastic stage 14 in Pattern No. 9). It is possible that from this result diagonal type modes can only develop (when using square or rectangular elements) if all nodes of the elements on the diagonal are plastic allowing sufficient reduction in bending resistance to form a mechanism. This might explain why the band of plasticity extended to the supports since in Pattern No. 9 all the diagonal elements have four plastic nodes.

It is not to be concluded that because the diagonal mode developed in this solution gives only a 2% error in collapse load that the use of square elements will always give as small an error when diagonal type modes are involved. The simply supported slab is not the best type of problem to solve in attempts to investigate this accuracy because of the little redistribution involved. The limit analysis collapse load is only about 3% above the elastic limit load and the computer collapse load is of the same order above the limit analysis value.

6.3 Comparison with Lower Bound Solutions

The generalized stress field at collapse ($P/P_c = 1.021$) is compared with those for the unique solutions (1) and (2) outlined in Chapter 1. Comparisons are made across one half of the slab span ($L/2$) at three positions as shown on the figure with Graphs 6.1 to 6.4. The solution referred to as "Wood" is actually due to Prager as reported in Chapter 1 but has been summarized by Wood[4].

It is clear that the Vallance solution is very similar to the finite element results. The Wood solution is a good indication of the absurd generalized stress fields which can sometimes occur for lower bound solutions. It is quite unreasonable to believe that, for the simply supported slab which is almost in a collapse state at the end of the elastic limit, the final generalized stress field would look anything like Prager's solution.

The error in generalized stress perpendicular to the boundary in the element method is shown in Graph 6.2 and represents less than 2% of the maximum value.

In Graph 6.4 the support reaction between slab and beam results in the distribution of load on the support as shown. In addition to the distributed load there exists a concentrated corner reaction acting upwards on the beam, downwards on the corner of the slab. This reaction is the same for computer and lower bound solutions. Again the Vallance and F.E.M. solutions are similar. The integration of these reaction distributions around the slab periphery combined with the concentrated corner reactions should equal the collapse intensity of load. For the Vallance and Wood solutions this is so. In the F.E.M.

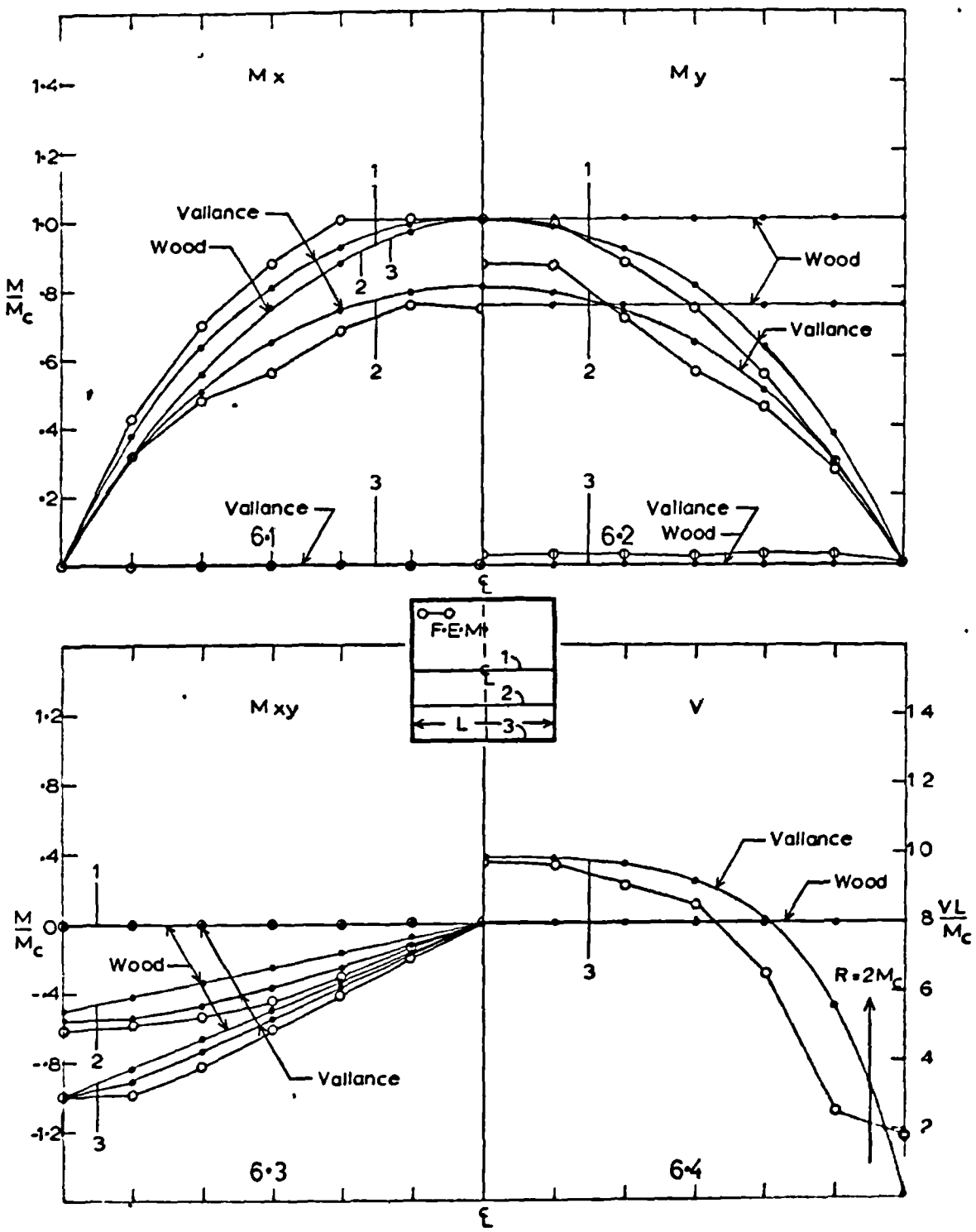
Mx
My
Mxy
V
Vallance
Wood
F·E·M
L
R=2Mc
6·1
6·2
6·3
6·4
M/Mc
VL/Mc

solution an underestimate of total reaction results in a difference of 12% between reaction and applied load. This error is partially due to the approximate nature of the element method along boundaries.

The distinct difference between the lower bound solutions and that by the element approach is the indication of redistribution of generalized stresses resulting in irregularly shaped distributions.

Square Slab with Free Edges and Corner Supports

6.4 Plastic Flow Pattern

This solution resulted in 27 plastic nodes forming out of the 28 possible. The collapse load was .5% below the limit analyses value. This error is most likely due to round off errors occuring in the scaling procedures to determine plastic nodes. The collapse mechanism in Pattern No. 10 is the same as that given by limit analysis with the first indication of plasticity occuring in the most highly stressed area at mid-span on the edges. The final plastic node occurs at the center resulting in collapse of the plate.

6.5 Comparison with a Lower Bound Solution

This solution when compared with the unique solution (3) of Chapter 1 shows a remarkable similarity as indicated by Graphs 6.5 to 6.7. For the comparison, γ_p = o when determining the twisting generalized stress of equation 1.17. The lower bound Mx and My generalized stresses shown here are identical to those previously given for the "Wood" simply supported case and in fact these values are the same in the next solution that is presented. Wood has based these solutions on the Prager stress field mentioned earlier. The only difference between the "Wood" lower

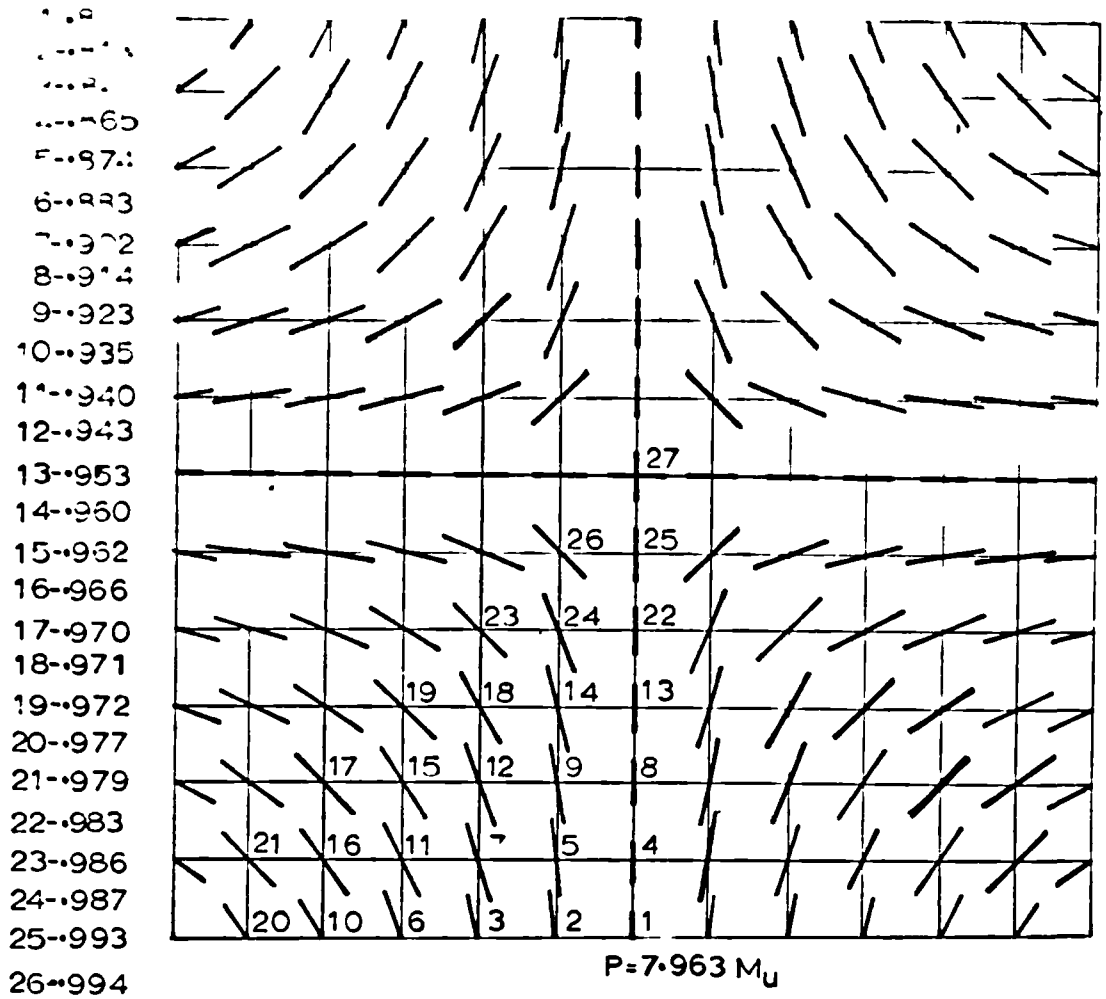

ν =·15

M_u=1·0 D/L

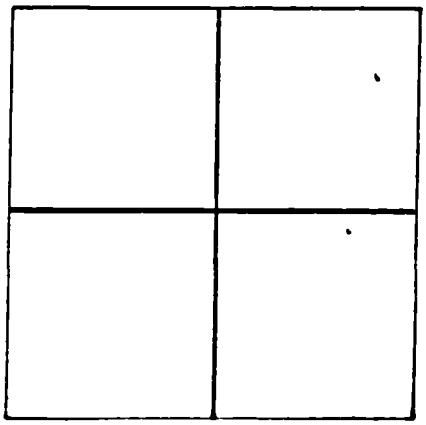

$\frac{P_e}{P_c}$ =·804

$\frac{P}{P_c}$ =·995

P_c=·814

Pattern No.10

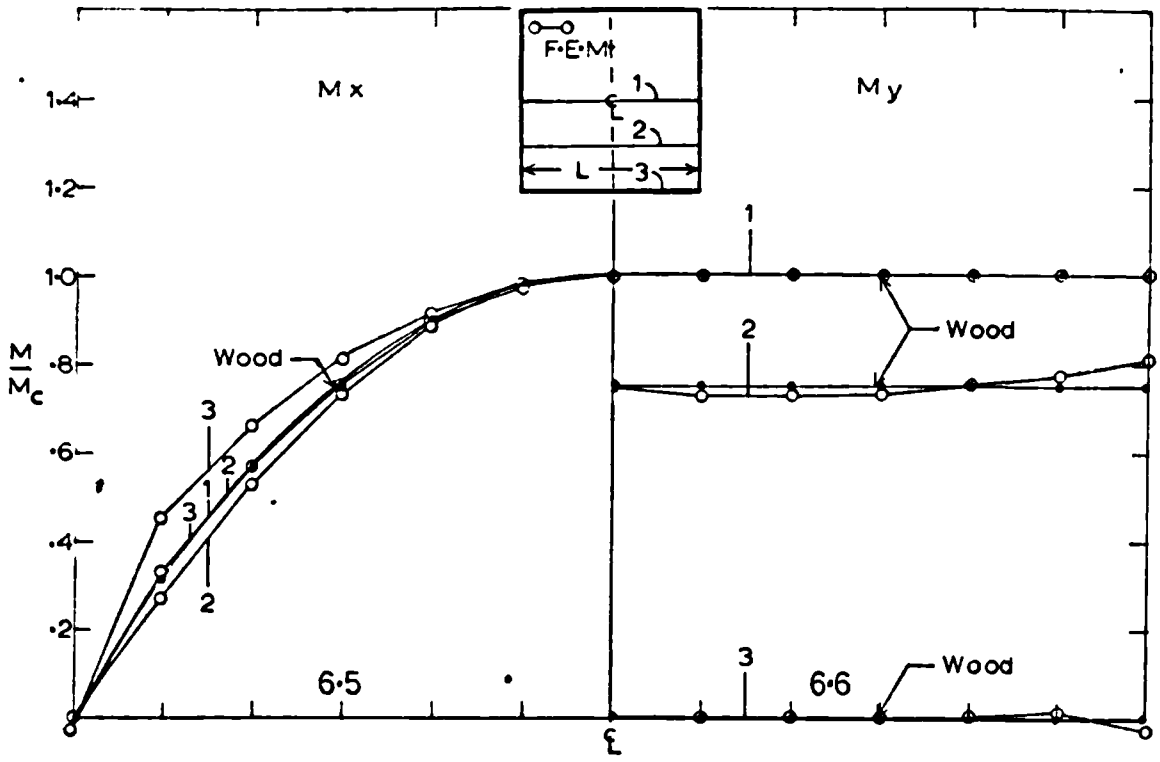
F·E·M
M x
M y
L
1
2
3
1·4
1·2
1·0
·8
·6
·4
·2
M/Mc
Wood
Wood
Wood
6·5
6·6
ℓ

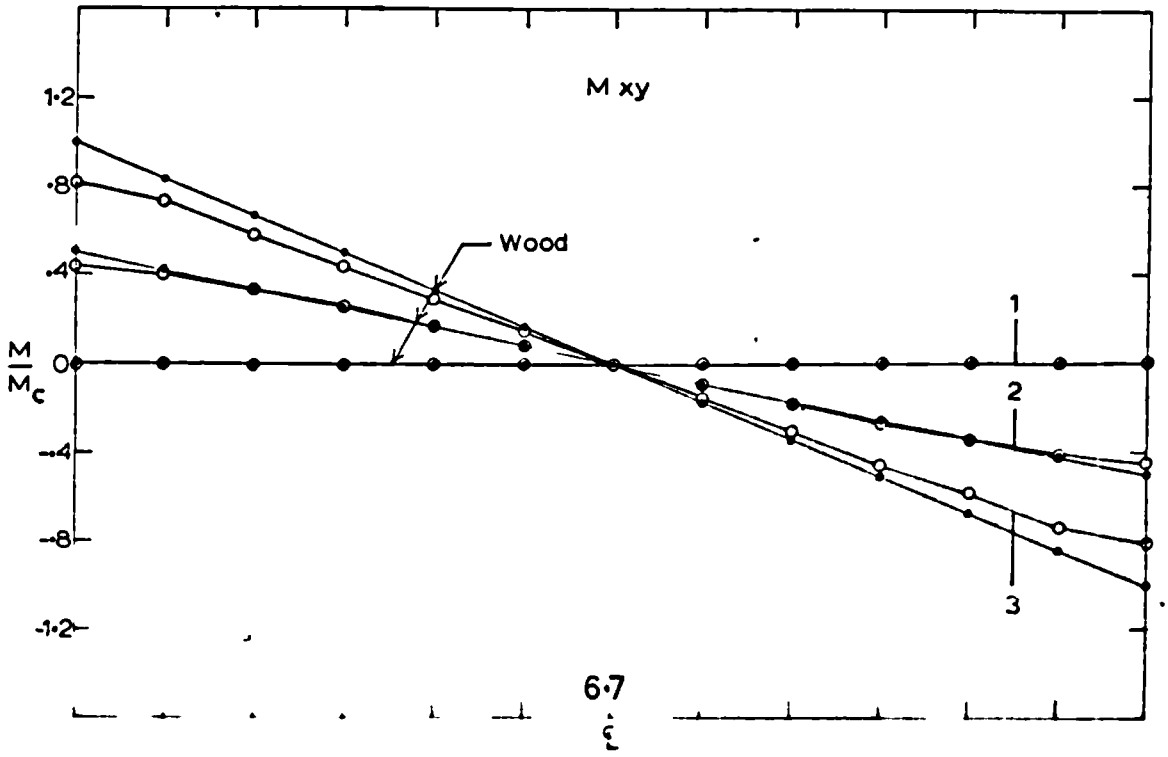
M xy
1·2
·8
·4
0
-·4
-·8
-1·2
M/Mc
Wood
1
2
3
6·7
ℓ

bound generalized stress fields is the value of Mxy.

From Graph 6.7 the F.E.M. gives Mxy to be less than M_c which means that the corner reaction between slab and support is less than it should be. The results show that since the corner node did not become plastic, the reaction is approximately 17% below the required value to support the collapse load indicated by Pattern No. 10. This error could be due to the usual inconsistencies experienced on boundaries in finite element analysis. However, this difference is larger than is usually experienced on boundaries and some may be due to the way in which plastic flow is allowed only along element boundaries (see section 3.5b) resulting in a displacement field which does not permit the twisting generalized stresses to increase properly. This may also explain the small differences between the analytical and unique collapse loads that occur in all three solutions presented here.

The reasons for the discrepancies in support reactions, variation of twisting generalized stress, errors in generalized stresses on boundaries that do occur have not been investigated in this study and therefore the statements made above are strictly conjectures on the part of the writer.

Square Slab with Edge Beams and Corner Supports

6.6 Plastic Flow Pattern

This solution results in the plastic flow distribution of Pattern No. 11 in which 23 stages of plasticity are experienced before the final collapse mode forms. This problem is an example of the "junction mode"

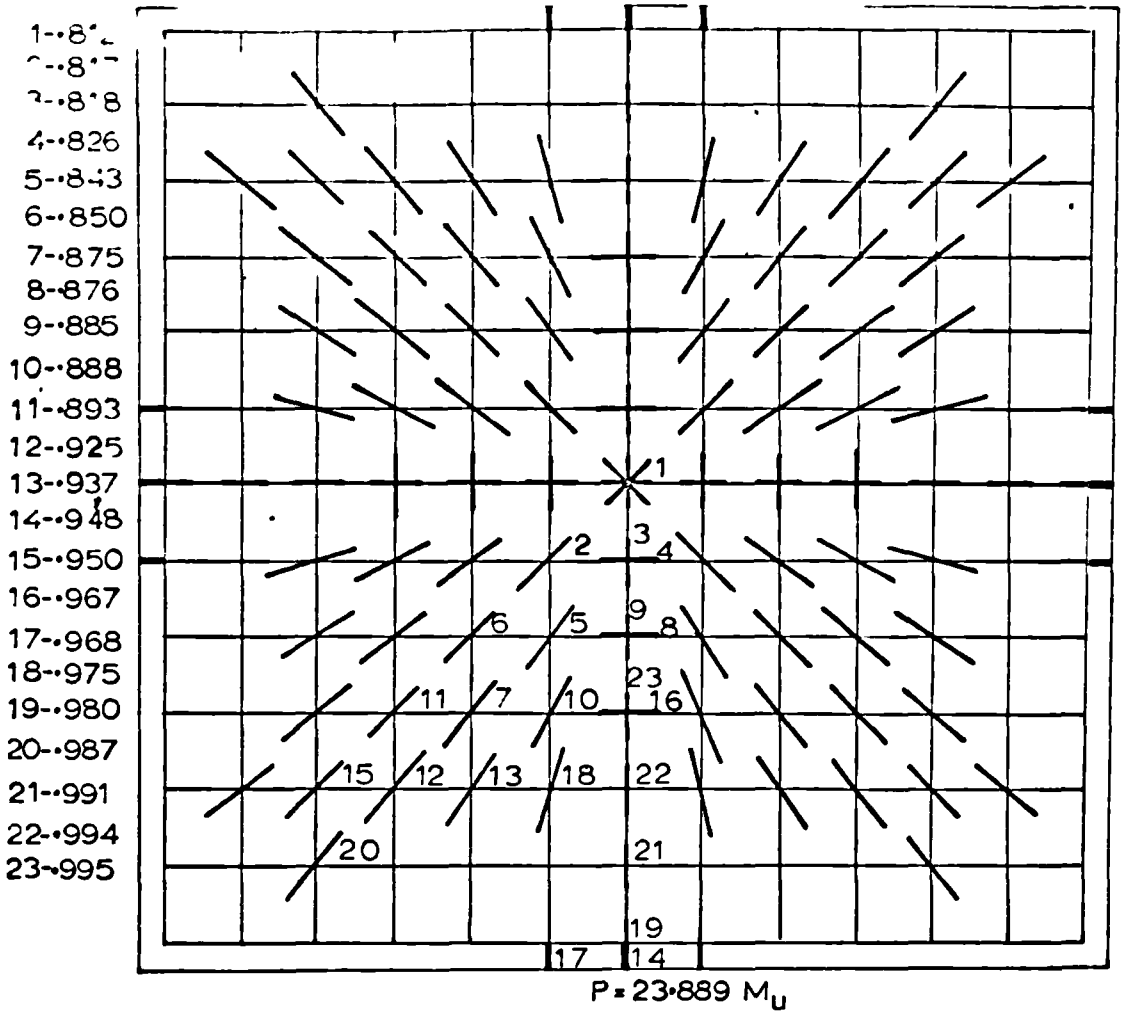

ν = ·15

M_u = 1·0D/L

γ_e = 2·0

γ_p = 1·0

γ_t = 0·0

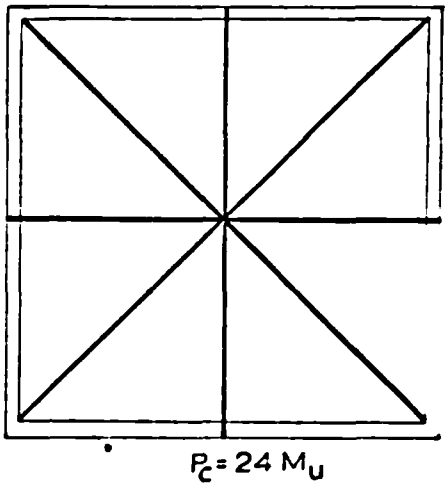

$\frac{P_e}{P_c}$ = ·812

$\frac{P}{P_c}$ = ·995

Pattern No.11

cases presented by Wood[22]. From Pattern No. 11 it is quite evident that the combined diagonal and rectangular modes have almost completely formed. The actual collapse mechanism is a rectangular type involving collapse of the edge beams and the slab.

The $\gamma_e = 2$ value was chosen arbitrarily as a possible practical value. This may explain why the diagonal mode did not extend closer to the corner. As γ_e is made larger, the principal generalized stresses perpendicular to the diagonals increase in magnitude and could result in more plastic behaviour along the diagonal. However, the results of Pattern No. 11 are proof of the existence of junction modes for the critical beam ratio, $\gamma_p = 1.0$. The collapse load again occurs .5% below the limit analysis value.

6.7 Comparison with a Lower Bound Solution

The results from the computer analysis for generalized stresses are again compared with the statically admissible stress field for the unique solution (3) of Chapter 1 with $\gamma_p = 1.0$ in equations 1.15 to 1.19. The stress fields are quite dissimilar as seen in Graphs 6.8 to 6.11. In Graph 6.8 the generalized stress Mx shows a wide region of plasticity covering one half of the span length (along line 1). It also shows that at the slab-beam interface (line 3) where the beam is plastic, there is a sharp increase in Mx resulting in the slab becoming plastic after the beam.

A further difference between these solutions is the edge reaction between slab and beam. The load delivered to the beam from the slab is shown in Graph 6.11. The concentrated reaction from the F.E.M. solution is 25% less than that given by Wood. This is evident from Pattern No.11 in which the corner of the slab does not become plastic and therefore

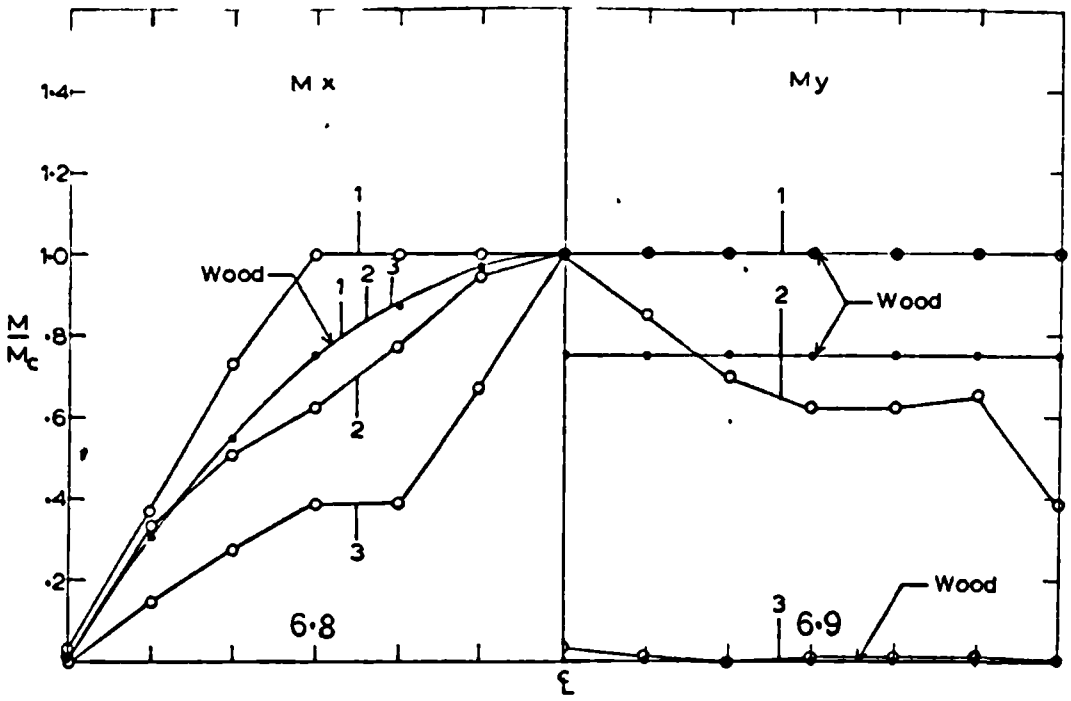
M x
My
1·4
1·2
1·0
·8
·6
·4
·2
M/Mc
Wood
1
2
3
Wood
Wood
6·8
6·9
℄

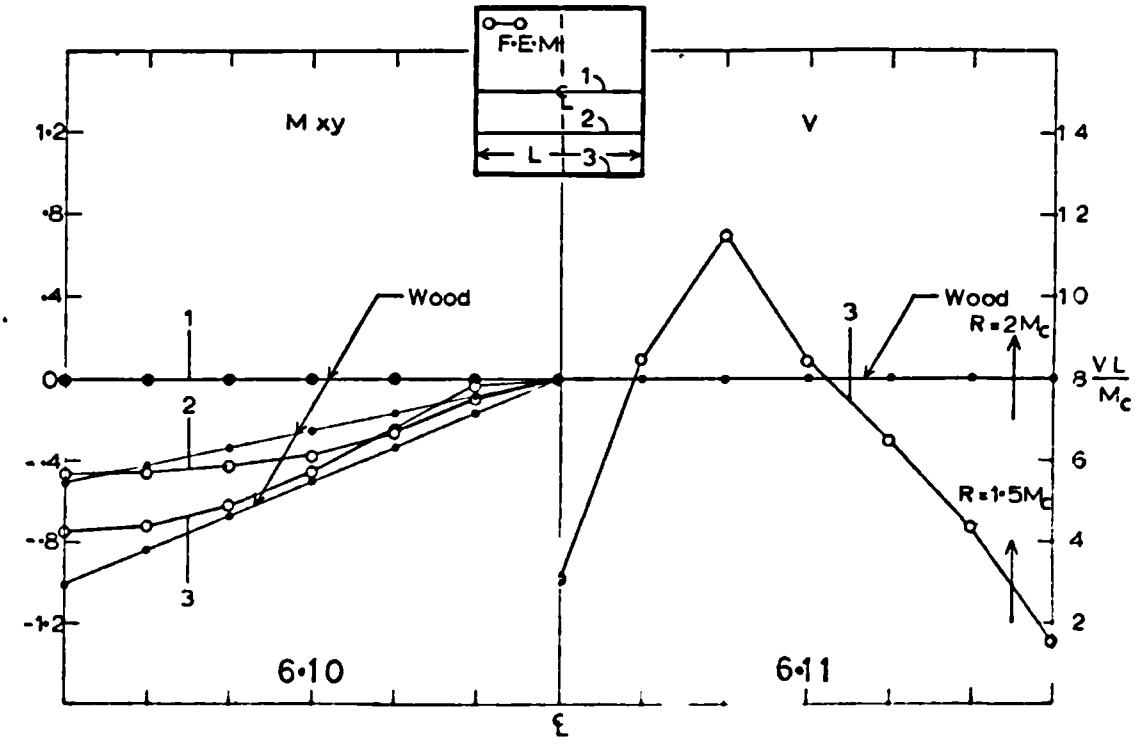
F·E·M
M xy
V
L
1·2
·8
·4
0
-·4
-·8
-1·2
1·4
1·2
1·0
·8
·6
·4
·2
Wood
Wood
R=2Mc
R=1·5Mc
VL/Mc
6·10
6·11
℄

R = 2Mxy is less than Wood's result. It is also quite evident from Graph 6.11 that due to the plasticity at mid-span on the beams, the beams shed their load from the center of the span towards the ends. Comparing support reaction with applied load results in an 8% under-estimate of reaction.

6.8 Concluding Remarks

The lower bound generalized stress fields used in comparison with the F.E.M. analyses were each based on the Prager solution (1) in Chapter 1 with the important exception of the Vallance solution (2). It is quite clear that for the simply supported slab, Vallance has given an excellent stress field when compared with the F.E.M. results.

For the other two solutions the lower bound comparisons show that Wood's stress fields are excellent for the case of free edges but rather questionable (from the practical point of view) for the simply supported slab and the "junction mode" solution.

CHAPTER 7 - CONCLUDING DISCUSSION AND FUTURE RESEARCH

7.1 General Discussion

Few attempts have been made to produce elastic-plastic analyses of two dimensional plate continua in bending. In this respect, the present application of the finite element method to the solution of elastic-plastic plate and slab problems is the first of its kind to be reported. As is usual with first attempts, more questions remain at the end of the study than were present at the beginning.

The foundations of the present proposal lie within the development of the finite element method. With the present state of knowledge on the use of displacement functions for elastic element bending behaviour, it is not surprising that application to elastic-plastic problems has not appeared previously.

The procedures developed in this thesis have been successfully used in producing computer solutions which when compared with experimental results show good agreement.

In each of eight solutions that are compared with experiment, the computer collapse load is identical to the limit analysis upper bound value (no lower bound solutions exist for these plates and slabs). A good deal of redistribution of generalized stress occurs in each of these solutions. The ranges of load over which plastic behaviour is traced varies from 35% to 60% of the collapse range, thereby testing the reliability of the method to predict plastic behaviour over a wide range of load.

The computer collapse loads for three analyses that are not compared with experiment differ from the limit analyses values. The largest difference is 2% above the limit analysis value and the

smallest 0.5% below.

The collapse mechanisms of the eleven solutions presented are clearly indicated by computer. A rectangular mode developed in all but the simply supported case, in which a wide band of plasticity formed a diagonal mode.

A comparison of computer results with experiment shows the generalized stresses for the slab tests to be the least satisfactory. The primary cause of discrepancy is the flexural stiffness assumed for the F.E.M. model. The stiffness of the uncracked concrete section was of the order 10 times greater than that for a cracked section. Consequently, the early elastic behaviours showed little agreement. Better agreement is seen when the elastic-plastic portion of the computer generalized stress curves are superimposed on the experimental. The agreement here indicates that the computer closely reproduces the general form of variation in generalized stress.

A further difficulty with investigations of generalized stresses in slabs is the uncertainty of determining generalized stresses from curvature measurements made in the slab.

The comparisons of experimental edge beam bending moments with analytical for the slabs shows better agreement than do those for generalized stresses. The effects of slab flexural stiffness on the beam curvature are less than on the slab generalized stresses during the early experimental elastic behaviour. Also, the measurement of curvature on the steel beams and subsequent determination of bending moments is more reliable than similar measurements made for the slab.

The correlation between experimental and analytical generalized stresses for the plates was much better than for the slabs. The plate

results include effects of edge supporting beams and two different point load arrangements.

For three of the plates, the variation of principal plane orientation at a point off lines of symmetry was investigated. The F.E.M. model closely reproduces the form of variation with the difference in magnitude between experimental and analytical being only a few degrees.

Deflections measured at the center and mid-span on the edges of both plates and slabs were also compared with computer predictions. For the slabs, the computer overestimates deflections and underestimates for the plates. For the plates the agreement is reasonably good over the entire load range but for the slabs, the early elastic-plastic range of deflections is not as good as the agreement closer to collapse. The underestimate of slab flexural stiffness assumed for the analyses is again responsible for the discrepancies.

Evidence of inhomogeneous plastic deformation in the form of Lüder's lines is seen in two of the plates tested. Only one of these plates shows a shearing type failure in the plane of the plate. This behaviour occurs close to the corners of the plate and indicates that the experimental generalized stress field satisfies the +, - yield condition of the Tresca criterion in the plane of the plate. The other plate indicates shear failure plate-to-atmosphere at 45°. The computer solutions for the four plate tests performed give generalized stress fields based on a square yield criterion and therefore do not reproduce the +, - Tresca yield behaviour. However, it is interesting to note that of the four plate solutions produced only one would have satisfied the +, - condition in the plane of the plate. This solution was for

the same plate mentioned above and indicates the same region near the corner of the plate where the Lüders lines form.

7.2 The Composite Plate-Beam Behaviour

One of the most important features of the finite element method in elastic analysis is its ability to deal with different types of elements (shape and material properties). For plate bending analyses, this feature allows the effects of edge beams to be included. The same is now true for elastic-plastic analyses when it includes the composite plate-beam yield behaviour developed in this study. The procedures outlined herein are simple and are based on well established principles of structural mechanics and idealized plastic behaviour. The reliability of the composite model in predicting edge beam effects is substantiated by four experiments (two on plates and two on slabs). The experimental bending moment distributions and evidence of plastic behaviour is closely reproduced by computer.

Generally, the method described in this study has been well supported experimentally. The procedures reported have been developed to solve plate and slab problems within the category to which the experimental tests reported belong. Any extension of these procedures to more complex problems (non-developable collapse surfaces involving membrane forces and the use of other yield criteria) must be made with the knowledge of the limitations of the present approach.

7.3 Limitations of the Method

(a) The Use of Rectangular Elements and the Flow Rule

Probably the most severe limitation of the method is the vectoral representation of plastic deformation used. By resolving the total

plastic rotation into components along the orthogonal element boundaries, a double plastic fold develops at the nodes rather than a single line of discontinuity. If the total rotation vector is directed along an element boundary, only then can the actual plastic rotation be introduced.

Wherever yielding occurs in two orthogonal directions such that the total rotation vectors have magnitudes of opposite sign and whose components along element boundaries cancel each other, no (plastic rotation) discontinuity can occur. The total plastic rotations can still be solved for and the yield stress condition maintained in the analysis. However, no kinematical representation of plastic flow can be realized. For the procedures present herein, this limitation would mean that the +, - Tresca condition occuring on lines of symmetry could not be satisfied kinematically if the plastic straining occurs at 45^{o} to the element boundaries.

(b) The Use of Other Element Shapes

The severity of the previously mentioned limitation is not fully appreciated until elements with shapes other than rectangular are considered.

Because of the vectoral representation of the total plastic rotation, only two component rotations can be introduced along element boundaries. Inorder to allow discontinuity between two adjacent elements, the boundaries of the elements must be straight and when extended pass through the node. At least two continuous straight lines (boundaries) must exist at a plastic node inorder to allow components of plastic rotations to be imposed between elements. Figure 7.1 illustrates a

number of elements at a common node. None of the boundary lines are continuous through the node and therefore plastic rotations cannot be allowed. For example, if a component of α

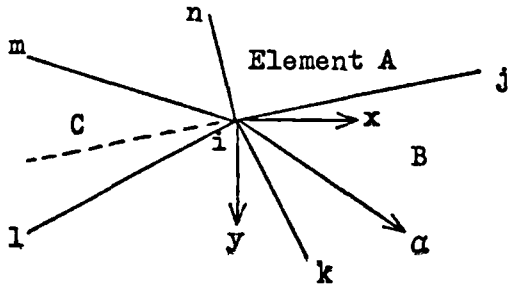

Figure 7.1

is specified along the boundary ij, the discontinuity in slope will occur between elements A and B. However, this cannot be allowed since element C would have to fold about the dotted line of ij produced. Similar arguments hold for the other boundaries and elements. Figure 7.2 illustrates the necessary and sufficient conditions (minimum of two straight lines) for using the vectoral representation of plastic rotations. Boundaries ik and il are straight and continuous.

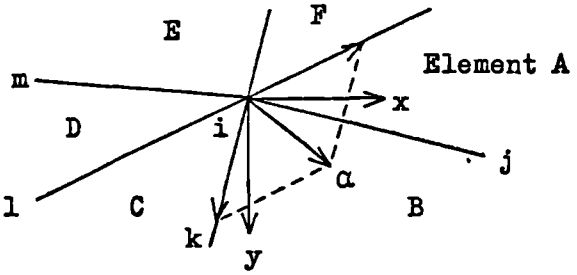

Figure 7.2

The two components of α are shown along these boundaries. Slope discontinuity develops only between elements B and C, C and D, E and F, and F and A. If more than two straight lines occur, a choice of two must be made. The best choice being the pair that produces plastic flow as close as possible to what the actual plastic rotation would produce.

In summary, the type of flow rule used in this study has definite limitations for general application in finite element analyses and if used, care should be exercised in assessing its value to the analytical results.

(c) Monotonic Load Application

A further limitation of the method is its inability to deal with reversal of applied loading. The loads must be monotonically increasing throughout the elastic-plastic analysis. This does not preclude stress reversal in the non-plastic areas but it does restrict it to a study of reversal under increasing load. Stress reversals in the non-plastic regions did occur both experimentally and analytically in this study.

Stress reversals in plastic regions, regardless of load application, cannot be investigated by the procedures outlined herein.

(d) Linear Approximations to Non-Linear Behaviour

This limitation is not peculiar to the present method but is found in all linear elastic-plastic plate bending analyses in which the principal generalized stress equations are the yield functions. The non-linear form of these functions must be approximated by a linear relationship that is assumed to apply over small intervals of the plastic load range. This linearization can be accomplished by writing the principal generalized stress equations

$$M^{1,2} = \tfrac{1}{2}\left[Mx+My \pm \sqrt{(Mx-My)^2+4Mxy^2}\right] \qquad 7.1$$

in a form

$$M^{1,2} = f(Mx,My,Mxy,\emptyset) \qquad 7.2$$

Since Mx, My and Mxy are linear functions of load between any two stages of plastic behaviour, the only variable is the angle ϕ of which the

$$\text{Tangent } (2\phi) = 2Mxy/(My-Mx) \qquad 7.3$$

Therefore, by maintaining ϕ constant over small increments of load, an approximation to equations 7.1 can be made. For the present study, this approximation in the form of equations 7.2 is

$$M^{1,2} = \tfrac{1}{2} \left\{ Mx+My \pm \left[(Mx-My)\cos(2\phi) - 2Mxy \sin(2\phi) \right] \right\} \qquad 7.4$$

Equation 7.4 has proved to be an excellent approximation for the present proposal.

The use of equations 7.4 results in an approximation to equations 7.1 once the angle ϕ is assumed constant during a load interval. This assumption is not strictly true at points off lines of symmetry where the orientations of principal planes change as redistribution of generalized stresses occurs.

(e) Limitations of Present Computer Size

Another disadvantage of the present method is the size of computer required to produce the solutions. In the present study, the computer program required all the available compilation store of the Atlas computer at the University of London Computer Center. Since this program analyses only one eighth of the square plate, any extension of the method to more complex studies will probably meet with some difficulty in acquiring sufficient computer store and computational time. However, the current limitations on computer store and available

time (a problem of computer speed) are not likely to be present in the future as computers continue to become larger and more complex.

7.4 Comparison with Unique Solutions

The generalized stress fields and support reactions from three computer solutions are compared with those from the lower bound solutions to the unique collapse loads. These comparisons show how unrealistic lower bound stress fields can be. Even for the same problem, completely different stress fields are possible.

The theoretical requirements to be satisfied in producing lower bounds on collapse loads do not ensure that the admissible stress field is a realistic one. In this respect lower bound solutions have really only one purpose, i.e. to bound the collapse load. Consequently, it is one matter to produce unique collapse loads by coincidental upper and lower bounds but an entirely different matter to suggest that design should follow using the generalized stress fields from the lower bound solutions. As an example of such a suggestion a recent statement by Massonnet[23] is quoted here:

"The aim of the present paper is to show that,....., we can .....(d) find, for simply supported slabs, several new complete solutions which, up to now, were only known as kinematically admissible solutions, with the advantage of guaranteeing the correctness of the value found for the limit load and of giving the distribution of moments and of support reactions - this makes it possible to distribute the reinforcement of the slab judiciously and to design its supporting beams.....;"

Admittedly, this quotation is puzzling since at the beginning

it mentions simple supports and at the end, supporting beams. However, the point is quite clear - the unique collapse load is determined and the generalized stress field with support reactions allows the slab and supporting beams to be designed. If this attitude is to be the aim of lower bound solutions then the present gap in the communication link between the academic and the designer is certain to widen.

The writer finds it difficult to accept lower bound fields as possible realistic ones unless they are intuitively obvious (most are far from it) or if they have been supported by experimental evidence. The lack of experimental evidence in support of lower bound solutions is obvious, especially for reinforced concrete slabs where most research effort to determine unique solutions has been directed.

Of the very few unique solutions in existence, those reproduced in this thesis when compared with the F.E.M. solutions (which are likely to be the most realistic of existing ones for the problem presented) show that a realistic limit analysis generalized stress field is not always produced. Except for the Vallance solution to the simply supported slab, the lower bound solutions reported herein give constant intensity of support reaction regardless of the supporting conditions. Indeed, most lower bound solutions (whether for unique solutions or not) result in constant support reaction since their admissible stress field variations are usually of a parabolic nature. It is doubtful whether such lower bound solutions give any reliable information about support reactions.

7.5 Future Research

In the application of finite elements to elastic-plastic slab analysis, the problem of cracking of concrete and subsequent reduction

in flexural stiffness should be included. This could be done in the present proposal by assuming an uncracked stiffness before cracking and after cracking to allow the elements about a "cracked" node to reduce their stiffnesses. Until a cracking response is included, the generalized stress fields etc. developed over the elastic and early elastic-plastic load ranges will not compare favourably with the experimental.

Beyond the cracking stage the problem of satisfying the flow rule associated with the yield criterion chosen is of primary importance. The present proposal does not allow the correct plastic flow to develop. However, this is governed by the number and type of displacements allowed at the element nodes. Consequently, other forms of displacement functions should be investigated that will allow a better approximation to the real plastic flow than does the function presented herein. Possible alternative approaches might be considered using the developments of previously mentioned current research[45,46].

If a more realistic way of representing the flow rule can be established, the application to metal plates will require the use of the Tresca or von Mises criteria. Therefore, additional research will be needed to investigate analytically the use of these types of criteria.

The problem of strain hardening for plates can also be studied. The present proposal could include an idealized linear work hardening rule. For example if an expanding square yield locus with a stationary origin is represented in plane space by functions such as

$$M_q^t = M + hR_q^t \qquad 7.5$$

in which h is a constant, then substituting into equations 3.60 gives

$$M_q^t = \left| K_{qn}^t \quad K_{qp}^{ts} - h \right| \left| \begin{matrix} D_n \\ R_p^s \end{matrix} \right| \qquad 7.6$$

Therefore, linear strain hardening can be included into the general scheme for the present plate analyses.

Future work on the effects of membrane forces on the elastic-plastic behaviour of plates and slabs is required. Here the finite element method may prove a useful tool.

With the facility of finite elements to deal with elements of different shapes, physical and material properties, it would be interesting to explore the use of this facility for yield behaviour of elements with different yield properties. This might be attempted by assuming independent yield behaviour for each element at a common node and introducing a concept similar to that used herein for plate-beam composite yield behaviour.

It may prove more profitable to use other numerical variational methods such as the Localized Rayleigh-Ritz[59] method in which the Rayleigh functions describe behaviour over small regions of the continuum rather than over the complete continuum. The use of the finite difference technique should also be more fully investigated for use in elastic-plastic analysis than it has been up to the present.

Finally, more experiments on metal plates are definitely required, particularly for medium thick plates like those reported herein. The fact that collapse behaviour is observed at loads close to those predicted by limit analysis means that generalized stress fields can

be studied and compared with lower bound fields. Although, these types of metal plates have less obvious application than do reinforced concrete slabs, their investigation may lead to a better understanding of admissible stress field distributions. The question of edge supports and load transfer from plate to beam can be studied. The important experimental consideration is to reproduce as closely as possible the boundary and loading conditions assumed analytically.

APPENDIX I - MATRICES FOR ELASTIC ANALYSIS

A1.1 Non-Dimensional Parameters

The non-dimensional form of the parameters used in the derivation of the matrices contained in Chapter 3 are as follows:

L - is a representative length of the plate system

$X = x/L \quad Y = y/L$

$W = w/L \quad A = a/L \quad B = b/L$

$P = qL^3/D$ (for a uniformly distributed load q)

$P = pL/D$ (for a concentrated point load p)

$\tau = D_1/D \quad \sigma = Dy/D \quad \mu = Dxy/D$

$\gamma_e = \frac{D_b}{DL}$ $\qquad w,x = W,X$

$\gamma_p = \frac{M_b}{ML}$ $\qquad w,xx = W,XX/L$

$\gamma_t = \frac{GJ}{D_b}$ $\qquad w,xxx = W,XXX/L^2$ etc.

Table A1.1

A1.2 Rectangular Finite Element Displacement Function

The displacement function of equations 3.7 when written in non-dimensional form is

$$W = A_1+A_2X+A_3Y+A_4X^2+A_5XY+A_6Y^2+A_7X^3+A_8X^2Y+A_9XY^2+A_{10}Y^3+A_{11}X^3Y+A_{12}XY^3 \qquad \text{A1.1}$$

The coordinate positions for nodes i, j, k and l of the rectangular element (see Figure 3.12) are simply

$$\begin{aligned} i &= (0,0) \\ j &= (A,0) \\ k &= (A,B) \\ l &= (0,B) \end{aligned} \qquad \text{A1.2}$$

with respect to the individual element system of axes.

The nodal displacements of equations 3.8 in non-dimensional form for node i as an example are

$$U_i = \begin{vmatrix} W_i \\ \theta x_i \\ \theta y_i \end{vmatrix} = \begin{vmatrix} W \\ W,Y \\ -W,X \end{vmatrix}_i = \left|U(X,Y)\right|_i \left|A\right| \qquad \text{Al.3}$$

Substituting the values of X and Y of equation Al.2 into equations Al.3, the displacements for all four nodes become

$$U = CA \qquad \text{Al.4}$$

which when written in full produces

(See next page)

$$
\begin{bmatrix} W_i \\ \theta x_i \\ \theta y_i \\ W_j \\ \theta x_j \\ \theta y_j \\ W_k \\ \theta x_k \\ \theta y_k \\ W_l \\ \theta x_l \\ \theta y_l \end{bmatrix} =
\begin{bmatrix}
1 & 0 & 0 & 0 & 0 & 0 & 0 & 0 & 0 & 0 & 0 & 0 \\
0 & 0 & 1 & 0 & 0 & 0 & 0 & 0 & 0 & 0 & 0 & 0 \\
0 & -1 & 0 & 0 & 0 & 0 & 0 & 0 & 0 & 0 & 0 & 0 \\
1 & A & 0 & A^2 & 0 & 0 & A^3 & 0 & 0 & 0 & 0 & 0 \\
0 & 0 & 1 & 0 & A & 0 & 0 & A^2 & 0 & 0 & A^3 & 0 \\
0 & -1 & 0 & -2A & 0 & 0 & -3A^2 & 0 & 0 & 0 & 0 & 0 \\
1 & A & B & A^2 & AB & B^2 & A^3 & A^2B & AB^2 & B^3 & A^3B & AB^3 \\
0 & 0 & 1 & 0 & A & 2B & 0 & A^2 & 2AB & 3B^2 & A^3 & 3AB^2 \\
0 & -1 & 0 & -2A & -B & 0 & -3A^2 & -2AB & -B^2 & 0 & -3A^2B & -B^3 \\
1 & 0 & B & 0 & 0 & B^2 & 0 & 0 & 0 & B^3 & 0 & 0 \\
0 & 0 & 1 & 0 & 0 & 2B & 0 & 0 & 0 & 3B^2 & 0 & 0 \\
0 & -1 & 0 & 0 & -B & 0 & 0 & 0 & -B^2 & 0 & 0 & -B^3
\end{bmatrix}
\begin{bmatrix} A_1 \\ A_2 \\ A_3 \\ A_4 \\ A_5 \\ A_6 \\ A_7 \\ A_8 \\ A_9 \\ A_{10} \\ A_{11} \\ A_{12} \end{bmatrix}
\qquad \text{A1.5}
$$

A1.3 Internal Generalized Stress Matrix

The curvatures of equations 3.10 in non-dimensional form become

$$\begin{vmatrix} -W,XX \\ -W,YY \\ W,XY/L \end{vmatrix} = \begin{vmatrix} 0\ 0\ 0\ -2\ 0\ 0\ -6X\ -2Y\ 0\ 0\ -6XY\ 0 \\ 0\ 0\ 0\ 0\ 0\ -2\ 0\ 0\ -2X\ -6Y\ 0\ -6XY \\ 0\ 0\ 0\ 0\ 1\ 0\ 0\ 2X\ 2Y\ 0\ 3X^2\ 3Y^2 \end{vmatrix} \begin{vmatrix} A_1 \\ \vdots \\ A_{12} \end{vmatrix} \qquad \text{A1.6}$$

That is

$$K = BA \qquad \text{A1.7}$$

Substituting the coordinate positions of the nodes (equation A1.2) into equations A1.6 and substituting the result into equation 3.12 leads to the generalized stress matrix of

$$M = DBC^{-1}U \qquad \text{A1.8}$$

If the inverse of matrix C in equations A1.5 is

(See next page)

$$C^{-1} =$$

1	0	0	0	0	0	0	0	0	0	0	0
0	0	-1	0	0	0	0	0	0	0	0	0
0	1	0	0	0	0	0	0	0	0	0	0
$-\frac{3}{A^2}$	0	$\frac{2}{A}$	$\frac{3}{A^2}$	0	$\frac{1}{A}$	0	0	0	0	0	0
$-\frac{1}{AB}$	$-\frac{1}{A}$	$\frac{1}{B}$	$\frac{1}{AB}$	$\frac{1}{A}$	0	$-\frac{1}{AB}$	0	0	$\frac{1}{AB}$	0	$-\frac{1}{B}$
$-\frac{3}{B^2}$	$-\frac{2}{B}$	0	0	0	0	0	0	0	$\frac{3}{B^2}$	$-\frac{1}{B}$	0
$\frac{2}{A^3}$	0	$-\frac{1}{A^2}$	$-\frac{2}{A^3}$	0	$-\frac{1}{A^2}$	0	0	0	0	0	0
$\frac{3}{A^2B}$	0	$-\frac{2}{AB}$	$-\frac{3}{A^2B}$	0	$-\frac{1}{AB}$	$\frac{3}{A^2B}$	0	$\frac{1}{AB}$	$-\frac{3}{A^2B}$	0	$\frac{2}{AB}$
$\frac{3}{AB^2}$	$\frac{2}{AB}$	0	$-\frac{3}{AB^2}$	$-\frac{2}{AB}$	0	$\frac{3}{AB^2}$	$-\frac{1}{AB}$	0	$-\frac{3}{AB^2}$	$\frac{1}{AB}$	0
$\frac{2}{B^3}$	$\frac{1}{B^2}$	0	0	0	0	0	0	0	$-\frac{2}{B^3}$	$\frac{1}{B^2}$	0
$-\frac{2}{A^3B}$	0	$\frac{1}{A^2B}$	$\frac{2}{A^3B}$	0	$\frac{1}{A^2B}$	$-\frac{2}{A^3B}$	0	$-\frac{1}{A^2B}$	$\frac{2}{A^3B}$	0	$-\frac{1}{A^2B}$
$-\frac{2}{AB^3}$	$-\frac{1}{AB^2}$	0	$\frac{2}{AB^3}$	$\frac{1}{AB^2}$	0	$-\frac{2}{AB^3}$	$\frac{1}{AB^2}$	0	$\frac{2}{AB^3}$	$-\frac{1}{AB^2}$	0

A1.

then the generalized stresses for an anisotropic rectangular element are given by

(See next page)

$$
\begin{bmatrix} Mx_i \\ My_i \\ Mxy_i \\ Mx_j \\ My_j \\ Mxy_j \\ Mx_k \\ My_k \\ Mxy_k \\ Mx_l \\ My_l \\ Mxy_l \end{bmatrix} =
\begin{bmatrix}
\frac{6}{A^2}+\frac{6\tau}{B^2} & \frac{4\tau}{B} & -\frac{4}{A} & -\frac{6}{A^2} & 0 & -\frac{2}{A} & 0 & 0 & 0 & -\frac{6\tau}{B^2} & \frac{2\tau}{B} & 0 \\
\frac{6\tau}{A^2}+\frac{6\sigma}{B^2} & \frac{4\sigma}{B} & -\frac{4\tau}{A} & -\frac{6\tau}{A^2} & 0 & -\frac{2\tau}{A} & 0 & 0 & 0 & -\frac{6\sigma}{B^2} & \frac{2\sigma}{B} & 0 \\
-\frac{2\mu}{AB} & -\frac{2\mu}{A} & \frac{2\mu}{B} & \frac{2\mu}{AB} & \frac{2\mu}{A} & 0 & -\frac{2\mu}{AB} & 0 & 0 & \frac{2\mu}{AB} & 0 & -\frac{2\mu}{B} \\
-\frac{6}{A^2} & 0 & \frac{2}{A} & \frac{6}{A^2}+\frac{6\tau}{B^2} & \frac{4\tau}{B} & \frac{4}{A} & -\frac{6\tau}{B^2} & \frac{2\tau}{B} & 0 & 0 & 0 & 0 \\
-\frac{6\tau}{A^2} & 0 & \frac{2\tau}{A} & \frac{6\tau}{A^2}+\frac{6\sigma}{B^2} & \frac{4\sigma}{B} & \frac{4\tau}{A} & -\frac{6\sigma}{B^2} & \frac{2\sigma}{B} & 0 & 0 & 0 & 0 \\
-\frac{2\mu}{AB} & -\frac{2\mu}{A} & 0 & \frac{2\mu}{AB} & \frac{2\mu}{A} & \frac{2\mu}{B} & -\frac{2\mu}{AB} & 0 & -\frac{2\mu}{B} & \frac{2\mu}{AB} & 0 & 0 \\
0 & 0 & 0 & -\frac{6\tau}{B^2} & -\frac{2\tau}{B} & 0 & \frac{6}{A^2}+\frac{6\tau}{B^2} & -\frac{4\tau}{B} & \frac{4}{A} & -\frac{6}{A^2} & 0 & \frac{2}{A} \\
0 & 0 & 0 & -\frac{6\sigma}{B^2} & -\frac{2\sigma}{B} & 0 & \frac{6\tau}{A^2}+\frac{6\sigma}{B^2} & -\frac{4\sigma}{B} & \frac{4\tau}{A} & -\frac{6\tau}{A^2} & 0 & \frac{2\tau}{A} \\
-\frac{2\mu}{AB} & 0 & 0 & \frac{2\mu}{AB} & 0 & \frac{2\mu}{B} & -\frac{2\mu}{AB} & \frac{2\mu}{A} & -\frac{2\mu}{B} & \frac{2\mu}{AB} & -\frac{2\mu}{A} & 0 \\
-\frac{6\tau}{B^2} & -\frac{2\tau}{B} & 0 & 0 & 0 & 0 & -\frac{6}{A^2} & 0 & -\frac{2}{A} & \frac{6}{A^2}\ \frac{6\tau}{B^2} & -\frac{4\tau}{B} & -\frac{4}{A} \\
-\frac{6\sigma}{B^2} & -\frac{2\sigma}{B} & 0 & 0 & 0 & 0 & -\frac{6\tau}{A^2} & 0 & -\frac{2\tau}{A} & \frac{6\tau}{A^2}\ \frac{6\sigma}{B^2} & -\frac{4\sigma}{B} & -\frac{4\tau}{A} \\
-\frac{2\mu}{AB} & 0 & \frac{2\mu}{B} & \frac{2\mu}{AB} & 0 & 0 & -\frac{2\mu}{AB} & \frac{2\mu}{A} & 0 & \frac{2\mu}{AB} & -\frac{2\mu}{A} & -\frac{2\mu}{B}
\end{bmatrix}
\begin{bmatrix} W_i \\ \theta x_i \\ \theta y_i \\ W_j \\ \theta x_j \\ \theta y_j \\ W_k \\ \theta x_k \\ \theta y_k \\ W_l \\ \theta x_l \\ \theta y_l \end{bmatrix}
$$

A1.10

A1.4 Elastic Stiffness Matrix

The elastic stiffness matrix for the anisotropic rectangular element as derived by equations 3.18 is presented here in explicit form in the following nodal force-displacement relationships. (See next page)

A1.5 Edge Reaction Matrix

For the present study the edge reaction between plate and edge support was determined only along the boundary Y = L/2 of Figure 3.3. This reaction is given by

$$Vy = -D(\sigma W,YYY+\eta W,XXY)/L^2 \qquad \text{A1.12}$$

in which $\eta = \tau + 4\mu$ and acts downwards on the plate. These reactions are computed only at the boundary nodes. The required reaction matrix for nodes k and l of the element shown in equations A1.11 is

$$\begin{vmatrix} Vy_k \\ Vy_l \end{vmatrix} = \frac{D}{L^2} \begin{vmatrix} 6\eta/A^2B, 0, -2\eta/AB, -12\sigma/B^3 - 6\eta/A^2B, -6\sigma/B^2, -4\eta/AB, \\ \quad 12\sigma/B^3 + 6\eta/A^2B, -6\sigma/B^2, \quad 4\eta/AB, -6\eta/A^2B, 0, 2\eta/AB \\ -12\sigma/B^3 - 6\eta/A^2B, -6\sigma/B^2, \quad 4\eta/AB, 6\eta/A^2B, 0, 2\eta/AB, \\ -6\eta/A^2B, 0, -2\eta/AB, 6\eta/A^2B + 12\sigma/B^3, -6\sigma/B^2, -4\eta/AB \end{vmatrix} \begin{vmatrix} W_i \\ \vdots \\ W_j \\ \vdots \\ W_k \\ \vdots \\ W_l \\ \theta x_l \\ \theta y_l \end{vmatrix} \qquad \text{A1.13}$$

A1.6 Applied Load Matrices

In the finite element method, external loading can only be applied at the nodes of elements. These loads must be in equilibrium with the nodal forces. For bending analyses such as those described herein, the applied loads can consist of vertical point loads, bending couples or a combination of these. The bending couples can only be applied in the orthogonal directions dictated by the bending forces (mx and my) at nodes.

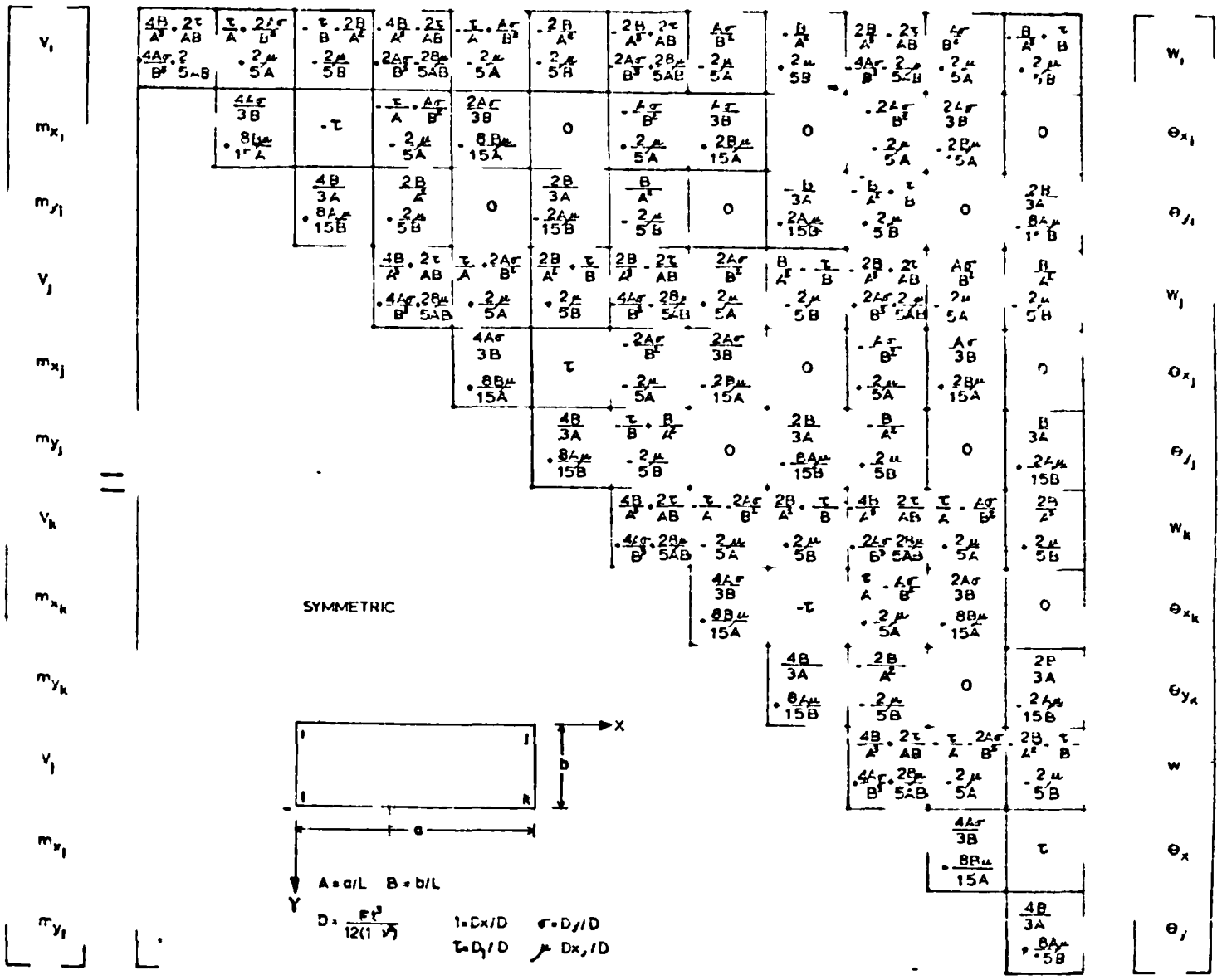

A1·11

As an example, consider a loading case in which vertical point loads P_i and P_j are applied at nodes i and j respectively and the bending couples $C_{x\,k}$ at node k. If there are only nine nodes in the entire structure (i.e. i to q) the structure's nodal force matrix would be

$$\begin{vmatrix} F_i \\ \cdot \\ \cdot \\ \cdot \\ \cdot \\ \cdot \\ F_q \end{vmatrix} = \begin{vmatrix} \Sigma V_i \\ \Sigma mx_i \\ \Sigma my_i \\ \vdots \\ \Sigma V_q \\ \Sigma mx_q \\ \Sigma my_q \end{vmatrix} \qquad \text{Al.14}$$

In order to maintain equilibrium with externally applied loading this force vector is simply replaced by the load vector. That is

$$\begin{vmatrix} \Sigma V_i \\ \Sigma mx_i \\ \Sigma my_i \\ \Sigma V_j \\ \Sigma mx_j \\ \Sigma my_j \\ \Sigma V_k \\ \Sigma mx_k \\ \Sigma my_k \\ \cdot \\ \cdot \\ \cdot \\ \cdot \\ \cdot \\ \cdot \\ \cdot \\ \Sigma my_q \end{vmatrix} = \begin{vmatrix} P_i \\ 0 \\ 0 \\ P_j \\ 0 \\ 0 \\ 0 \\ Cx_k \\ 0 \\ \cdot \\ \cdot \\ \cdot \\ \cdot \\ \cdot \\ \cdot \\ \cdot \\ 0 \end{vmatrix} \qquad \text{Al.15}$$

For a uniformly distributed load, two approaches are possible in representing this load by nodal equivalents. One approach is to divide the distributed load on one element into equal vertical concentrated loads at each of the element nodes.

A second approach[42] is more consistent with the derivation of the stiffness matrix and is based on the virtual work principle that results in nodal forces equivalent to the distributed loading.

Consider a set of nodal forces N equivalent to the distributed loading on one element. The work done by these nodal forces during the unit virtual displacements $\delta u = I$ is

$$W_N = (\delta u)^T N = IN = N \qquad \text{A1.16}$$

The work done by the distributed loading q is

$$Wq = \iint (\delta w)^T q dx dy \qquad \text{A1.17}$$

Restating equation 3.7 in matrix form as

$$w = La \qquad \text{A1.18}$$

and recalling equations 3.9

$$\delta w = LC^{-1} \delta u = LC^{-1} I = LC^{-1} \qquad \text{A1.19}$$

Substituting equations A1.19 into A1.17 and equating the work done gives the nodal forces to be

$$N = \iint (LC^{-1})^T q dx dy = (C^{-1})^T \iint L^T q dx dy \qquad \text{A1.20}$$

When written in non-dimensional form equations A1.20 become

$$\frac{L}{D}\begin{vmatrix} N_1 \\ Nx_i \\ Ny_i \\ N_j \\ Nx_j \\ Ny_j \\ N_k \\ Nx_k \\ Ny_k \\ N_l \\ Nx_l \\ Ny_l \end{vmatrix} = \frac{qL^3}{D}\begin{vmatrix} AB/4 \\ AB^2/24 \\ -A^2B/24 \\ AB/4 \\ AB^2/24 \\ A^2B/24 \\ AB/4 \\ -AB^2/24 \\ A^2B/24 \\ AB/4 \\ -AB^2/24 \\ -A^2B/24 \end{vmatrix} \qquad \text{A1.21}$$

It is apparent from equation A1.21 that to properly represent the distributed load, bending couples must be included at the nodes in addition to the vertical point loads. At interior nodes where four elements join, these couples cancel one another and only the vertical point loads remain. However, along the boundaries of plates carrying uniform loading these couples exist, producing bending normal to the boundaries.

In the three analytical solutions presented in Chapter 6 with distributed loads, these loads are represented by a set of nodal forces given by equation A1.21.

A1.7 Beam Element Stiffness Matrix

The beam element stiffness matrix is derived by following the same procedures as those for plate elements. Based on the derivation of

section 3.8b the stiffness equation for beam elements given by equations 3.86 are as follows:

- for a beam element with longitudinal axis along the x axis with nodes 1 and k

$$\frac{1}{D}\begin{vmatrix} V_1 L \\ mx_1 \\ my_1 \\ V_k L \\ mx_k \\ my_k \end{vmatrix} = \begin{vmatrix} \frac{12\gamma_x}{A^3} & 0 & \frac{-6\gamma_x}{A^2} & \frac{-12\gamma_x}{A^3} & 0 & \frac{-6\gamma_x}{A^2} \\ 0 & \frac{\gamma_{xt}\gamma_x}{A} & 0 & 0 & \frac{-\gamma_{xt}\gamma_x}{A} & 0 \\ \frac{-6\gamma_x}{A^2} & 0 & \frac{4\gamma_x}{A} & \frac{6\gamma_x}{A^2} & 0 & \frac{2\gamma_x}{A} \\ \frac{-12\gamma_x}{A^3} & 0 & \frac{6\gamma_x}{A^2} & \frac{12\gamma_x}{A^3} & 0 & \frac{6\gamma_x}{A^2} \\ 0 & \frac{-\gamma_{xt}\gamma_x}{A} & 0 & 0 & \frac{\gamma_{xt}\gamma_x}{A} & 0 \\ \frac{-6\gamma_x}{A^2} & 0 & \frac{2\gamma_x}{A} & \frac{6\gamma_x}{A^2} & 0 & \frac{4\gamma_x}{A} \end{vmatrix} \begin{vmatrix} W_1 \\ \theta x_1 \\ \theta y_1 \\ W_k \\ \theta x_k \\ \theta y_k \end{vmatrix} \qquad \text{Al.22}$$

in which $\gamma_x = D_{bx}/DL$ and $\gamma_{xt} = GJ/D_{bx}$.

- for a beam element directed along the y axis with nodes i and 1

$$\frac{1}{D}\begin{vmatrix} V_i L \\ mx_i \\ my_i \\ V_1 L \\ mx_1 \\ myl \end{vmatrix} = \begin{vmatrix} \frac{12\gamma_y}{B^3} & \frac{6\gamma_y}{B^2} & 0 & \frac{-12\gamma_y}{B^3} & \frac{6\gamma_y}{B^2} & 0 \\ \frac{6\gamma_y}{B^2} & \frac{4\gamma_y}{B} & 0 & \frac{-6\gamma_y}{B^2} & \frac{2\gamma_y}{B} & 0 \\ 0 & 0 & \frac{\gamma_{yt}\gamma_y}{B} & 0 & 0 & \frac{-\gamma_{yt}\gamma_y}{B} \\ \frac{-12\gamma_y}{B^3} & \frac{-6\gamma_y}{B^2} & 0 & \frac{12\gamma_y}{B^3} & \frac{-6\gamma_y}{B^2} & 0 \\ \frac{6\gamma_y}{B^2} & \frac{2\gamma_y}{B} & 0 & \frac{-6\gamma_y}{B^2} & \frac{4\gamma_y}{B} & 0 \\ 0 & 0 & \frac{-\gamma_{yt}\gamma_y}{B} & 0 & 0 & \frac{\gamma_{yt}\gamma_y}{B} \end{vmatrix} \begin{vmatrix} W_i \\ \theta x_i \\ \theta y_i \\ W_1 \\ \theta x_1 \\ \theta y_1 \end{vmatrix} \qquad \text{Al.23}$$

in which $\gamma_y = D_{by}/DL$ and $\gamma_{yt} = GJ/D_{by}$.

A1.8 Beam Element Bending and Twisting Moment Matrix

The bending moments given by equations 3.78 and twisting moments by the convention of Figure 3.16 are combined into the following matrix equations:

- for beams along the x axis with node 1 and k

$$\frac{1}{D}\begin{vmatrix} Mx_1 \\ T_1 \\ Mx_k \\ T_k \end{vmatrix} = \begin{vmatrix} \frac{6\gamma_x}{A^2} & 0 & \frac{-4\gamma_x}{A} & \frac{-6\gamma_x}{A^2} & 0 & \frac{-2\gamma_x}{A} \\ 0 & \frac{\gamma_{xt}\gamma_x}{A} & 0 & 0 & \frac{-\gamma_{xt}\gamma_x}{A} & 0 \\ \frac{-6\gamma_x}{A^2} & 0 & \frac{2\gamma_x}{A} & \frac{6\gamma_x}{A^2} & 0 & \frac{4\gamma_x}{A} \\ 0 & \frac{-\gamma_{xt}\gamma_x}{A} & 0 & 0 & \frac{\gamma_{xt}\gamma_x}{A} & 0 \end{vmatrix} \begin{vmatrix} W_1 \\ \theta x_1 \\ \theta y_1 \\ W_k \\ \theta x_k \\ \theta y_k \end{vmatrix} \qquad \text{A1.24}$$

APPENDIX II - COMPUTER PROGRAM

A2.1 Type of Computer and Language

The computer program was developed for use on the Atlas computer housed at the University of London's Computing Center. The language used was EXCHLF autocode because of its simplicity of statement form and its ability to manipulate large arrays of numbers with the very minimum of program effort.

The Atlas computer performs approximately 10,000 machine instructions per minute and operates a vast execution store. The compilation store available (store required for compiling the object program) has an economical limit specified by the U.L.C.U. and is approximately 150 blocks (one block consists of 512 storage locations, each comprising one 14 digit number). In single length form the Atlas provides 12 decimal digits in its computation. Double length facilities are also available.

A2.2 General Remarks

At the outset of this study a computer program was developed to solve only the simply supported uniformly distributed load case of elastic-plastic plate bending as a trial for the finite element approach. Once this solution was complete and the method appeared to work sufficiently well, an automated program was next developed to analyse other types of plates. However, it was quite obvious during the development of the first program that the total compilation store required for such a program would be large even for the Atlas computer. In fact the final program store exceeded the allowable capacity of 150 blocks. To overcome this difficulty the program was semi-compiled onto magnetic tape and

fully compiled in sections that were not interconnected by the general program flow. Once one section was fully compiled, portions of the storage area used could be cleared out and made available for the following sections of program. In this way the program was compiled into the computer from its magnetic store library requiring 135 blocks of final compiled store. Unfortunately, the size of the program placed it in the stream of Complex Work at U.L.C.U. and thereby reduced the availability of computer time for this study.

Approximately one year was required to complete the analytical portion of this study which included the development and use of the automated program.

A2.3 Purpose of Computer Program

The final program was developed to analyse isotropic square plates supported and loaded symmetrically about the central axes and diagonals, i.e. only one eight of the plate was analysed. This required the use of 28 nodes for a 12 x 12 subdivision into finite elements (see Figure 3.3).

The loading and boundary conditions were specified by indices placed in the input stream. The program also included the effects of edge beams on the elastic-plastic behaviour of the plate.

Each time a node becomes plastic the program outputs complete descriptions of the generalized stress and displacement fields, the applied load causing plasticity, the edge reactions and the edge beam bending and twisting moments if they exist.

Although many plate problems could be solved by this program, only those reported in this thesis were produced because of the lack of

available computer time.

A2.4 Compilation and Execution T me Used

The U.L.C.U. allowed 30 minutes of computer time per month to each university user (based on compilation of program, execution of analysis and running cost time). This amount of time on the Atlas computer is quite sufficient for normal computer work. Table A2.1 is a summary of the times required for the solutions presented herein.

SOLUTION	COMPILATION	EXECUTION	TOTAL TIME*	PLASTIC NODES
	min.	min.	min.	N
Slab No. 1	0.4	3.87	10.82	8
Slab No. 2	"	5.25	13.76	11
Slab No. 3	"	3.87	10.82	8
Slab No. 4	"	8.58	21.39	19
Plate No. 1	"	3.87	9.27	8
Plate No. 2	"	5.64	14.76	12
Plate No. 3	"	7.00	15.94	15
Plate No. 4	"	6.45	17.14	14
Simple Supports	"	6.39	16.48	14
Free Edges	"	12.67	30.20	27
Edge Beams γ_p=1.0	"	11.25	27.26	20

* Total time available per month = 30 minutes.

Table A2.1

On the basis of the solutions presented here approximate time and cost formulae are:

Program Compilation + Execution Time = .5(N+1) minutes

Total Computer Time = 1.25N minutes

Total Cost ≐ (£6.0s.0d.)N

where N = number of plastic nodes in the analysis.

A2.5 Discussion of Program

Only a brief outline of the program is given here. The actual program typescript consisted of approximately 130 foolscap pages and consequently is not presented here. Furthermore, any complex program if presented in computer language is of little value to the reader. Therefore the program is discussed here in accordance with the flow diagram of Figure A2.1.

The program consisted of 65 routines, 7 programmes (subprograms) and the supervisory chapter controlling the flow. Each section of the flow diagram is described below in the order in which they are entered during program execution.

(1) Specify input data according to analysis desired.

There are sixteen items that are standard input data.

n_1 - the number of times the complete set of stiffness equations are output for inspection before they are solved. This allows the checking of elastic-plastic coefficients at each stage of plasticity if desired.

n_2 - the number of times the solution of the equations is to be refined during each stage of plasticity.

ν - Poisson ratio of plate material.

τ - D_1/D where $D = Et^3/12(1-\nu^2)$

σ - Dy/D

μ - Dxy/D

$\frac{M_c L}{D}$ - non-dimensional limiting value for yield criterion of plate material.

$\gamma_e = \frac{D_b}{DL}$ - elastic stiffness ratio (beam/plate)

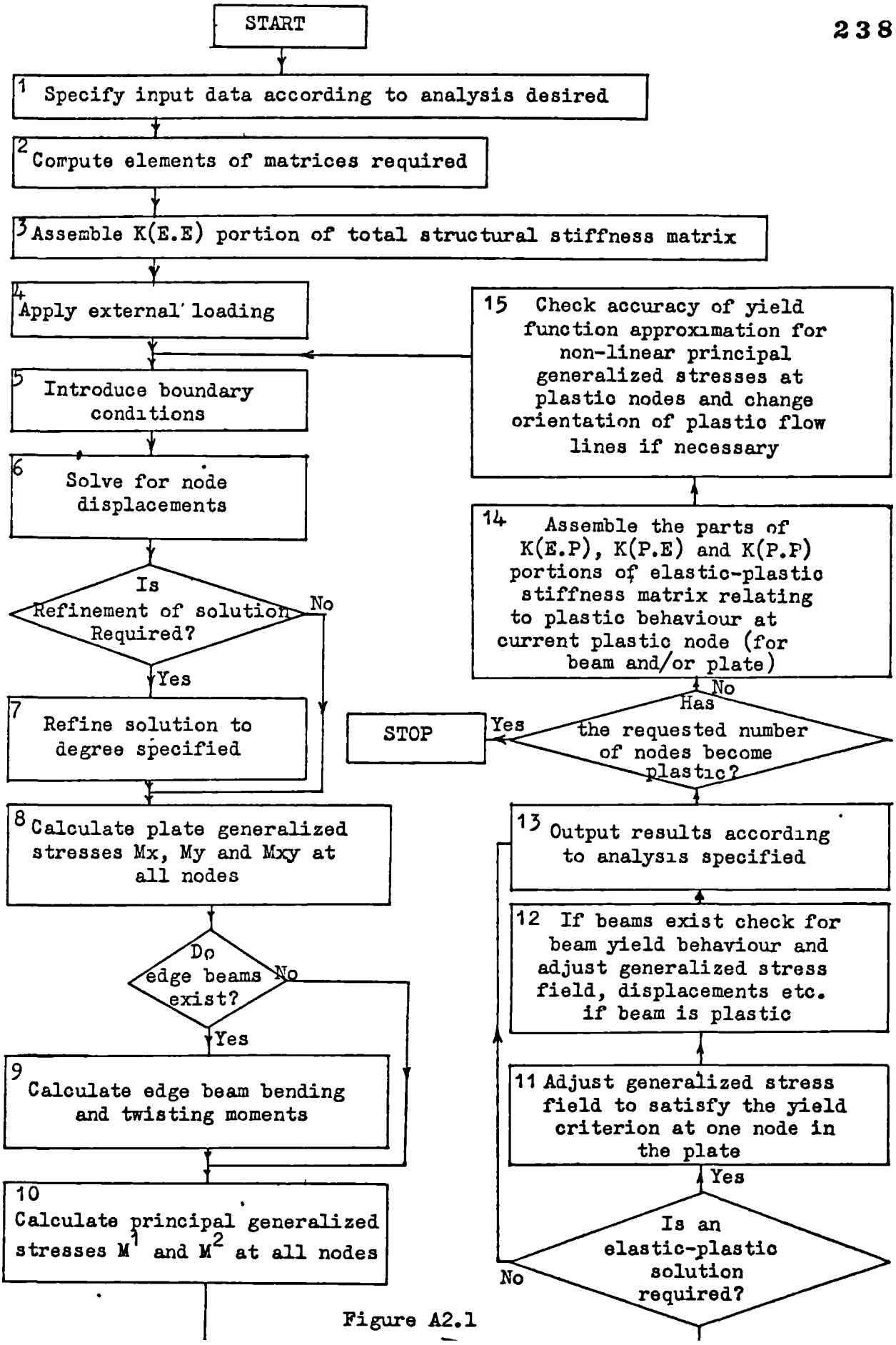
START
1 Specify input data according to analysis desired
2 Compute elements of matrices required
3 Assemble K(E.E) portion of total structural stiffness matrix
4 Apply external loading
5 Introduce boundary conditions
6 Solve for node displacements
Is Refinement of solution Required?
No
Yes
7 Refine solution to degree specified
8 Calculate plate generalized stresses Mx, My and Mxy at all nodes
Do edge beams exist?
No
Yes
9 Calculate edge beam bending and twisting moments
10 Calculate principal generalized stresses M1 and M2 at all nodes
15 Check accuracy of yield function approximation for non-linear principal generalized stresses at plastic nodes and change orientation of plastic flow lines if necessary
14 Assemble the parts of K(E.P), K(P.E) and K(P.P) portions of elastic-plastic stiffness matrix relating to plastic behaviour at current plastic node (for beam and/or plate)
Has the requested number of nodes become plastic?
No
Yes
STOP
13 Output results according to analysis specified
12 If beams exist check for beam yield behaviour and adjust generalized stress field, displacements etc. if beam is plastic
11 Adjust generalized stress field to satisfy the yield criterion at one node in the plate
Is an elastic-plastic solution required?
Yes
No

Figure A2.1

$\gamma_t = \frac{GJ}{D_b}$ - beam torsional stiffness ratio

$\frac{M_b}{D}$ - limiting bending moment for edge beams

$\gamma_p = \frac{M_b}{M_c L}$ - plastic strength ratio

n_3, n_4 } - round off parameters for comparing numerical values
eg. $n_3 = 10^6$, $n_4 = .5$ rounds off to six places of decimal

n_5 - applied load index

100 - indicates a uniformly distributed load

20 - indicates point loads

3 - indicates applied bending couples

123 - indicates a combination of all three load types

n_6 - the number of nodes that are to become plastic before the solution terminates. If $n_6 = 0$ only an elastic solution is presented.

n_7 - if $n_7 > 0$ the approximation to the yield function is checked at plastic nodes off lines of symmetry and if necessary, updating procedures are used.

The remaining input data describes the applied load values and boundary conditions.

n_8 - value of uniformly distributed load if n_5 contains 100

n_9 - number of nodes at which point loads are applied if n_5 contains 20

n_{10} - node number
n_{11} - point load value } repeated n_9 times

n_{12} - number of nodes at which bending couples are applied

n_{13} - node number
n_{14} - value of bending couple } repeated n_{12} times

n_{15} - number of nodes at which boundary conditions must be satisfied

n_{16} - number of nodes where boundary condition exists

n_{17} - boundary condition index

100 - indicates vertical displacement is zero

20 - indicates slope about y axis is zero

3 - indicates slope about x axis is zero

$\overline{123}$ - indicates encastered boundary

The n_{16} and n_{17} integers are repeated in pairs n_{15} times.

The loading and boundary conditions specified by the n_5 and n_{17} indices are made symmetrical about the central axis and diagonals of the square plate.

(2) Compute elements of matrices required

These matrices were derived and presented explicitly in Chapter 3 and Appendix I respectively.

(3) Assemble K(E.E) portion of total structural stiffness matrix

This portion of the total stiffness matrix is established at the outset of the analysis and remains unaltered during the elastic-plastic analysis except where the composite yield behaviour of plate-beam elements requires the separation of nodal force equilibrium as described in section 3.9c.

(4) Apply external loading

The external loading is applied in accordance with the n_5 index described above.

(5) Introduce boundary conditions

The boundary conditions are satisfied in accordance with the n_{17}

index described above and results in rows and corresponding columns being removed from the analysis.

(6) Solve for node displacements

The equations are solved by Gaussian elimination with row interchanges to reduce rounding off errors. There is a maximum of 154 equations for plate-beam systems. That is, five degrees of displacement freedom at each of 28 nodes in the plate, seven equilibrium and seven yield equations for the beams.

(7) Refine solution to degree specified

Following the initial solution for the unknown displacements at each stage of plasticity, the solution can be refined as many times as desired. The refinement procedures were applied to two of the solutions contained in this thesis. The increase in accuracy was so small that refinement was not necessary. The equations were well conditioned throughout the elastic-plastic analysis.

(8) Calculate plate generalized stresses at all nodes

Each of the generalized stresses Mx, My and Mxy were computed at each node for each separate element and averaged so that only one generalized stress state existed at any one node. These were stored and made available for calculating principal generalized stresses and computing scale factors for the yield behaviour of the plate.

(9) Calculate edge beam bending and twisting moments

These were computed and averaged at nodes joining beam elements and made available for the investigation of their composite yield behaviour with plate elements.

(10) Calculate principal generalized stresses at all nodes

These are computed using the generalized stresses of (8) above and the equations discussed in sections 3.4d and e. These are stored for use in the next section of the program and constitute the major output quantities required from the analysis.

(11) Adjust generalized stress field to satisfy yield criterion

This portion of the program determines the plastic behaviour at nodes in the plate and functions in accordance with the procedures outlined in section 3.7. It specifies which of the nodes has become plastic during an increase in load and gives the load causing plasticity. The node number is recorded and the responsible principal generalized stress indicated by a plasticity index. This index is simply an integer such that if its value is

0 - the node is non-plastic.

2 - the principal generalized stress $M^2 = M$.

10 - the principal generalized stress $M^1 = M$.

$\overline{12}$ - both principal generalized stresses M^1 and $M^2 = M$.

(12) Check for beam yield behaviour

Once the yield criterion is satisfied in the plate at one node, the beam bending moments are checked and if any exceed the limiting value for the beams, the load given by (11) above must be reduced such that the beam becomes plastic and not the plate. The beam node affected is noted and a plasticity index computed for this node. This index is

0 - if neither beam nor plate element joining at the node is plastic.

1 - if plate is plastic but not beam such that beam has continuous slope but different from that of the plate.

2 - if beam has reached plasticity.

(13) Output results according to analysis specified

Output is presented after an elastic analysis or for an elastic-plastic analysis after each stage of plastic behaviour whether it occurs in the plate, beam or both simultaneously. The output for the collapse stage of the third solution described in Chapter 6 is shown in Tables A2.2, A2.3 and A2.4.

In Table A2.2 the input items n_{16} and n_{17} are shown. In this solution only the vertical displacement at node 28 (corner of the plate) was prevented. In Table A2.3 the displacement field at collapse is shown with the column matrix of displacements of equations 3.61 indicated. Here the subscripts n and p have the range of values 1 to 28. Also shown in this table are the angles of principal plane orientations and of plastic flow lines as described for Figure 3.13a. In Table A2.4, the violation of the yield criterion is indicated. This occurs as a result of assuming ϕ_q constant in equations 3.38. The change $\Delta\phi_i$ is also shown. From the results it is clear that for node 5 with $\Delta\phi_5 = 19.29^\circ$ equations 3.38 underestimates the true yield limit by only 2.36% and correspondingly overestimates the smaller principal generalized stress by 3%. This node became plastic with $M_5^1 = M$ at a load equal to 84% of the collapse load. This solution is a good indication of the importance of equations 3.38 in approximating the yield function for large changes in the angle ϕ_i.

Also in Table A2.4 are shown the beam slope θ_y' and plastic rotations α_b that were described for the composite plate-beam yield behaviour of Figure 3.18. The plasticity index for the slab at node 22 indicates that $M_{22}^1 = M$. The beam index indicates that the beam bending moment

```
0 1.00000, +0   0 6 0 1+9, +4   0 1,00000, +6   0 1.00000, +6   0 7   0 7   0 1.00000, +4   0 1.00000, +4
                    ELASTIC-PLASTIC SOLUTION

                                          TO A

                                      SQUARE PLATE


STRENGTH PARAMETERS
          SLAB FULLY PLASTIC MOMENT = 1 00000000000  D/L
          EDGE BEAM STIFFNESS RATIOBEAM/SLAB = 2 00
          EDGE BEAMS STIFFNESS RATIO TORSIONAL/BENDING= 0.00
          FULLY PLASTIC MOMENT RATIO BEAM/SLAB = 1 00
          POISSON RATIO = 0.15000


APPLIED LOADS AND BOUNDARY CONDITIONS SYMMETRICAL ABOUT X AND Y AXIS AND DIAGONALS

APPLIED LOADING
          UNIFORMLY DISTRIBUTED LOAD TO SLAB = 50.0000000000  D/LLL


BOUNDARY CONDITIONS

          NODE  20   100
               n16   n17


APPLIED LOADS CAUSING PLASTICITY AT NODE  7

          UNIFORMLY DISTRIBUTED LOAD = 23.0604050701+  D/LLL

 ✓        VERTICAL EDGE REACTION (D/L)
22  -3.6720500020     23  -6.5193376+970     24  -11.9+570043070     29  -8.47494177109
          26  -6.9160049166?     27  -4 37373340250     20  -1.9220107106+
```

Table A2.2

NODE	PLASTICITY INDEX	VERTICAL DISPLACEMENTS (L) D_n	SLOPE X D_n	SLOPE Y D_n	ROTATION 1 R_p^1	ROTATION 2 R_p^2
1	19	0.21487998814	0.00926645789	-0.00926646836	0.01053292198	0.01053292198
2	19	0.21947008859	-0.07779172488	-0.00449952529	0.00499095237	0.07884280070
3	18	0.21207590140	-0.07919908852	-0.14705730720	0.10167828360	0.000 000000
4	19	0.20007641967	-0.22113201406	-0.00241260152	0.04184012980	0.00482958882
5	18	0.19499711186	-0.21613799810	-0.13275007935	0.07013012838	0.0 0 00 0000
6	16	0.18337267722	-0.19225180950	-0.24997037918	0.08021216713	0.0 000000000
7	19	0.17917246749	-0.33446000429	-0.000000 0135	0.00455107423	0.000 0000000
8	16	0.17721036278	-0.32901906608	-0.10918049079	0.04705592046	0.000000000000
9	18	0.16037312197	-0.39215197911	-0.21412018022	0.05459800034	0.000000000000
10	18	0.14019361843	-0.7672 070964	-0.30911400909	0.05961790116	0.000000000000
11	18	0.14407043127	-0.40153778473	-0.00106723922	0.00213448427	0.000000 0000
12	16	0.14081961884	-0.40184274802	-0.00078889975	0.01437631781	0.000000 0 00
13	18	0.13024742907	-0.38320051336	-0.17906875570	0.02100585848	0.000000000000
14	10	0.11299409980	-0.34541830926	-0.25423131379	0.02062491444	0.000000000000
15	18	0.08999035817	-0.20629711289	-0.31347747905	0.02422598381	0.000000000000
16	16	0.10494094858	-0.43016704179	-0.00243670298	0.00487399968	0.000000000000
17	6	0.10949015918	-0.43921092473	-0.08826397554	0.000000000000	0.000000 0000
18	6	0.09909539480	-0.47645034190	-0.14486045911	0.000000000000	0.000000000000
19	6	0.08139567871	-0.39256721886	-0.20219274139	0.000000000000	0.000000000000
20	16	0.06254649261	-0.33947628132	-0.24476472453	0.00137954124	0.000000000000
21	6	0.04073390817	-0.27417974301	-0.27417974361	0.000000000000	0.000000000000
22	16	0.07721864290	-0.44105029923	-0.01800170702	0.02008359418	0.000000000000
23	8	0.06439187388	-0.44645906987	-0.07564765908	0.000000000000	0.0 0000000000
24	6	0.05007046797	-0.43567507324	-0.12229203764	0.000000000000	0.000000000000
25	6	0.04409957940	-0.40109613103	-0.15797111721	0.000000000000	0.000000 0000
26	6	0.03372289831	-0.34879519908	-0.18407230612	0.000000000000	0.000000000000
27	6	0.01734532457	-0.28310798080	-0.20419092231	0.000000000000	0.000000000000
28	6	0.00000000000	-0.21048758049	-0.21048758049	0.000000000000	0.000000000000

NODE	PRINCIPAL MOMENTS (D/L) M1	PRINCIPAL MOMENTS (D/L) M2	CARTESIAN MOMENTS (D/L) MX	CARTESIAN MOMENTS (D/L) MY	MXY	PRINCIPAL ANGLE ϕ_1	ANGLE 1 (DEGREES) Φ_1^1	ANGLE 2 Φ_1^2
1	0.99999999924	0.99999999904	0.99999999924	0.99999999904	-0.00000001827	0.00	90.00	0.00
2	0.99999999877	1.00000000094	0.99999999877	1.00000000094	0.00000000382	0.00	90.00	0.00
3	0.99999999885	0.88943073358	0.94471986627	0.94471986686	-0.05528013268	45.00	135.00	0.00
4	1.00000000050	1.00000000080	1.00000000080	1.00000000050	0.00000001143	90.00	180.00	90.00
5	0.99999999938	0.82702367149	0.87153466450	0.95548900621	-0.10235988625	36.86	126.86	0.00
6	1.00000000110	0.54850779217	0.77425389666	0.77425380663	-0.22574618448	45.00	135.00	0.00
7	1.00000000030	1.00000000001	1.00000000001	1.00000000030	-0.00000001931	90.00	180.00	90.00
8	0.99999999947	0.80028271234	0.94513697630	0.85514573553	-0.19073706038	27.01	117.01	0.00
9	0.99999999972	0.47205648484	0.77036364452	0.70169284206	-0.24239280278	39.25	129.25	0.00
10	0.99999999942	0.24419659716	0.67204829880	0.62204829851	-0.37795170114	45.00	135.00	0.00
11	1.00000000001	0.73453142247	1.00000000001	0.73453142247	0.00000007834	0.00	90.00	0.00
12	0.99999999908	0.67124384809	0.99177277187	0.67907187609	-0.05050587010	15.93	105.93	0.00
13	1.00000000087	0.44970627464	0.84409722549	0.60444989321	-0.24776494677	33.03	123.03	0.00
14	0.99999999994	0.13699420967	0.62907700022	0.51101712930	-0.42791098588	40.10	130.10	0.00
15	0.99999999908	-0.10389501714	0.44809249132	0.44809249145	-0.55194750893	45.00	135.00	0.00
16	0.99999999907	0.37265694630	0.99999999997	0.37265694440	0.00000000949	0.00	90.00	0.00
17	0.91900029323	0.39061947114	0.91540119076	0.39402754463	-0.04795707223	5.10	[illegible]	0.00
18	0.80126790 182	0.26785203450	0.77177520370	0.38734969250	-0.24910793342	25.00	[illegible]	0.00
19	0.96973894087	0.02210671143	0.69202038990	0.33981680552	-0.44735889044	38.10	[illegible]	0.00
20	1.00000000001	-0.22714974229	0.47309337997	0.29984684481	-0.69738073229	49.09	139.09	0.00
21	0.94908972425	-0.44588006892	0.29159358706	0.25190358707	-0.60747769958	45.00	[illegible]	0.00
22	0.99999999 871	0.83534590414	0.99999999821	0.03593455816	-0.03000014404	9.00	99.00	0.00
23	0.84900170966	0.01154473521	0.84807754910	0.01344880940	-0.03539484972	9.00	[illegible]	0.00
24	0.58270847579	-0.1170 849730	0.39179948216	0.00240444827	-0.24510041040	24.16	[illegible]	0.00
25	0.88614914140	-0.7873 677464	0.39304302082	0.01440309403	-0.44030751390	31.46	[illegible]	0.00
26	0.77247149 125	-0.47724347307	0.27077920478	0.01999659341	-0.61078969917	38.00	[illegible]	0.00
27	0.70041303838	- 6302 648404	0.14014894041	0.01020041172	-0.71594848888	42.93	[illegible]	0.00
28	0.74870883213	- 74747301908	0.03090740820	0.00030740815	-0.74787122410	45.00	[illegible]	0.00

Table A2.3

$\Delta\phi_1$

PRINCIPAL MOMENT DATA (TRUE/APPROX PERCENT)

NODE	PLASTICITY INDEX	M1	M2	ANGLE DIFFERENCE (TRUE LESS APPROX DEGREES)
1	12	0.0000	-0 0000	0.00
2	19	0 0000	-0 0000	0 00
3	10	0 0000	0. 000	0.00
4	19	0 0000	-0 0000	0.00
5	10	2 3979	-3 0073	19 20
6	10	0 0000	-0. 000	0 00
7	19	0 0000	-0.0000	0 00
8	10	0 1420	-0.1700	4 01
9	10	0 0657	-0 1394	2.02
10	10	0 0000	-0 00 0	0 00
11	10	0 0000	0. 000	0.00
12	10	0 2283	-0.3471	-4 75
13	10	0 0159	-0.0370	-0 95
14	10	0 0260	-0 1904	0 99
15	10	0 00 0	0.0000	0 00
16	10	0 0000	0 0000	0 00
17	0	0 0000	0.0000	0 00
18	0	0 0000	0.0000	0 00
19	0	0 0000	0.0000	0 00
20	10	0 0009	0.0304	-0 05
21	0	0 0 00	0. 030	0 00
22	10	0 0000	0 000	0.00
23	0	0 0000	0 0000	0 00
24	0	0 0000	0.0000	0 00
25	0	0 0000	0.0000	0 00
26	0	0 0000	0.0000	0.00
27	0	0 0000	0 0000	0.00
28	0	0 0000	0.0000	0.00

θ'_y α_b

NODE	PLASTICITY INDEX (SLAB)	(BEAM)	BENDING MOMENT	TWISTING MOMENT	BEAM SLOPE	BEAM ROTATION
22	10	2	1 00000000001	0 00000000000	-0.02918208104	0 05092509220
23	9	2	1.0 000000021	0 00000000000	-0 03109040944	0 01919043400
24	0	0	0 93346670123	0 00000000000	0 00000000000	0 0 0 0 00 00
25	0	0	0 78099010760	0 00000000 0	0 0 000000000	0 0000000 00
26	0	0	0 56765585785	0 00000000000	0 0 0000 0 00	0 000 0 00 00
27	0	0	0 30201012960	0 00 00000009	0.00000000000	0 00000 0 00
28	0	0	0.00069114513	0 0000 00 003	0 00000000000	0 000 000 00

```
0 7  0 2  0 49  0 78  0 2  0 3  0 129  0 176  0 4  0 181  0 182  0 3  0 5  0 237  0 238  0 4
0 7  0 349  0 350  0 8  0 405  0 406  0 5  0 9  0 461  0 462  0 6  0 11  0 573  0 574  0 7
0 3  0 674  0 675  0 676  0 677  0 479  0 680  0 681  0 683  0 685  0 686  0 687  0 689
0 691  0 693  0 695  0 697  0 699  0 701  0 703  0 711  0 715  0 14  0 730  0 731  0 732
0 733  0 735  0 736  0 737  0 739  0 741  0 742  0 743  0 745  0 747  0 749  0 751  0 753
0 755  0 757  0 759  0 767  0 771  0 8  0 15  0 787  0 788  0 9  0 17  0 9 9  0 910  0 10
0 19  0 1021  0 1022  0 11  0 21  0 1133  0 1134  0 12  0 23  0 1245  0 1246  0 13  0 25
0 1357  0 1358  0 14  0 27  0 1469  0 1470  0 15  0 29  0 1581  0 1582  0 16  0 31  0 1603
0 1604  0 28  0 30  0 2141  0 2142  0 22  0 43  0 2365  0 2366  0 4 99980, -1  0 1 00000, +4
0 1 00000, +4  0 4 9990 , +1  0 1 00000, +4  0 1.00000, +4  0 2 72220, +4  0 5 55550, +4
0 40  0 42  0 9 15450, +0  0 1.50141, +0  0 2 00000, +1  0 99990  0 1 48440, -1  0 9 000317 -1
0 5 43004, -9  0 19  0 46  0 1 21840, +0  0 3 49235, +7  0 1 21880, -4  0 1 00000, +4  0 6 00000, +0
0 6.00000, +0  0 99909  0-2 28381,-11  0 1 00000, -0  0 3 79208, -2  0 31  0 44  0 1 00140, -0
0 2 00294, +7  0 1 00170, +4  0 1.00000, +4  0 1 60000, -1  0 1 40000, +1  YIELD CRITERION VIOLATED (P-9)-5 10

END OUTPUT   09 0 OCKS
```

Table A2.4

at this node is also at its limit. For node 23 the index for the slab indicates that no plasticity has occured in the slab. However, the beam index shows that the beam is plastic at node 23. These are two examples of composite yield behaviour.

At the begining of Table A2.2 and at the end of Table A2.4 are samples of "query printing". This allows the flow of the program to be traced before and after output. Queries are made by placing a question mark after a calculation or at the end of any program statement. This facility was used a great deal in the program development. It can be easily suppressed and need not appear with the output. However, it was included here to illustrate what happens when the elastic-plastic analysis results in collapse of the plate or slab. When collapse occurs no solution to the equations is possible and the yield criterion is violated at previous plastic nodes. In the present example node 16 had reached plasticity previous to the collapse stage shown and the yield criterion was satisfied during subsequent increases in applied loading. But when node 7 became plastic and allowed a rectangular collapse mechanism to form, further increase in load resulted in node 16 violating the yield criterion. The underlined query printing gives the principal generalized stress $M^1_{16} > M$, the value of $M = 1.0$ and the node number 16 along with the caption indicating violation of the yield criterion.

(14) Assemble parts of elastic-plastic stiffness matrix for plate and beams

This portion of the program required the most programming effort and resulted in complicated but systematic procedures for building the coefficients in the total structural elastic-plastic stiffness matrix.

The plasticity indices for indicating plate and beam plastic behaviour were used throughout this section and they completely controlled the calculation and placement of the required coefficients. Of the total store required for the program, this portion required approximately one third.

(15) Update orientation of principal planes at plastic nodes where necessary

This updating procedure and reasons for its use are described in section 3.4e. None of the analyses presented in this study required these procedures since the yield criterion was never violated more than the 2.36% of Table A2.4. In fact, all the other solutions gave errors of less then 1%.

APPENDIX III - MISCELLANEOUS EXPERIMENTAL DATA

A3.1 General R marks

On each of the metal plates deflections and strain recordings were made at more locations than the results indicate in Chapter 5. However, these additional measurements were made to establish the degree of symmetry produced for curvature and deflections, since symmetry about the central axes and diagonal is assumed in the computer analyses. These results have not been presented. The symmetry conditions were very good in all plate tests. The positions where measurements were taken are reported in this appendix along with general comments on membrane strain measured in the plate tests.

For both plates and slabs, various control beam tests and other miscellaneous material tests were performed. The results of these tests are included in this appendix.

Each of the plate and slab tests was performed over a period of 4 to 6 hours except for slab No.2 which was loaded over a period of 7 hours.

A slow rate of straining was used in all tests. The accuracy of strain measurement recorded by the data logger was to the nearest 4 micro-strain on the maximum gain. But since most of the strain readings were made during inelastic strain ranges, this gain had to be reduced. The estimated accuracy of strain measurement is about $\pm 5\%$. Since generalized stresses were determined from experimental generalized stress-curvature curves, an additional 5% error could be introduced. Therefore, the maximum possible error in determining generalized stresses is approximately $\pm 10\%$.

All graphs and figures are placed at the end of the appendix.

Reinforced Concrete Slab Tests

A3.2 Slab No.1

(a) Flexural Stiffness for Slab

For this slab the flexural stiffness had to be computed theoretically. It was assumed that the concrete was cracked to the neutral axis, everywhere in the slab. The calculation of D for this slab follows:

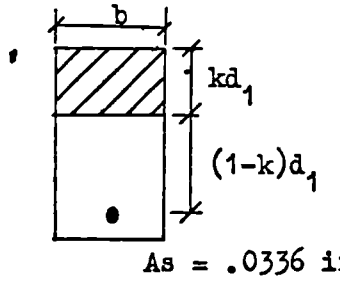

As = .0336 in.^{2}

$n = \frac{Es}{Ec} = 10 \quad Ec = 3x10^6$ p.s.i.

$d_1 = 1.31"$ $\quad b = 3"$ $\quad \nu = .15$

$bk^2 = 2nAs(1-k) \quad k = .375"$

$Ic = \frac{1}{3}bd_1^3 = .0525$ in.^{4}

$Is = nAs(1-k)^2 = .2940$ in.^{4}

$I/b = .1155$ in.^{3}

$$D = \frac{EI}{(1-\nu^2)} = 354{,}000 \text{ lb in.} \qquad \text{A3.1}$$

If based on an uncracked section, D = 810,000 lb in.

(b) Control Beam for Determining M_u of Slab

The load-deflection curve for the control beam specimen for this slab is shown in Graph A3.1. From this graph, $P_{ultimate} = .81$ tons giving

$$M_u = 1260 \text{ lb in/in} \qquad \text{A3.2}$$

Since for this slab, L = 36" and D is given by equation A3.1, the non-dimensional limiting generalized stress is

$$\frac{M_u L}{D} = .1280 \qquad \text{A3.3}$$

A3.3 Slab No.2

(a) Flexural Stiffness for Slab

The theoretical stiffness based on a cracked section is given below.

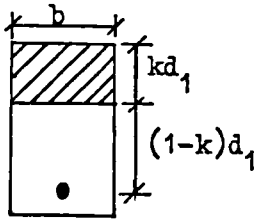

$d_1 = 1.313"$ $b = 4"$

$k = .449$

$Ic = .1207\ in.^4$

$Is = .3485\ in.^4$

$I/b = .1173\ in.^3$

$As = .0468\ in.^2$

$$D = \frac{EI}{(1-\nu^2)} = 360{,}000\ lb\ in. \qquad A3.4$$

(b) Control Beam for Slab

The generalized stress-curvature diagram for this control beam is presented in Graph A3.2. The limiting generalized stress is seen to be $M_u = 1040$ lb in/in with an ultimate curvature of $.0024\ in.^{-1}$

The flexural stiffnesses for this slab as determined from Graph A3.2 are:

Before Cracking - $D = 3{,}100{,}000$ lb in. A3.5

After Cracking - $D = 353{,}000$ lb in. A3.6

For the other slabs, only theoretical stiffnesses could be used since no curvature measurements were made. These stiffnesses were based on a cracked (to the neutral axis) concrete section.

(c) Flexural Stiffness of Edge Beam

For the edge beam section ($\frac{3}{8}" \times 1\frac{1}{2}"$) on this slab, the theoretical bending stiffness is

$$EI = 3{,}170{,}000\ lb\ in.^2 \qquad A3.7$$

(d) Control Beam for Edge Beam

The experimental bending moment-curvature characteristics of the edge supporting beams are shown in Graph A3.3.

The fully plastic bending moment is M_b = 8000 lb in. and the bending stiffness is slightly greater than the theoretical value (equation A3.7); i.e. experimentally

$$EI = 3{,}640{,}000 \text{ lb in.}^2 \qquad \text{A3.8}$$

The non-dimensional limiting values for slab and edge beams with L = 36" are:

$$\frac{M_u}{D} L = .1060 \qquad \text{A3.9}$$

using D = 353,000 lb in.

$$\frac{M_b}{D} = .0226 \qquad \text{A3.10}$$

A3.4 Slabs No.3 and No.4

(a) Flexural Stiffness for Slabs No.3 and No.4

The stiffness for these slabs based on the cracked section is as follows:

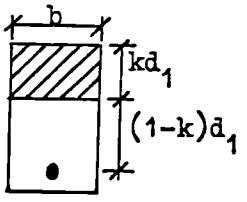

b = 1" d_1 = .625"
k = .2675
Ic = .00637 $in.^4$
Is = .0128 $in.^4$
As = .0104 $in.^2$ I/b = .01917 $in.^3$

$$D = \frac{EI}{(1-\nu^2)} = 58{,}800 \text{ lb in.} \qquad \text{A3.11}$$

(b) Control Beam for Slabs

The load-displacement graph for the control specimen for these slabs is shown in Graph A3.4, from which

$$M_u = 170 \text{ lb in/in} \qquad \text{A3.12}$$

Therefore, the non-dimensional value becomes (for L = 16")

$$\frac{M_u L}{D} = .0464 \qquad \text{A3.13}$$

(c) Control Beam for Edge Beams on Slab No.4

The moment-curvature characteristics of these edge beams are shown in Graph A3.5. The fully plastic bending moment for the beams is

$$M_b = 290 \text{ lb in.} \qquad \text{A3.14}$$

with a bending stiffness of

$$EI = 16{,}200 \text{ lb in.}^2 \qquad \text{A3.15}$$

The non-dimensional fully plastic value using equation A3.11 is

$$\frac{M_b}{D} = .00493 \qquad \text{A3.16}$$

Mild Steel Plate Tests

A3.5 Plates No.1 to No.4

(a) Stress-strain Characteristics of Plate Material

A portion of the stress-strain relationship for the metal plates is shown in Graph A3.6. Tensile coupon tests were made for all the plates. Graph A3.6 is a typical relationship since very little difference in properties was found between the tests.

(b) Control Beam for Plates

The bending stiffness of the plates was determined from the generalized stress-curvature results of a control beam test. This relationship is shown in Graph A3.7.

From this graph the stiffness

$$D = 325{,}000 \text{ lb in.} \qquad \text{A3.17}$$

The theoretical value is

$$D = \frac{Et^3}{12(1-\nu^2)} = 332{,}000 \text{ lb in.} \qquad \text{A3.18}$$

The limiting generalized stress value is

$$M_p = 2270 \text{ lb in/in} \qquad \text{A3.19}$$

and in non-dimensional form is

$$\frac{M_p L}{D} = .1120 \qquad \text{A3.20}$$

(c) Control Beam for Edge Beams

The bending moment-curvature diagram of Graph A3.8 for the edge beams used on plates No.2 and No.4 indicates that

$$EI = 4{,}700{,}000 \text{ lb in.}^2 \qquad \text{A3.21}$$

and

$$M_b = 7920 \text{ lb in.} \qquad \text{A3.22}$$

Using the plate stiffness of equation A3.17, the non-dimensional limiting value is

$$\frac{M_b}{D} = .0244 \qquad \text{A3.22}$$

(d) Strain Measurement

The locations on plate No.1 at which strains were recorded are shown on $\frac{1}{4}$ of the plate in Figure A3.1. Symmetry of curvature was checked by comparing the results of diagonally opposite pairs of gauges.

The maximum difference between curvature measurements made across the x and y axes was less than 3%.

Measurements of membrane strains were made at the locations shown in Figure A3.1. Of the 72 stages of loading at which strains were recorded, the average of membrane to bending strain was less than .05; i.e. 5% membrane strain. It was evident from the strain readings that this was compressive membrane strain.

Figures A3.2 to A3.4 give the position of strain gauges on plates No.2, No.3 and No.4 respectively.

From strain measurements (at more than 70 load stages) for each of the last three plate tests, the results indicated better symmetry of curvature than for plate No.1 and about the same order of membrane strain to bending (5%). In-plane strains were, of course, largest near the cable point loads. Here the membrane strain was largest in plate No.3 where it reached 35% of the bending strain close to the collapse load. It increased rapidly at collapse to more than 1.5 times the bending strain.

A3.6 Loading Cables

The cables used in loading plates No.3 and No.4 were purchased from British Ropes Limited, London S.E.7, and have the following particulars:

N.B.L.(Tons)	Size	Thread
4	$\frac{5}{8}$" B.S.F.	5/16" dia. 6/9x9x1 W.S.C.
6	$\frac{3}{4}$" B.S.F.	$\frac{3}{8}$" dia. 6/9x9x1 I.W.R.C.
10	$\frac{7}{8}$" B.S.R.	$\frac{1}{2}$" dia. 6/9x9x1 I.W.R.C.

Table A3.1

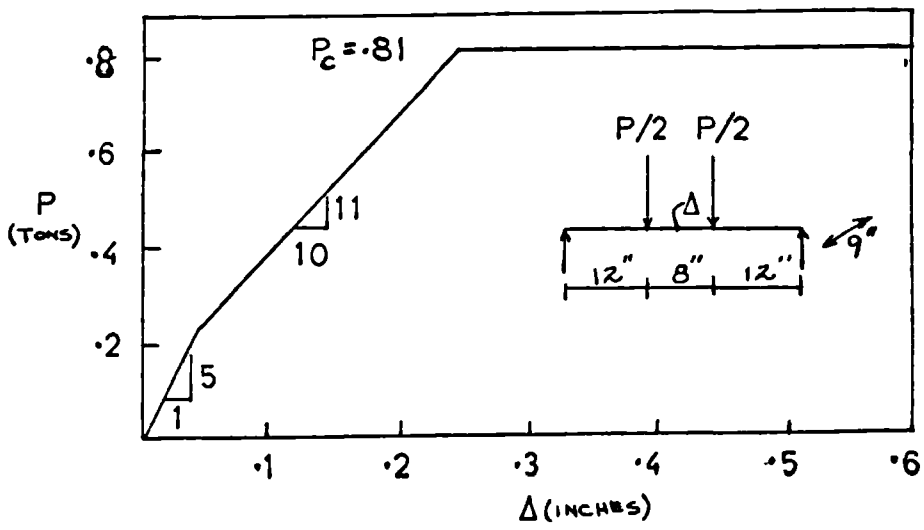

Slab No.1

Control Beam

Graph A3.1

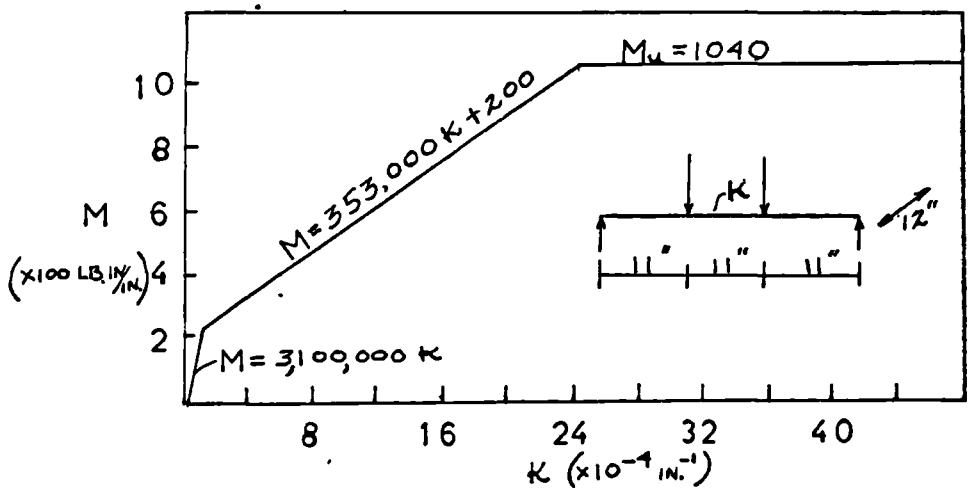

Slab No.2

Control Beam

Graph A3.2

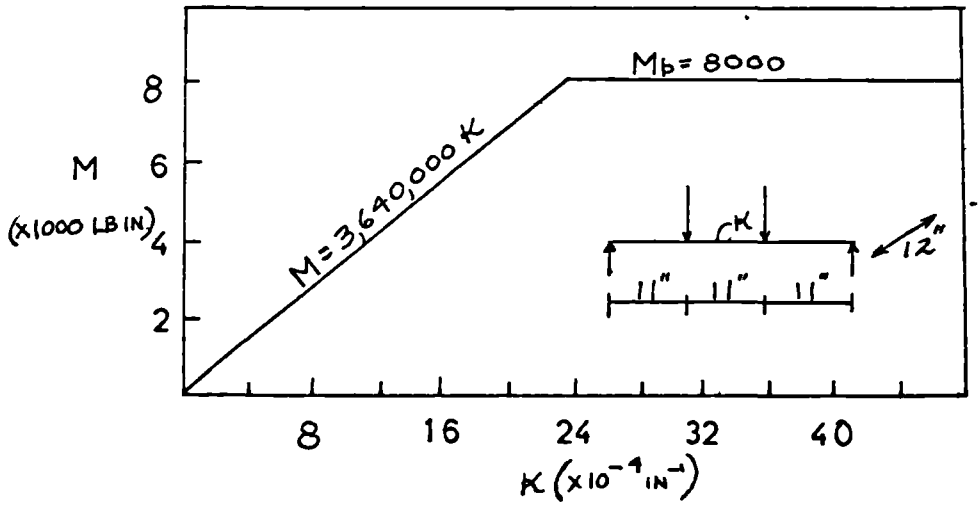

Slab No.2

Edge Beam
Control Beam

Graph A3.3

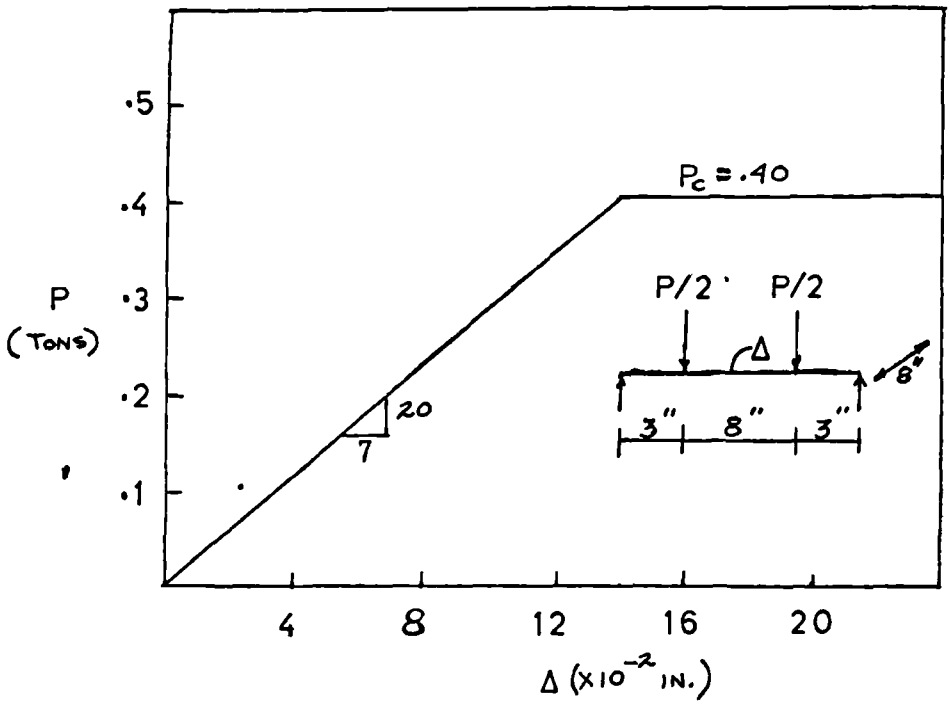

Slabs No.3 & 4

Control Beam

Graph A3.4

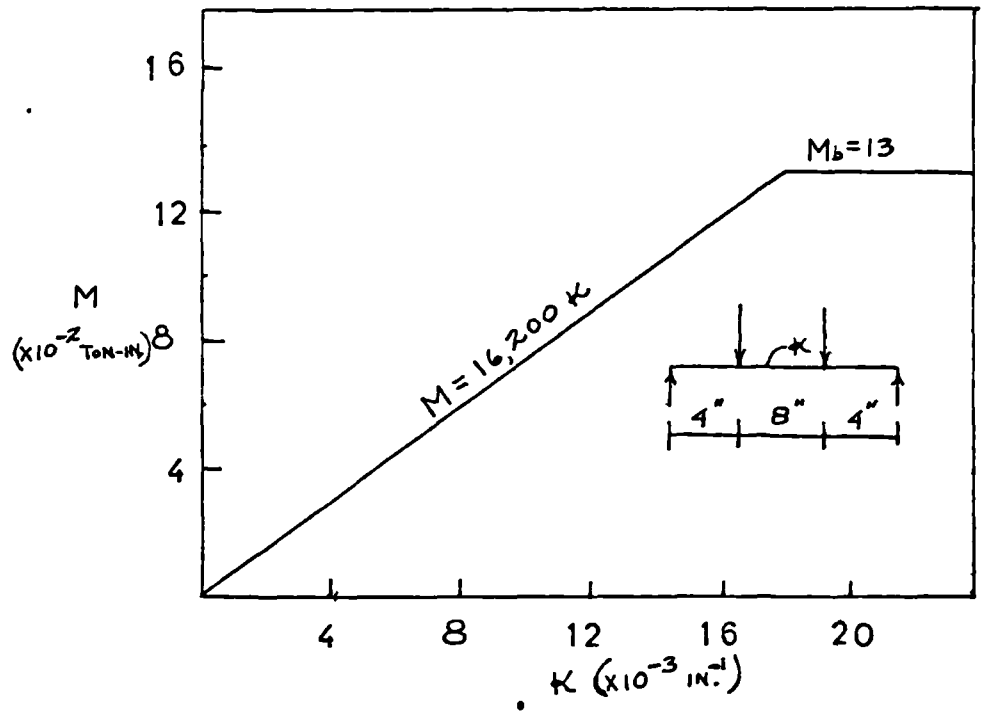

Slab No.4

Edge Beam
Control Beam

Graph A3.5

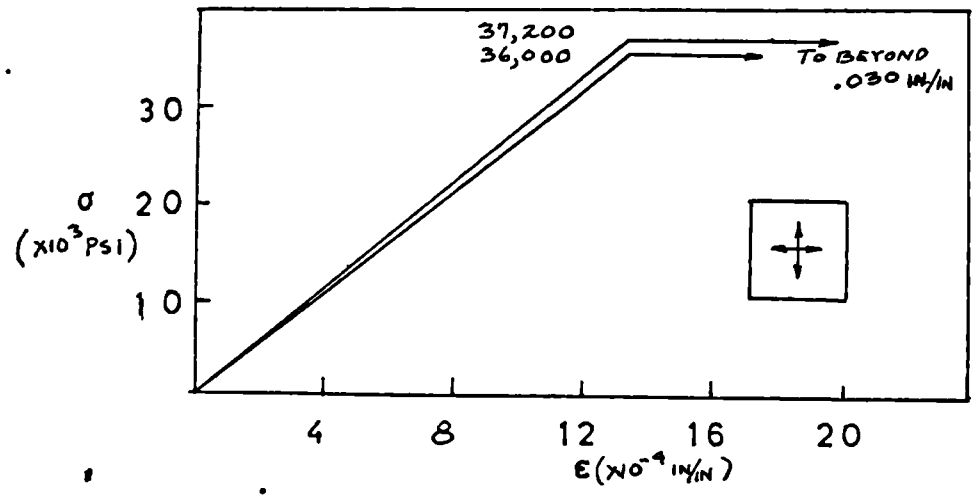

Plates No.1 to

Typical Stress-Strain Properties for Plate Material

Graph A3.6

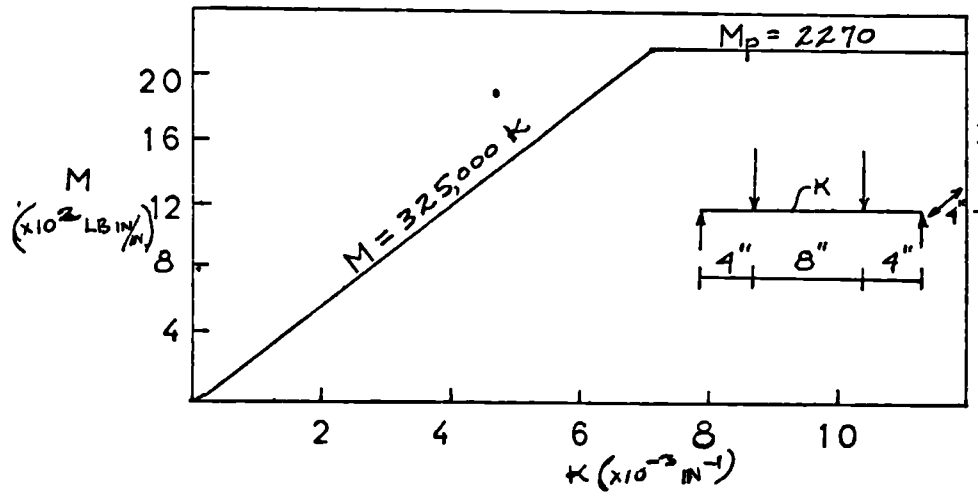

Plates No.1 to

Control Beam

Graph A3.7

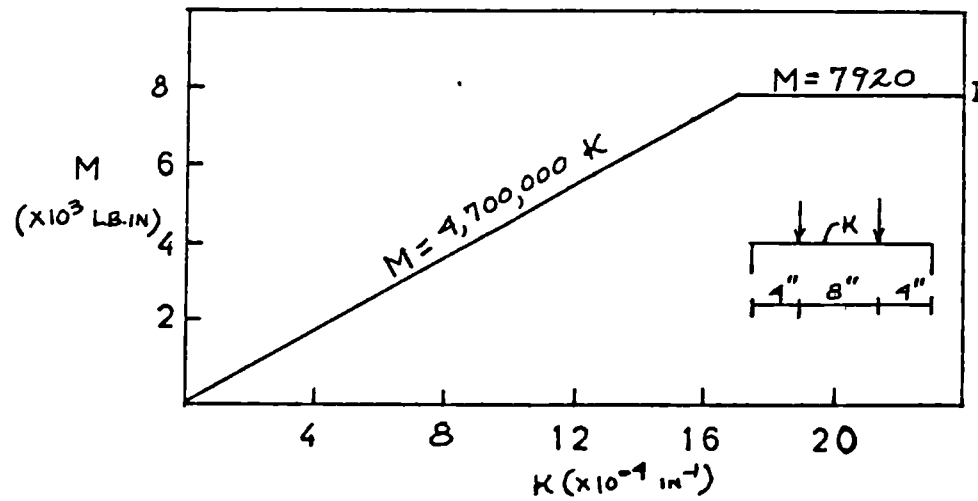

Plates No. 2 & 4

Edge Beam
Control Beam

Graph A3.8

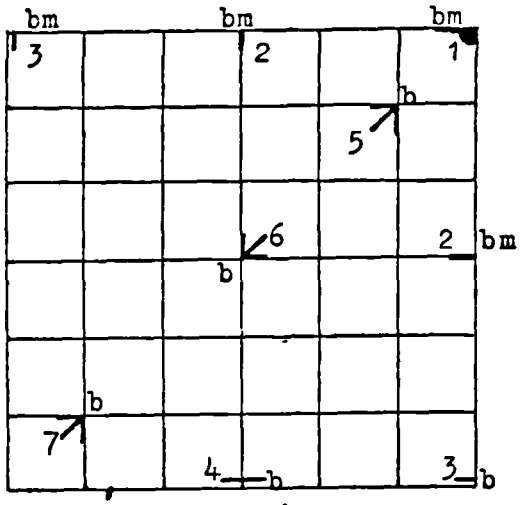

Plate No.1

Figure A3.1

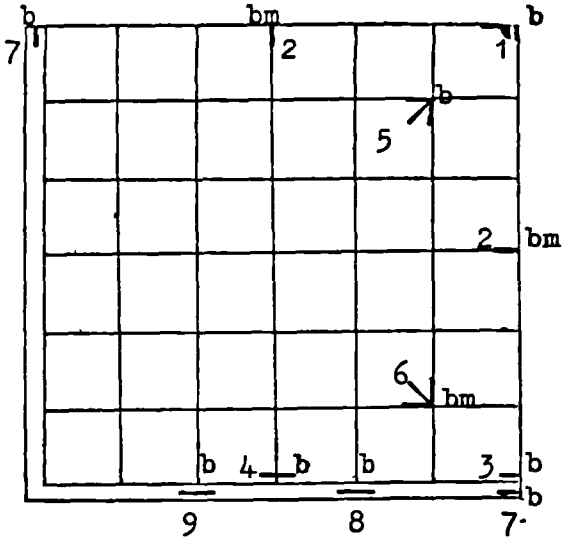

Plate No.2

Figure A3.2

Metal Plate Tests - Strain Gauge Positions

b-bending strain

m-membrane strain

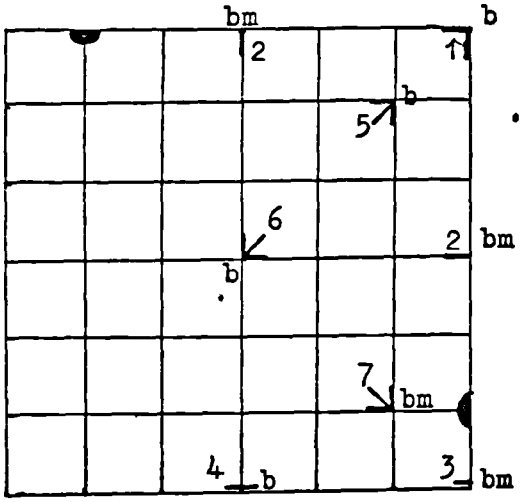

Plate No.3

Figure A3.3

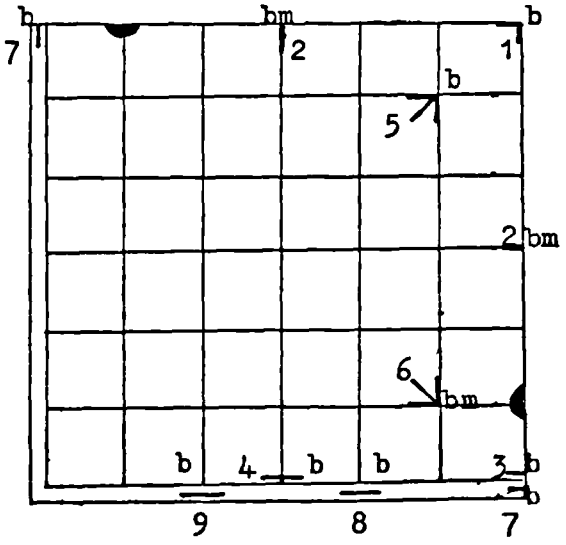

Plate No.4

Figure A3.4

BIBLIOGRAPHY

1. Westergaard, H.M. and Slater, W.A., Moments and Stresses in Slabs. Proc. A.C.I., 1921.

2. Bach, C. and Graf, O., Versuche mit allseitig aufliegenden, quadratischen and rechteckigen Eisenbetonphatten, Deutscher Ausschuss für Eisenbeton, Vol. 30. Berlin, 1915.

3. Timoshenko, S.P., and Woinowsky-Krieger, S., Theory of Plates and Shells, McGraw-Hill Book Co. Inc. 2nd edition, 1959.

4. Wood, R.H., Plastic and Elastic Design of Slabs and Plates, Thames and Hudson, London, 1961.

5. Johansen, K.W., Pladeformler. Formelsamling, 2 volumes. Polyteknisk Forenig, Copenhagen, 1949, 1951.

6. Johansen, K.W., Brudlinieteorier, Copenhagen, 1952.

7. Johansen, K.W., Yield-Line Theory. English translation of the thesis presented to the Danmarks Tekniske Højskole in 1943, Cement and Concrete Association, London, 1962.

8. Comité Européen du Béton, Bulletin d'Information No. 27, September, 1960, English translation, Cement and Concrete Association, London.

9. Comité Européen du Béton, Bulletin D'Information No. 35, March,1962. English translation, Cement and Concrete Association, London.

10. Comité Européen du Béton, Bulletin D'Information No. 56, August,1966, English translation, Cement and Concrete Association, London.

11. Kemp, K.O., Yield of a square reinforced concrete slab on simple supports, allowing for membrane forces, The Structural Engineer. Vol. 45, No. 7, July,1967.

12. Jones, L.L., Ultimate Load Analysis of Reinforced and Prestressed Concrete Structures, Chatto and Windus, London, 1962.

13. Wood, R.H. and Jones, L.L., Yield-Line Analysis of Slabs, Thames and Hudson, Chatto and Windus, London,1967.

14. Prager, W., The theory of plasticity: A survey of recent achievements, James Clayton Lecture, Inst. Mech. Eng., London,1955.

15. Drucker, D.C., Greenberg, H.J. and Prager, W., Extended limit design theorems for continuous media, Quart. Appl. Math., Vol. 9, 1952.

16. Hill, R., On the state of stress in a plastic-rigid body at the yield point. Phil, Mag., Vol. 42,1951.

17. Haythornthwaite, R.M. and Shield, R.T., A note on the deformable region in a rigid-plastic body. J. Mech. Phys. Solids Vol.6,1958.

18. Hodge, P.G., Limit Analysis of Rotationally Symmetric Plates and Shells, Prentise-Hall Inc., 1963.

19. Prager, W., An Introduction to Plasticity. Addison-Wesley Pub. Co. Inc. 1959.

20. Hodge, P.G., Plastic Analysis of Structures, McGraw-Hill Book Co. Inc., 1959.

21. Shull, H.E., and Hu, L.W., Load-Carrying Capacity of Simply Supported Rectangular Plates, J. App. Mech., December,1963.

22. Wood, R.H., Studies in Composite Construction. Part 2, The Interaction of Floors and Beams in Multi-Storey Buildings, Her Majesty's Stationery Office, London,1955.

23. Massonnet, Ch., Complete solutions describing the limit state of reinforced concrete slabs. Magazine of Concrete Research, Vol. 19, No. 58, March,1967.

24. Hillerborg, A., Strip method for slabs on columns, Australian C.S.I.R.O., Division of Building Research, Translatio No.2, Melbourne, 1964.

25. Levi, F., Superfici di influenza e fenomeni di adattamento nelle lastre piane, Giornale del Genio Civile, May,1950.

26. Callari, C.E., Tentative d'établissment d'une méthode générale pour le calcul anélastique des dalles en flexion. C.E.B. Bulletin D'Information No.30,Paris March,1963.

27. Callari, C.E., Méthode générale de calcul des dalles en flexion dars le domaine anélastique, Annales de l'Institut Technique du Batiment et des Travaux Publics, No.201, September,1964.

28. Somigliana, C., Sulle deformazioni elastiche non regolari, Archives du IV° Congrès des Mathematiciens, Vol. III, Rome, 1908.

29. Massonnet, Ch., Théorie générale des plaques élasto-plastiques, C.E.B. Bulletin D'Information No. 56, August,1966.

30. Cornelis, A., Étude à l'aide d'une calculatrice électronique du comportement des dalles en béton armé en phase de fissuration, C.E.B. Bulletin D'Information No.56, August,1966.

31. Cyrus, N.J. and Fulton, R.E., Finite difference accuracy in structural analysis, J. Str. Div., Proc. Amer. Soc. of Civil Eng., Vol. 92, No.ST6, December,1966.

32. Parkhill, D.L., The flexural behaviour of slabs at ultimate load, Magazine of Concrete Research, Vol. 18, No. 56, September,1966.

33. Kemp, K.O., Contribution to discussion on Parkhill[31] approach, Magazine of Concrete Research. Vol. 19, No. 59, June,1967.

34. McNeice, G.M., Contribution to discussion on Parkhill[31] approach, Magazine of Concrete Research. Vol. 19, No.59, June, 1967.

35. Turner, M.J., Clough, R.W., Martin, H.C. and Topp, L.J., Stiffness and Deflection Analysis of Complex Structures, J. Aero. Sci, Vol. 23, No. 9, September,1956.

36. Clough, R.W., The Finite Element Method in Structural Mechanics, Chapter 7 of Stress Analysis, John Wiley and Sons Ltd., 1965.

37. Zienkiewicz, O.C., Finite Element Procedures in the Solution of Plate and Shell Problems, Chapter 8 of Stress Analysis, John Wiley and Sons Ltd., 1965.

38. Zienkiewicz, O.C., The Finite Element Method, in Structural and Continuum Mechanics, McGraw-Hill Pub. Co. Ltd., 1967.

39. Proceedings of the Conference on Matrix Methods in Structural Mechanics, Air Force Institute of Technology, Wright Patterson Air Force Base, Ohio, U.S.A., October,1965.

40. Argyris, J.H., On the analysis of complex elastic structures, App. Mech. Rev., Vol. 11, July,1958.

41. Gallagher, R.H., A Correlation Study of Methods of Matrix Structural Analysis, Pergamon Press, 1964.

42. Zienkiewicz, O.C. and Cheun , Y.K., The finite element method for analysis of elastic isotropic and orthotropic slabs. Proc. Inst. Civ. Eng., Vol. 28, August,1964.

43. Bazeley, G.P., Cheung, Y.K., Irons, B.M., Zienkiewicz, O.C., Triangular ele ents in plate bending - conforming and non-conforming s lutions. Proc. Conf. on Matrix Methods, Air Force. Inst. of Tech., Wright Patterson Air Force Base, Ohio, U.S.A., October,1965.

44. Clough, R.W. and Tocher, J.L., Finite element stiffness matrices for analysis of plates in bending. Proc. Conf. on Matrix Methods, Air Force. Inst. of Tech., Wright Patterson Air Force Base, Ohio, U.S.A., October,1965

45. Herrmann, L.R., A bending analysis for plates. Proc. Conf. on Matrix Methods, Air Force. Inst. of Tech., Wright Patterson Air Force Base, Ohio, U.S.A., October,1965.

46. Hansteen, H., Finite element displacement analysis of plate bending based on rectangular elements. International Symposium on the use of Electronic Digital Computers in Structural Engineering, Paper No. 14, Working Session No. 4, University of Newcastle-upon-Tyne, Department of Civil Engineering.

47. Argyris, J.H., Continua and discontinua. Proc. Conf. on Matrix Methods, Air Force. Inst. of Tech., Wright Patterson Air Force Base, Ohio, U.S.A., October,1965.

48. Pope, G.G., A discrete element method for the analysis of plane elasto-plastic stress problems. Aer. Quart. Vol.XVI February,1966.

49. Ngo, D. and Scordelis, A.C., Finite Element Analysis of Reinforced Concrete Beams. J. A.C.I., March,1967.

50. Norris, C.H., and Wilbur, J.B., Elementary Structural Analysis. McGraw-Hill Pub. Co. Inc., 1960.

51. Livesley, R.K., Matrix Methods of Structural Analysis. Pergamon Press, 1964.

52. Prager, W., An Introduction to Plasticity. Addison-Wesley Pub. Co.Inc., 1959.

53. Hill, R., The Math matical Th ory of Plasticity. Oxford University Press.,1950.

54. Kemp, K.O., The yield criterion for orthotropically reinforced concrete slabs. Int. J. Mech. Sci., Vol. 7,1965.

55. Save, M., A corsistert limit-analysis theory for reinforced concrete slabs. Magazine of Concrete Research, Vol. 19, No. 58, March,1967.

56. Morley, C.T., Experim nts on the yield criterion of isotropic reinforced concrete slabs. J. A.C.I., January,1967.

57. Lenschow, R. and Sozen, M.A., A yield criterion for reinforced concrete slabs, J. A.C.I., May,1967.

58. Seely, F.B. and Smith, J.O., Advanced Mechanics of Materials. John Wiley and Sons Inc., 2nd edition, August,1961.

59. Thompson,J.M.T., Localized Raleigh functions in structural and stress analysis. Int. J. Sol. and Str., Vol. 3, 1967.

ADDENDUM I - VIOLATION OF YIELD CRITERION IN SINGLE ELEMENTS

ADD1.0 Variation of Maximum Principal Generalized Stresses in Elements

In order to determine if and to what extent the yield criterion has been violated within elements, principal generalized stresses were computed at nine locations (in addition to nodal points) on elements selected from five of the eleven analyses presented. The five chosen consisted of Metal Plate Tests No. 1 and No. 3 and the three additional solutions reported in Chapter 6. The first two were selected because the gradients of principal values were larger for plates without beams and also they were essentially the same type of analyses as those for Slab Tests No. 1 and No.3. The three additional solutions were selected since they involved different loading and to some extent different supporting conditions from the previous eight solutions.

From each of the five analyses, one element was selected. These elements (with one exception) involved plastic behaviour at one node at the end of the elastic range and considerable nodal plasticity at the collapse state.

The values of largest principal generalized stresses were computed using equations 3.20 at thirteen positions on the element. This was done by combining equations 3.9 (u = displacements at the node which are known at each stage once the elastic-plastic analysis is complete) with equations 3.19 to determine Mx, My and Mxy at each point selected.

The results are shown in Figures ADD1.0 to ADD1.4. The node numbers are indicated and correspond to those given in Figure 3.3. In addition to the computed largest principal values, the largest nodal principal generalized stresses produced during the elastic-plastic analyses are indicated (based on average values of Mx, My and Mxy - see section 3.3c). The comparison of nodal values indicates that discrepancies of about 10% exist between individual element values and those determined by the averaging procedures.

From the distributions of largest principal generalized stresses in each of Figures ADD1.0 to ADD1.4 it is clear that the greatest values occur at nodes. The averaged nodal values used in the elastic-plastic

analyses were maintained at unity for plastic nodes. However, the actual nodal values (using one element only) appear to violate the yield criterion by less than 10%. Consequently, it is reasonable to suggest that the greatest violation exists at the nodes and can be of the order 10% in the class of problems considered.

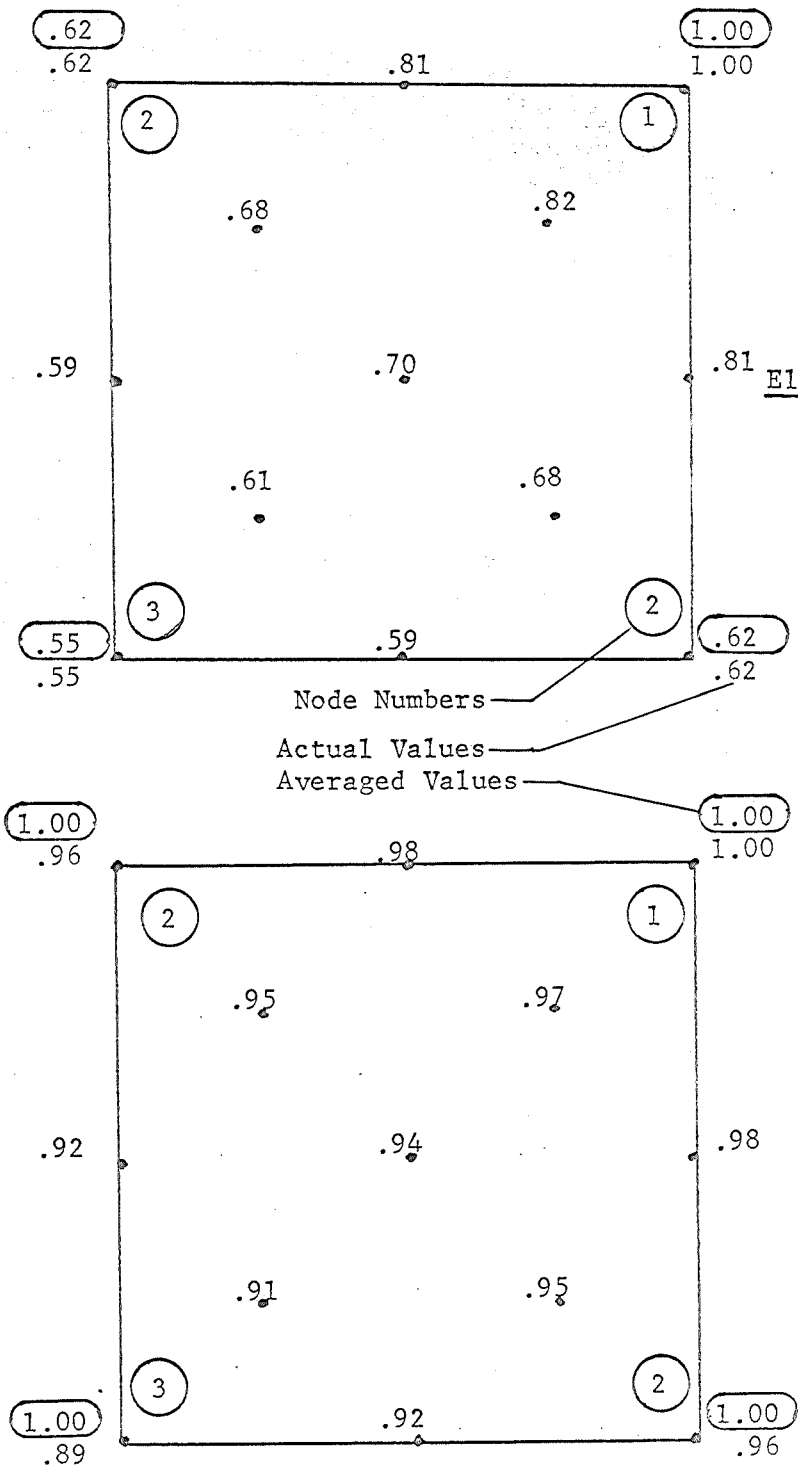

Maximum Principal Generalized stresses

Metal Plate Test No.1 (see Pattern No.5)

Figure ADD 1.0

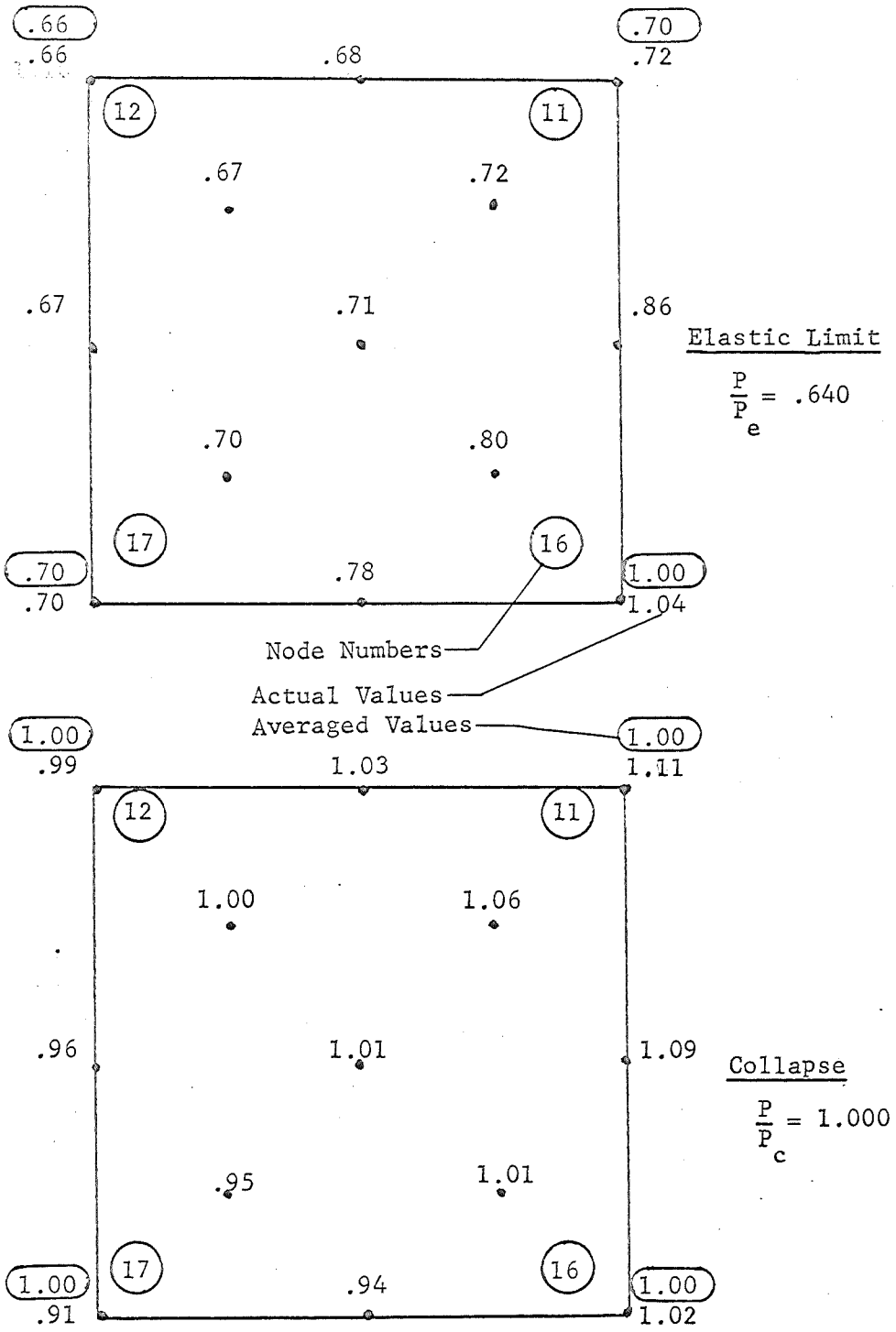

Maximum Principal Generalized Stresses

Metal Plate Test No.3 (see Pattern No.7)

Figure ADD 1.1

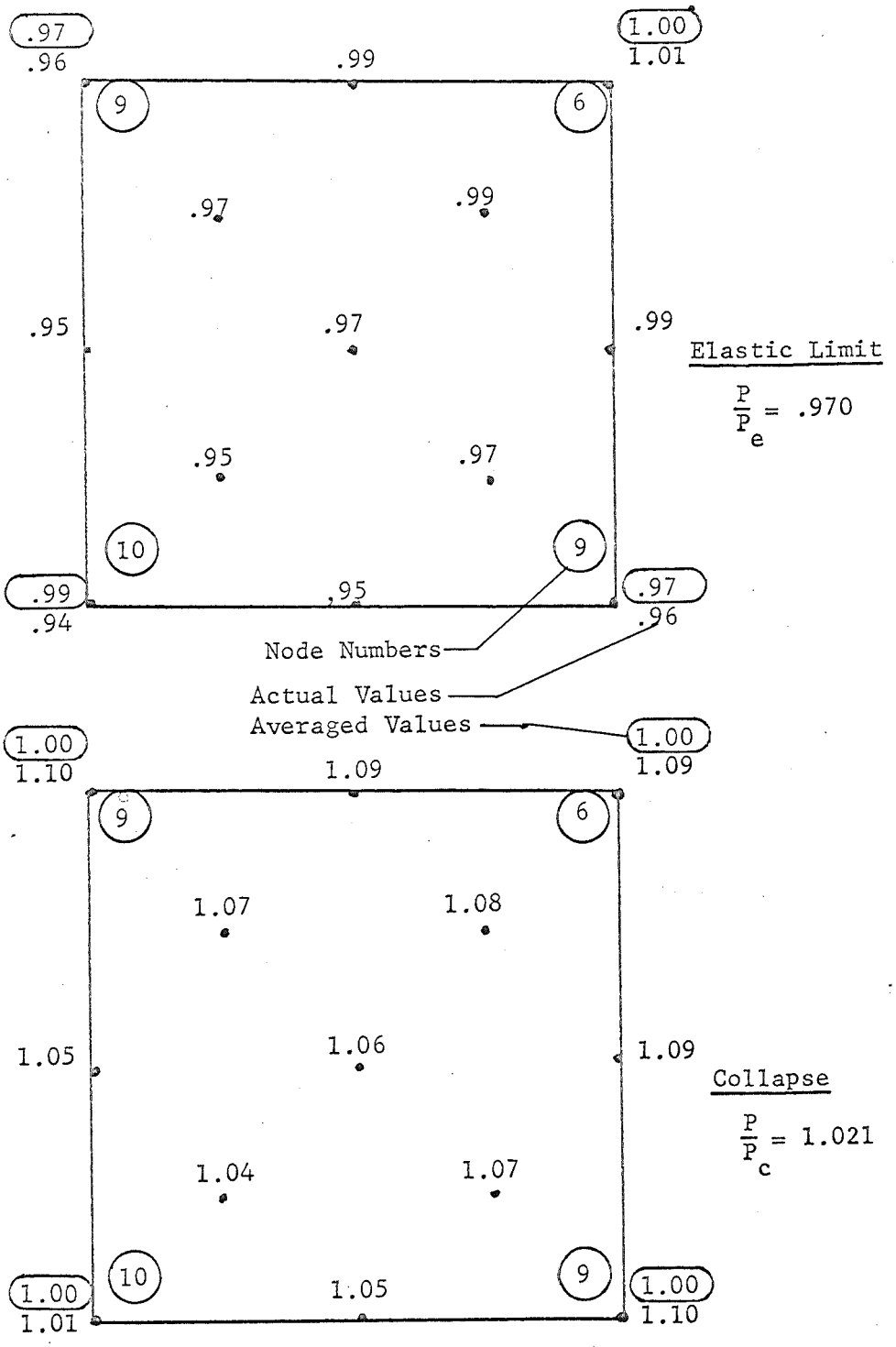

Maximum Principal Generalized Stresses

Simply Supported Square Slab (see Pattern No.9)

Figure ADD 1.2

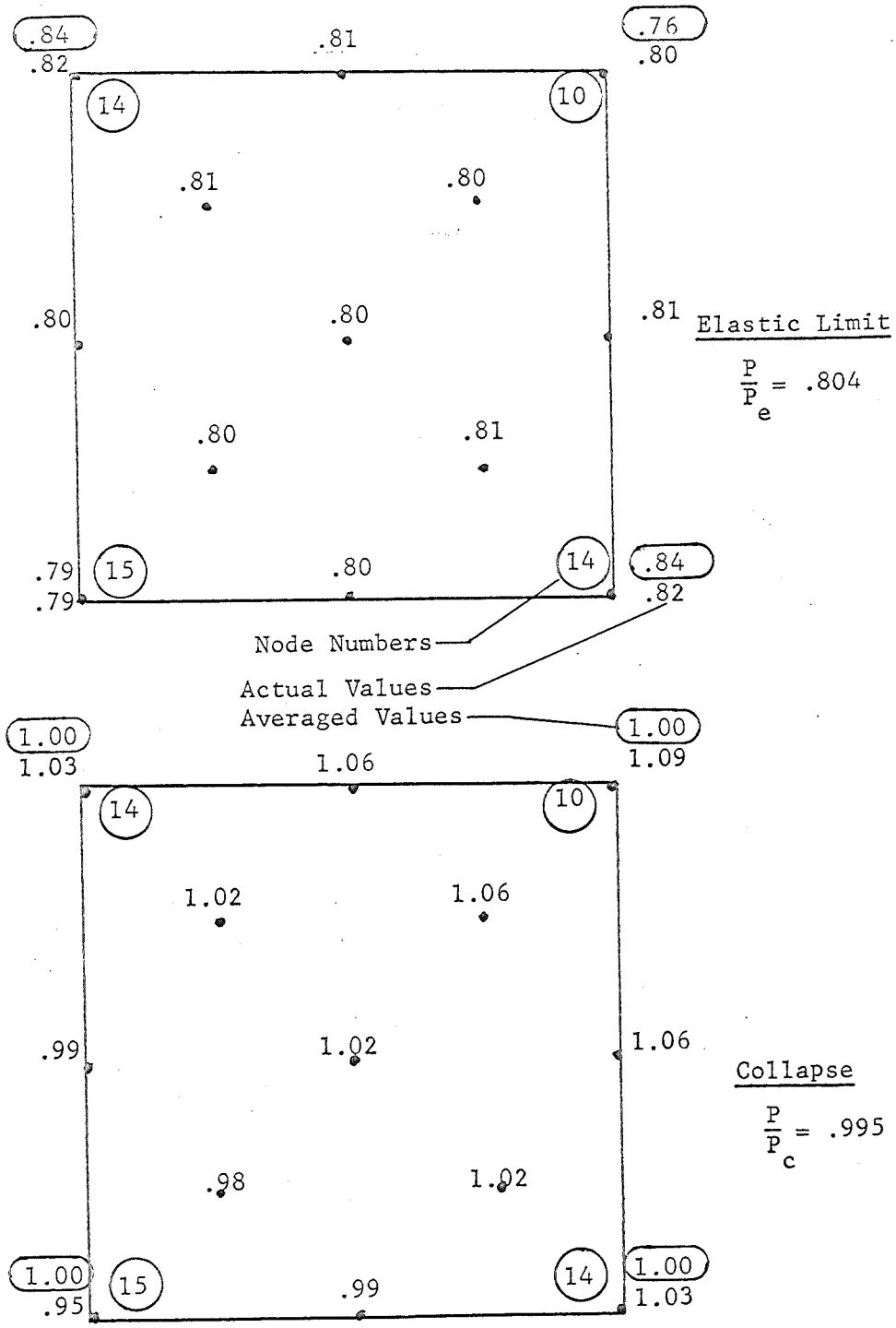

Elastic Limit

$\frac{P}{P_e} = .804$

Collapse

$\frac{P}{P_c} = .995$

Maximum Principal Generalized Stresses

Square Slab with Free Edges and Corner Supports (see Pattern No.10)

Figure ADD 1.3

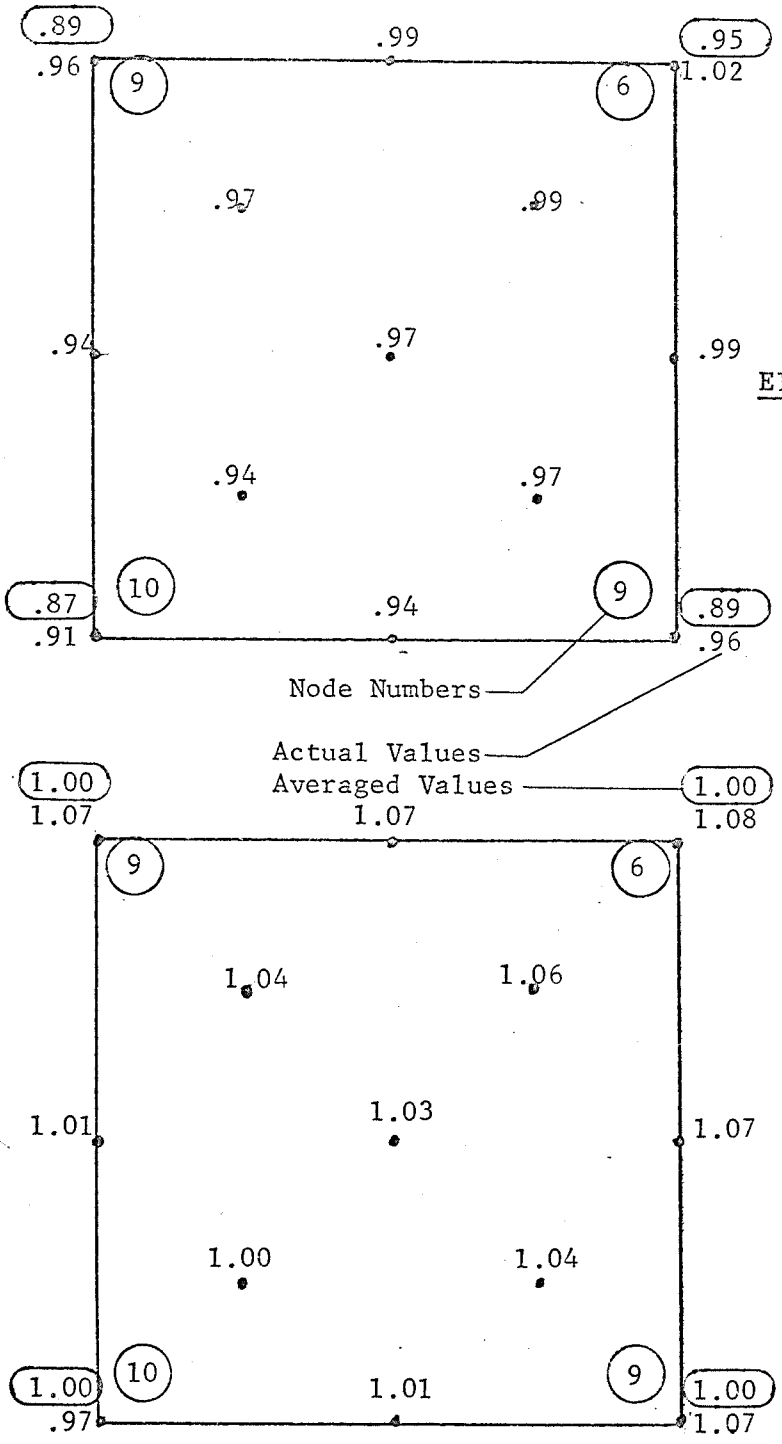

Maximum Principal Generalized Stresses

Square Slab with Edge Beams and Corner Supports (see Pattern No.11)

Figure ADD 1.4